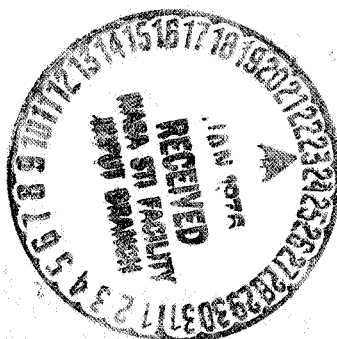**Rocketdyne**
North American Rockwell

6633 Canoga Avenue
Canoga Park, California 91304

R-7970

INVESTIGATION OF 17-HZ

CLOSED-LOOP INSTABILITY

ON S-II STAGE OF SATURN V

Contract NAS8-19

PREPARED BY
Rocketdyne Engineering
Canoga Park, California

APPROVED BY

P. D. Castenholz
J-2 Program Manager

NO. OF PAGES 268 & xiv   **REVISIONS**   DATE 29 August 1969

DATE	REV. BY	PAGES AFFECTED	REMARKS

FORM R18-G REV. 5-69

ABSTRACT

Following Apollo flight AS-503, and on flight AS-504, large-amplitude oscil-
lations in the 17-Hz frequency range were observed near the end of S-II
burn. Analytical and experimental programs were initiated to determine
the cause of these oscillations and methods of eliminating them. Rocketdyne's
efforts on the program consisted of three phases:

1. Analysis of flight data with support from stage static tests

2. Engine pulsing test program and analysis

3. LOX pump pulsing test program and analysis

From the analysis of the flight data, Rocketdyne was able to show that the
oscillations were the result of a closed-loop instability. The loop includes
the structure, the inboard LOX feedline, and the inboard engine. The in-
stability was demonstrated and parameter effects evaluated using an analog
model of the closed-loop system. The engine pulsing test program showed
that the flight oscillations are not engine self-excited oscillations, and
determined the engine transfer function $\Delta P_c/\Delta P_{in}$ (chamber pressure/LOX
pump inlet pressure) based on an inlet flow perturbation. This transfer
function is required in the closed-loop stability models. The primary
output of the pump test program was the pump termination impedance (G =
pump inlet pressure/flow) which was determined as a function of NPSH by
a combined analytical-experimental program. Using the pump termination
impedance and engine transfer function, the transmission of oscillations
from structural accelerations to chamber pressure could be determined.

ACKNOWLEDGEMENTS

CONTENTS

ILLUSTRATIONS

THIS SPACE INTENTIONALLY LEFT BLANK

TABLES

INTRODUCTION

Following Apollo flight AS-503, accelerometers and pressures were observed
to indicate a period of large amplitude oscillations in the latter part
of the second-stage burn. Data analysis revealed that the oscillations
were in the range of 18 Hz, that they appeared to be more prominent in the
parameters associated with the center engine of the second stage, and on
AS-503 that the engine pressure parameters indicated the problem more than
accelerometers. These pressure oscillations were large enough that analyses
were initiated to explain their origin. These analyses included review
of data from previous flights and from ground tests, investigation of in-
strumentation used in flight, and investigation of various hypotheses
relative to the cause of the oscillations. Effort was also directed to
obtaining more significant data on flight AS-504 to lead to a verification
of the source and nature of the oscillations.

The review of previous flight data revealed that similar, yet less severe,
oscillations were experienced on AS-501 and -502. Probably one of the
most significant results determined from this initial study was that the
accelerometers used were not adequate for obtaining valid data at 18 Hz,
and this inadequacy was corrected on flight AS-504. However, prior to
AS-504, the primary hypothesis relative to the cause of the oscillations
was that the engine had self-excited oscillations which coupled with the
structure to give large oscillation amplitudes. To help remedy this situ-
ation, the LOX pump NPSH was increased using step pressurization.

Flight AS-504 data looked very similar to flight AS-503 except that with
the new accelerometers the accelerations of the center engine and LOX tank
bottom on the second stage were very large. Using the AS-504 data, cor-
relating amplitude ratios and phase angle relationships between parameters,
Rocketdyne showed that the oscillation problem was actually the result of a
system closed-loop instability, not engine self-excited oscillations. The

THIS SPACE INTENTIONALLY LEFT BLANK

main components of the system are the structure, the LOX pump feed system, and the engine. The closed-loop instability is most easily defined by tracing the response of the components around the loop. The structural accelerations cause flow perturbations at the LOX pump inlet which result in inlet pressure oscillations as determined by the feedline-pump dynamics. These inlet pressures are transmitted through the engine to chamber pressure and result in thrust oscillations. The thrust oscillations act on the structure to cause structural accelerations. Thus, the loop is closed, and the system is unstable if, in going around the loop, the amplitude and phase relationships are such that the oscillation amplitudes tend to grow as in flight. (A mathematical definition of the loop stability is given in the text.) The instability occurred at a structural resonant frequency which is particularly associated with the cross-beam structure upon which the center engine is mounted.

Of course, previous to these flights, stability analyses had been performed to determine system stability, and these analyses had not revealed this instability. Since then, it has been found that the definition of the dynamics of the major elements of the system were inaccurate in these initial stability models. Rocketdyne performed tests pulsing the engine using an inlet piston pulser. These tests revealed that the engine transfer functions based on a model constructed to fit discharge pulsing data were not adequate for describing engine dynamics with an inlet pulse. Thus, tests were extended to get a new engine transfer function $\partial P_c / \partial P_{in}$ on the LOX side. Flight data also revealed that the structural model in these upper modes was giving inaccurate results, and attempts, both analytical and experimental, were initiated by NAR Space Division and MSFC to improve this part of the system model. Also, both Rocketdyne and NASA-MSFC performed tests to determine more accurately the dynamics of the LOX feedline-turbopump model.

The present report describes Rocketdyne's efforts in solving this S-II 18-Hz oscillation problem. The report has two major divisions. First is presented the flight data and their analysis including Rocketdyne's analog computer model of the system which was based on flight results and used to study parameter variation effects on stability. In this first section, a definition of the closed-loop instability, the arguments that proved the problem to be an instability, and a rating of the degree of instability as determined from the closed-loop damping factor, also are presented.

The second division of the report describes Rocketdyne's engine pulsing tests and the LOX turbopump pulsing tests. The results of these tests are presented and, where possible, correlation with data from MSFC tests is mentioned. There were difficulties in obtaining the data required to establish the dynamic relationships of interest. In some cases, these difficulties could be handled, but the final results still depended on a combined experimental-analytical analysis.

It should be mentioned, also, that to eliminate the oscillation problem, the center engine on the second stage was cut off early, at a time before the instability occurred. This solution has since been verified to be effective on both flights AS-505 and -506.

FLIGHT DATA, AS-504

The data obtained from flight AS-504 were more complete, permitting more detailed analysis of the dynamic performance of the vehicle than the three previous flights. Thus, the data from flight 504 will be discussed first in detail, and then the data from the other flights will be summarized, highlighting the differences and similarities between flights. Certain flight parameters have been most heavily relied upon to reach an understanding of the nature of the 17-Hertz (Hz) oscillation problem. These parameters are the five engine chamber pressure measurements (P_{c1}, P_{c2}, ..., P_{c5}) and longitudinal accelerometers on engine No. 1 ($\ddot{X}_1$), engine No. 5 ($\ddot{X}_5$), and the LOX tank bottom ($\ddot{X}_{LTB}$). These parameters, being considered primary, will be discussed first followed by a general review of other measured parameters used for corroboration.

There are significant oscillation amplitudes (particularly in certain of the accelerometer data) at frequencies other than 17 to 18 Hz. For example, a subharmonic frequency (1/2*18 Hz) and a 10-Hz frequency oscillation have been observed. Although these oscillations may be partially related, they will be discussed individually, all emphasis initially being on the data in the 17-Hz frequency range.

Chamber Pressure Measurements

The five engine chamber pressure measurements are shown for the full S-II burn time in Fig. 1. All five measurements have the same full-scale amplitude of 100 psi. The region of large oscillation amplitude is evident near the end of flight on the center engine (engine No. 5). During this same time period, the four outboard engines do indicate slight increases in oscillation amplitude. The parameters are shown again in Fig. 2 at the same amplitude range but with an expanded time scale in

THIS SPACE INTENTIONALLY LEFT BLANK
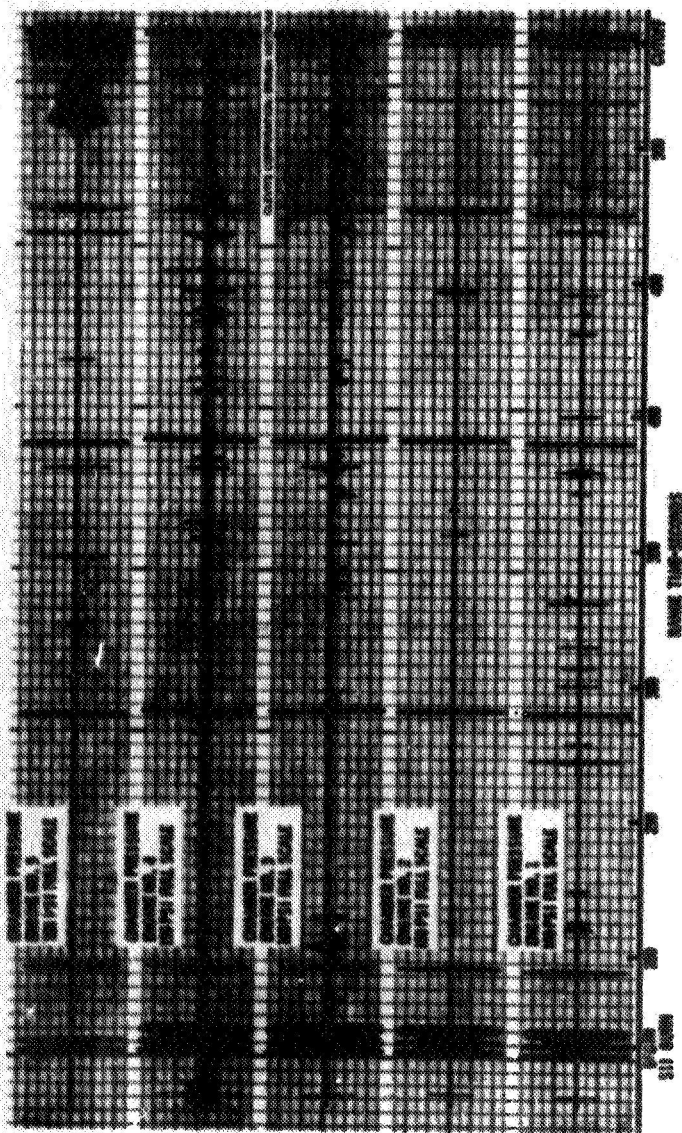
Figure 1. AS-504 S-II 17-Hz Oscillations (15- to 20-Hz Band Pass Filtered Data)
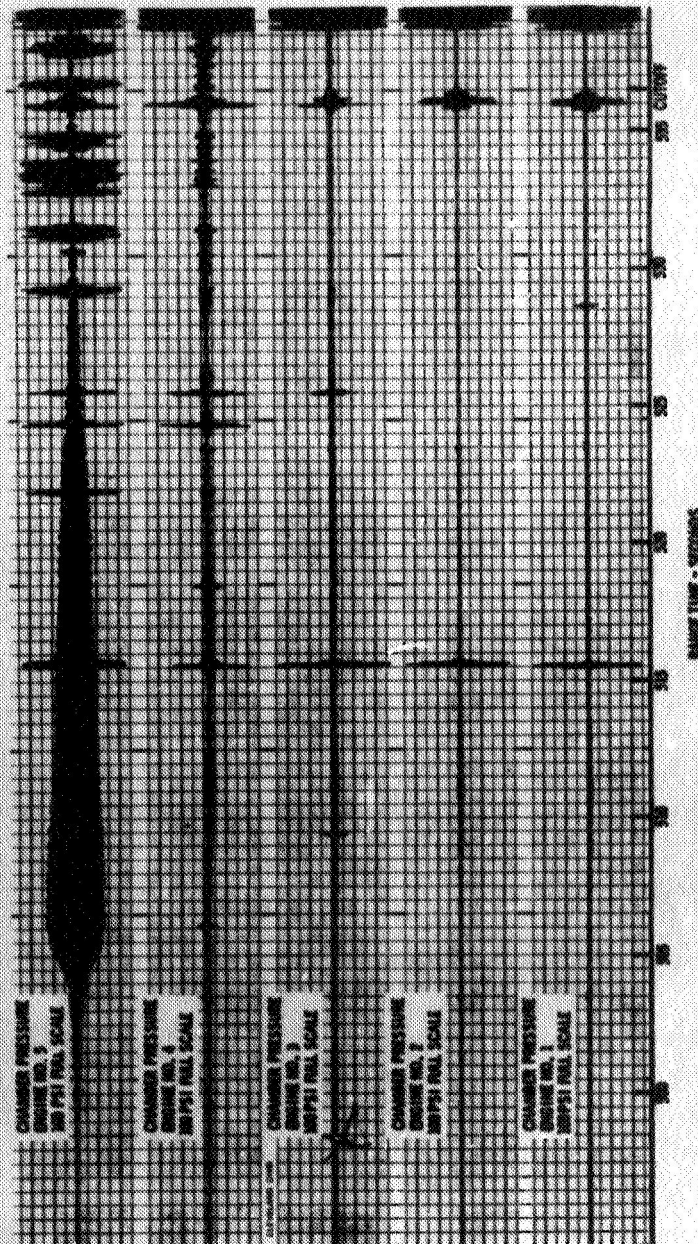
Figure 2. AS-504 S-II 17-Hz Oscillations (15-to 20-Hz Band Pass Filtered Data)

the region of large oscillations. It should be noted that both Fig. 1 and 2 present data band-pass filtered from 15 to 20 Hz. The oscillations on the center engine would be obvious without the filtering, but not those on the outboard engines.

The frequency and amplitude for F_{c5} and P_{c1} are shown in Fig. 3. The frequency was counted for each 1-second interval from filtered Brush records. The amplitudes were determined from a tracking filter of 2-Hz bandwidth. This amplitude represents a continuous average value over an 0.30-second time slice. The amplitude of P_{c5} is slowly diverging from range time (RT) 497 seconds. At RT 504.5 to 506 seconds, the amplitude rapidly diverges reaching a limit at approximately 506.5. During this period of rapid divergence, the frequency drops by a few tenths of a cycle. The amplitude then slowly decreases as the frequency slowly increases from a minimum value of 16.7 Hz to approximately 19.0 Hz. The amplitude divergence is definitely caused by a closed-loop instability (which will be described and discussed in a later section). The abrupt limit of the amplitude indicates a limit cycle resulting from system non-linearities. The gradual decrease in amplitude after 507 seconds is indicative of a return to stability.

The outboard engine measurement has a much lower amplitude and a different characteristic than the inboard measurement. It will subsequently be shown that the outboard engines are not a significant participant in the 17-Hz oscillation problem.

For comparison purposes, the maximum amplitude of the unfiltered data for P_{c5} was 75 psi, peak-to-peak (p-p). With the narrow (2 Hz) band-pass filtering of Fig. 3, the maximum amplitude was 51.2 psi, p-p. At range times prior to 497 seconds, the peak amplitudes in F_{c5} in the 10- to 25-Hz frequency range were from 0.5 to 2.1 psi, p-p, as determined from power-spectral-density plots (PSD's) with a 1-Hz bandwidth. The larger peaks which represent higher signal power during this earlier burn time occur
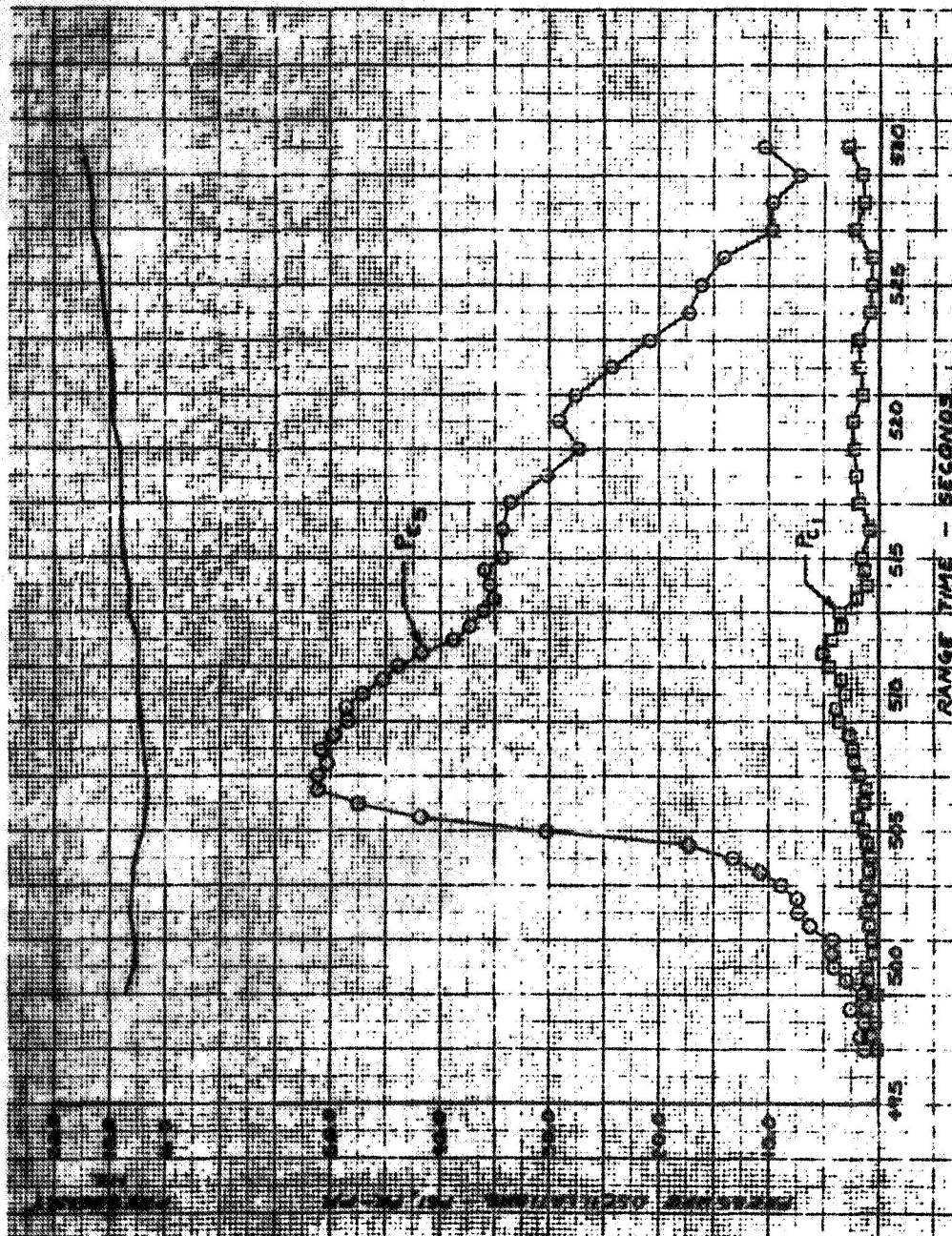
Figure 3. AS-504 S-II Oscillations, Amplitudes of Filtered Data

at frequencies close to structural resonant frequencies so that some
feedback from the structure through inlet pressure is suspected. As a
result, these peaks are not an accurate gage of the thrust oscillations
expected from the engine with no coupling to the structure. The actual
uncoupled oscillations are believed to be less than 1.0 psi (p-p) at a
given frequency, based on ground test results and the flight data at
frequencies which do not correspond to structural resonances. The ampli-
tude for the complex wave (unfiltered) of chamber pressure is generally
4 to 5 psi, p-p, and can be as high as 10 psi, p-p. This noise level
is high enough so that the data must generally be filtered to establish
accurate amplitudes in a given frequency range.

It was necessary to verify that the chamber pressure flight instrumenta-
tion was giving accurate data, because these data were used so extensively
to analyze the oscillation problem. The chamber pressure instrumentation
consists of a constricted flow channel (about 7 inches in length) followed
by a long sense line (about 41 inches) filled with hydrogen gas through a
purge line from the fuel manifold. The effect of the long sense line and
the hydrogen was determined by an engine test on the ground using a close-
coupled instrument and a flight instrument. The two instruments were in
phase at low frequencies and, at 70 Hz, the phase shift had become 45 degrees.
This indicated that the first acoustic resonance of the sense line was in
excess of 70 Hz. The effect of the constricted flow channel on the first
resonance was calculated analytically and indicated that, at most, the
first resonance of the feedline would be reduced to approximately 50 Hz.
Thus, the flight instrument used to measure chamber pressure shou.d have
a first resonant frequency in excess of 50 Hz and would, therefore, provide
valid data in the 18-Hz region.

Phase relationships between P_c and accelerometer measurements will be
discussed in the section on the accelerometer data.

Main Acceleration Measurements ($\ddot{x}_1$, $\ddot{x}_5$, $\ddot{x}_{LTB}$)

Three acceleration measurements are of primary interest in the study of the 17-Hz oscillation problem--the acceleration of engine No. 1 ($\ddot{x}_1$), engine No. 5 ($\ddot{x}_5$), and the LOX tank bottom, or sump ($\ddot{x}_{LTB}$). These three accelerations are shown in Fig. 4 for both the full S-II burn time and the time period of the large oscillations, in both cases the data being band-pass filtered from 15 to 20 Hz. The shape of the envelope of the amplitude for $\ddot{x}_5$ and $\ddot{x}_{LTB}$ is similar to that of P_{c5}. The amplitudes of these accelerations appear to diverge earlier in time than does P_{c5}, but this is believed to be caused by the much higher signal-to-noise ratio on the accelerometers. As in the case of the chamber pressures, the response of engine No. 1 is very small in comparison to the response of engine No. 5.

Another factor evident in Fig. 4, because of the low noise level, are the regions of increased amplitude at earlier times in flight. These regions begin at approximately 250, 280, 300, and 400 seconds RT. Because the region of rapidly diverging amplitudes of RT 504 has been revealed to be caused by a closed-loop instability, these earlier increases in amplitude could be indicative of a marginally stable system. These earlier phenomena will be discussed further below as the acceleration data are broken down into specific frequency content.

The amplitudes of the accelerations as determined from the tracking filter are shown in Fig. 5 for the time period of large oscillations. The frequency plot is identical to that for P_{c5} shown in Fig. 3. The maximum amplitudes observed in unfiltered data were $\ddot{x}_1 = 2.1$, $\ddot{x}_5 = 23.8$, and $\ddot{x}_{LTB} = 16.0$, all in units of g's, p-p. Earlier in time, i.e., previous to 497 RT, the maximum amplitude in $\ddot{x}_5$ was 1.0 g, p-p, and the majority of the data was less than 0.5 g, p-p.
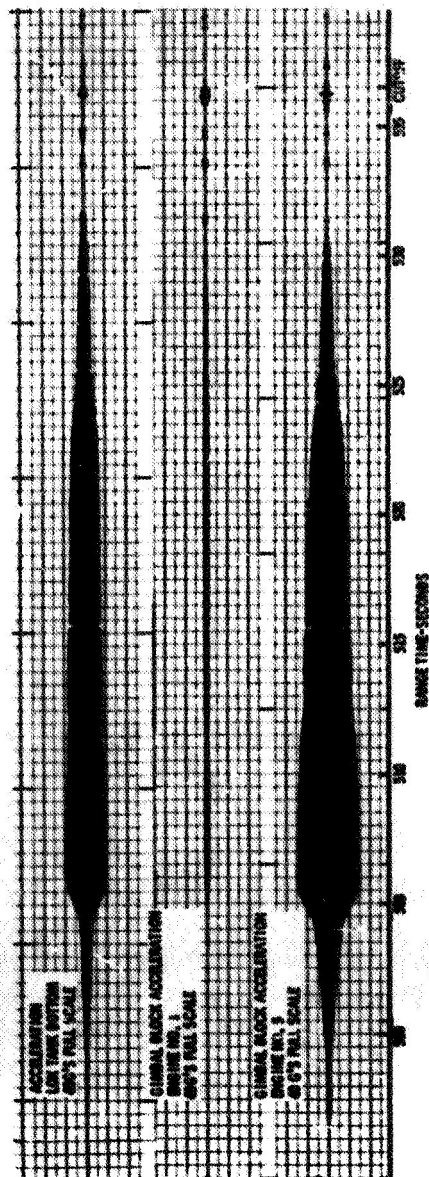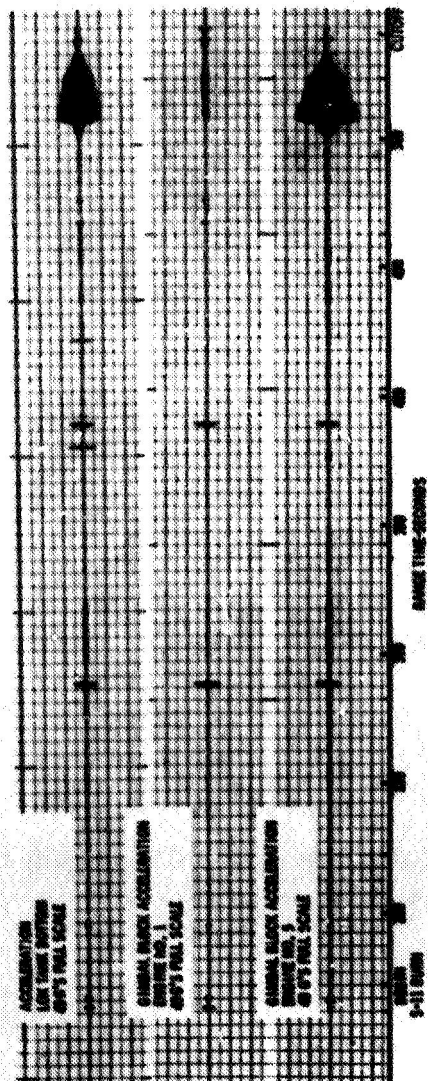
Figure 4. AS-504 S-II 17-Hz Oscillations (15- to 20-Hz Band Pass Filtered Data)
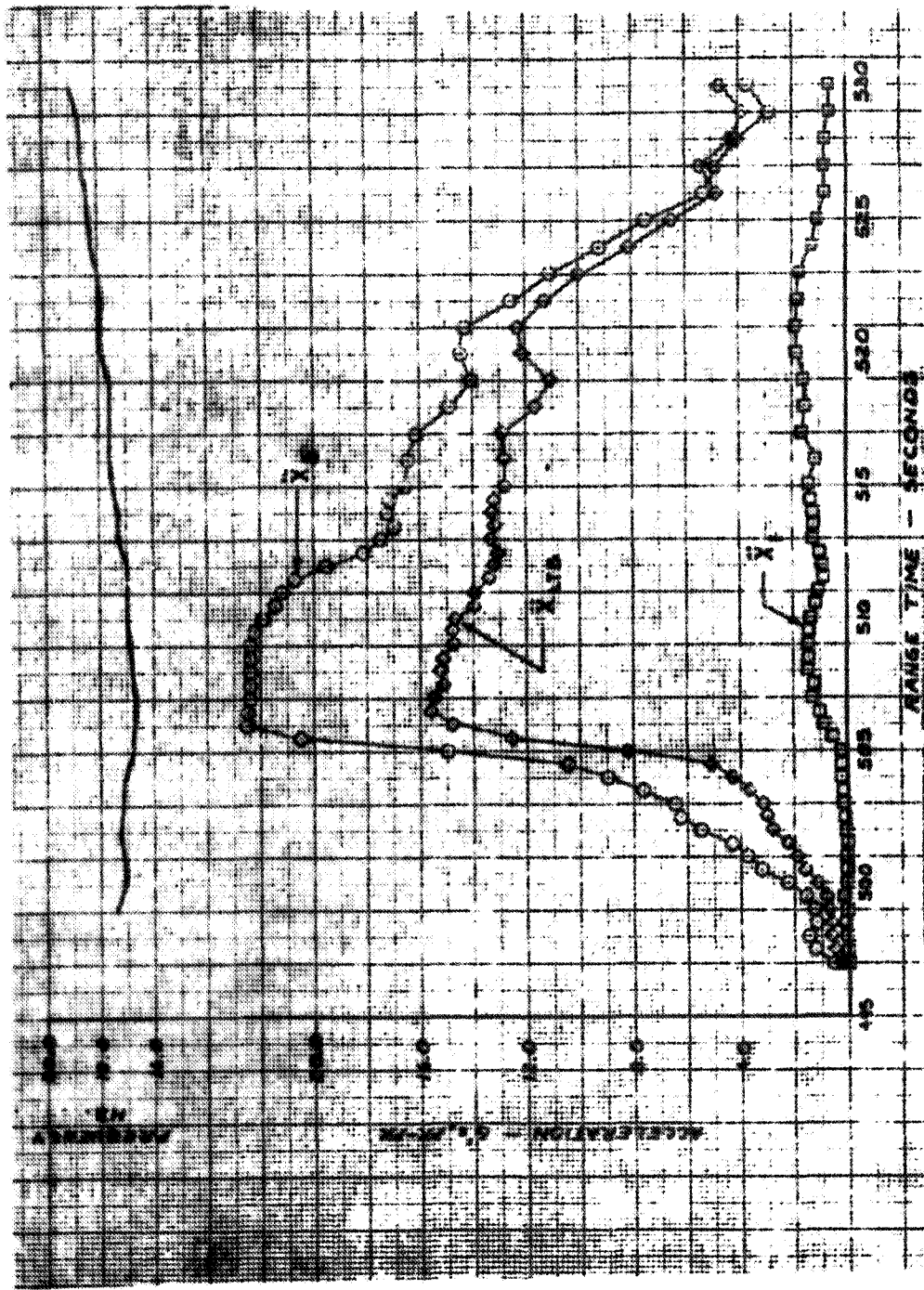
Figure 5. AS-504 S-II Accelerations, Amplitudes of Filtered Data

The phase relationships between acceleration and pressure measurements
as determined from Rocketdyne's tracking filter were probably the primary
data which eventually led to an understanding of the oscillation problem.
On flights 501 and 502 there were fewer accelerometers used and, on flight
503, the particular type accelerometers used provided data at low frequen-
cies and at steady state but had a sharp roll-off at approximately 10 Hz
so that at 17 Hz, amplitudes and phase relationships could not be estab-
lished. (These accelerometers were adequate for studying instabilities
involving the first longitudinal mode of the structure. Until flight
AS-503, no problem involving the higher modes had been anticipated.)
These accelerometers were changed on flight 504 to get good response at
17 Hz but used a circuit that blocked steady-state acceleration. Initial
investigations of the phase relationships revealed that there was an error
in interpretation of the tape data. Further investigation was pursued
to determine the source of the error. It was found that phase corrections
had to be made to account for the following:

1. The accelerometers ($\ddot{x}_1$, $\ddot{x}_5$, $\ddot{x}_{LTB}$) were mounted upside down so
   that positive acceleration was aft. This introduces an 180-
   degree phase error in acceleration-to-pressure.

2. There were charge amplifiers between the accelerometer and the
   data transmission package which introduce an extra 20-degree
   phase lead at 18 Hz in acceleration relative to pressures.

3. There is a phase roll-off characteristic associated with each
   of the FM tape IRIG channels so that in comparing data from
   different channels the proper correction must be made.

The phase relationships between the LOX tank bottom and engine No. 1 accel-
eration and the engine No. 5 chamber pressure relative to the engine No. 5
acceleration are shown in Fig. 6 for the time period of the large oscilla-
tion amplitudes. The LOX tank bottom and engine No. 5 accelerations are
seen to be in phase to within ±10 degrees. The outboard engine is in
phase with the center engine until the time when the amplitudes begin to
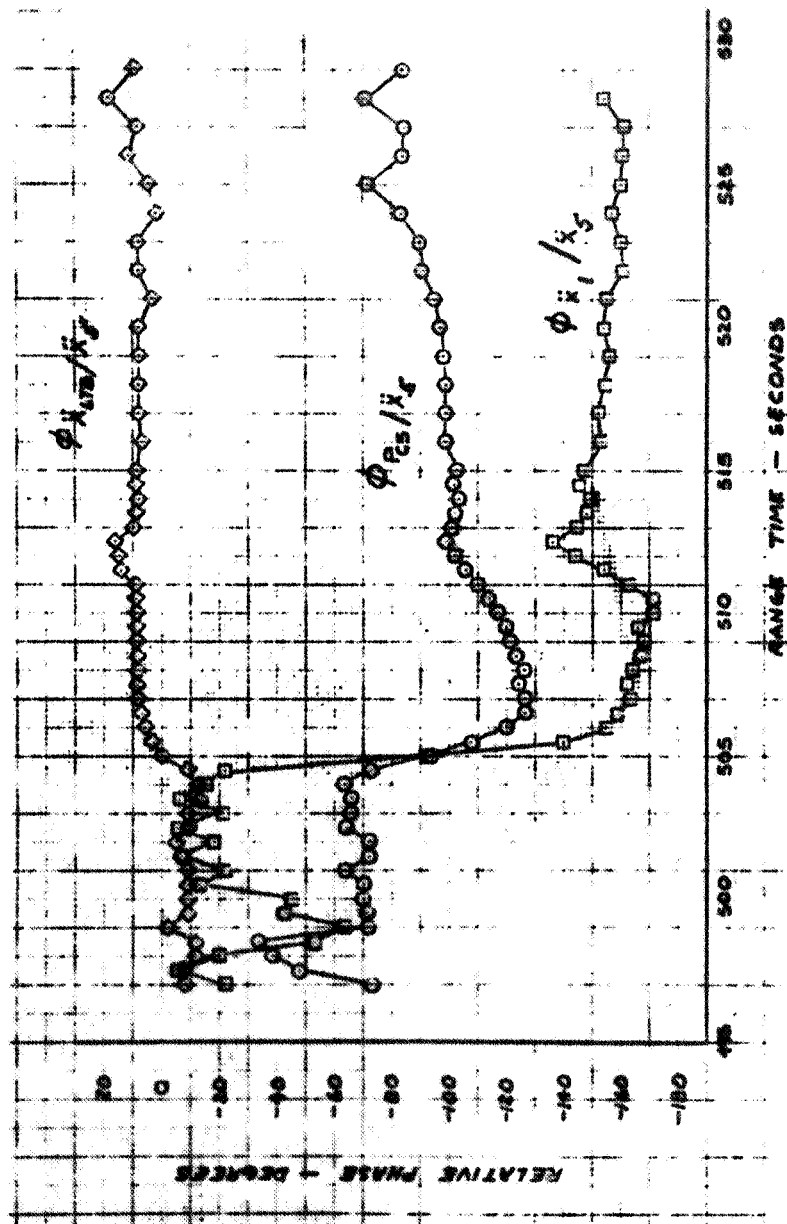
Figure 6. AS-504 S-II Oscillations, Relative Phase Angles From Tracking A-Bars

rapidly diverge, and then the outboard engine becomes approximately 180 degrees out of phase with the center engine. With these two engines out of phase, there must be a node point between the two with zero acceleration. Before the phase shift of engine No. 1 relative to engine No. 5, the node point had to be outside of the outboard engine, thus along the thrust structure. Because the acceleration amplitude of engine No. 1 is always small compared to that of engine No. 5, the nodal point must always lie close to the gimbal point of the outboard engine.

The phase relationship between P_{c5} and $\ddot{x}_5$ determines the amount of work done per cycle by the thrust force. For a sinusoidal force of amplitude, A, acting on a linear structural system with resulting displacement, B, the work done per cycle by the force is

$$W = A.B \sin(-\phi) \tag{1}$$

where ϕ is the phase angle of the force relative to the acceleration. As long as $-180 < \phi < 0$, there is positive work being done, and the maximum work is accomplished when $\phi = -90$ degrees. Figure 6 shows that the force of the center engine is always putting energy into the system (or doing positive work) and that at the time when the rate of divergence of the oscillation amplitudes is greatest (RT = 505 seconds) the center engine force is doing the maximum work because P_{c5} lags $\ddot{x}_5$ by 90 degrees. Having established the phase relationship between force and acceleration, the relative gain or amplitude of the structure can be determined as shown in Fig. 7. This figure presents the nondimensional amplitude of the acceleration and the phase angle for a single degree of freedom forced-vibration system. (It is true that the 17-Hz oscillation problem is a closed-loop stability problem, not a simple forced vibration, but the structural portion of the loop can be looked upon as a forced vibration.) From Fig. 6, the positions A and B on the phase curve can be established at any required time. Then the corresponding points on the amplitude curve can be located. Thus, at the time when the amplitudes are diverging most rapidly, the system is oscillating right at one of the structural resonant frequencies.

DAMPING RATIO = ζ = 1.5 %

AMPLIFICATION RATIO

PHASE, $\left(\phi_{\omega} - \phi_{s}\right)$ - DEGREES

FREQUENCY RATIO, ω/ω_n
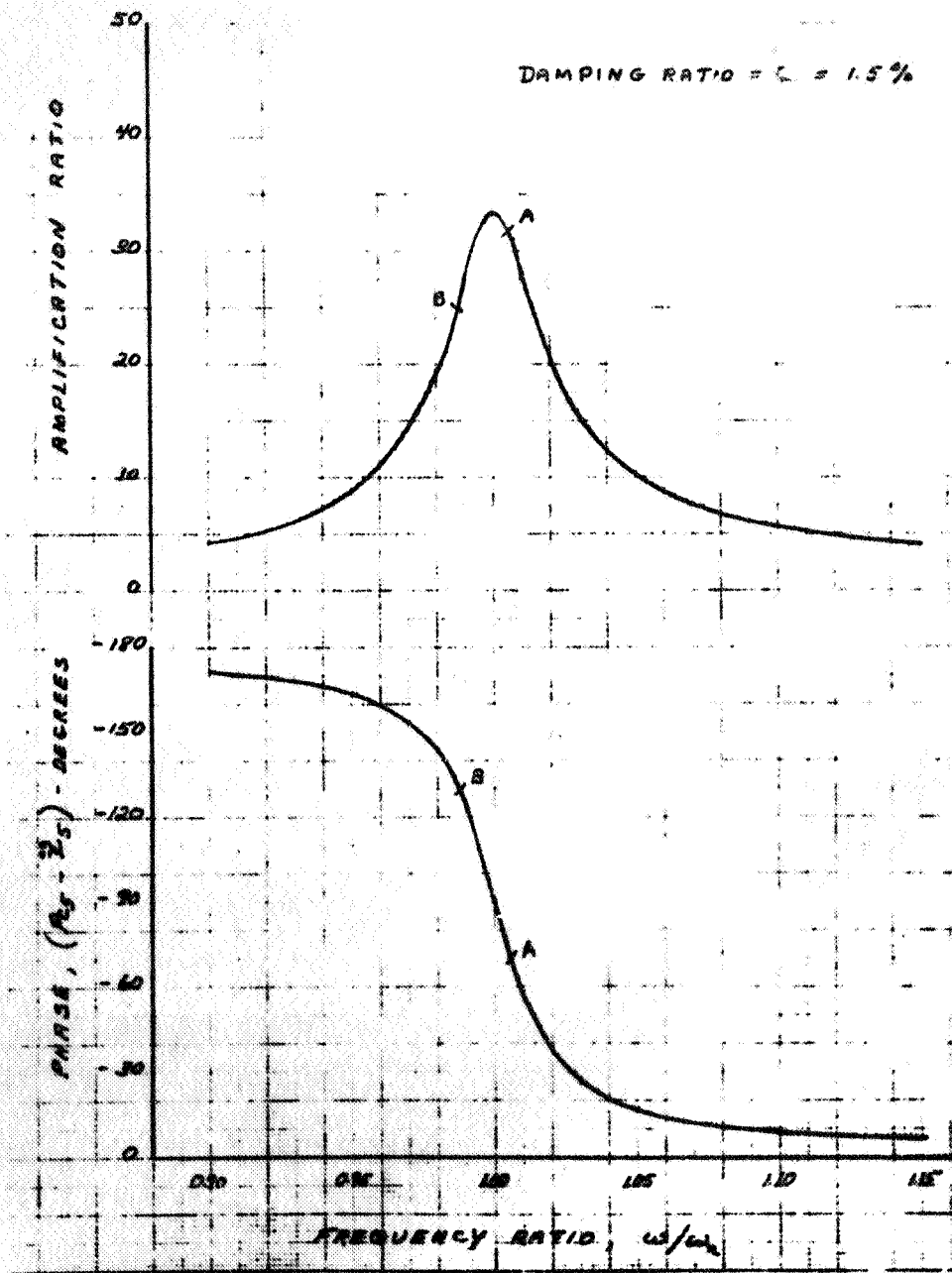
Figure 7. Acceleration Response Curve, Single-Degree-of-Freedom System

The phase relationship between force (P_{c1}) and acceleration ($\ddot{X}_1$) of engine No. 1 is shown in Fig. 8. Inserting this phase angle in Eq. 1 reveals that during a portion of the time the No. 1 engine is taking energy out of the system, or acting as a damper, and at other times it is putting energy into the system. However, at all times the amount of energy being put in or taken out is small because the phase angle is close to 180 degrees and because the amplitude of the force (P_{c1}) and acceleration, thus displacement, are small. Figure 8 presents the phase relationship for only one outboard engine because only one outboard engine acceleration was measured. However, all outboard engine chamber pressures were in phase and at approximately the same amplitude, and it is believed that at this frequency all outboard engines would experience similar in-phase accelerations. Therefore, the data rather conclusively prove that the 17-Hz oscillation problem has the center engine as its energy source, and the outboard engines are not contributing to the problem.

It has been established from the flight data that in the frequency range of interest (i.e., 16 to 19 Hz), the LOX tank bottom is in phase and the outboard engine is first in phase then out of phase with the inboard engine. These relative phases then define the structural mode shape experienced by the vehicle. A comparison of the predicted mode shapes for vehicle AS-504 in the same frequency range over the last 85 seconds of S-II burn time is given below.

Frequency Range, Hz	Predicted Structural Modes			Flight Data 16.7-19.0
	Mode 4 14.8-16.9	Mode 5 17.3-17.7	Mode 6 18.6-21.3	
Relative Phase Between Outboard and Inboard Engines	In phase	In phase	Out of phase	Out of phase last 31 seconds
Relative Phase Between Inboard Engine and LOX Tank Bottom	In phase until last 10 seconds	Out of phase	Out of phase	In phase
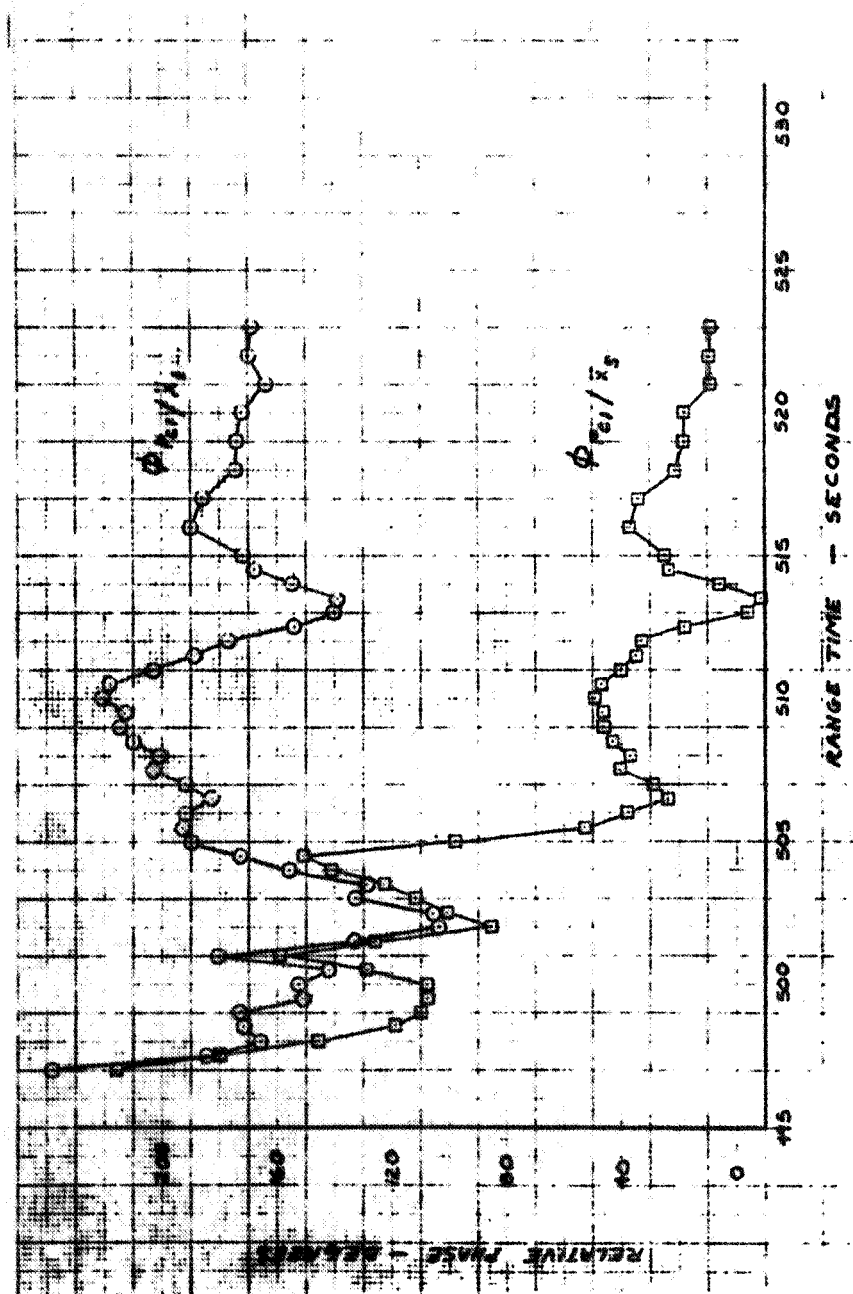
Figure 8. AS-504 S-II Oscillations, Relative Phase Angles From Tracking A-Bars

It is seen that the predicted modes are not in agreement with the modes experienced during flight. This led to an attempt to define structural modes based on the flight data itself for use in performing a closed-loop stability analysis. The first attempt to define the structural mode consisted of examining the frequency and phase relationship between the LOX tank bottom and center engine acceleration. These data were obtained by counting frequencies, where possible, on Brush records and examining the phase on tracking filter records. These early results are shown in Fig. 9 and indicate a tendency for these two parts of the structure to respond at different frequencies so that more than one structural mode was involved. However, at selected times they responded at the same frequency, and whenever they did, the amplitudes of the accelerations were higher and the two were in phase. It was thus felt that the data indicated a primitive mode of the cruciform beam at approximately 17 Hz and a LOX tank bottom mode which began at 15 Hz and swept up through the 17-Hz mode near the end of flight. This change with time of the resonant frequency of the LOX tank mode is consistent with the reduction of LOX in the tank with time. With two structural modes approaching each other, the structural gain is larger (being the sum of the two) so that the instability could be the result of this increased gain in the structural part of the system.

This effort to define structural modes from the data was continued using more sophisticated data transcription techniques. North American Rockwell Space Division obtained PSD's of the more significant variables at time slices scattered throughout the burn time. Bellcomm analyzed the same parameters using voice prints which are particularly useful for tracing the frequencies of various modes with time. Rocketdyne also obtained Sonograms of certain parameters which are similar to the voice prints in appearance and use. From these various representations of the data, a series of structural modes were constructed. Figures 10 and 11 present the frequency of these modes versus time and the SG4 data from which they were primarily obtained. The data points represent significant peaks in the PSD's for $\ddot{x}_5$ (Fig. 10) and $\ddot{x}_{LTB}$ (Fig. 11). Of course, the frequencies
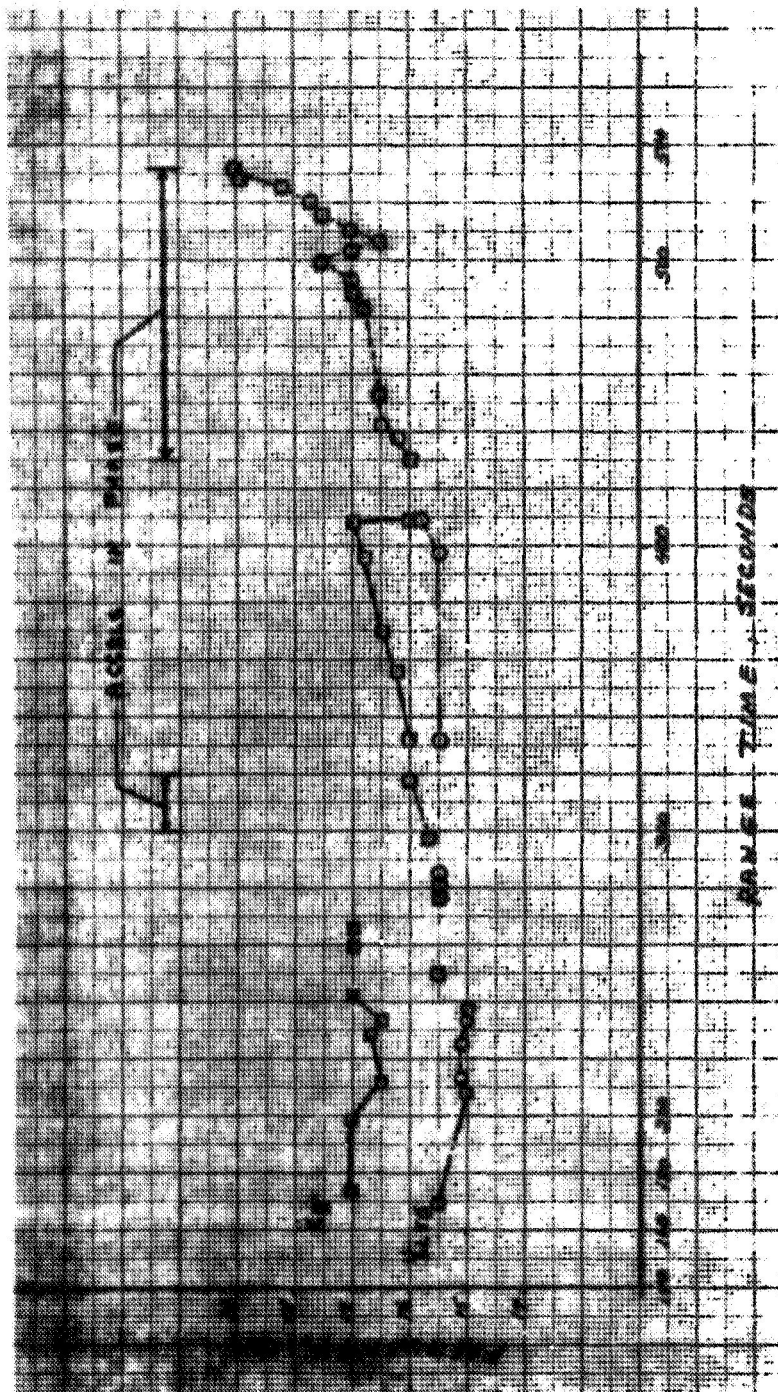
Figure 9. AS-504 S-II Oscillations, Acceleration Frequencies Seen in Flight
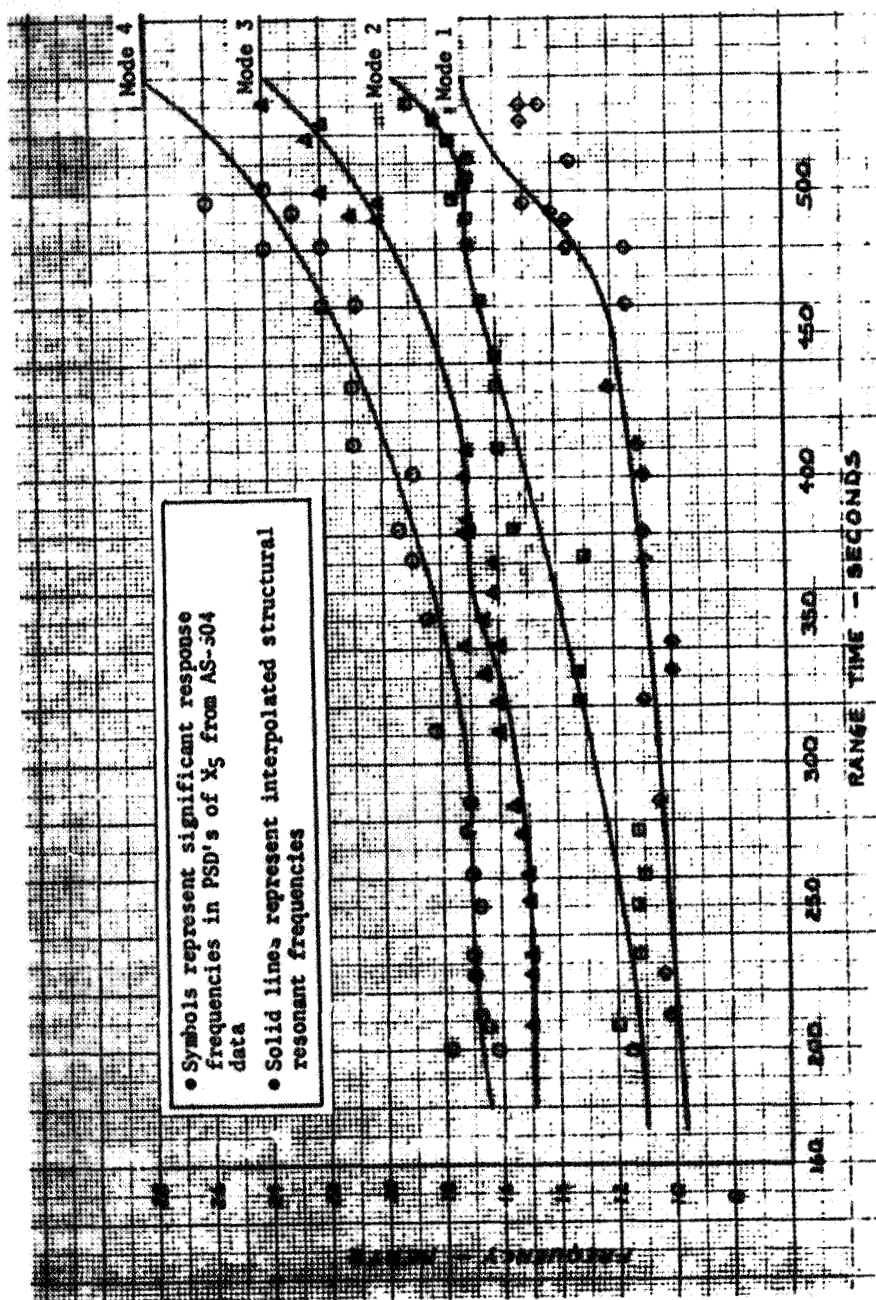
Figure 10. Frequency of Structural Modes Constructed From AS-504 Flight Data
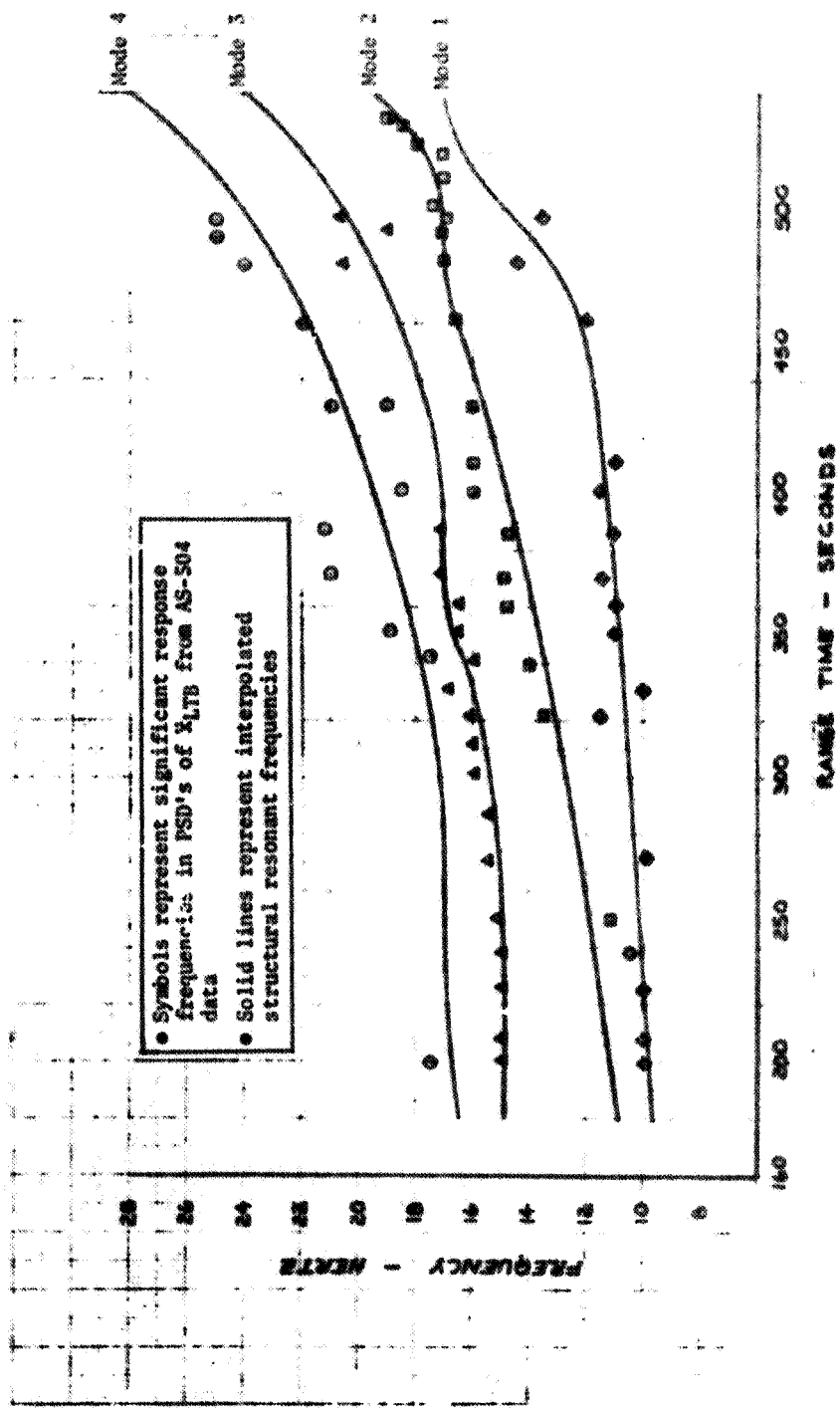
Figure 11. Frequency of Structural Modes (Constructed From AS-504 Flight Data)

of significant amplitude in a PSD are system response frequencies which do not necessarily correspond to structural resonant frequencies. However, in a linear system with light damping in the structure and with engine noise, which tends to be broad band in low-frequency content, as the forcing function, the structural response is going to be close to the structural resonances. With an interconnected spring-mass-dashpot model of the structure, it was shown that for continuous variations of the parameters, the resonant frequencies do not cross but will approach each other as shown in Fig. 10 and 11. However, the primitive mode of the cruciform beam does exert its influence on the structural modes in the 17-Hz region.

Assuming the modes determined from the data are reasonable, the modal gain for each mode was determined. This information was obtained by first reading the amplitudes of $\ddot{X}_5$, P_{c5}, and X_{LTB} from the PSD's at each of the data points shown in Fig. 10 and 11, unless there was no significant response peak at that frequency for that parameter. By assuming that these measured peak amplitudes represent the response due only to these four modes and by assuming reasonable damping, the generalized mass (M_i), or its inverse representing the modal gain $(1/M_i)$, for each of the four modes can be calculated. The gain values $(= \ddot{X}_5/P_{c5})$ determined from the flight data are shown in Fig. 12 along with a simple curve fit of the data. Resulting values for the modal gains, assuming all four modes have 1.5 percent of critical damping, are shown in Fig. 13. These structural modes were later used in Rocketdyne's analog computer model study.

Other Parameters

LOX Discharge Pressure. The LOX pump discharge pressure measurement on the inboard engine (P_{od5}) had similar characteristics as to the envelope of its amplitude and its frequency as the chamber pressure measurement. The unfiltered maximum amplitude of this parameter was 260 psi, p-p.
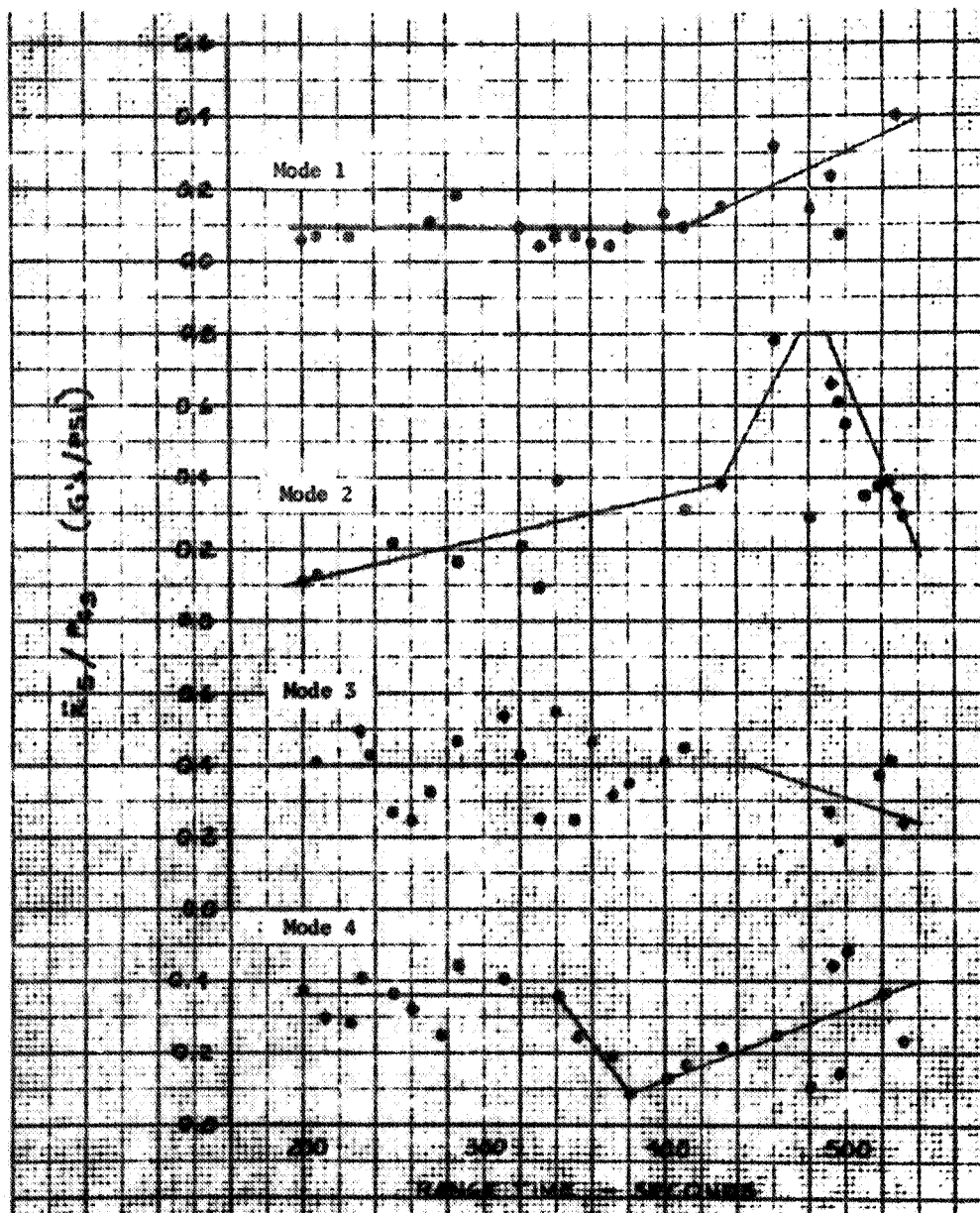
Figure 12. Gains for Four Modes Constructed From Flight Data ($\bar{x}_5$ and P_{c_5} Read From PSD's)
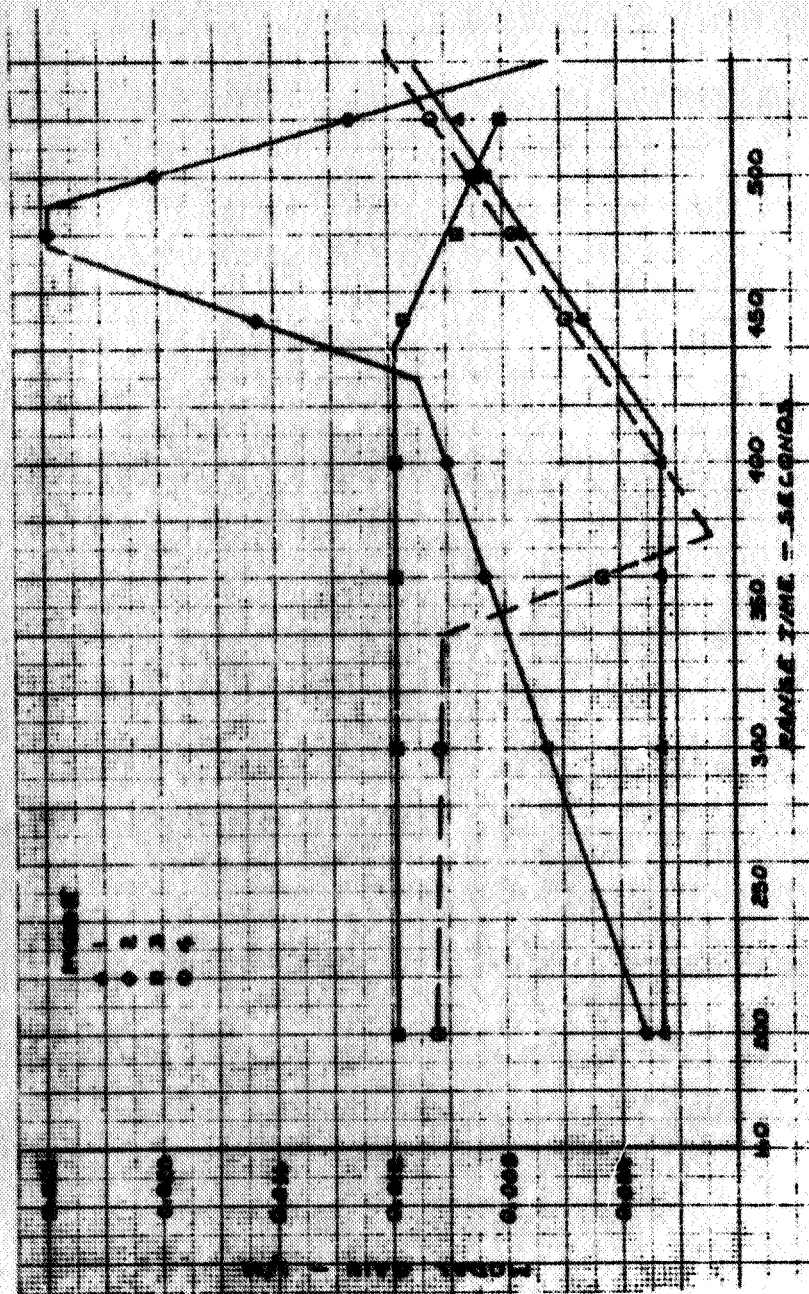
Figure 13. S-II Structure Modal Gain Reconstructed From Flight Data

However, the transducer measuring this parameter is at the end of a 4-foot sense line which has the potential of containing two-phase fluid and a resulting low resonant frequency. This potential was realized in flight, and on flight AS-503, this pump discharge pressure was proved to be too high by a factor of approximately 2.0 at 18 Hz. This was proved by four arguments:

1. The LOX pump discharge pressure trace as a function of time had a significantly different envelope than engine P_c, acceleration, fuel pump inlet pressure, and LOX pump injection pressure. These differences are shown in Fig. 14.

2. Ground tests on a J-2 engine were made using both a close-coupled and a simulated flight instrument line to measure LOX pump discharge pressure. The flight-type instrumentation consistently reads higher than the close-coupled instrument. These results are shown in Fig. 15.

3. Tests were performed using a straight duct flowing LOX with a siren on the inlet side to get oscillatory flow and pressure and a throttle valve on the discharge side to achieve desired steady-state pressures. Both a close-coupled transducer and a transducer on a flight sense line were used to measure the pressure oscillation amplitudes. The resulting resonant frequency of the sense line and its amplification of the true signal could easily be determined. Typical results are presented in Fig. 16. At 18 Hz, the amplification is approximately 2.0.

4. The transfer function expressing the relationship between LOX pump discharge pressure and chamber pressure was established in ground tests of the engine. This transfer function at 18 Hz requires $\Delta P_c/\Delta P_{od} = 0.48$. On AS-503, $\Delta P_c = 55$ psi, p-p, which using the transfer function would yield $\Delta P_{od} = 115$ psi, p-p.
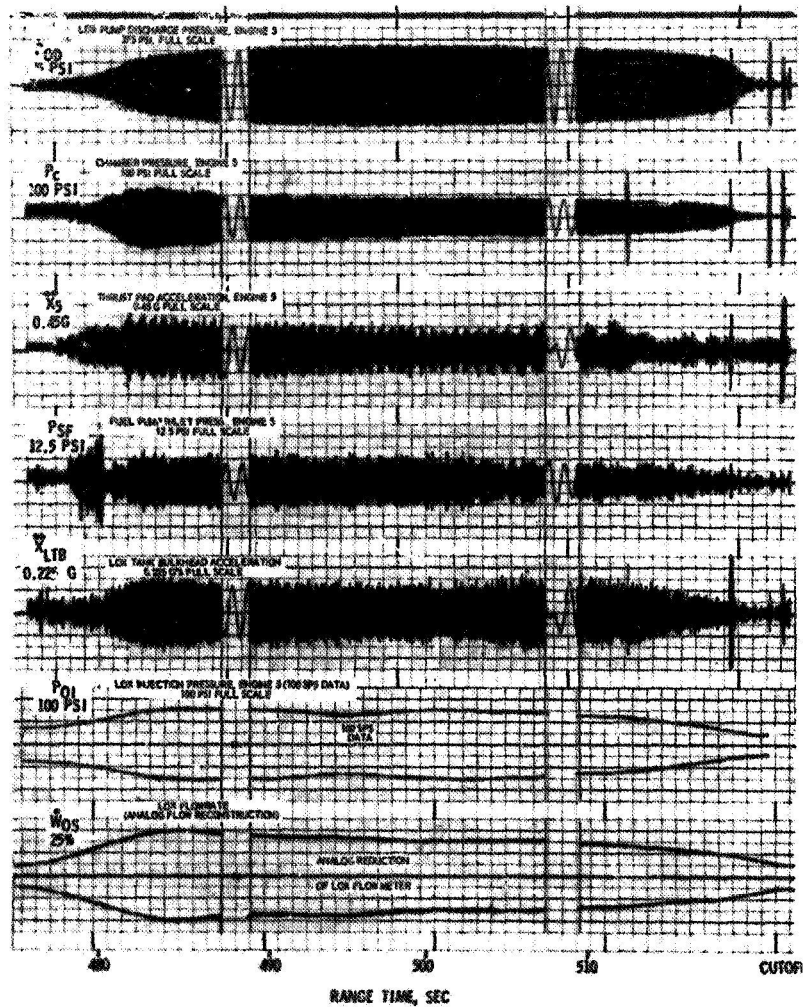
Figure 14. AS-503 18-Hz Oscillations (15- to 20-Hz Band Pass Filtered Data)
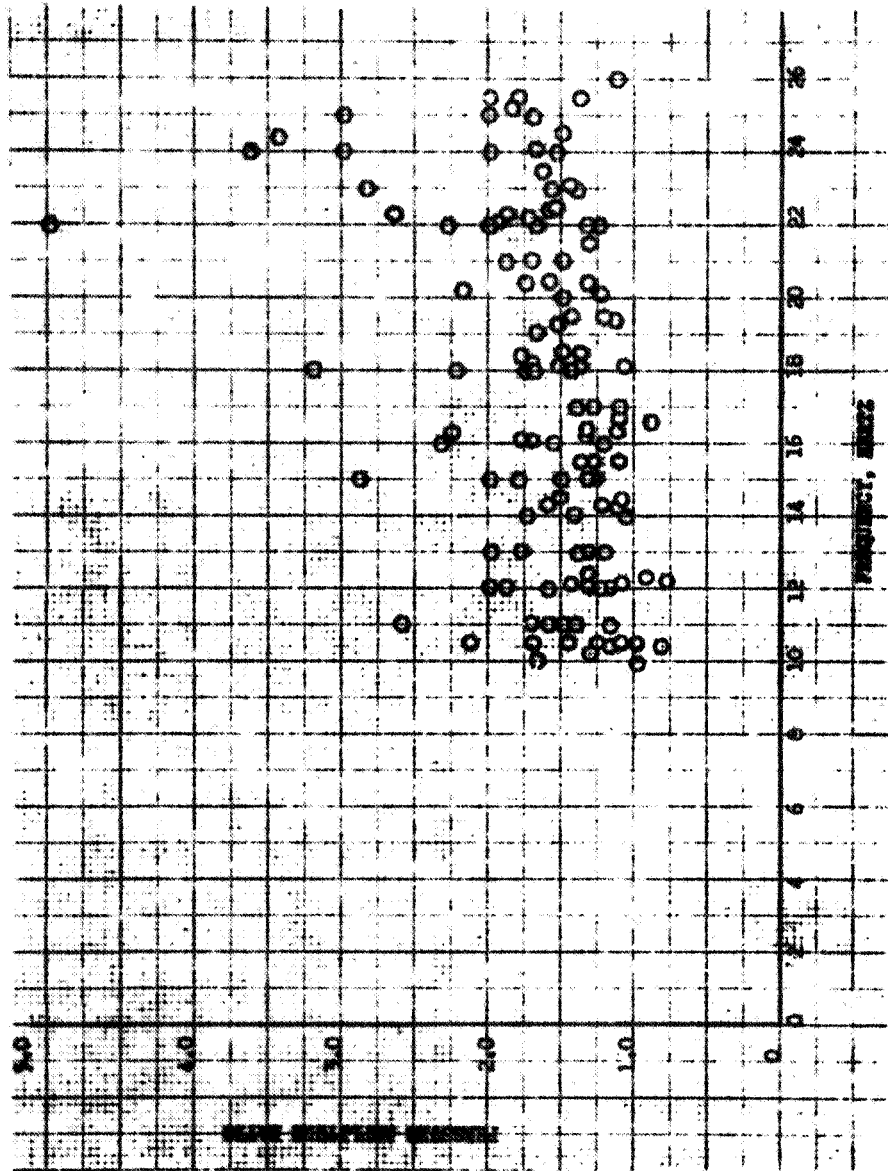
Figure 15. J-2 Engine Tests With Inlet Pulser. LOX Pump Discharge Pressure Ratio
(Ratio = Flight Instrument/Close-Coupled Instrument)
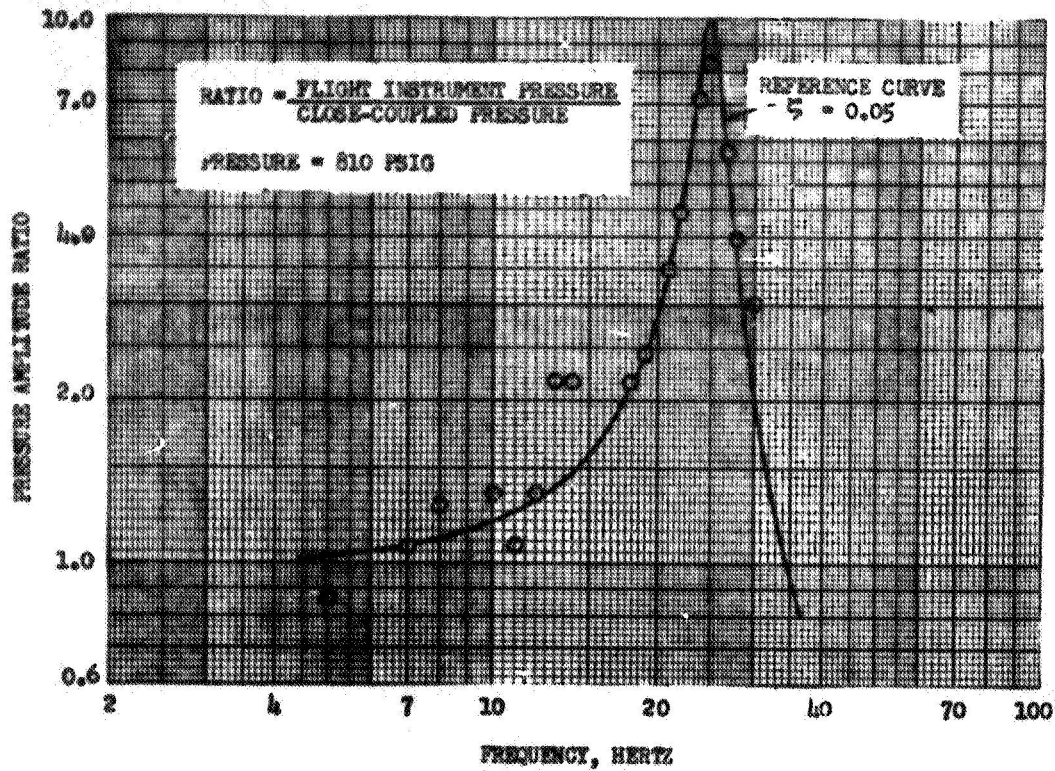
PRESSURE, PSIO	670	690	790	810	840
RESONANT FREQUENCY, HZ	21.5	22.5	23.0	25.0	27.0
PERCENT OF CRITICAL DAMPING = ζ	0.087	0.085	0.087	0.055	0.04

Figure 16.   LOX Pump Discharge Pressure Flight Instrument Resonance
Characteristic (Siren Tests at BRAVO in LOX)

Using the factor of 2.0 correction for P_{od} from flight 504 would give the true value of P_{od} as 130 psi, p-p. Using the transfer function and the unfiltered P_{c5} value of 75 psi yields P_{od} = 75/0.48 = 156 psi, p-p. Thus, in conclusion, the actual value of P_{od} is assumed to be within these bounds:

$$130 \leq P_{od5} \text{ (maximum)} \leq 156$$

LOX Inlet Pressure. The LOX pump inlet pressure was measured on flight 504 for the inboard engine. However, this measurement also had a relatively long sense line of 18 inches. For the lower inlet steady-state pressures an even shorter sense line is required to prevent the sense line from acting in the two-phase regime. The inlet pressure measurement was recorded as 120 sample-per-second data rather than as continuous (FM/FM) data. The inlet pressure tap location relative to the inducer inlet is also significant because the tap is only 3 inches upstream of the pump inlet flange. The significance of this location will be indicated below.

The chamber pressure on engine No. 5 was seen to slowly diverge from RT 497 to approximately RT 504 and then rapidly diverged, peaking out because of a limit cycle at about RT 506. During the initial period when the amplitudes were slowly diverging, the LOX pump inlet pressure was also slowly building up, was oscillating at the same frequency, but was tracking at approximately one-half of the amplitude of P_c. At RT 504 when P_c rapidly diverged, the inlet pressure showed a sudden decrease in both steady-state and oscillating components. A similar decrease in steady-state value was observed in AS-503 flight data, but that data sampling rate was too low to indicate the 18-Hz oscillation amplitudes. This shift in the steady-state inlet pressure is believed to be a characteristic of the tap location more than anything else. As the inlet pressure oscillations increase, the conditions at the pump inlet become more conducive to cavitation at the pump inlet and severe backflow at the pump periphery with an associated strong vortex action. Ground tests

have indicated that a pressure measurement in such an environment quite
frequently shows similar shifts in the steady-state value. For example,
in Fig. 17, data from ground tests reveal a shift in the inlet pressure
measurement 8 inches upstream of the pump inlet and no shift in the meas-
urement 32 inches upstream of the pump.

The decrease in the oscillation amplitude is probably primarily related
to cavitation at the tap location and to two-phase fluid in the sense
line. Even in the low-oscillation amplitude region, the amplitude of
the oscillations are too low, the sense line in this case tending to
attenuate the signal level rather than amplify it as on the pump discharge
pressure. (The signal will be attenuated or amplified depending on
whether the sense line resonant frequency is sufficiently below or above,
respectively, the signal frequency.) The proof that the signal is too
low is founded on three arguments:

1. Ground tests of the engine using close-coupled and simulated
    flight sense line measurements reveal that the flight measure-
    ment is too low at 18 Hz, the amount of attenuation increasing
    as oscillation amplitude level increases. This trend is shown
    in Fig. 18 for Rocketdyne engine tests. Actually, the sense
    line on the inlet pressure used by Rocketdyne was 24 inches long
    rather than 18 inches as in flight. MSFC used an 18-inch line
    in ground tests and got the same trend as shown in Fig. 18,
    except the response ratio was a little lower. Thus, the sense
    line can very easily attenuate the signal by a factor of 2.0
    at low-amplitude oscillations and by a factor as high as 5.0
    to 7.0 at high-oscillation amplitudes.

2. The transfer function, $\Delta P_c/\Delta P_{os}$, established from ground tests
    has a gain of approximately 1.0 at 18 Hz for operating conditions
    similar to those in flight. Thus, if flight data give ratios
    of approximately 0.5, they appear too low by a factor of 2.0.
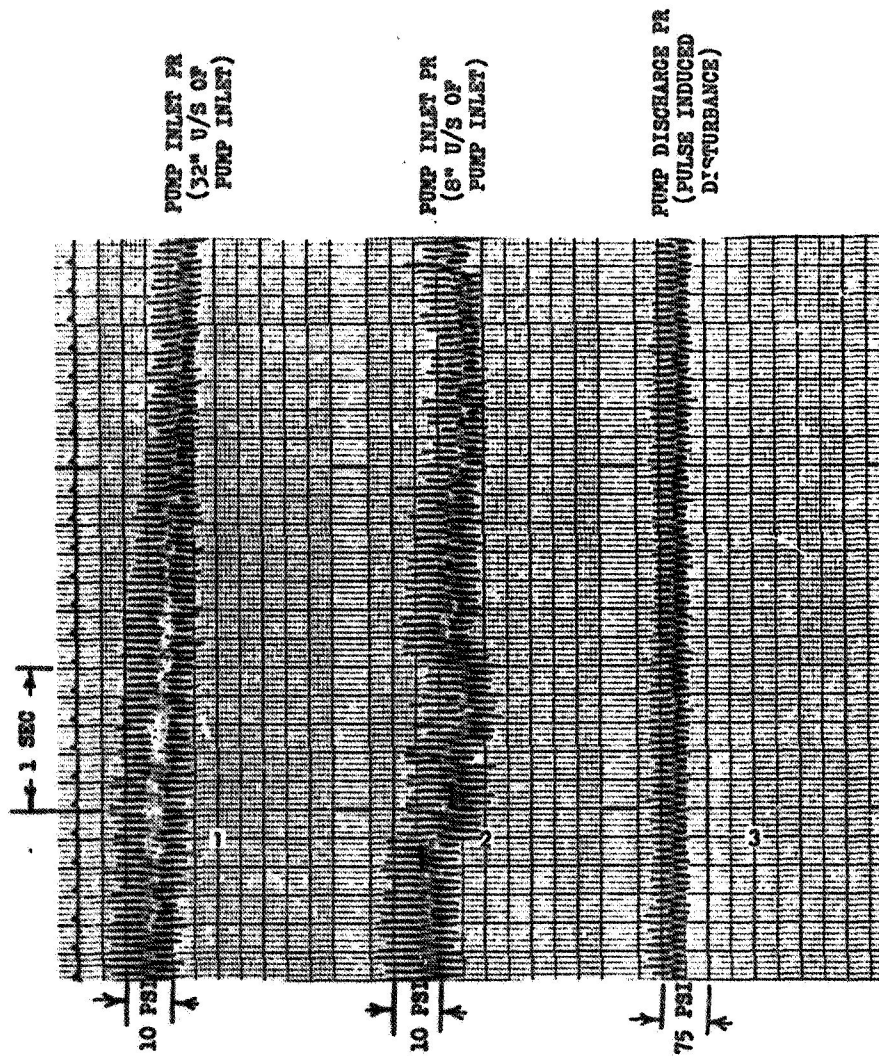
Figure 17. J-2 LOX Pump Inlet Pressure Characteristics
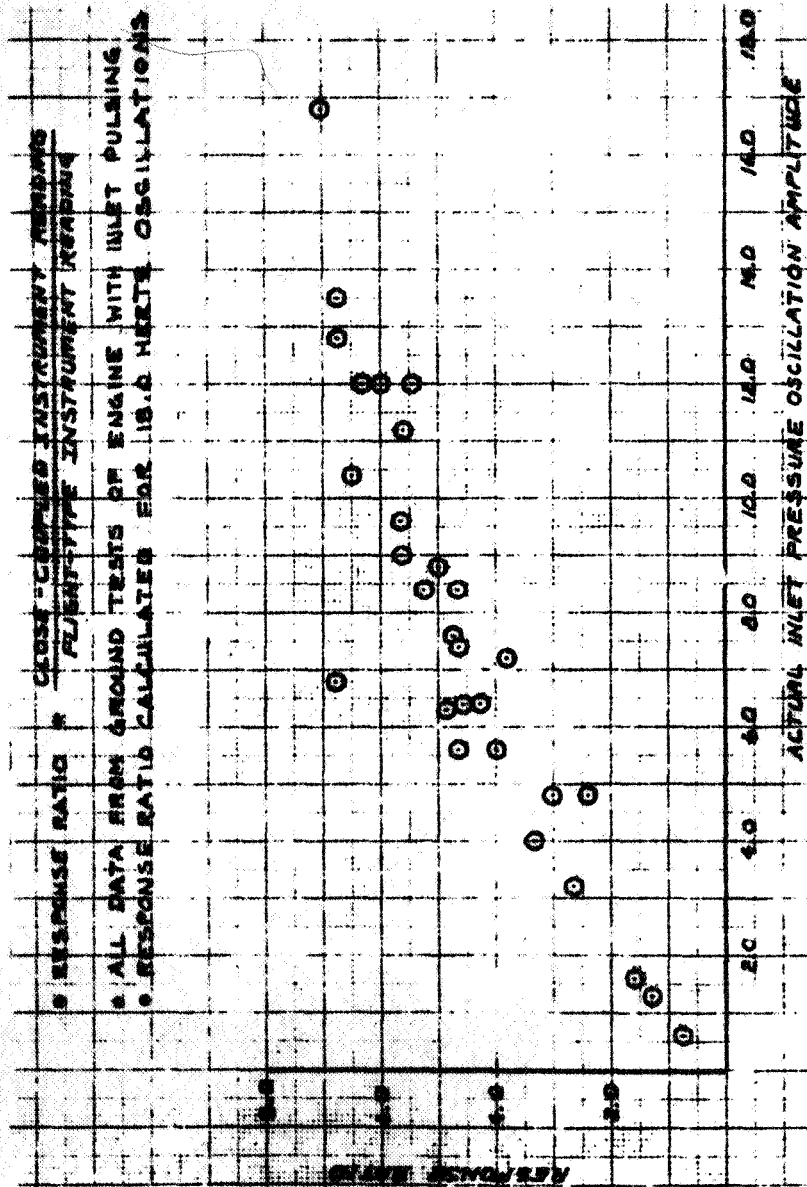
Figure 18. Instrumentation Comparison, LOX Inlet Pressure

3. The acceleration levels of the structure (i.e., the cruciform
    beam at the center engine and the LOX tank bottom) are suffici-
    ently high that even ignoring for present purposes the dynamics
    of the inlet line, the inlet pressure oscillations should be a
    factor of 2.0 or more higher. For example, near 500 seconds RT,
    the liquid level in the LOX tank is approximately 8 feet above
    the pump inlet. With a column of fluid of weight 70 lb/cu ft
    and 8 feet high vibrating at a given g level, the pressure
    oscillation at the bottom of the column is given by

$$\Delta P = \frac{8 \cdot 70 \cdot}{144} \; g \quad \text{psi, p-p} \tag{2}$$

At 500 RT, from Fig. 5, $\ddot{x}_S = 2.2$ g, $\ddot{x}_{LTB} = 1.1$ g giving an average of
1.65 g. Substituting this value into Eq. 2 gives

$$\Delta P = 6.41 \; \text{psi, p-p}$$

but the measured value is 3.1 psi, p-p. If similar calculations are made
at 504 RT, the calculated ΔP is 25.6 psi, p-p, but the measured value is
8.9 psi, p-p. Thus, at the lower amplitude oscillations, the inlet pres-
sure appears to be too low by a factor of approximately 2.0. As the
actual amplitudes rapidly diverge, the flight instrument attenuates the
18-Hz oscillation component by a large factor (5 to 7), and the instru-
ment also indicates a shift in the steady-state pressure which shift is
related to the tap location.

Other Parameters. Data were reviewed from several other parameters, but
none of these others significantly influenced the study of the problem.
Several parameters that were observed are mentioned here for completeness
relative to the 17-Hz oscillation performance of each. Dome accelerom-
eters for each engine were obtained from the single side-band data. The
engine No. 1 dome accelerometer channel was overdriven invalidating the
data. The engine No. 3 and No.4 dome accelerometers indicated no sig-
nificant 17-Hz oscillations above the noise level. The engine No. 5

dome accelerometer had a similar response to the engine No. 5 accelerometer on the cruciform beam. The dome accelerometer was noisier throughout most of the burn time (probably because of its wider bandwidth and less sensitive scale) but had lower oscillation amplitudes in the range time of the instability. Amplitudes determined from 15 to 20 Hz band-pass filtered data are compared below.

Range Time, seconds	500	502	504	505	506	508	510	512
E-5 Dome Accelerometer*	1.34	3.6	6.7	10.3	16.6	17.5	16.6	15.3
E-5 Beam Accelerometer*	2.23	5.43	8.99	15.01	22.5	22.4	21.9	19.51

*Amplitude in g, p-p

The engine No. 2 dome accelerometer did not appear to have an overdriven tape, but its amplitude was much too large, being as high or higher than the engine No. 5 dome accelerometer. This amplitude and wave shape is believed to be erroneous and appears very similar to data in which the coaxial cable from the accelerometer was slapping against hardware. Physical distortion of the cable can directly affect the charge amplifier output.

Two other accelerometers that were observed but indicated no significant change in response in the region of the instability were the body modal lateral forward skirt accelerometer and the body modal radial aft skirt accelerometer. There were some velocity measurements which definitely contained strong 17-Hz data in the region of the instability. These velocity measurements were designated as pitch angular velocity, yaw angular velocity, and roll angular velocity.

Several other pressure measurements were examined. Gas generator chamber pressures were available on all five engines. The outboard gas generator P_c's indicated no significant 17-Hz oscillations above the noise level, but the inboard engine measurement had a response similar to the main P_c

with a maximum amplitude of 40 psi, p-p. On engine No. 1, the LOX pump
discharge pressure and injection pressure had some stronger response at
17 Hz in the region of the instability, but their response was not nearly
so pronounced as observed on engine No. 5 parameters. The maximum ampli-
tude for this discharge pressure was only about 5 psi, p-p, and for the
injection pressure was 9 psi, p-p. The fuel inlet pressure on engine
No. 5 had a response envelope with a similar shape to the main P_c and a
maximum amplitude of approximately 5.5 to 6.0 psi, p-p. Using the
unfiltered amplitude of main P_c = 75 psi, p-p and the engine transfer
function, $\Delta P_c/\Delta P_{fs}$, evaluated at 17 Hz, the predicted value of ΔP_{fs}
would be 6.4 psi,p-p, which is in good agreement with the data. (The
transfer functions are presented in a later section.)

Performance Shift of Engine

During the time of the instability, a performance shift was experienced
on engine No. 5 on both flight AS-503 and -504. The shift has been ex-
plained as caused by a performance loss in the LOX pump. By varying the
LOX pump efficiency and the head-flow characteristic, the computed shifts
in engine performance were matched successfully to the observed shifts for
the two flights. The parameter changes required to match the data are
given below.

Parameter	Percentage Change	
	AS-503	AS-504
LOX Pump Efficiency	4.0	1.7
LOX Pump Head-Flow Relationship	4.2	1.2

Table 1 shows the observed and computed parameter changes for AS-504.
A typical parameter LOX pump speed, is shown in Fig. 19 indicating the
performance shift and the fitted values.

One rather significant implication from these results is that the type of
performance shift observed is typical of the shift that occurs when the
LOX pump cavitates. Because of the large oscillation amplitudes on the

TABLE 1

ENGINE J2066 (POSITION 5 ON S-II STAGE OF AS-504)

INDEPENDENT

LOX PUMP PSI (%CHG/100)	-3.012
LOX PUMP EFF (%CHG/100)	-0.017

TIME= 505.00

DEPENDENT		OBSERVED	COMPUTED
ENG LOX FLOW	(LB/SEC)	-12.300	-7.467
ENG FUEL FLOW	(LB/SEC)	-0.210	-0.390
ENGINE THRUST	(LBS)	0.C	-3082.682
GG CHAMB P	(PSIA)	-8.400	-8.527
ENGINE MIXTURE RATIO		-0.150	-0.064
THRUST CHAMB P	(PSIA)	-13.000	-9.705
FUEL TURB IN TEMP	(DEGR)	0.0	-13.373
FUEL PUMP DISCH P	(PSIA)	-17.400	-14.381
FUEL PUMP DISCH T	(DEGR)	-0.170	-0.150
LOX PUMP DISCH P	(PSIA)	-11.400	-20.374
FUEL TURB SPEED	(RPM)	-144.000	-144.000*
LOX TURB SPEED	(RPM)	-51.4CC	-51.400*
ENGINE ISP	(SEC)	0.0	0.475
LOX TURB INLET P	(PSIA)	-0.916	-1.097
LOX TURB DISCH P	(PSIA)	-0.337	-0.405
LOX TURB INLET T	(DEGR)	-0.CO	-9.676
LOX TURB DISCH T	(DEGR)	0.0	-8.308
TC FUEL INJECT P	(PSIA)	-13.5C0	-10.652
TC LOX INJECT P	(PSIA)	-18.300	-15.927
GG FUEL INJECT P	(PSIA)	-11.200	-11.176
GG LOX INJECT P	(PSIA)	-23.300	-10.490

* COMPUTED COLUMN IS BASED ON THE INDEPENDENT VARIABLE CHANGES
NECESSARY TO MATCH THE OBSERVED CHANGES IN THESE PARAMETERS
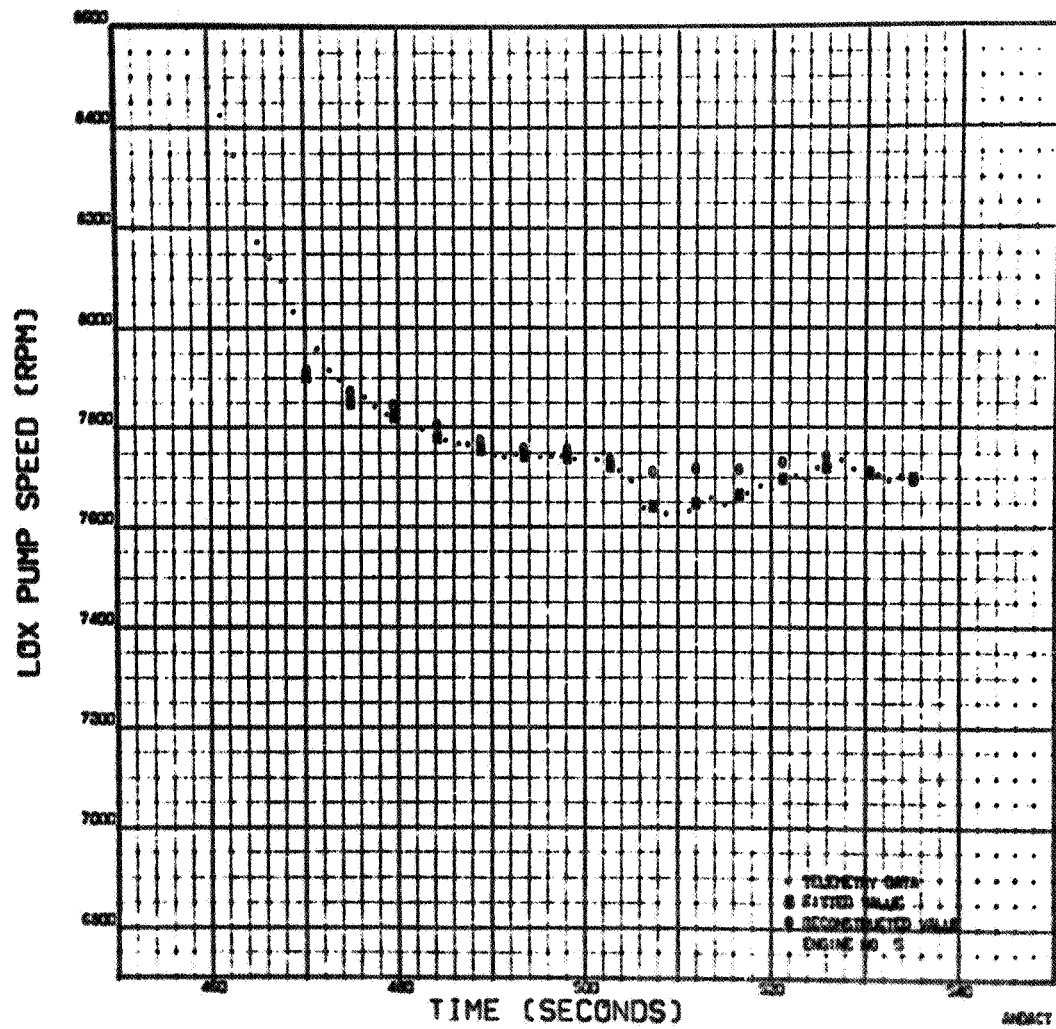
Figure 19. AS-504 S-II LOX Pump Speed

LOX side, cavitation would certainly be expected, and the performance shift appears to confirm the expectation. This pump cavitation would place a lower limit on the amplitude of LOX pump inlet pressure which could be a major factor producing the limit cycle performance of the oscillations. However, this will be discussed more fully in a later section.

FLIGHT DATA, AS-501, -502, AND -503

AS-501

The parameters showing significant 18-Hz oscillations on AS-501 were the five engine chamber pressures. These pressures are shown in Fig. 20 after band-pass filtering to clearly distinguish the data at 18 Hz.

In these data, a general noise level of about 3 psi, p-p, exists. However, at about 300 seconds RT, all five engines show an increase in amplitude to about 5 psi, p-p, and lasting for approximately 40 seconds. At 390 seconds RT, a similar increase in amplitude occurs and reaches a maximum amplitude of about 9 psi, p-p. The duration of this latter burst is approximately 50 seconds except for engine No. 5. Engine No. 5 maintains a 9- to 10-psi amplitude from 400 seconds to 480 seconds at which time its amplitude suddenly increases to about 22 psi, p-p. (The corresponding unfiltered amplitude is 42 psi, p-p.) This amplitude is maintained for only 1 second after which time it suddenly decreases to about 8 psi, p-p, and then disappears into the noise level by 500 seconds RT. The sudden increase in amplitude starting at 480 seconds is the typical 18-Hz closed-loop instability problem that was so evident on vehicle AS-503 and AS-504. It is of interest to note that the increase in oscillation amplitude that occurred earlier on all five engines had disappeared from all outboard engines at least 30 seconds prior to the 18-Hz closed-loop instability. Thus, it appears that the increases in amplitude that occur in the earlier time periods are a different phenomena than that which occurs primarily on engine No. 5 at the later time.
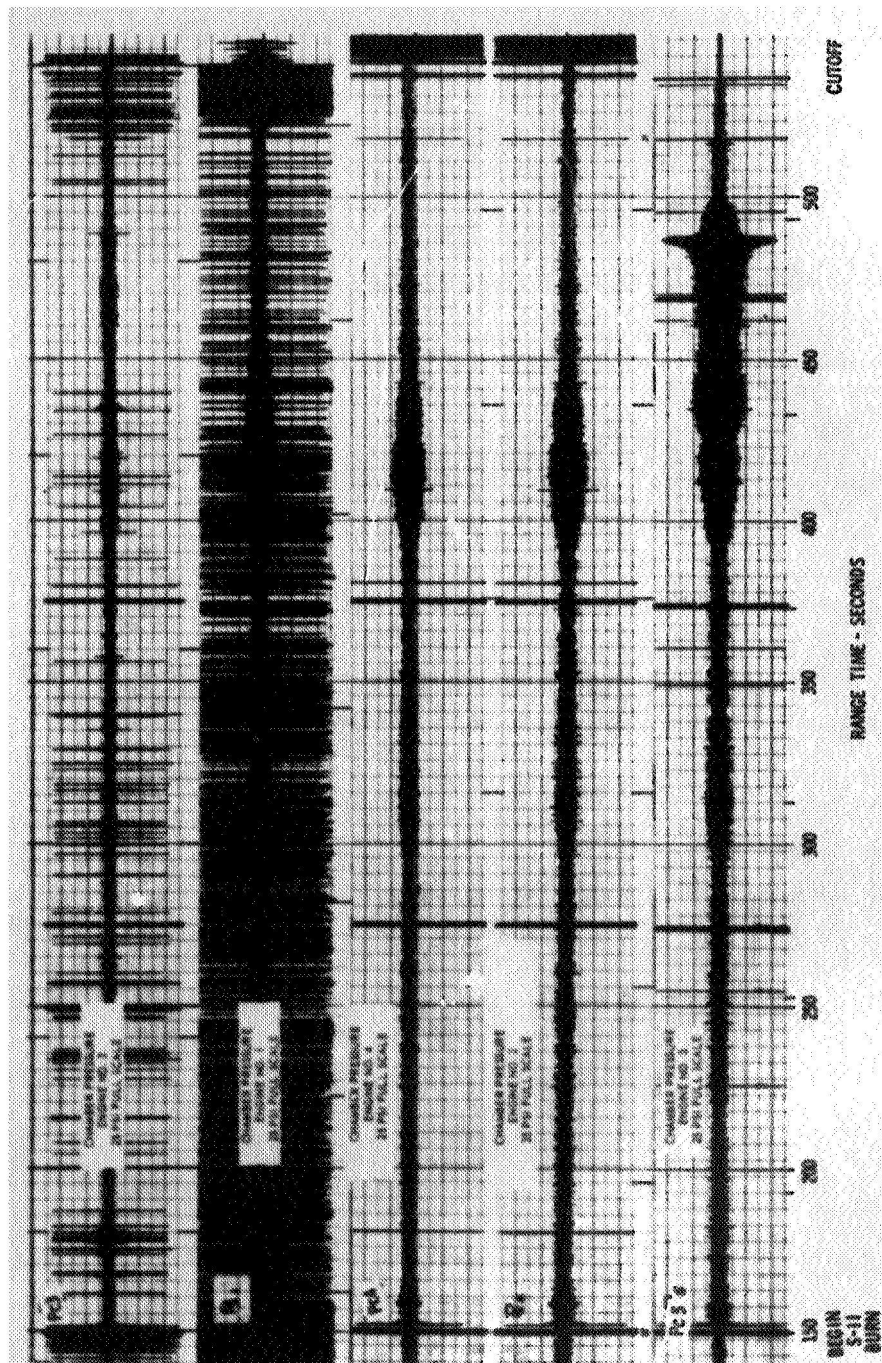
Figure 20. AS-501 S-II 18-Hz Oscillations (15- to 20-Hz Band Pass Filtered Data)

The predominant frequency in the oscillation of engine No. 5 at 400 seconds RT was 16 Hz. This frequency gradually increased to 17 Hz at 440 seconds and then to 18 Hz at 470 seconds. Eighteen Hz was also the predominant frequency during the high-amplitude burst of the closed-loop instability.

AS-502

Only the five engine chamber pressure measurements were considered significant in the flight data of AS-502. The amplitudes of these five measurements vs range time are shown after filtering with a 15- to 20-Hz band-pass filter in Fig. 21. All P_c measurements exhibit a 3-psi noise level throughout the flight. The first increase in amplitude above this noise level occurs at 300 seconds RT when the amplitude reaches 6 psi for a period of about 50 seconds. A second increase in amplitude starts at 400 seconds RT and lasts for 100 seconds in engines 1, 4, and 5 only. Engines 2 and 3 had already shut down and therefore would not be expected to exhibit P_c oscillations. At 500 seconds RT, engine No. 5 chamber pressure suddenly increased to 13 psi, p-p (24 psi, p-p, unfiltered). This high-amplitude burst has been identified as the 18-Hz closed-loop instability.

The predominant frequency throughout the high-amplitude burst was 18 Hz. It has been reported that a second burst had been observed later in flight having a frequency of 20 Hz and reaching an amplitude of 40 psi, p-p, unfiltered. The Rocketdyne data reduction was done from the KSC tape which after 550 seconds was not clear because of a high-amplitude noise level. It is interesting to note that the envelope of the oscillations at the point of the 18-Hz instability is different on 502. The amplitudes on 502 do not appear to be diverging exponentially like they do on the other flights.

AS-503

A comparison of the P_c measurements of all five engines of the S-II stage of AS-503 is shown in Fig. 22. It is seen that AS-503 has many characteristics that are similar to the flights of AS-501 and AS-502. At 265 seconds RT, the amplitude of the P_c measurements increased from the noise
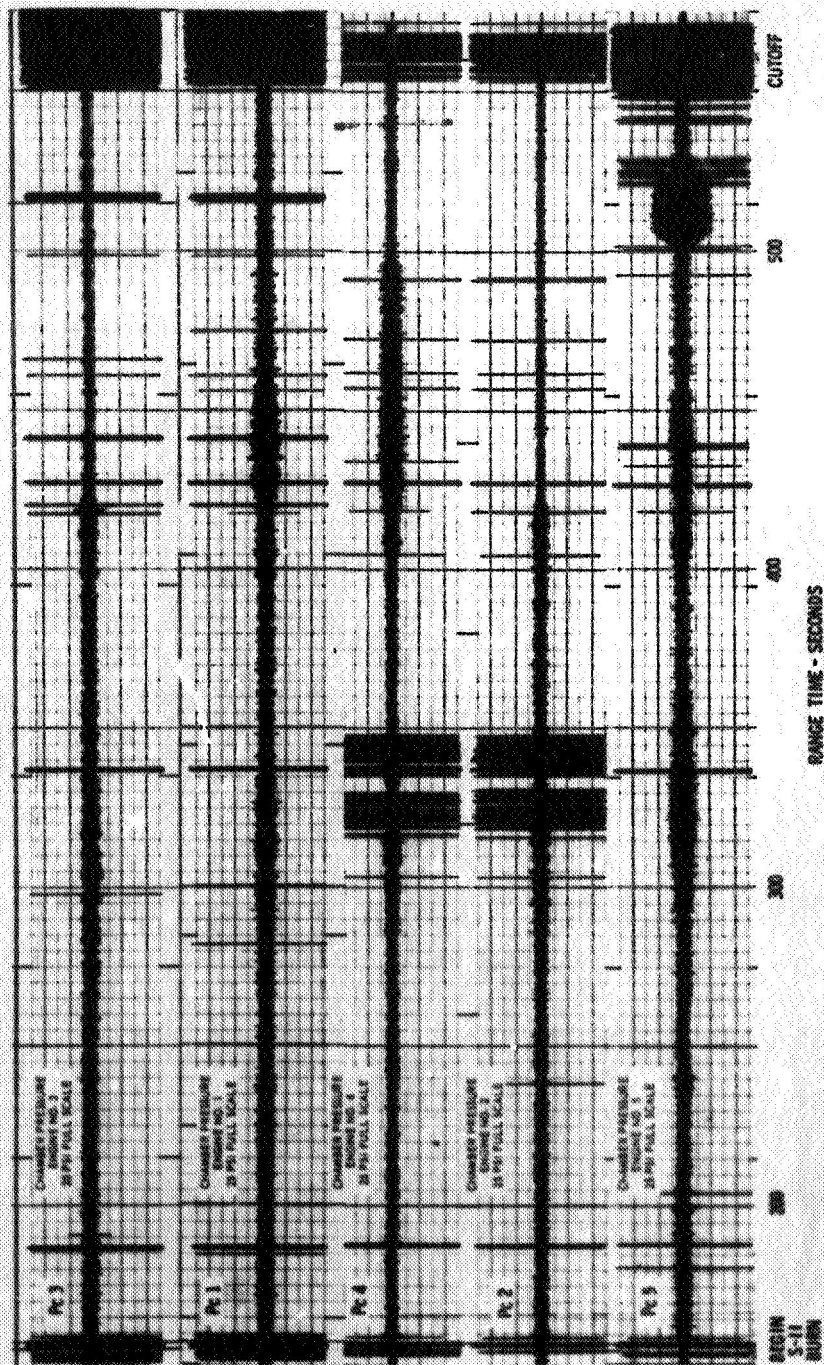
Figure 21. AS-502 S-II 18-Hz Oscillations (15- to 20-Hz Band Pass Filtered Data)
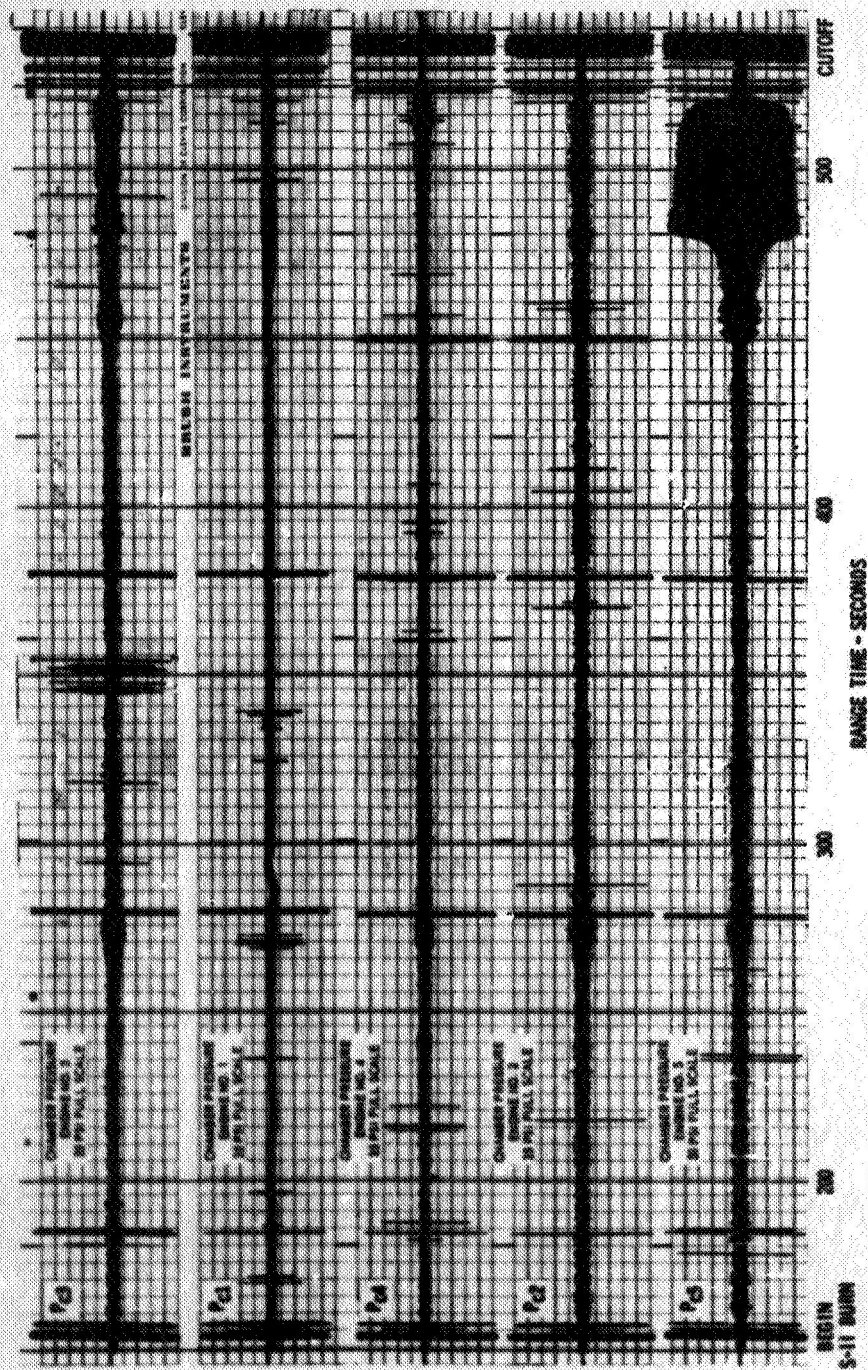
Figure 22. AS-503 S-II 18-Hz Oscillations (15- to 20-Hz Band Pass Filtered Data)

RANGE TIME - SECONDS

CUTOFF

BEGIN
S-II BURN

R-7970

level to about 8 psi, p-p, on the inboard engine and 4 psi, p-p, on the outboard engines. This initial increase in P_c lasts for approximately 65 seconds. The second increase in P_c amplitude started at about 450 seconds RT and reached an amplitude of 15 psi, p-p, (filtered) on the center engine and 6 psi, p-p, on engine No. 3 with lesser increases on the other outboard engines. Thus, the center engine shows a different behavior than the four outboard engines.

Figure 23 shows a plot of frequency and filtered P_c amplitude as a function of range time. At 470 seconds RT, a gradual increase in amplitude occurs in engine No. 5 P_c. At 480 seconds, a more rapid divergence of amplitude occurs, and a maximum pressure of 50 psi, p-p, (65 psi, p-p, unfiltered) is reached. After reaching the maximum amplitude, the oscillations decrease to about 30 psi, p-p, until at 520 seconds there is a sudden decrease, and the amplitude disappears into the noise level at 522 seconds. At 450 seconds RT, concurrent with the second increase in P_c amplitude, a predominant 17.5-Hz frequency is apparent in the unfiltered oscillograph. The predominant frequency gradually increases to 18.1 Hz, then drops rather suddenly to 17.3 Hz during the period of rapidly diverging amplitudes. As the limit cycle is reached at 484 seconds RT, the predominant frequency again gradually increases until it reaches 19.6 Hz at 521 seconds. At this time, the predominant signal disappears into the general noise level. During this latter time period, the maximum amplitudes in P_c on the outboard engines at 18 Hz are 6 to 8 psi, p-p, unfiltered, appearing primarily in engines No. 1 and No. 3.

The LOX pump discharge pressure on engine No. 5 had large oscillations in the 18-Hz region, reaching amplitudes of 300 psi, p-p. However, as was mentioned previously, the sense line for this measurement contains a two-phase fluid which gives a low line resonance amplifying the signal by a factor of approximately 2.0 at 18 Hz. The actual maximum unfiltered amplitude is assumed to be in the range

$$130 \leq P_{od5} \text{ (maximum)} \leq 150$$
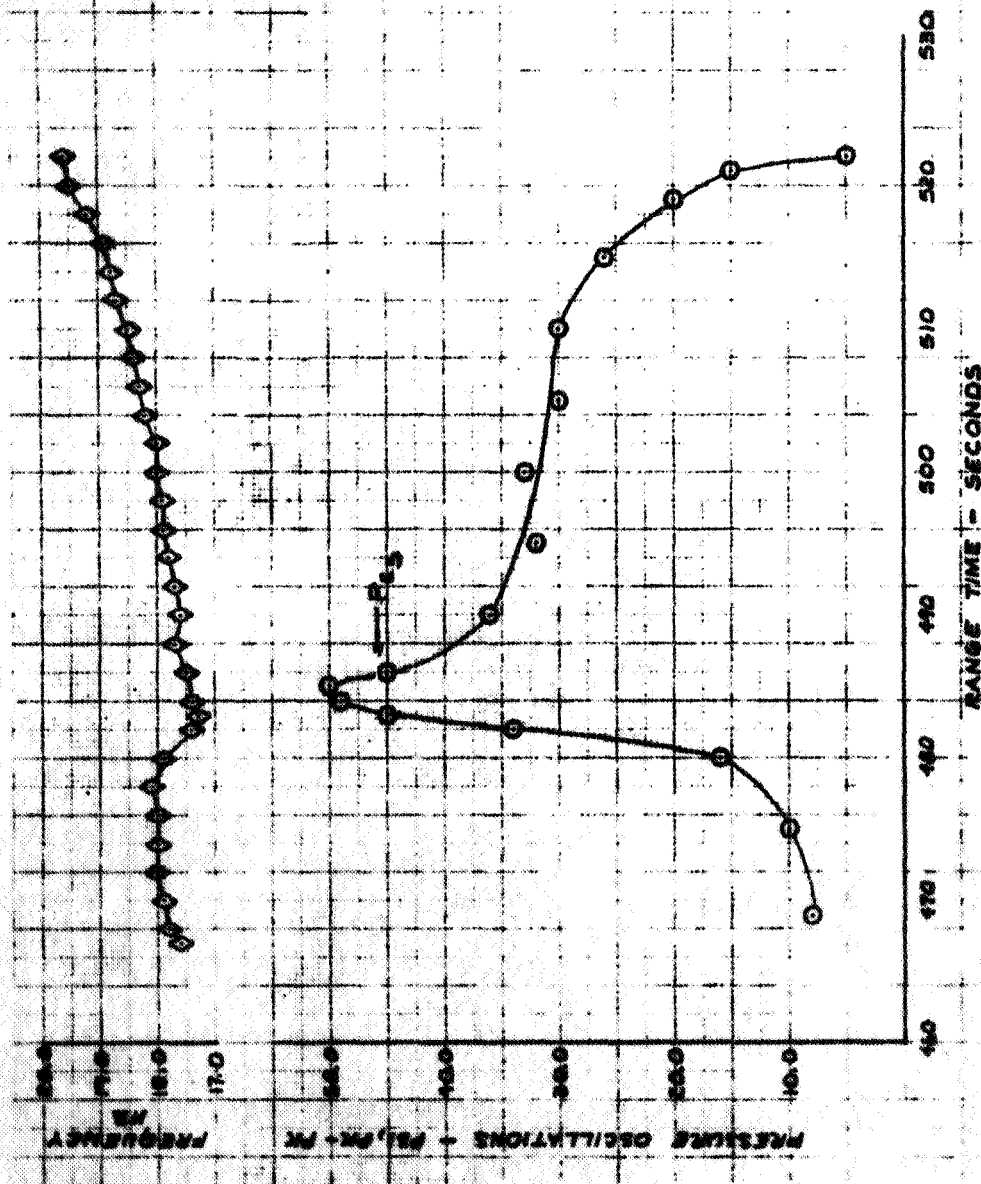
Figure 23. AS-503 S-II Oscillations, Amplitudes of Filtered Data

R-7970

the lower bound determined from the transfer function which gives $\dot{W}_c/\Delta P_{od} \sim 0.5$, and P_c maximum is 65 psi, unfiltered. There were 18-Hz data observable in an unfiltered record of the outboard LOX pump discharge pressure. However, there were strong data of higher frequencies, particularly 26 to 28 Hz, which were usually predominant over the 18 Hz. Engine No. 4 appeared to have the highest 18-Hz amplitudes with maximum values of from 30 to 35 psi, p-p, unfiltered. Probably, this value is larger than the actual signal because of the sense line.

The LOX injection, GG P_c, and fuel inlet pressures on engine No. 5 all had predominant 18-Hz oscillations in the latter portion of the burn. Maximum values observed were 75 psi, unfiltered, in LOX injection pressure; 33 psi, unfiltered, in GG P_c; and 5 to 6 psi, filtered, in fuel inlet pressure, all values being p-p.

Essentially the same accelerometer measurements were made on flight 503 as on flight 504, but the accelerometers were of a different type. On flight 503, the accelerometers had a sharp response roll-off at approximately 10 Hz. This is illustrated by the response curve of Fig. 24 which gives the gain of the engine No. 5 thrust pad accelerometer. Note that at 18 Hz the gain is down to 0.0115 of its actual value. Similar data for the phase response is not even available. As a result, the accelerometer data are of very little use on flight 503. No phase relationships can be determined between acceleration and force (P_c). Acceleration amplitudes could be estimated by multiplying by the correction factor from curves similar to Fig. 24, but these correction factors are so large that their reliability is questionable. As a result, the amplitudes will be primarily reported as determined from the data with no attempts to correct or to interpret the amplitude.

Much of the 18-Hz data were not discernible because of the oscillations in the 10-Hz region where the attenuation by the accelerometer roll-off is small. However, when the instability occurs near 480 RT, the maximum unfiltered values observed were as follows.
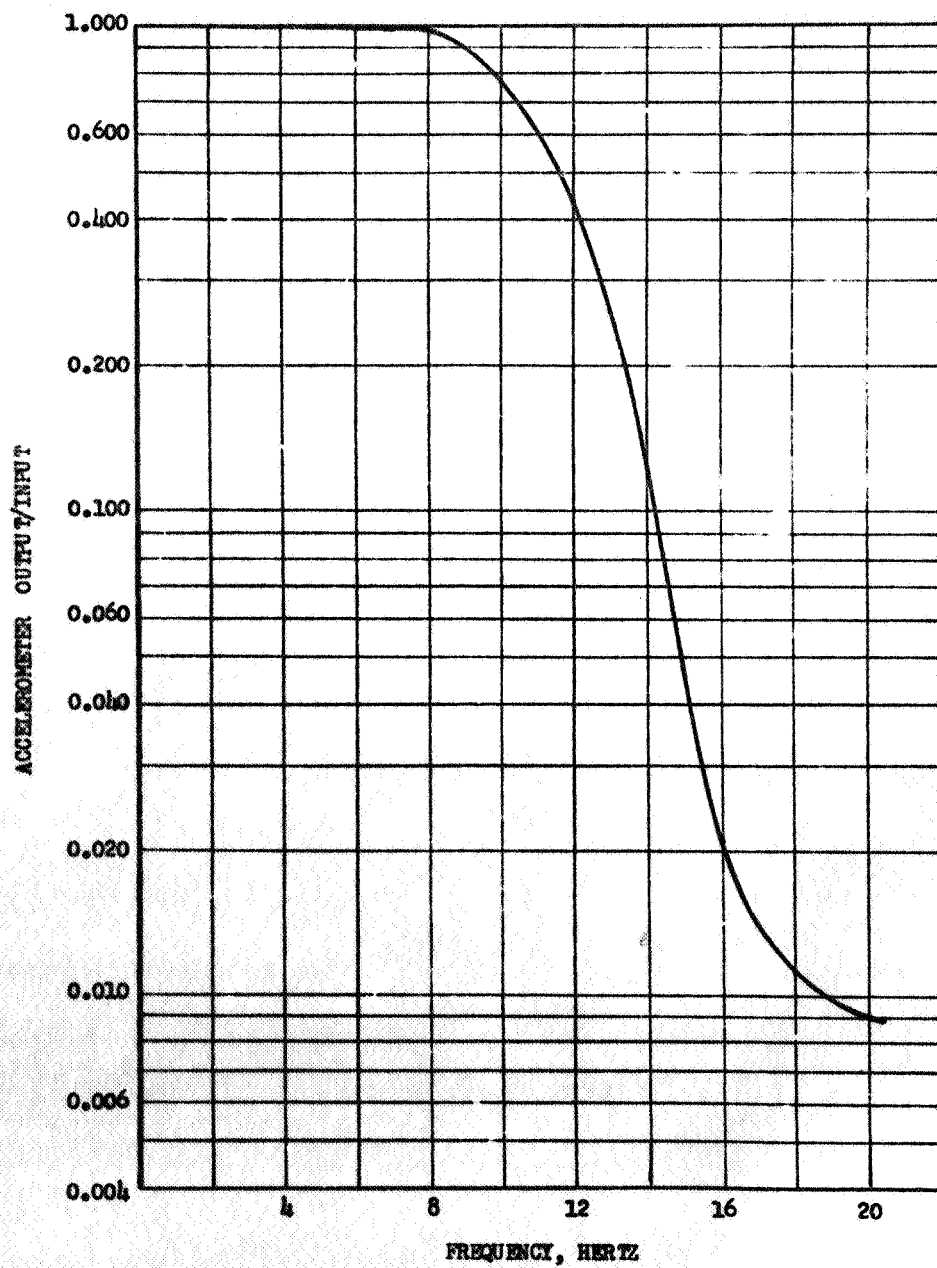
Figure 24.   Engine 5 Thrust Pad Accelerometer Response on AS-503

R-7970

$$\ddot{x}_5 \simeq 0.29 \text{ g, p-p}$$

$$\ddot{x}_{LTB} \simeq 0.16 \text{ g, p-p}$$

$$\ddot{x}_1 \simeq 0.10 \text{ g, p-p}$$

Applying the correction factor to $\ddot{x}_5$ yields

$$\ddot{x}_5 \simeq 0.29/0.0115 \simeq 25 \text{ g, p-p}$$

which compares well with the value 23.8 observed on flight 504. The dome accelerometer on flight 503 did not have the same roll-off characteristic as the other accelerometers. These dome accelerometers are used to measure high-frequency vibrations, and their response is good at the high frequencies, but they begin to attenuate the signal in the low-frequency range. This was observed in the 504 data where the dome accelerometer measurement on engine No. 5 was from 60 to 80 percent of the beam accelerometer measurement of engine No. 5. The maximum amplitude of the dome accelerometer on engine No. 5 for 503 was 9.6 g p-p, band-pass filtered from 15 to 20 Hz. If the signal was attenuated by 60 percent, then the actual value would be 16.0 g, p-p, which is comparable to signal values observed on flight 504. The dome accelerometers on engines No. 1 and No. 2 indicate no significant 18-Hz data above the noise level.

Accelerometers on the third stage of the vehicle had predominant 18-Hz oscillations during the S-II burn time. The gimbal block accelerometer on the third stage engine had maximum accelerations of 0.375 g, p-p, and the dome accelerometer of 0.45 g, p-p. The gimbal block accelerometer value is larger than the reading on the gimbal block of engine No. 5 on the second stage; however, no information is available on the required correction factors for these measurements.

The 18-Hz oscillations were seen in parameters in the I.U. package; e.g., yaw accelerometer and x-axis gyro servo, and in actuator ΔP's for the outboard engines. These oscillations appeared as early in time as

453 seconds RT and led initially to speculation that the 18-Hz problem
was caused by the guidance control system. Investigation of this poten-
tial cause revealed that the 18-Hz control signal to the actuator servo-
valves was negligible, and, even more significant, the phasing of the
engine oscillations was contrary to the control system logic. Thus, the
signals present could not be called for by the control system but only
represented response to the existing 18-Hz oscillations.

DATA CORRELATIONS

Flight Results

There are four characteristics of the oscillations other than frequency
which can be compared from flight-to-flight with an attempt to explain
these characteristics based on correlations with flight hardware or oper-
ating conditions. These four characteristics are time of occurrence of
the instability, oscillation amplitude changes before the instability,
maximum amplitude levels, and the amplitude envelope during the insta-
bility. The major hardware items and operating conditions which may
have contributed to differences from flight-to-flight were reviewed and
are presented in Table 2. Most of these items are not sufficiently dif-
ferent to explain any variations, but reference will be made to some of
the items in the following discussion.

After flight 503, the occurrence of the large-amplitude oscillations was
found to correlate well with two parameters, LOX liquid level in the
tank and LOX pump NPSH. The correlation with LOX level is shown in Fig. 25,
and the correlation is seen to hold for flight 504 as well. This liquid
level has a strong influence on the frequencies and gains of certain of
the structural modes. Thus, as the LOX level decreases the frequencies
increase such that modes in the 17- to 18-Hz region have a larger gain,
and the instability results.

TABLE 2

COMPARISON OF MAJOR FLIGHT ITEMS S-II 503 AND 504 Vs 501 AND 502

Item	504	503	501 and 502
Thrust Structure	Redesign (lighter)	Original design	Original design
Fuel Tank	Same as 503	Forward bulkhead gore section taper change	Original design
LOX Tank	Same on all		
LOX Tank Sump Baffles	Same as 503	16 Triangular sump baffles removed	Baffles redesigned for 501 and 502
LOX Tank Sump Screen	Same as 503	Inverted screen near bottom of sump(20 mesh)	Cooley hat screen above sump baffles (4 mesh)
Stage LOX Prevalves	Opening moment 375 to 557 in. lb (spring only) plus friction plus flow forces	Opening moment 59 to 115 in. lb (spring only) plus friction, plus flow forces	Opening moment 3554 to 3772 in. lb (pressure and spring) plus friction, plus flow forces
Stage Fuel Ducting (Straight Pressure Carrying Sections)	Same as 503	0.040-inch wall thickness	0.020-inch wall thickness
Flight Operation PU System	Closed loop	Open loop	Closed loop
Engine MR at Minimum PU	4.7	4.5	Approximately 4.7
Engine Outboard Inlet Ducting Fuel and LOX	All light weight	All light weight except No. 1 engine fuel and No. 2 engine both ducts	501 All heavy weight except position 3; 502 all light weight except position 4
RKD Insulation LOX System	Same all engines		
S-II Insulation Center Engine LOX	Same as 503	Same as 502 except for sealing between sections of insulation	502 Preformed fiberglass batting enclosed in stainless-steel half shells
LOX Tank Step Pressurization	In effect	Not in effect	Not in effect
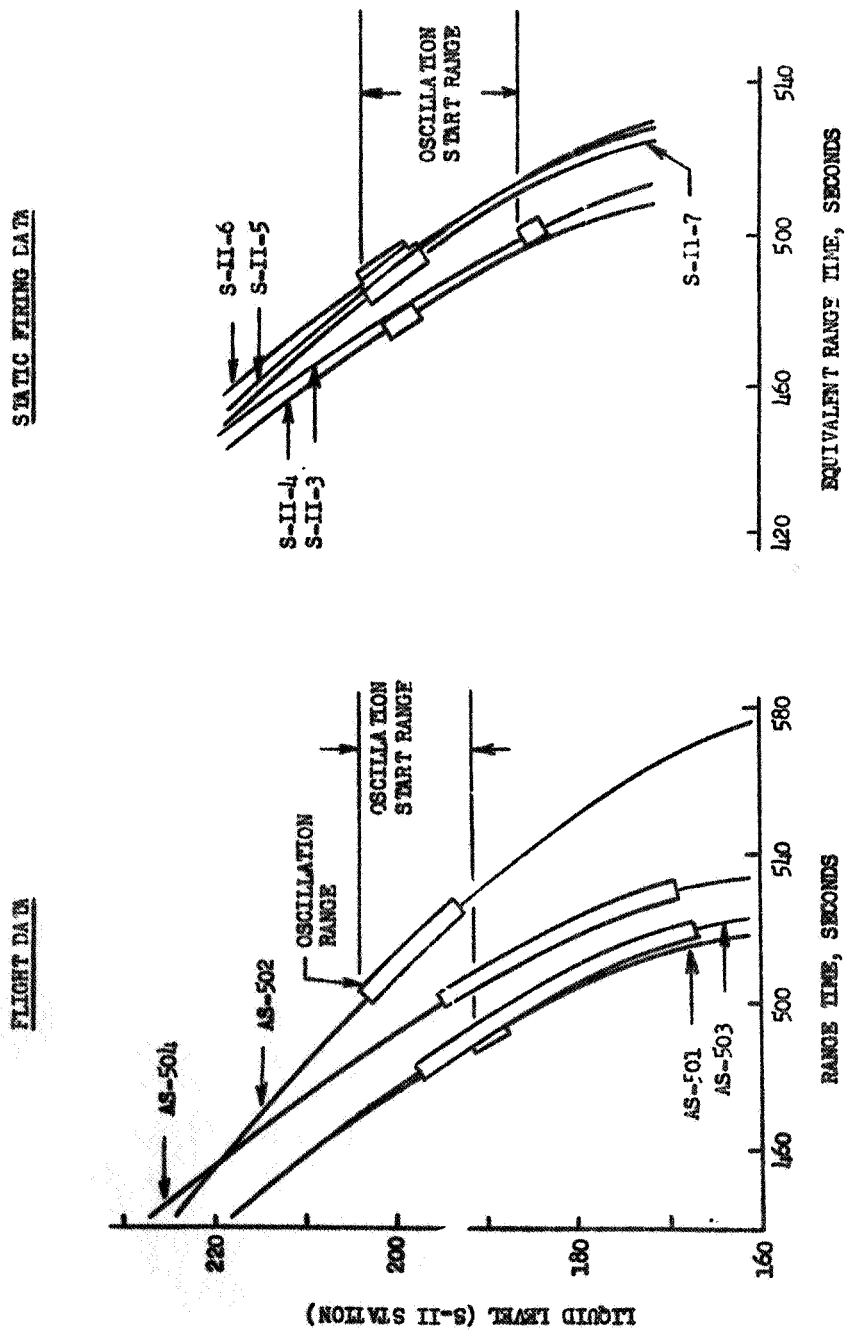
Figure 25. Oscillation Start Range as a Function of LOX Level In Tank

Although the LOX level in the tank during flight could not easily be changed, step pressurization was used on flight 504 to keep the NPSH higher at the end of burn. It must be kept in mind, also, that before flight 504 the generally accepted explanation of the cause of the oscillation problem was that the engine was self-driving at 18 Hz. Thus, increasing the NPSH would reduce the potential for the engine to self-drive (although ground tests have shown that on all flights the NPSH was higher than those values at which self-driven oscillations occur). The resulting correlation of instability with NPSH is shown in Fig. 26. The correlation does not hold for flight 504 proving that NPSH is not a significant enough parameter to eliminate the instability, and the 504 data proved that the problem was an instability, not engine self-driven oscillations.

However, the step pressurization with resulting increased NPSH is believed to be of benefit. For example, on flights 501, 502, and 503 there were periods of time prior to the instability at which amplitude levels of the P_c's increased. These early bursts in amplitude were not evident in the P_c measurements on 504 (compare Fig. 1 with Fig. 20 through 22). They did appear in accelerometer measurements on 504, but comparable data are not available for the other flights. If these early bursts on the first three flights indicate marginal stability, the increased NPSH could have produced enough additional margin to render these bursts indiscernible in P_c.

Another possible influence of the step pressurization is the effect on the amplitude envelope during the instability as seen in comparing flights 503 and 504 (Fig. 22 and Fig. 1, respectively). The P_{c5} amplitude converged faster on flight 504 than on flight 503. Also, the instability occurred later in time on 504 as compared with 503. These results could, again, be indicative of a slightly better margin of stability with the higher NPSH. However, in comparing all four flights, the amplitude envelope and the maximum amplitude level variations from flight to flight are for the most part unexplained. These maximum amplitude levels are summarized on the following page. Flights 503 and 504 were very similar, and
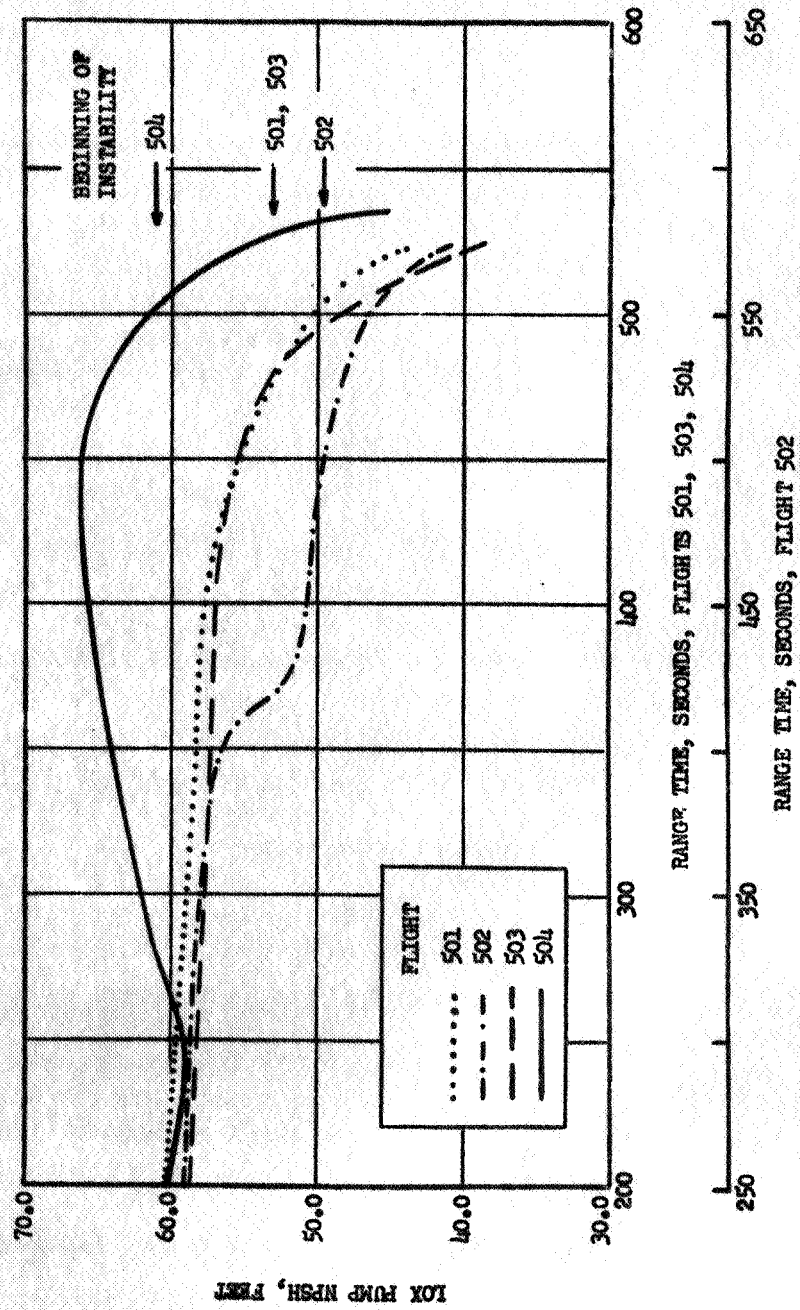
Figure 26. Flight LOX Pump NPSH History

indications are that the amplitudes on these flights were limited by cavitation at the LOX pump inlet. However, the oscillation amplitudes on 501 and 502 were not large enough to reach the vapor pressure when the oscillating pressure is subtracted from the steady-state pressure.

Parameter	501	502	503	504
P_{c5}, psi, p-p, unfiltered	42.0	24.0	65.0	75.0
P_{c5}, psi, p-p, filtered	22.0	13.0	50.0	51.2

Stage Static Test Results

The stage static tests have also indicated significant oscillations in the 15- to 18-Hz region, associated with the center engine near the end of the burn. The frequency of the oscillations is generally slightly less than in flight, and the amplitudes are much less. However, in the static tests the structure is tied down, and as a result the gains and frequencies of the structural modes are shifted. Still, there is sufficient similarity between the oscillation behavior of static tests and flight to lead to the conclusion that both are related. In Fig. 25, the correlation of time of the larger oscillations with LOX level in the tank is seen to be in good agreement with the flight data.

Some typical values seen in the static tests during the time of oscillation are:

Test S-II-7, at 330-second burn time:

$$\ddot{x}_{LTB} = 2.2 \text{ g, p-p, maximum}$$

$$P_{os} = 7.4 \text{ psi, p-p}$$

Both at a frequency of 16.0 Hz

These data were obtained from analyses by Space Division using a Gulton Process which gives a narrow bandwidth PSD over every 8 seconds of burn time. The static test data were also used to indicate the structural

modes of the LOX tank bulkhead. The result is shown in Fig. 27. The data
points were taken from the Gulton analysis, and the solid lines were based
on both the indicated symbols and on voice prints of the same measured
parameter which were obtained from Bellcomm. The resemblance of these curves
to the modes taken from flight data and shown in Fig. 11 is obvious, the
static firing frequencies tending to be a little lower than the flight
frequencies.

17-HERTZ CLOSED-LOOP INSTABILITY

Definition of the Closed-Loop Instability

Before discussing the instability associated with the S-II stage, a brief
discussion of what is meant by closed-loop instability, or what consti-
tutes the instability, is in order. The instability is a system problem,
the system being composed of three main components:

1. The structure

2. The turbopump feed system

3. The engine

These three components are connected in such a way that they form a
closed loop as sketched below. That is, given a thrust force acting on

F = Thrust   [Structure] $\ddot{X}$ = Acceleration

[Engine]   P = Inlet Pressure   [Feed System]
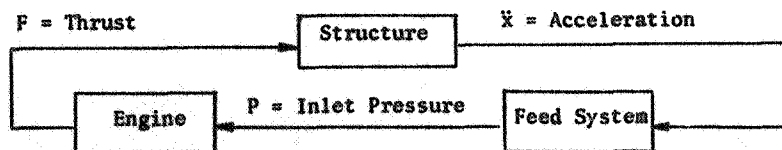
the structure, the structure responds with a given acceleration. The
acceleration of the structure causes corresponding inlet pressure varia-
tions which are transmitted through the engine resulting in a thrust
which again acts on the structure. Thus, the loop is closed, all three
components have a direct influence on the loop, and the path around the
loop is identical regardless of which response (thrust, acceleration, or
inlet pressure) is taken initially.
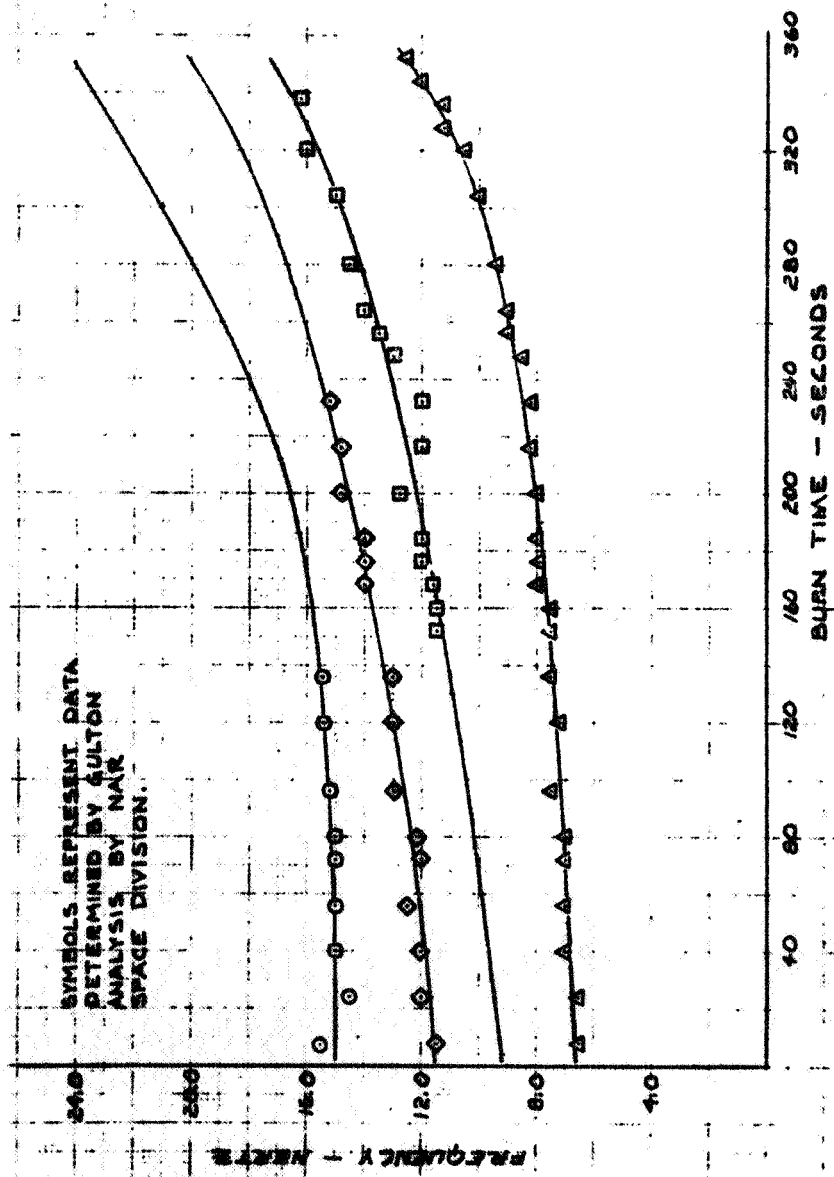
Figure 27. LOX Bulkhead Modes From S-II-7 Static Firing

R-7970

Having then defined the loop, consider now the dynamic stability of the loop. For a given frequency, at any point of time, the output of any of the three boxes in the above sketch can be represented by a gain and phase relation to the input. That is,

$$\text{output} = Ke^{i\phi} \cdot \text{input}$$

where K is a numerical gain factor and ϕ is a phase angle, and both are generally frequency dependent. Therefore,

$$\ddot{x} = K_1 e^{i\phi_1} F \tag{3}$$

$$P = K_2 e^{i\phi_2} X \tag{4}$$

$$F = K_3 e^{i\phi_3} P \tag{5}$$

If Eq. 4 and 5 are used in Eq. 3, the resulting equation is

$$\ddot{x} = K_1 e^{i\phi_1} \left[K_3 e^{i\phi_3} \left(K_2 e^{i\phi_2} X \right) \right]$$

or simplifying

$$\ddot{x} = K_1 K_2 K_3 e^{i(\phi_1 + \phi_2 + \phi_3)} \ddot{x}$$

If subscripts are added to the acceleration parameter to indicate successive cycles,

$$\ddot{x}_i = K_1 K_2 K_3 e^{i(\phi_1 + \phi_2 + \phi_3)} \ddot{x}_{i-1} \tag{6}$$

If

$$\phi_1 + \phi_2 + \phi_3 = 0$$

$$K_1 K_2 K_3 > 1.0 \tag{7}$$

then X will diverge, and the system is unstable. Therefore, Eq. 7 constitutes the conditions for defining an instability.

R-7970

One further comment concerns the relation of POGO to the closed-loop instability. POGO is a closed-loop instability. However, the classical POGO problem occurs near the frequency of the first longitudinal structural mode of the vehicle, and many definitions of POGO found in the literature restrict POGO to only this mode. Thus, a closed-loop instability involving a different mode at a higher frequency, as for example, on the S-II stage of the Apollo, would not fit these more restrictive definitions of POGO and is, therefore, referred to as a closed-loop instability.

Indications of the Instability on the S-II

Four arguments will be presented to show that the 17-Hz phenomenon on the S-II stage was a closed-loop instability involving the vehicle structure, the LOX pump feed system, and the center engine.

1. The gains and phases of the three main elements of the loop are partially known from flight data and ground tests, and the other gains and phases required to have an instability are easily realized based on current information. The instability occurred on flight 504 at an NPSH of approximately 60 feet and with the PU valve at 10 degrees from full-open position. Ground tests have established that at this operating point the engine transfer function has a gain and phase at 17 Hz of

$$K_3 = 320.0*(0.566)$$

$$= 181 \frac{\text{pounds thrust}}{\text{psi inlet pressure}}$$

and

$$\emptyset_3 = -50 \text{ degrees}$$

The value of K_3 comes from the product of the value of $\Delta P_c/\Delta P_{os}$ (=0.566) and the pounds of thrust per psi chamber pressure (=320). From flight data, $\ddot{x}$ and P_c of engine 5 are known. For example, at RT 500 where the

amplitudes are beginning to rapidly diverge

$$\ddot{x}_5 \quad = \quad 2.1 \text{ g, p-p (see Fig. 5)}$$

$$P_{c5} \quad = \quad 4.0 \text{ psi, p-p (see Fig. 3)}$$

both at a frequency = 17.0 Hz

and the phase between the two

$$\phi_{P_{c5}} / \ddot{x}_5 \quad = \quad -70 \text{ degrees}$$

Therefore, referring to Eq. 3,

$$K_1 \quad = \quad \frac{2.1}{4.0 \ (320.)} \quad = \quad 0.00164 \ \frac{\text{g acceleration}}{\text{pounds thrust}}$$

$$\phi_1 \quad = \quad 70 \text{ degrees}$$

Substituting the values of K_1, K_3, ϕ_1, and ϕ_3 into Eq. 7 and solving for K_2 and ϕ_2 yields

$$\phi_2 \quad = \quad -20 \text{ degrees}$$

$$K_2 > 3.37 \ \frac{\text{psi inlet pressure}}{\text{g acceleration}}$$

It was previously shown that at the time of the instability, the height of LOX above the pump inlet is approximately 8 feet so that the pressure at the inlet because of a 1-g acceleration was

$$\frac{\Delta P}{g} \quad = \quad \frac{8 \ * \ 70 \ * \ 1}{144} \quad = \quad 3.89 \ \frac{\text{psi inlet pressure}}{\text{g acceleration}}$$

Thus, the value K_2 required to get the instability is less than the static value which would be obtained if the LOX column acted like an incompressible mass of liquid. The inlet line dynamics could tend to

increase or decrease this static gain depending on the resonant frequencies of the feedline. Current analysis of ground test data has revealed that the feedline response at 17 Hz is as large, or larger, than the static response and that the phase angle at this frequency is very close to the -20 degrees which is needed for instability. (A detailed description of these ground tests and their results is presented in a later section.)

Thus, the current best estimate of the gains and phases of the three main elements of the closed loop do satisfy Eq. 7, and the closed-loop system is unstable. This is the most direct and conclusive proof of an instability, but other arguments are presented to add weight to the conclusion.

2. It was pointed out previously (Fig. 6 and 7), based on the phase relationship between P_c and $\ddot{x}_s$, that the oscillations are occurring at a resonant frequency of the structure. A structure-engine closed-loop instability will always occur at, or very near, a resonance of the structure because the structural gain, thus, the loop gain, is significantly larger at this frequency. Because the structural resonance is frequently characterized by a change in frequency with time, the change in the frequency of the instability with time indicates that the instability is tending to follow the resonance.

3. The shape of the oscillation amplitude curve is in itself indicative of an instability. For example, in Fig. 1 or 4, the amplitudes are seen to diverge in an exponential fashion until abruptly limited. This type of behavior is characteristic of an instability with nonlinearities resulting in a limit cycle.

4. Immediately after flight AS-503, it was proposed that the oscillation problem was caused by self-driven oscillations of the engine rather than an instability. It had been noticed that the J-2 engine under certain operating conditions would tend to produce low-frequency oscillations.

Ground tests both at Rocketdyne and MSFC were performed to establish at what operating conditions these self-driven oscillations occur. The results are shown in Fig. 28. The region of pump self-driven oscillations is below the operating NPSH values during each of the flights. A comparison of Fig. 26 and Fig. 28 reveals that the flight oscillation region continued to an NPSH of 40 feet on AS-503 (full-open PU valve position). This is within 5 feet of the self-excited oscillation region yet the oscillations stopped, clearly showing that the self-excited region had not been reached. One further important characteristic noted concerning the self-excited oscillations is that the amplitudes in inlet, discharge, or chamber pressure never exceed a few psi. There have been no self-excited oscillation amplitudes observed on the J-2 engine which are as large as those seen in flight. Thus, the flight oscillations cannot be engine self-excited oscillations.

The above four arguments offer conclusive evidence that the flight 17 Hz oscillations are caused by a closed-loop instability.

The Degree of Instability During Flight

The flight data can also be used to indicate the times of instability and the degree of instability at least as indicated by the closed-loop damping factor. Before presenting this information, a brief discussion of the analytical background of the subject is in order.

A typical second-order system can be represented by the differential equation

$$\ddot{x} + 2\zeta\omega_n \dot{x} + \omega_n^2 x = 0 \tag{8}$$

e.g., the structural modes of the vehicle are represented in this manner. Thus, if a force F is applied to the structure, then the acceleration and velocity could be found using the block diagram

$$F \longrightarrow \boxed{\dfrac{K_o S^2/\omega_n^2}{1 + 2\zeta_s S/\omega_n + S^2/\omega_n^2}} \xrightarrow{\ddot{x}} \boxed{\dfrac{1}{S}} \xrightarrow{\dot{x}}$$
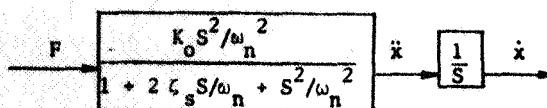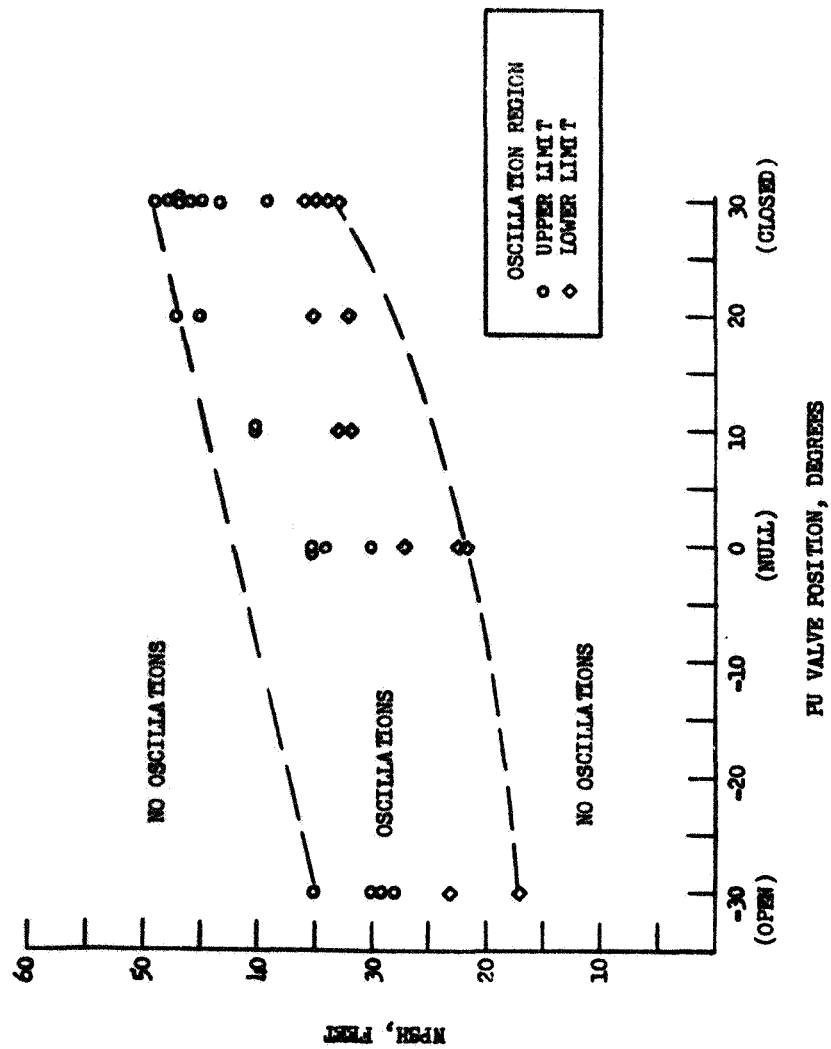
Figure 28. Region of J-2 LOX Pump Self-Excited Oscillations

If, now, a feedback term is introduced which relates engine thrust to velocity as in the closed-loop instability problem, then the block diagram becomes

$$F \xrightarrow{} \boxed{\Sigma} \xrightarrow{} \boxed{\dfrac{K_o \, S^2/\omega_n^2}{1 + 2\zeta_s S/\omega_n + S^2/\omega_n^2}} \xrightarrow{\ddot{x}} \boxed{\dfrac{1}{S}} \xrightarrow{\dot{x}}$$

$$\boxed{K_1}$$
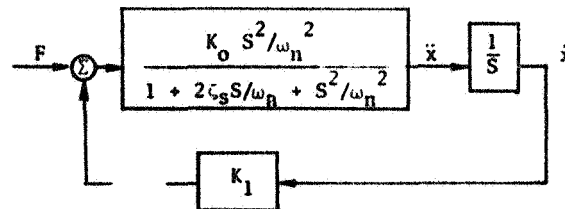
where for simplicity only a single gain is used in the feedback block. This diagram can be reduced to the form

$$F \xrightarrow{} \boxed{\dfrac{K_o \, S^2/\omega_n^2}{1 + (2\zeta_s - K_1 K_o/\omega_n) \, S/\omega_n + S^2/\omega_n^2}} \xrightarrow{\ddot{x}}$$
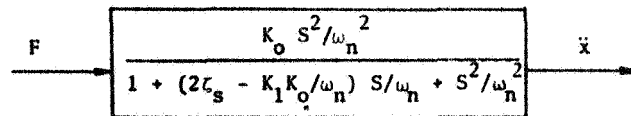
In other words, the feedback term has changed the effective structural damping, or yielded a closed-loop damping factor of $2\zeta_\ell = (2\zeta_s - K_1 K_o/\omega_n)$.

More complex feedback terms could now be assumed, but each one could be effectively simplified to the above form to establish system stability. Thus, Eq. 8 can be used to indicate the response of the closed-loop system if the damping factor ζ is the closed-loop damping, ζ_ℓ.

A general solution of Eq. 8 for the displacement, given an initial displacement, ϵ, is

$$x = \epsilon \, e^{-\zeta_\ell \, \omega_n t} \cos q(t - \theta)$$

where

$$q = \omega_n \sqrt{1 - \zeta_\ell^2}$$

R-7970

clearly, the exponential term, exp $(-\zeta_\ell \omega_n t)$, determines the stability of the system. Three possibilities exist assuming $t > 0$:

$$\zeta_\ell \omega_n \begin{cases} < 0 \text{ , system unstable} \\ = 0 \text{ , system marginally stable} \\ > 0 \text{ , system stable} \end{cases}$$

Therefore, if the feedback term reduces the closed-loop damping to a negative value, an instability will result. Having established that the system stability is determined by the term

$$Z = e^{-\zeta_\ell \omega t}$$

note that

$$\dot{Z} = -\zeta_\ell \omega Z$$

so that

$$\zeta_\ell \omega = -\frac{\dot{Z}}{Z} \tag{9}$$

Thus, for the S-II oscillation problem, or any other instability, the closed-loop damping can be estimated from the slope and magnitude of the oscillation amplitude envelope, because the frequency (ω) is known. Note that the point of maximum instability is not the point of maximum amplitude, but the point where the slope divided by the amplitude is maximum. Also, for a limit cycle as on AS-504, where the amplitude is effectively constant, the slope is zero and the system is marginally stable.

Using the above technique, the slope and amplitude of the oscillation envelopes were determined from the data, and the effective closed-loop damping was determined from Eq. 9. The results for AS-501, 503, and 504 are shown in Fig. 29. On flight 504, the maximum instability is at the time when the amplitudes are just beginning to grow (however, at these times the signal-to-noise level is relatively low and accurate determination of the slope and amplitude of the oscillations is difficult and subject to inaccuracies). The system is becoming more stable then abruptly becomes less stable (corresponding to the time when the amplitudes
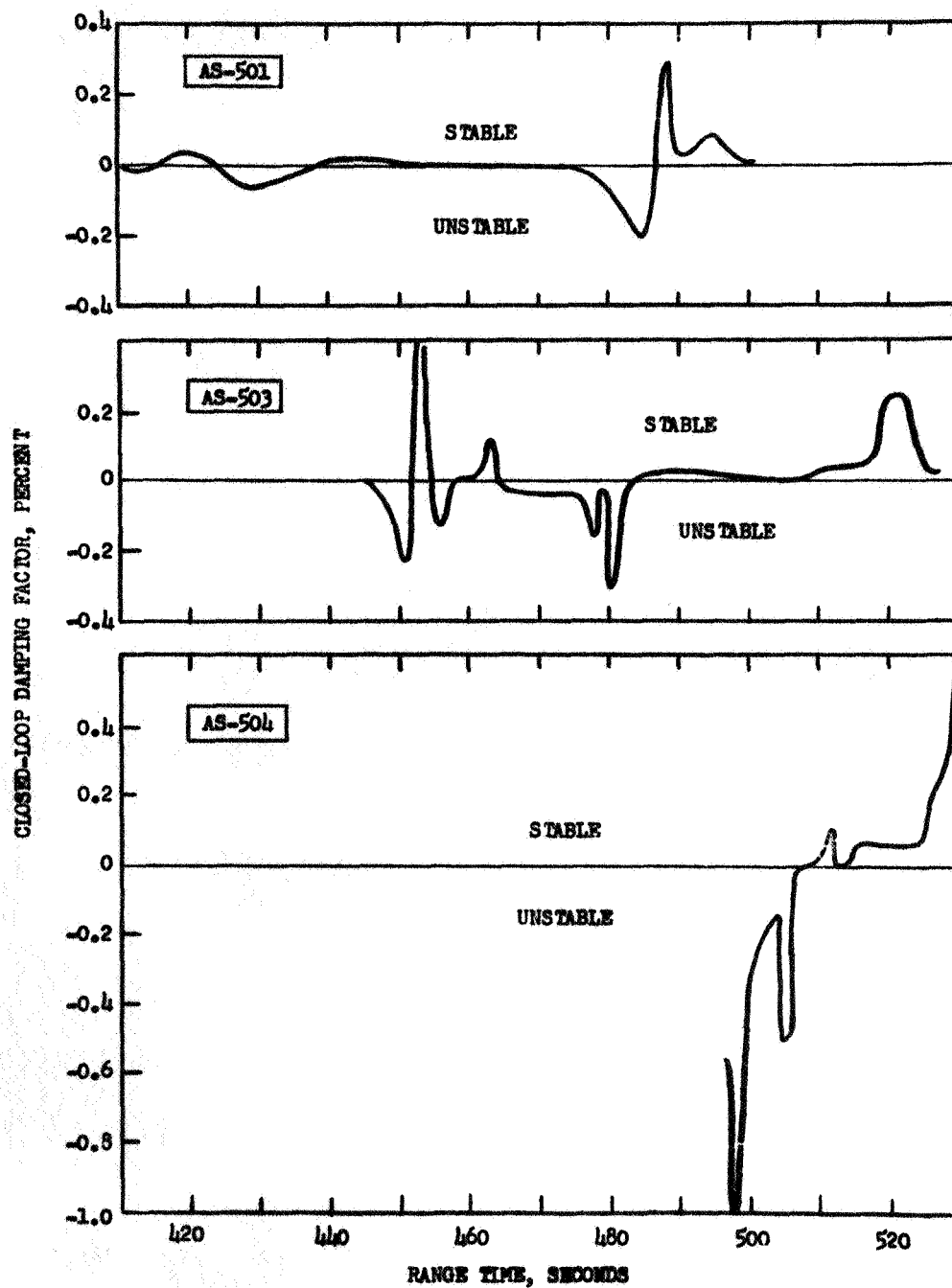
Figure 29.   Closed-Loop Damping vs Range Time

rapidly diverge). Because of the limit cycle, the system is marginally stable for a time, then becomes stable. The results of Fig. 29 indicate that the closed-loop damping reaches a maximum negative value of (-) 1.0 percent on 504. It is desirable to relate this closed-loop damping to the system stability in terms of db's.

By definition, the loop stability in db's is

$$db = 20 \log_{10} \text{ (open-loop gain)}$$

$$= 20 \log_{10} \text{ (output/input)}$$

Referring to the block diagram with the feedback term included, the input is F and the open-loop output is

$$\text{output} = F \left[\frac{K_o \, S^2/\omega_n^2}{1 + 2 \zeta_s \, S/\omega_n + S^2/\omega_n^2} \right] \left[\frac{K_1}{S} \right]$$

At the zero phase point, $S^2/\omega_n^2 = -1.0$, therefore,

$$\text{output} = \frac{F(-K_o) \, (K_1)}{-2 \zeta_s \, \omega_n} = \frac{F \, K_o K_1}{2 \zeta_s \, \omega_n}$$

Therefore

$$db = 20 \log_{10} \, (K_o K_1 / 2 \zeta_s \, \omega_n)$$

But
$$2 \zeta_\ell = 2 \zeta_s - K_o K_1 / \omega_n$$

So that

$$K_o K_1 / 2 \, \omega_n = (\zeta_s - \zeta_\ell)$$

and

$$db = 20 \log_{10} \left(\frac{\zeta_s - \zeta_\ell}{\zeta_s} \right)$$

For AS-504, the closed-loop damping factor reached a minimum value of
-1.0. Assuming that the structure had 1.5-percent damping, then the max-
imum instability was

$$db = 20 \log_{10} \left(\frac{1.5 - (-1.0)}{1.5}\right) = 4.5$$

Or if it is assumed that the structure had only 1.0-percent damping at
this frequency,

$$db = 20 \log_{10} 2.0 = 6.0$$

The other flights can be similarly rated using the data of Fig. 29.

Analog Model of Instability

Initial Model. When the 17-Hz phenomenon was realized to be a closed-loop
instability, the various elements of the loop (i.e., the structure, feed-
line, and engine) were not completely defined. In an analog computer
model, each of these elements must be defined, and the interdependence of
each is defined so that the closed-loop system exists on the computer.
Time can then be varied to correspond with actual flight time, and the
system response can be recorded so that any instability will be evident.
Lacking complete information on the loop elements, a simple analog model
was established initially to study the influence on stability of various
parameters appearing in the loop. This initial model was only applicable
to the last 100 seconds of range time. Following these initial studies,
the structure and LOX feedline dynamic description were expanded to
include the results of further analysis of both ground and flight data,
and the time period of the model was extended to include the full S-II
burn time.

The predicted structural modes in the frequency range around 17 Hz were inaccurate. Some of these inaccuracies were discussed in the section on the flight 504 main acceleration measurements. As a result, the predicted structural modes could not be used with any confidence, and Rocketdyne decided to use in the analog model a single structural mode with frequency and gain characteristics determined from the flight data itself. The acceleration of the center engine and LOX tank bottom, the chamber pressure (representing the force), and the phase relationship between the acceleration and force were all known. Assuming a single structural mode, which is equivalent to assuming that the structure can be represented by a mass-spring-dashpot system, then the acceleration of the structure caused by a force F is given by

$$\frac{\ddot{x}}{F} = \frac{\frac{1}{M}\left(\frac{S}{\omega_1}\right)^2}{1 + 2\zeta\left(\frac{S}{\omega_1}\right) + \left(\frac{S}{\omega_1}\right)^2} \tag{10}$$

where M is the mass, ω_1 the resonant frequency, and ζ the ratio of damping to critical damping for the structure and S is the Laplace operator, or the independent variable. Thus, the structure is defined by three parameters: M, ω_1, and ζ. The damping coefficient is assumed to be known and was set equal to 0.015, or at times to 0.01. Knowing the phase angle between the force and acceleration, the resonant frequency can be determined as was illustrated in Fig. 7 . Using Eq. 10 and the actual data for the amplitudes of $\ddot{x}$ and F, the value of M can be determined for any point in time. Thus, the complete structure is defined by a resonant frequency and gain varying with time as in the flight.

The LOX tank bottom and engine No. 5 acceleration are in phase throughout the region of large 17-Hz oscillations. Therefore, if Eq. 10 is used to define the structural acceleration of engine No. 5 ($\ddot{x}_5$), the LOX tank bottom acceleration can be found by using a single gain factor, K, which

relates the amplitude or $\ddot{x}_{LTB}$ to $\ddot{x}_5$ as a function of time. The liquid level in the LOX tank is also varying with time, and this variation is included in the analog model. The approximations to these flight results that were used to define the structure are shown in Fig. 30.

The next major element in the loop is the feedline system. Initially, both the LOX and fuel-side feed systems were included in the model. However, the fuel side was shown to have a very small influence on the stability and, therefore, all attention was directed to the LOX side. Since the LOX feedline dynamics were not known in the first part of the study, a very simple model was assumed consisting of a single inertance (L_1) and a compliance (B_1). A schematic diagram of the feedline is shown below with significant parameters defined in the diagram. Using these symbols,
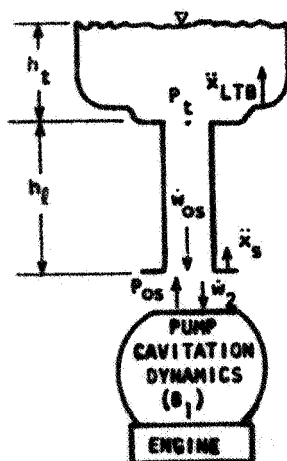
$$P_t = \frac{\rho h_t}{g} \ddot{x}_{LTB} \tag{11}$$

$$(P_t - P_{os})A = \frac{\rho h_\ell A}{g} \frac{dV_1}{dt} \tag{12}$$

$$P_{os} = \frac{B_1}{S}\left(\dot{w}_{os} + \frac{\rho A \ddot{x}_s}{S} - \dot{w}_{od}\right) \tag{13}$$

where ρ is the specific weight of the LOX, V_1 is the velocity of the flow relative to the duct, A is the area of the feedline, $\dot{w}_{od}$ is the pump discharge flowrate, and S is the Laplace operator ($S = d/dt$, where t = time). Equation 12 can be written as

$$P_t - P_{os} = L_1 S \dot{w}_{os} \tag{14}$$
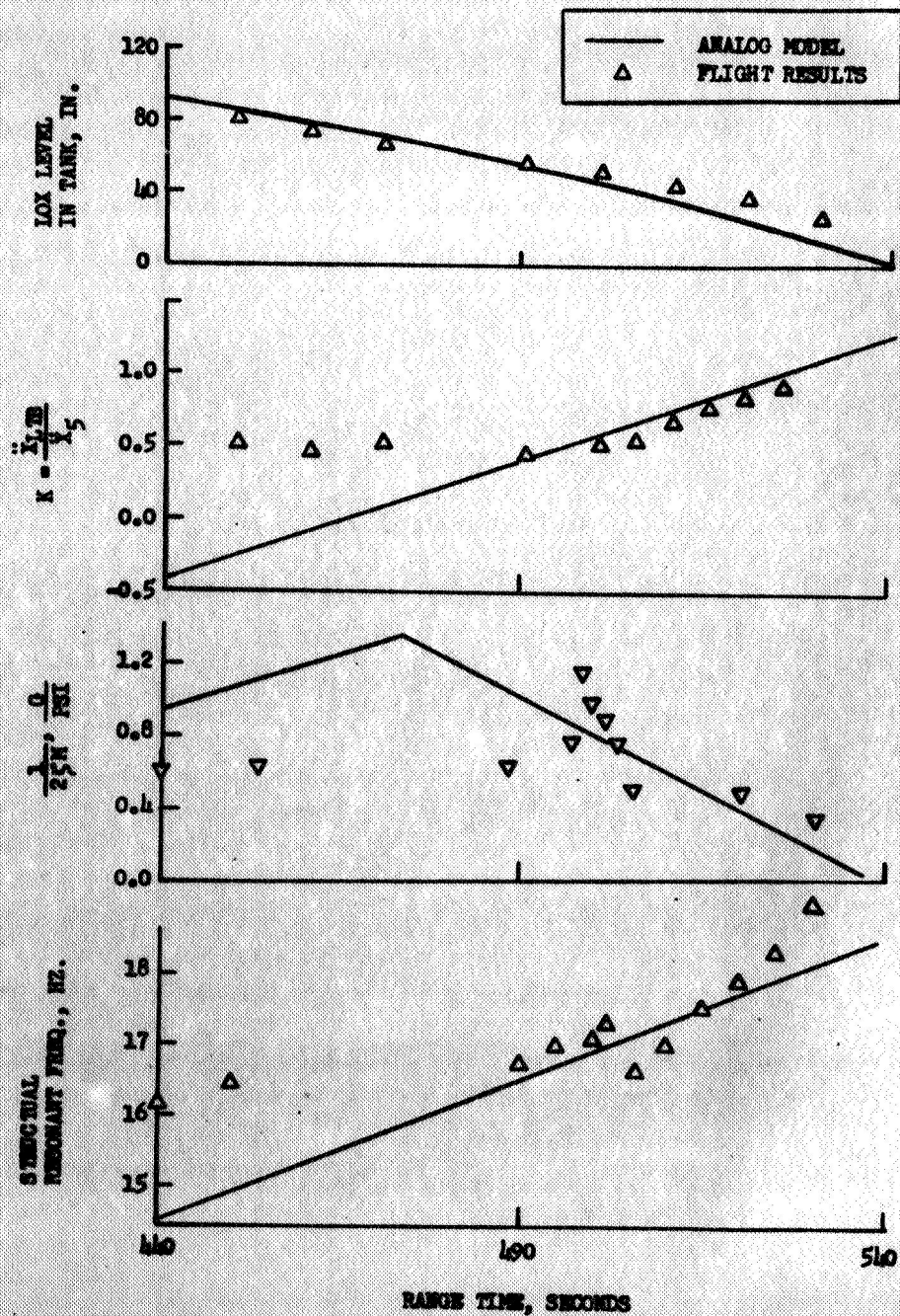
Figure 30. Analog Model Time Variant Parameters

where L_1 is the inertance ($= h_\ell/Ag$) and $\dot{w}_{os} = \rho AV_1$. In Eq. 13 the discharge flowrate, $\dot{w}_{od}$, is dependent upon the effective resistance of the engine. This flowrate is determined from the engine transfer function so that

$$\dot{w}_{od} = \frac{\partial \dot{w}_{od}}{\partial P_{os}} \, P_{os} \tag{15}$$

Thus, Eq. 11, 13, 14, and 15 describe the feedline and pump cavitation dynamics and couple these to the structure through $\ddot{x}_S$ and $\ddot{x}_{LTB}$. Note that this portion of the loop is equivalent to a fluid mass, represented by L_1, sitting on a fluid spring, represented by B_1, and although it is not obvious yet the real part of $\partial \dot{w}_{od}/\partial P_{os}$ represents damping caused by the engine.

The remaining element of the loop is the engine. The one engine transfer function has been introduced already; the other is the transfer function relating engine thrust to LOX pump inlet pressure ($\partial F/\partial P_{os}$). This transfer function was established through engine tests using a positive-displacement pulser on the inlet line. Initially, outboard engine effects were included in the model, but both the model and flight results revealed that the outboard engines were not contributing significantly to the 17-Hz problem. The curve fits of the engine transfer functions used in the analog model are shown in Fig. 31. The NPSH and PU valve position correspond to conditions near the region of instability on AS-504. Under these conditions, the pump appears to be rather nondynamic, particularly the gain. (To convert the gain of P_c to thrust use the relationship: thrust = 320 *P_c.)

These component elements can now be combined to form the closed loop. A block diagram of the loop is shown in Fig. 32. The structure is primarily from Eq. 10 the feedline from Eq. 11 through 15. The block diagram of Fig. 32 represents the analog model used to study the parameter influence on system stability. Essentially every parameter indicated in Fig. 32 was varied, and its resulting influence recorded. These results will be presented below.
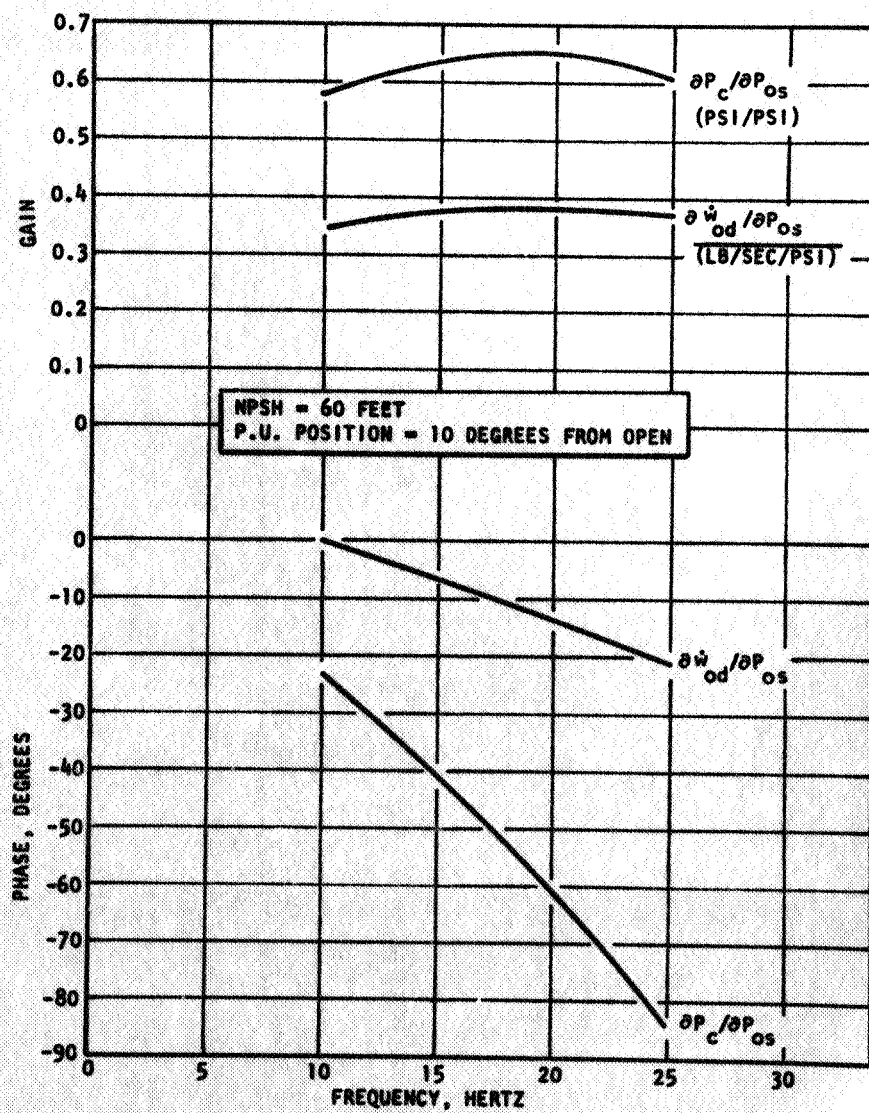
Figure 31. Curve Fit of Engine Transfer Function
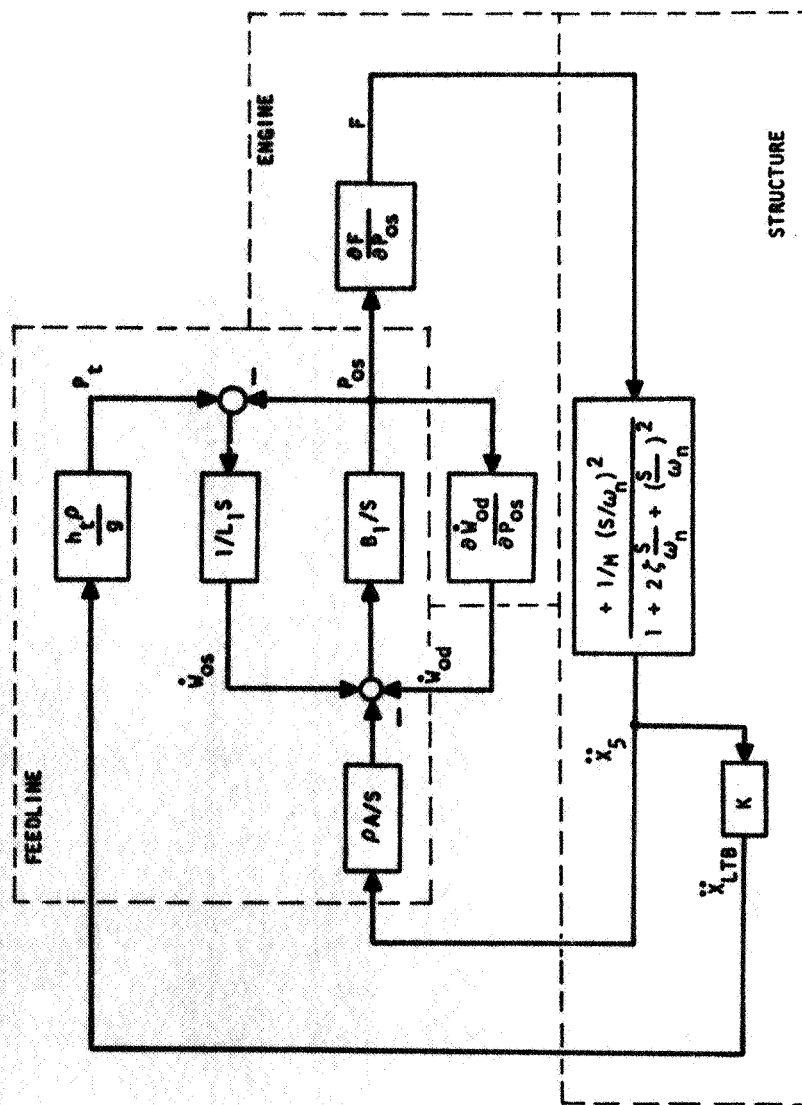
Figure 32. Analog Model Diagram

The equations for the feedline dynamics can be rewritten and put in different form. The result is shown in the block diagram of Fig. 33. In this diagram the inlet line resonant characteristics are more obvious. The resonant frequency of the line is

$$\omega_\ell \approx \sqrt{B_1/L_1} \qquad \text{rad/sec} \qquad\qquad (16)$$

and the role of $\partial \dot{w}_{od}/\partial P_{os}$ as a damping factor is evident. The magnitude of B_1 was varied over a large range, and the resonant frequency varied accordingly. As a reference case $B_1 = 180$ in.$^{-2}$ was used which probably represents an upper bound.

$$L_1 = \frac{h_\ell}{A g} = 0.003 \text{ sec}^2/\text{in.}^2$$

Therefore, with $B_1 = 180$

$$f_\ell = \frac{1}{2\pi} \sqrt{\frac{B_1}{L_1}} = 39 \text{ Hz}$$

Values of B_1 as low as 20 were used, which would yield an inlet line resonance of 13 Hz. The engine flow-feedback transfer function gives an effective damping ratio of about 4 percent if $f_\ell = 13$ Hz and of about 11 percent if $f_\ell = 39$ Hz.

Using this initial model, the system was stable until approximately 60 seconds prior to cutoff. Because the model was linear, the amplitudes during the instability continued to increase with no amplitude limit (except machine limitations as, e.g., amplifier overload). The system did return to the stable region before cutoff. From the gain curve ($1/2\zeta M$) of Fig. 30, the instability was initiated after the peak gain was reached and must, therefore, have depended partially on the resonant frequency of the structure as well.
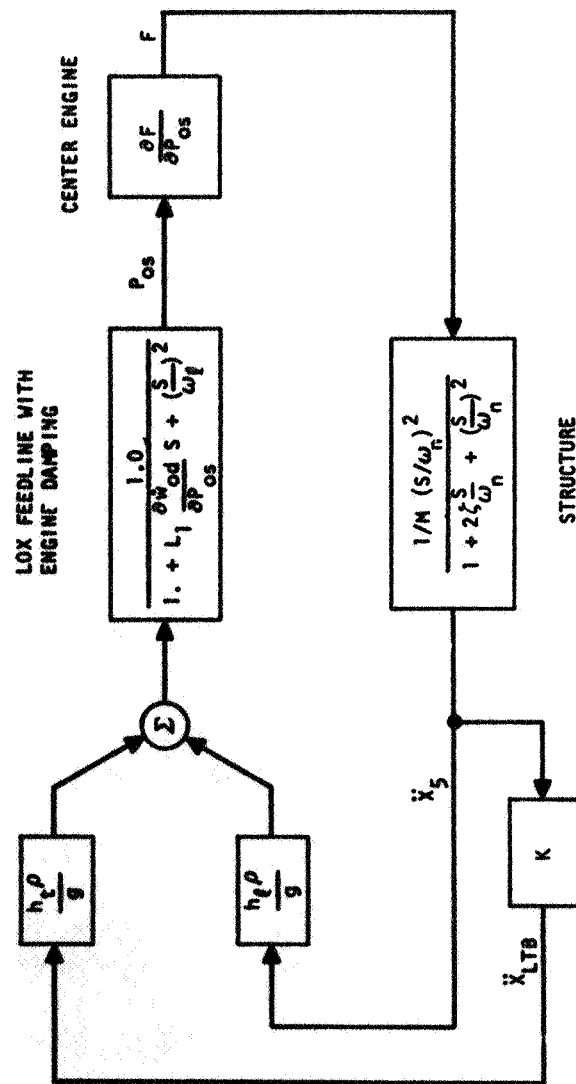
Figure 33. Analog Model Diagram

To establish the effect on the stability of the various parameters, a
gain factor was inserted into the loop, time was set at the point of
maximum instability, and the gain factor adjusted until the system was
marginally stable. The relative value of the gain required to make the
system stable would then indicate whether a parameter change was stabi-
lizing or not. In Fig. 34, the effects of changes of some of the gains
in the loop are presented. The abscissa for the curves is the magnitude
of the parameter divided by its normal magnitude. The ordinate is the
gain factor required for marginal stability divided by the gain factor
using the normal magnitude of the parameter. Thus, every curve is forced
to go through the point (1,1).

The stability is directly proportional to the magnitude, or gain, of the
structure (1/M) and of the engine transfer function ($\partial F/\partial P_{os}$). This is
readily seen from Fig. 32 or 33 because the total gain around the loop
is directly proportional to these gains. The influence of the fuel side
on the stability is seen from the curve for $\partial F/\partial P_{fs}$ to be extremely small.
A factor of 10 change in the gain of $\partial F/\partial P_{fs}$ results in only a 10-percent
change in the stability margin. The system is slightly more stable if the
gain of $\partial \dot{\omega}_{od}/\partial P_{os}$ is increased. This is best understood by comparing Fig. 33
which shows that increasing this gain increases the feedline damping, thus
decreasing the total loop gain.

The effect of the portion of the loop involving the LOX tank bottom is
only partially revealed in Fig. 34. This figure indicates that the change
in the gain (K) of LOX tank bottom acceleration has a small effect compared
to a change in the gain (1/M). However, the actual value of 1/M was deter-
mined from flight data, as was the resonant frequency of the structure.
These flight data represent system response resulting from the total struc-
ture such that the influence of the LOX tank bottom is partially accounted
for in the values of 1/M and ω_1. The significance of the value of K, or h_t,
on the stability must, therefore, be qualified. The result of Fig. 34 means
that if the gain of the structure at the cruciform beam could be kept at
the same level, and the transmission of the gain through LOX tank bottom
acceleration to the fluid could be independently reduced, then the effect
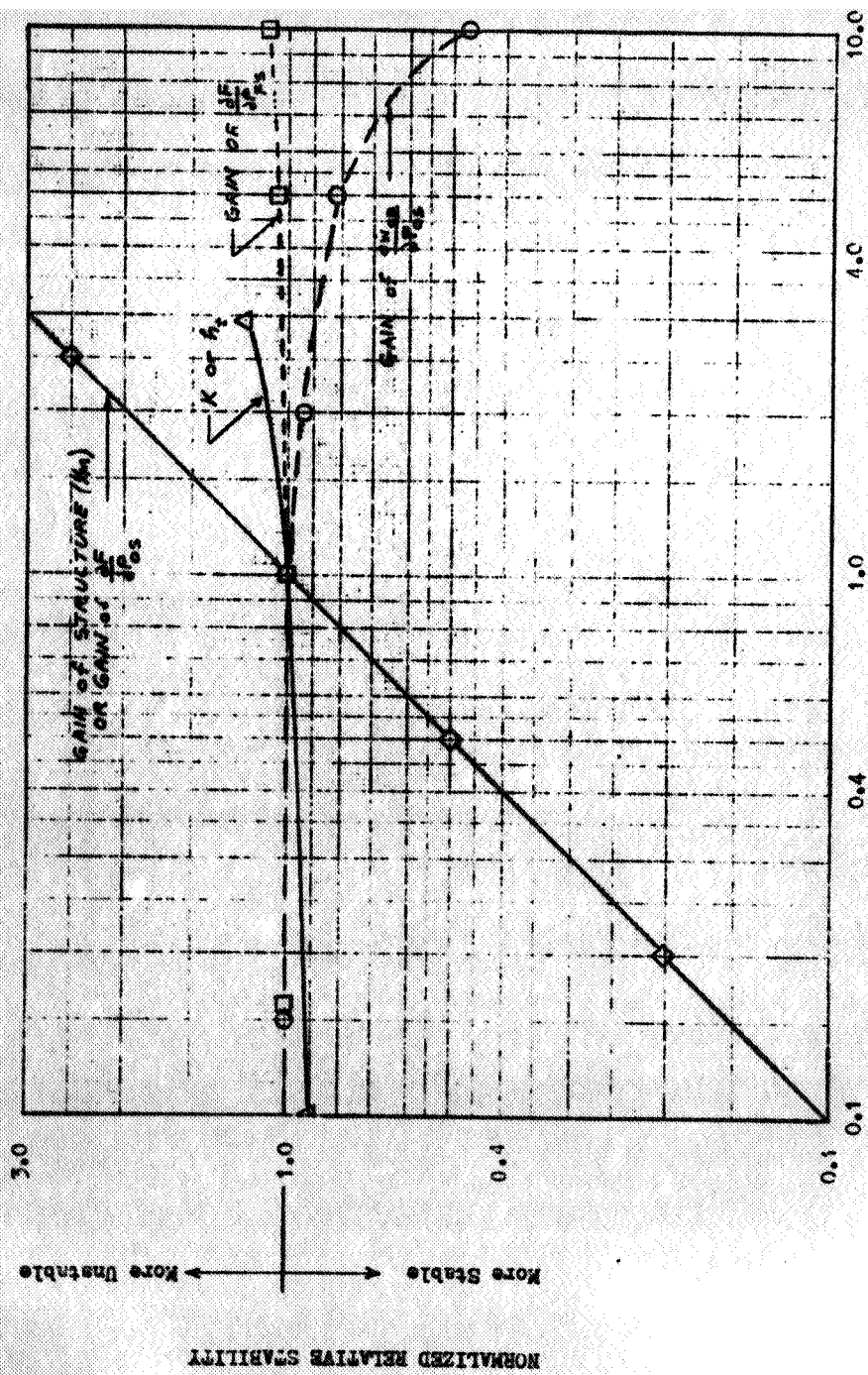
Figure 34. Analog Model Results, Effect on Stability of Various Parameter Gains

of the reduction would be as shown. Or, stated more simply, the system could be unstable with no tank bottom acceleration if the cruciform beam has large acceleration.

The next parameter to be considered is the LOX pump inlet compliance, B_1. The reference value used, $B_1 = 180$, was considered to be an upper bound, thus only lower values were investigated. The effect on stability of B_1 is shown in Fig. 35. As B_1 decreases, and in accordance with Eq. 16 the feedline resonant frequency decreases, the system becomes more unstable. The instability occurs at or very near the structural resonant frequency which for the model at this time is very nearly 15.9 Hz. The maximum instability of Fig. 35 occurs when $B_1 = 30$, $f_\ell = 15.9$ Hz; i.e., when the feedline resonance and structural resonance are the same. As the feedline resonance drops below the structural resonance, the system rather rapidly gets more stable. This stability is primarily achieved through the phase relationships around the loop. On flight 504, the actual instability occurred at 17 Hz, thus the feedline resonance would have to drop a few Hertz below this value to achieve stability. One means often used to reduce the feedline resonance below the structural resonance is to add an accumulator to the feedline (Ref. 2).

One further effect was noticed using the single inertance-compliance for the feedline dynamics. The portion of the loop from $\ddot{x}_5$ through to F appeared to have a larger gain than was seen in flight. This is indicative that there are either nonlinearities in the system which are not in the model, and/or the feedline dynamics are not adequately described by such a simple model. A more complex model was introduced and is described below.

The phase angles of the two engine transfer functions were also varied with the results shown in Fig. 36. Varying the phase of $\partial P_c/\partial P_{os}$ does not render the system significantly more unstable, but large changes in the phase angle can render the system phase stable. There are regions of
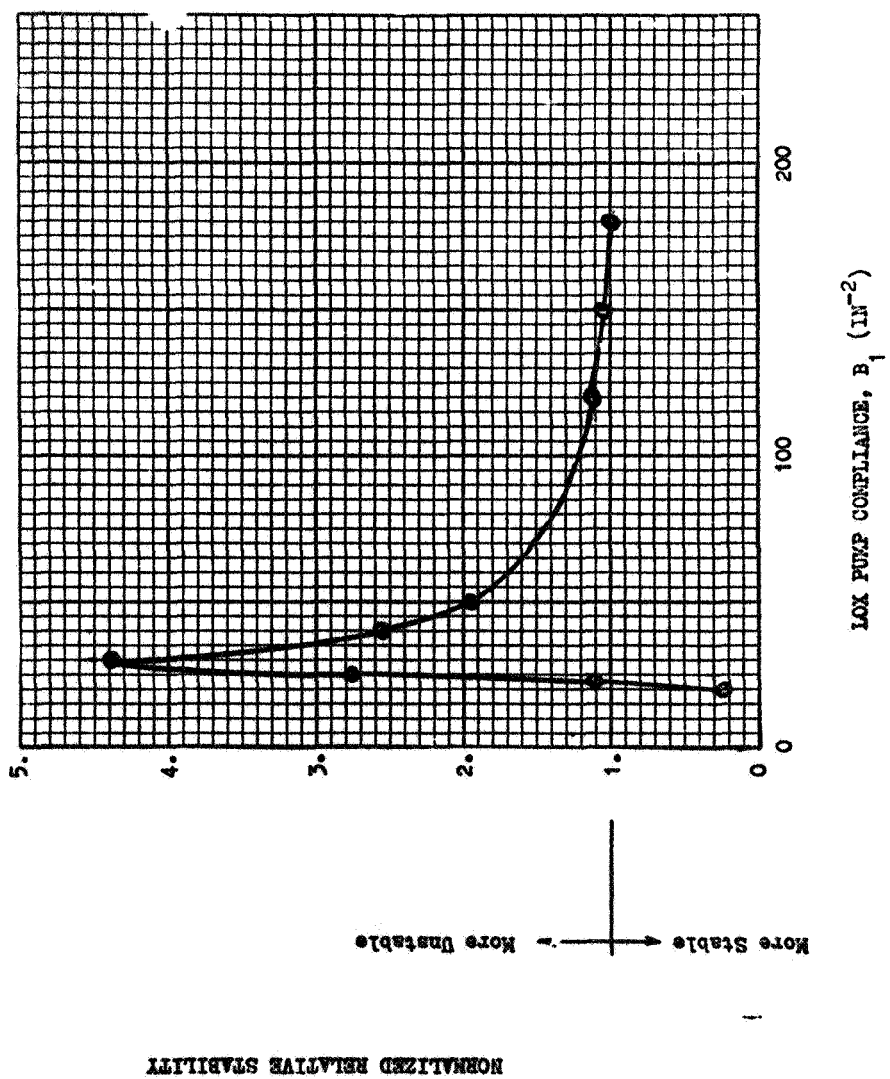
Figure 35. Analog Model Results, Effect on Stability of LOX Pump Inlet Compliance
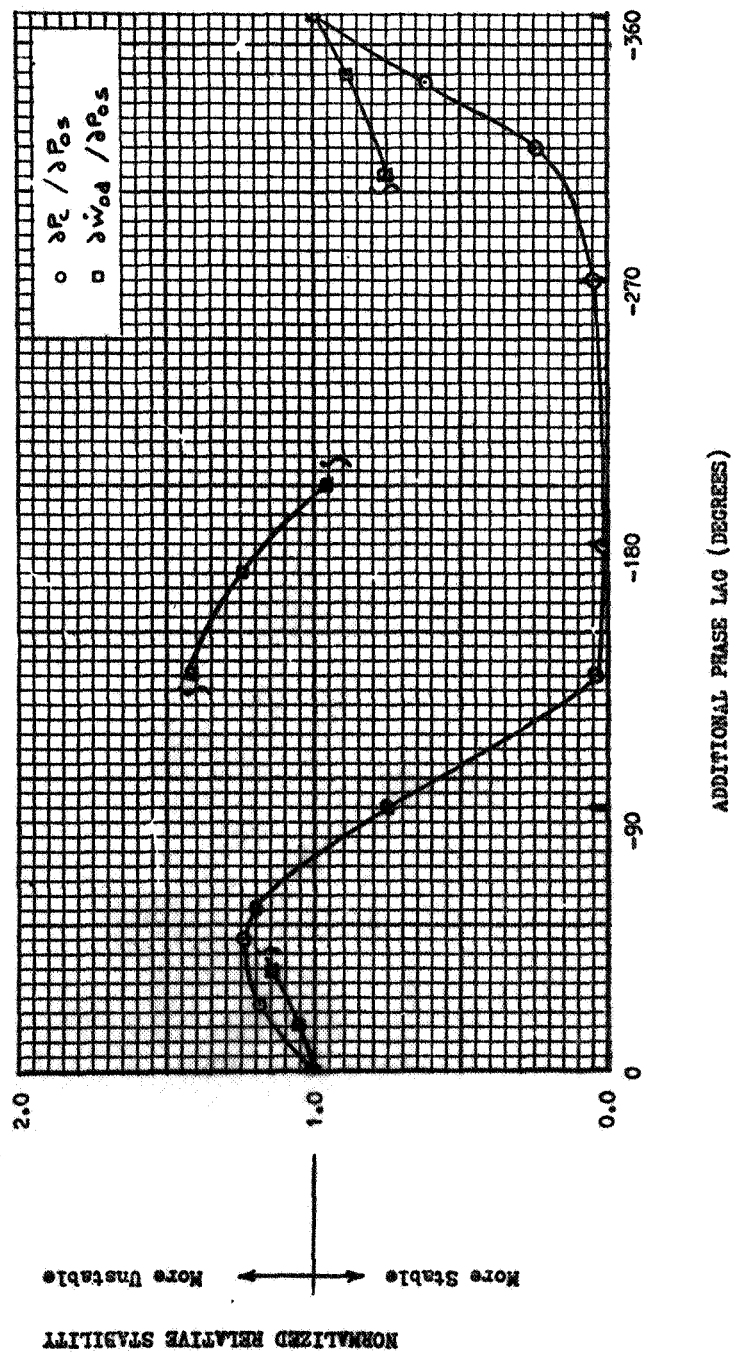
Figure 36. Analog Model Results, Effect on Stability of Adding Additional
Phase Lag to Engine Transfer Functions

phase lag in which the effect of $\partial \dot{w}_{od}/\partial P_{os}$ is not shown because the feed-line has its own instability, at a higher frequency, in these regions. This instability is not necessarily a characteristic of the engine system or of flight at all, but only a characteristic of the particular curve fit used for the transfer function and the simplifications used in the analog model. In these regions, the feedline appears to have little, or no, damping, but this condition is obviously not a flight characteristic.

Updated Analog Models. As analysis of flight and ground data continued, information was obtained concerning the structure and the feedline dynamics which was incorporated into the analog model. Some of these variations were made simultaneously, others being added individually. The various changes will be described, and their effect presented in chronological order.

The structural data presented in Fig. 30 were changed so that the model was in better agreement with the flight data. The new model representations are shown in Fig. 37. Using these new data, the model resulted in a system instability at a later time, the instability occurring at approximately 500 seconds RT, just past the peak in the gain curve. This time of instability corresponds much closer to that of flight.

The inlet line compliance, B_1, is primarily associated with cavitation at the turbopump inlet. Thus, the value of B_1 is characteristically represented as a function of the steady-state NPSH value. To attempt to model this type of behavior during the large variations associated with the instability, the magnitude of B_1 was made to vary with the instantaneous value of NPSH rather than the steady-state value. $\left|\text{NPSH, the net}\right.$ positive suction head, is given by: $\text{NPSH} = 144 \ (P_{os} - P_v)/\rho$, where P_{os} is total inlet pressure, P_v is the vapor pressure, and ρ the specific weight. $\left.\right|$ The magnitude of B_1 varied linearly from a value of zero at $\text{NPSH} = 0$ to some predetermined value at $\text{NPSH} = 60$ feet. The predetermined value was varied to determine its influence on system stability.
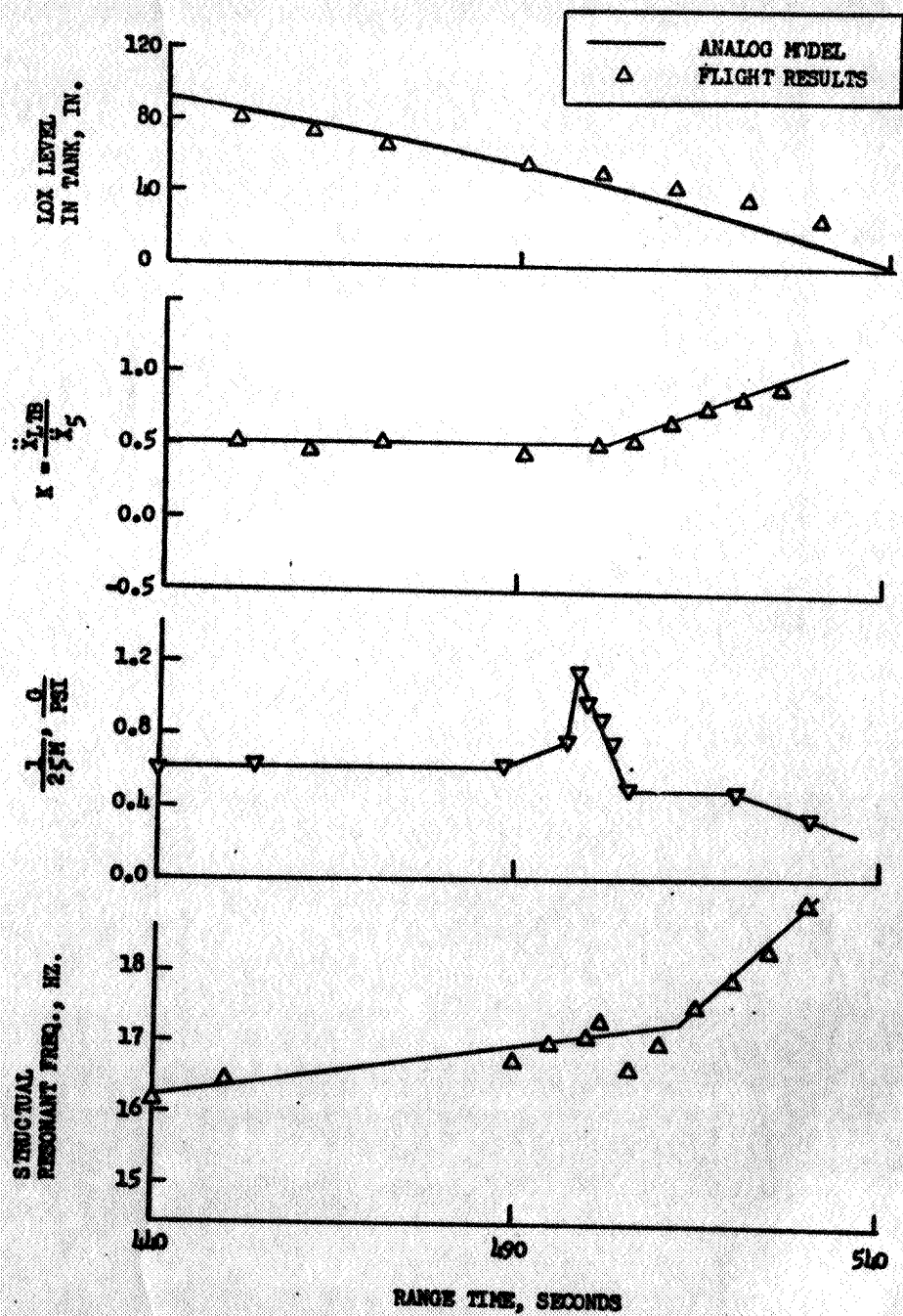
Figure 37. Analog Model Time Variant Parameters

The above variation of B_1 acts as a nonlinearity in the system. Its effects were threefold. First, the nonlinearity acted to limit the amplitudes during the instability although the limiting was not as pronounced as indicated in the flight data. Secondly, the frequency of the instability dropped a few tenths of a Hertz as the amplitudes began to diverge during the instability. A similar drop in the frequency was noted in the flight data. There is some indication that the drop in frequency could be caused by a shift in the structural mode at which the instability occurs, but the model does demonstrate that the shift could be explained by the nonlinear behavior of B_1. The third effect of B_1 was the change in the wave shape of the oscillations. These tended to be flattened out on the bottom with sharp peaks at the maximum values.

Data from ground tests were obtained to determine the value of B_1, or if a single compliance was not sufficient, to determine the required dynamic description for the turbopump termination to the feedline. Data indicated that there are two resonances required in this dynamic description. There are several dynamic models which could be used to match the data. The dynamic model used in the analog model represents a side branch associated with the turbopump. The electrical analog of this model is shown below with current expressed as weight flowrate and voltage as pressure.
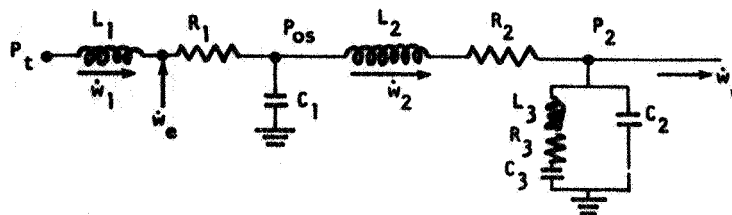
where R_i = resistance, L_i = hydraulic inertance, C_i = hydraulic compliance, $\dot{w}$ = weight flowrate, $\dot{w}_e$ = external input flowrate, and P is pressure. The physical interpretation of the model is as follows: with P_t = tank pressure and P_{os} = pump inlet pressure, L_1 and R_1 are the properties of the

feedline duct. C_1 is primarily the pump inlet compliance similar to $1/B_1$ with the simple model. L_2 and R_2 represent the inducer, and P_2 is the pressure downstream of the inducer. The side branch is represented by L_3, R_3, and C_3 and is only defined as being internal to the turbopump. C_2 is a very small compliance and need not be included. The flowrate $\dot{w}_d$ is the pump discharge flow.

Both tank pressure, P_t, and $\dot{w}_e$ are functions of the structural acceleration.

$$P_t = \rho \frac{h_t}{g} \ddot{x}_{LTB} \tag{17}$$

$$\dot{w}_e = \rho A \frac{\ddot{x}_5}{S} \tag{18}$$

The magnitudes of the dynamic parameters are shown in Table 3, and at the bottom of the table the resonant and antiresonant frequencies of the inlet pressure relative to acceleration are shown. The Bode plot of $P_{os}/\ddot{x}_5$ for case 2 is shown in Fig. 38. To obtain the results of Table 3 and Fig. 38 above 25 Hz, the transfer function $\partial \dot{w}_{od}/\partial P_{os}$ had to be arbitrarily extended because no test data were available above 25 Hz. The extension tended to continue the curves for $\partial \dot{w}_{os}/\partial P_{os}$ shown in Fig. 31 so that at 40 Hz the gain was 0.323 and the phase was -36 degrees. The only reason this arbitrary extension could be used was because of its relatively minor role in the overall feedline dynamic behavior. No similar extension could be applied to $\partial P_c/\partial P_{os}$ because it plays a major role in the system dynamics. (The comparison of these responses to test data is reserved for a later section.) The total impedance of the branch is given by

$$Z_B = \frac{P_2}{\dot{w}_2 - \dot{w}_d} = \frac{1 + SR_3 C_3 + S^2 L_3 C_3}{S(C_3 + C_2) + S^2 R_3 C_3 C_2 + S^3 L_3 C_3 C_2} \tag{19}$$

The analog model diagram using this more extensive feedline dynamic representation is given in Fig. 39.

TABLE 3

DYNAMIC PARAMETERS AND VARIABLES, LOX FEEDLINE
THREE-COMPLIANCE MODEL

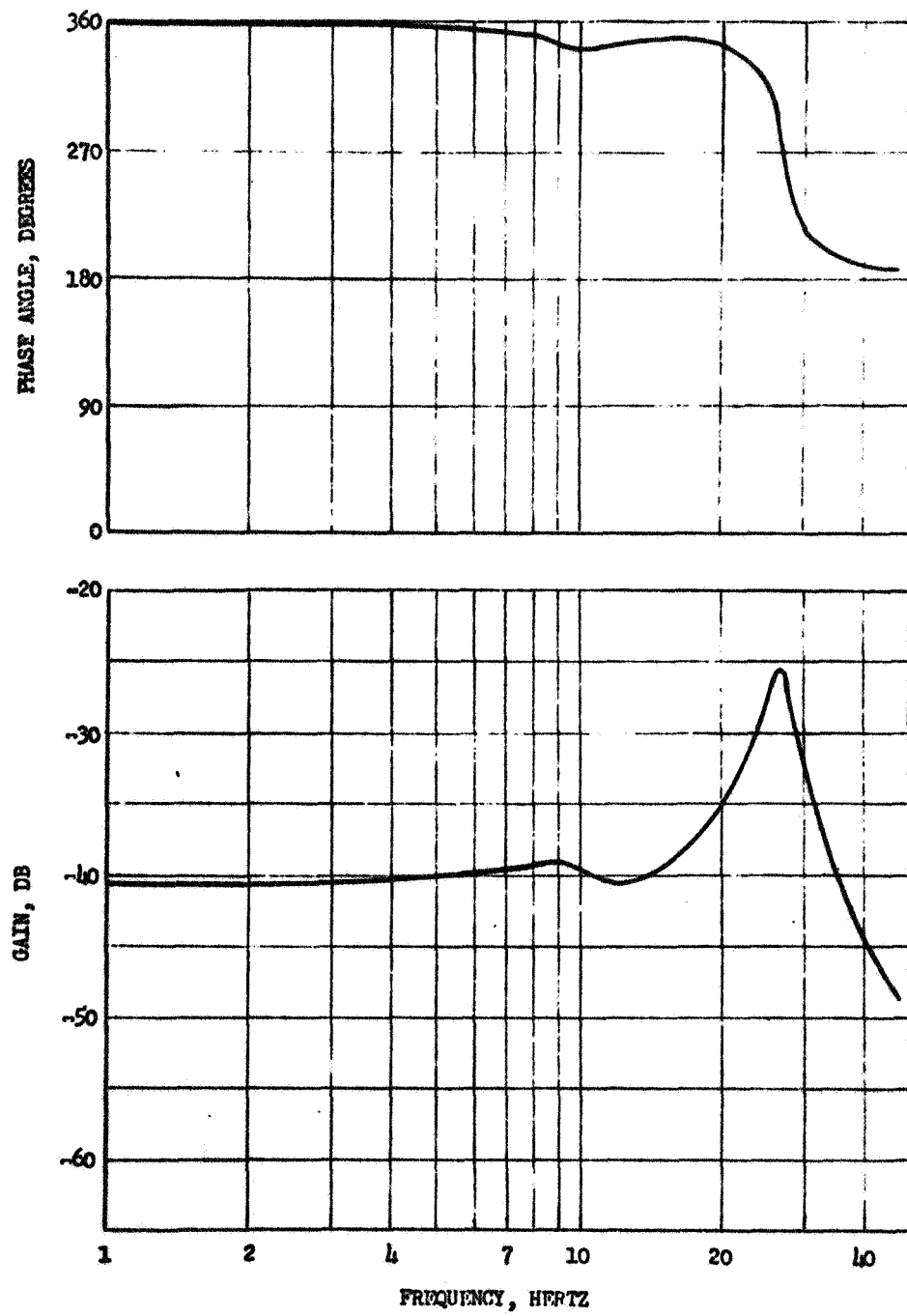| Parameter	Case No.			
	1	2	3	4
L_1, $(sec/in.)^2$	0.003 ———————————————————→			
R_1, $sec/in.^2$	0.0133 ——————————————————→			
$B_1 = 1/C_1$, $in.^{-2}$	150	75 ———→		37.5
L_2, $(sec/in.)^2$	0.0025 —————————————→			
R_2, $sec/in.^2$	0.36 ———————————————————→			
$B_2 = 1/C_2$, $in.^{-2}$	1000 ——————————————————→			
L_3, $(sec/in.)^2$	0.02 ————————————→			
R_3, $sec/in.^2$	0.3			
$B_3 = 1/C_3$, $in.^{-2}$	100 ————→		50 ————→	
f_1 = first resonance*, Hz	~8.5	~8.5	~6.0	~6.0
f_2 = first antiresonance*, Hz	~12.0	~12.0	~9.0	~8.5
f_3 = second resonance*, Hz	~37.5	~27.0	~27.0	~19.0

*From $P_{o3}/\dot{x}_S$

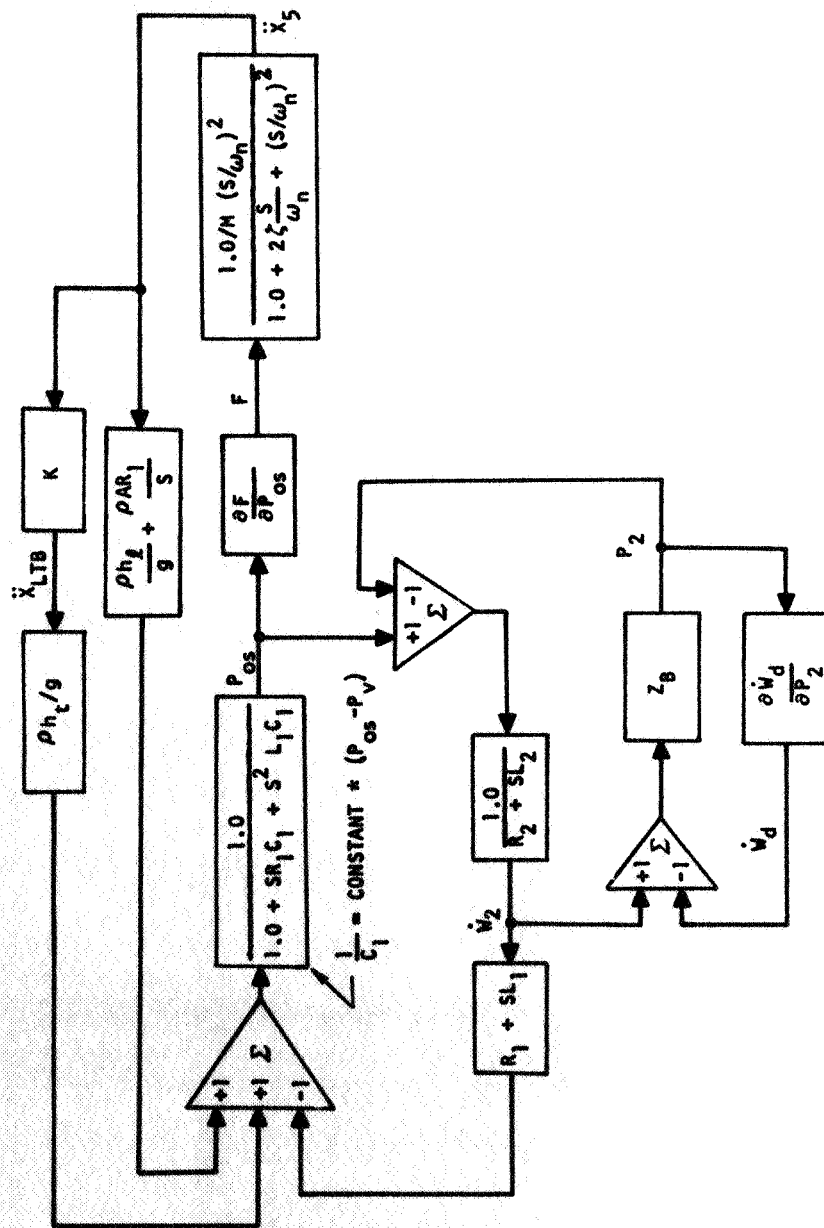Figure 38. Analytical Transfer Function, $P_{os}/\dot{x}_5$

Figure 39. Analog Model Diagram

The results of the closed-loop model analyses with this model were
similar in many respects to the results from the more simple model.
The loop was unstable at approximately the same range time and became
stable again toward the end of burn. The first compliance, C_1, or its
inverse B_1, was a function of the instantaneous pressure P_{os}, thus rep-
resents a nonlinearity in the system. The influence of this nonlin-
earity has already been discussed. One significant improvement in this
model is that the gain of thrust relative to $\dot{X}_5$ agrees much better with
the flight data. It was previously noted that in the simple model this
open-loop gain was much too high. This improvement is probably effected
by the ability of the side branch to receive flow, decreasing the flow
to the thrust chamber.

Parameter influences on stability were studied, varying in this updated
model only those parameters associated with the feedline and pump.
Figure 40 shows the influence on stability of the first compliance, B_1
($=1/C_1$). This effect is very similar to the effect of B_1 in the initial
model as seen by comparing Fig. 40 and 35. In Fig. 41 the effect of the
branch compliance, B_3 is shown. Its effect is not as large as that of
B_1 especially in the region $B_3<200$ which is the more reasonable range
of variation of this parameter. The influence of the inertance param-
eters is shown in Fig. 42. The most significant variable for the inlet
line is, thus, the inlet compliance, B_1. Actually, the effect of L_1
was not calculated because it would have a very similar effect as B_1
because the two determine the more significant inlet line resonance.

The next change made in the analog model was to use four structural
modes rather than a single mode and to extend the model to cover the
entire burn time of S-II. These four modes were determined from flight
data and were discussed previously. The frequency and gain characteris-
tics as a function of range time for the four modes were presented in
Fig. 10 and 12. Each mode was assumed to have 1.5 percent of critical
damping. Thus, in the analog model each mode is represented in the
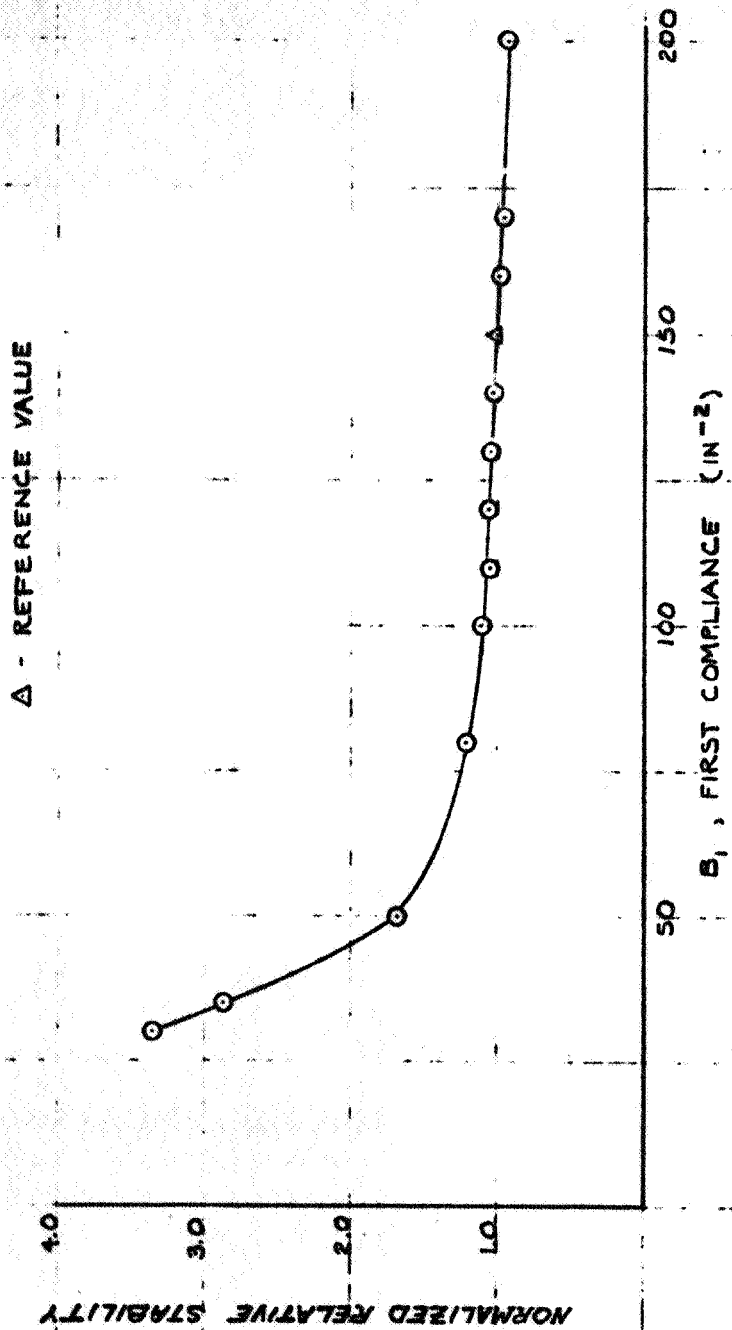same manner as the single mode was represented in Fig. 39 .

Figure 40. Analog Model Results, Effect on Stability of First Compliance Using a Double Compliance Model
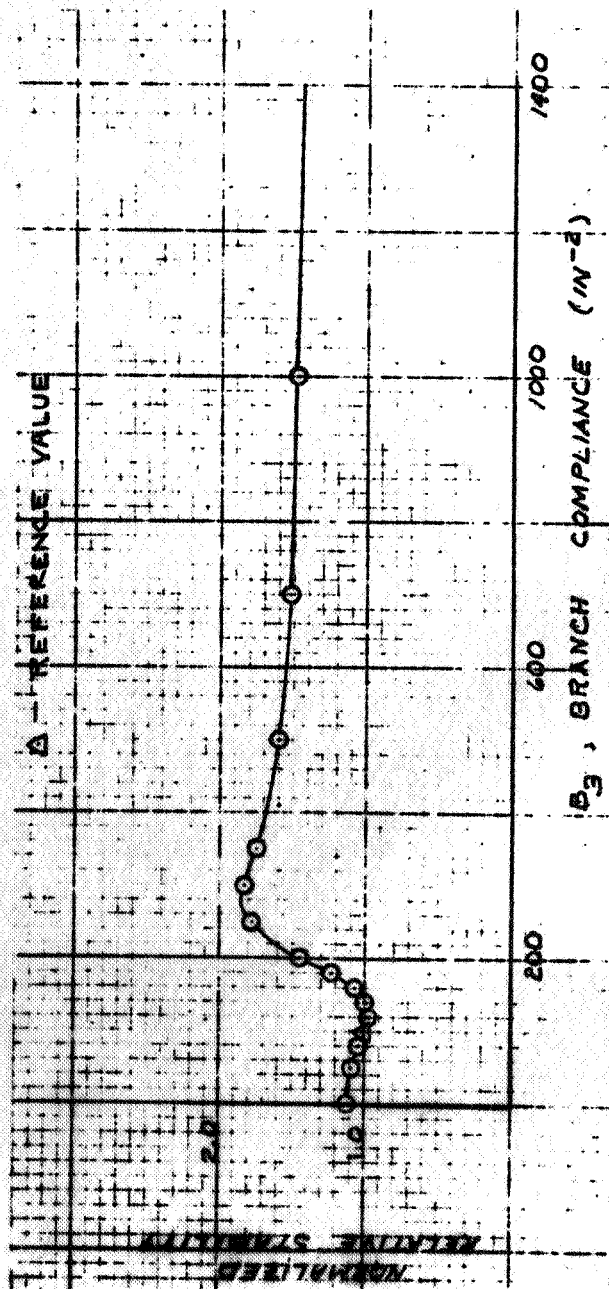
Figure 41. Analog Model Results, Effect on Stability of Branch Compliance Using a Double Compliance Model

Figure 42. Analog Model Results, Effect on Stability of Inertances Using the Double Compliance Model

Using the four structural modes, the system goes unstable at approximately 484 seconds RT, generally reaching a limit cycle, and then the instability ends around 515 seconds RT. The peak amplitude was reached at 500 seconds RT. Figure 43 shows some typical results in the region of the instability. Note that the paper speed is varied over two regions to permit a count of the frequency of the oscillations. The amplitudes in Fig. 43 are about one-half of those in flight 504, but the maximum amplitude observed in the instability is very sensitive. This was noticed to be especially true with regard to changes in B_1, the pump inlet compliance. The B_1 value used to obtain Fig. 43 was approximately 110 in.$^{-2}$. If B_1 is reduced even a few percent, the maximum amplitude increases significantly.

Because the full burn time is incorporated into the model and the various structural modes are represented, the margin of stability at other times in flight can be calculated. Of course, this margin of stability at any given time is only as good as the representation of the various elements at that time, and the confidence in the gains for the structural modes is particularly low. Nevertheless, the analysis was performed, and the results are presented in Fig. 44. These results indicate that the system is at most only a few db stable throughout the burn time. The frequency noted along the curve of Fig. 44 indicates that the mode closest to being unstable changes from the third to the second mode as defined in Fig. 10.

The one other analysis performed using this variation of the analog model was to establish the effect on the stability margin of variations in the inlet compliance, B_1, and the branch compliance, B_3. These results are shown in Fig. 45. The results are very similar to those of Fig. 40 and 41 which were determined using only a single structural mode.

One of the suggested means of eliminating the 17-Hz oscillations was to add a gas-filled accumulator to the LOX center-engine feedline. Assuming
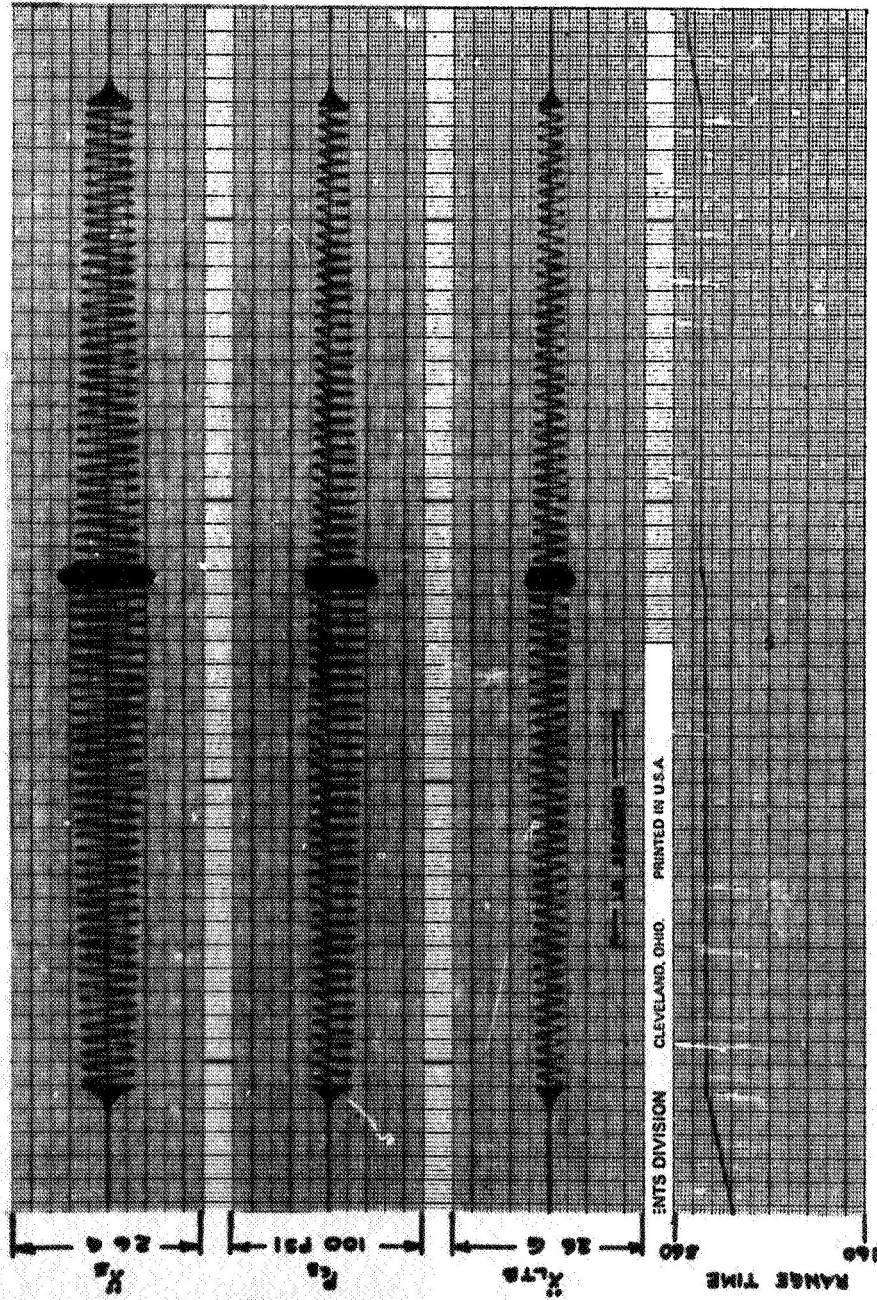
Figure 43. Analog Model Results

R-7970
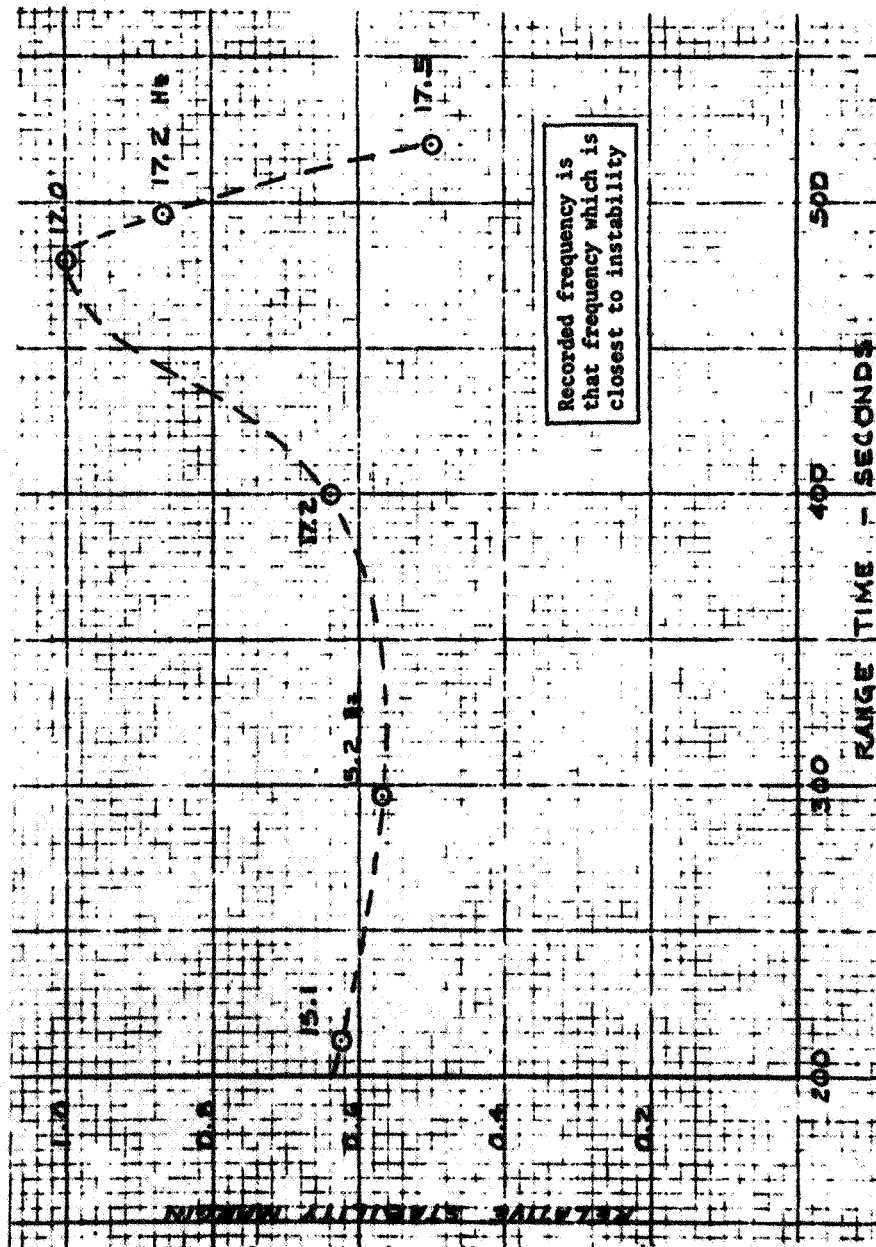
Figure 44. Analog Model Results, Relative Stability Margin vs Range Time

- Model uses double compliance feedline-pump dynamic representation
- Model uses four structural modes constructed from flight data
- Relative stability determined at 480 seconds range time

△ - B_1 = inlet compliance (with B_3 = 100)
⊙ - B_3 = branch compliance (with B_1 = 150)
▲,● = reference values

B = COMPLIANCE — IN^{-2}

RELATIVE STABILITY MARGIN
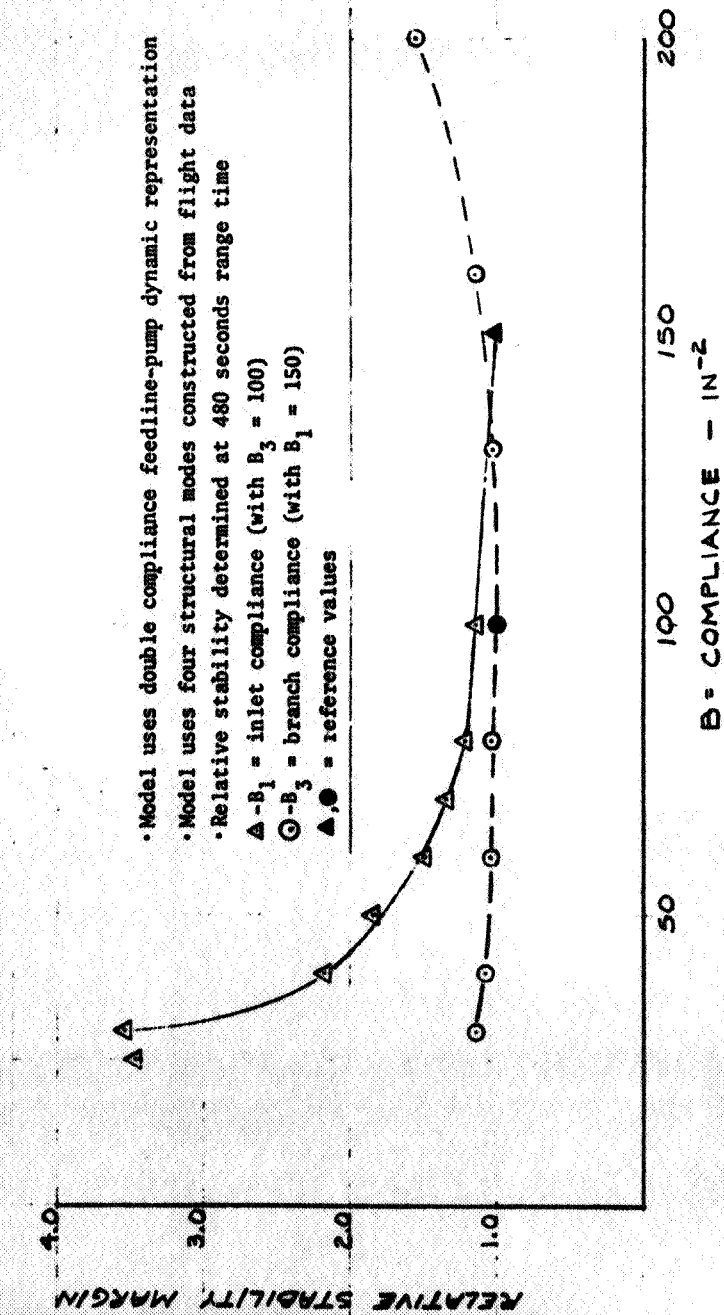
Figure 45. Analog Model Results, Effect on Stability of Pump Compliances

96

that the accumulator was placed at the pump inlet, the feedline-pump dynamic model would appear as represented below. The accumulator appears as
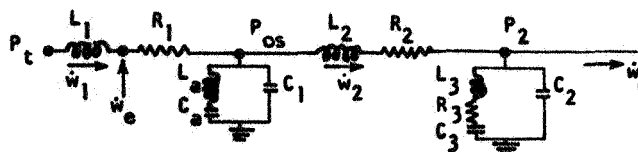
a side branch with an inertance, L_a, and a compliance, $B_a = 1/C_a$. The design objective for the accumulator is to fix its resonant frequency ($f_a = \sqrt{B_a/L_a}/2\pi$ Hz) at, or near, the frequency which is to be eliminated. Because the accumulator is a branch on the line, its resonance acts as an antiresonance for the main line. The important characteristic of the accumulator is then its resonance.

Initial concepts for an accumulator on the S-II feedline consisted of a helium gas volume of approximately 200 in.[3] connected to the main duct by 30 holes of 1/2-inch diameter and 0.07-inch length. Using these values, the accumulator characteristics were calculated

$$L_a = \frac{0.07 + 16\,(1/4)/3\pi}{\frac{\pi}{4}\left(\frac{1}{2}\right)^2 *386 * 30} = 2.17 * 10^{-4} \text{ (sec/in.)}^2$$

$$B_a = \frac{1.66\,(40)\,1728}{70\,(200)} = 8.2 \text{ in.}^{-2}$$

$$f_a = \sqrt{8.2/2.17 * 10^{-4}}/2\pi = 31.0 \text{ Hz}$$

where the static inlet pressure was assumed to be 40 psia. This frequency is higher than 17 Hz so was treated as an upper limit of the resonance, and this and lower values were used in the analog model. Using this accumulator eliminated the instability completely. The branch inertance was increased to determine at what value the instability returned.

Raising the inertance, of course, results in a lower resonant frequency
and makes the accumulator less effective at higher frequencies. It was
found that the inertance could be increased by a factor of over 20.0, or
that the accumulator resonant frequency had to drop below about 7.0 Hz,
before the instability reappeared. Thus, the inlet line accumulator can
stabilize the system based on current knowledge of the system components
by developing a system antiresonance which reduces the gain of the closed
loop.

A comparison of the effect of the accumulator on the feedline resonances
is of interest. Table 3 had presented the resonances and parameter values
without an accumulator. Table 4 presents the first two cases with the
accumulator. Figure 46 presents the Bode plot of $P_{os}/\ddot{x}_5$ for case 2 with
the accumulator and can be compared with Fig. 38.

TABLE 4

ANALYTICAL LOX FEEDLINE RESONANCES WITH AN ACCUMULATOR

Parameter	Case No.**	
	1	2
First Resonance, Hz*	7.5	7.5
First Antiresonance, Hz*	31.0	31.0
Second Resonance, Hz*	>50.0	>50.0

*From $P_{os}/\ddot{x}_5$

**Same cases as presented in Table 3 except
 accumulator added

This concluded the analytical effort using the analog computer model.
If more exact information becomes available concerning the feedline-pump
dynamics and the structural modes, further work would be performed to
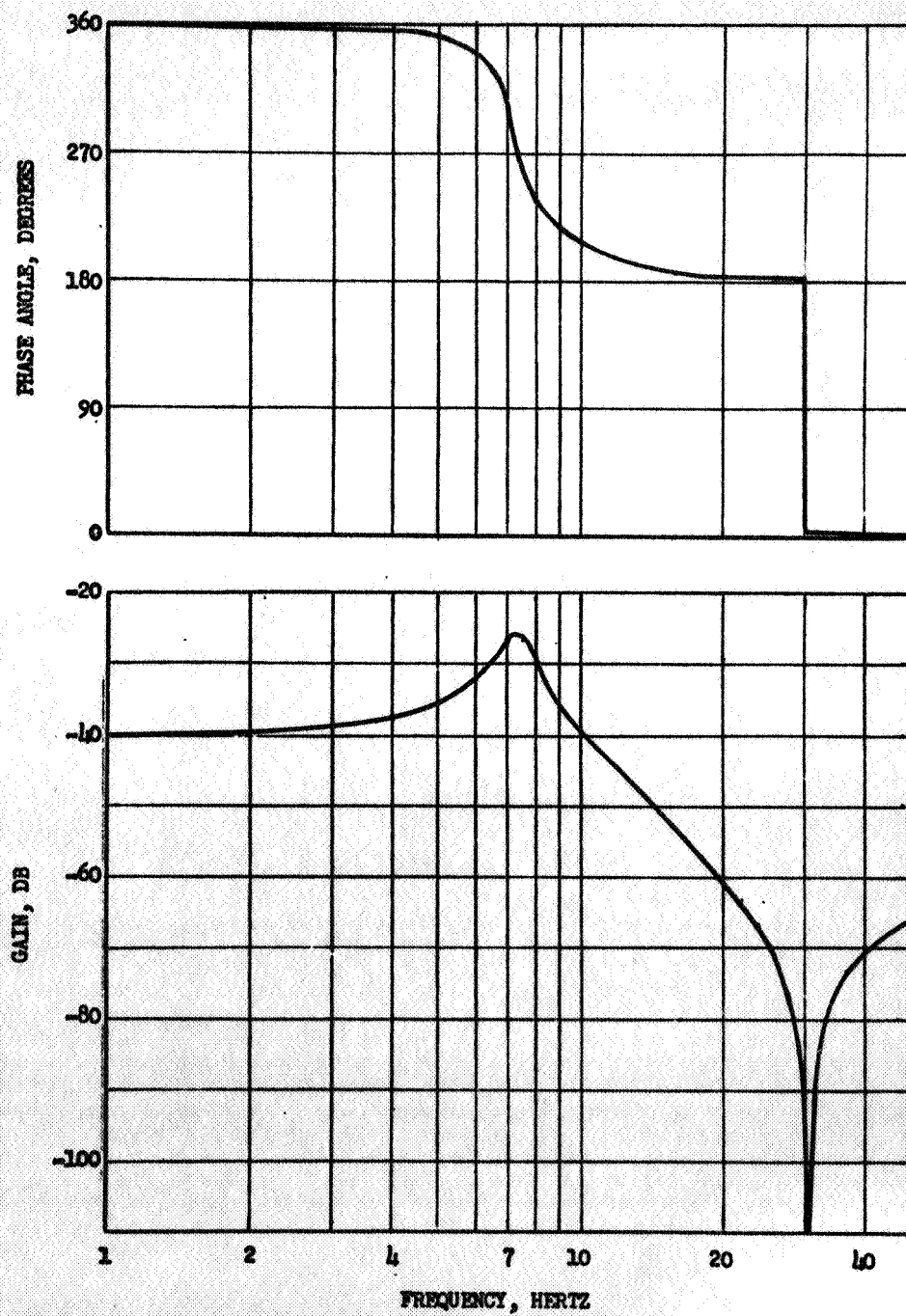analyze more completely the system dynamic response.

Figure 46. Analytical Transfer Function, P_{os}/X_5, With Accumulator

LOWER FREQUENCY OSCILLATIONS

There are two frequencies below the 17- to 18-Hz frequency which are generally present in several of the parameters during the S-II burn time. These two are (1) the subharmonic of the 17- to 18-Hz data, and (2) a 10- to 11.5-Hz oscillation. These two lower frequencies have not been characterized by large amplitudes in any particular parameter, but they are the frequencies which are transmitted to the command module and are felt by the astronauts during S-II boost. (The 17- to 18-Hz oscillations are not seen in the command module data.)

These two frequencies are in the frequency range of the first three structural modes predicted by NAR Space Division prior to flight AS-504. These first three modes are shown in Fig. 47. The oscillations at the 10- to 11.5-Hz frequency are suspected to be the ringing of the structure at the second or third mode resonant frequency. The oscillations at the subharmonic are probably generated by sloshing in the LOX tank, the sloshing frequency of a liquid in a tank being frequently at the subharmonic of the frequency of longitudinal vibration of the tank bottom according to Ref. 1.

On flight AS-501, the body modal radial aft and forward skirt accelerometers showed a subharmonic of the 17- to 18-Hz oscillations starting at RT 450 seconds and lasting until 500 seconds. Comparison of these times with Fig. 20 reveals that these subharmonic oscillations were present throughout the time of the largest oscillations at 17- to 18-Hz. The body modal longitudinal aft skirt accelerometer also experienced the subharmonic oscillation beginning at approximately 480 seconds RT, but this accelerometer response shifted to 10.5 Hz at 510 seconds, probably representing the second structural mode. At the same time, the body modal lateral aft skirt accelerometer changed from the subharmonic frequency to a 7-Hz frequency, probably representing the first mode of the structure.
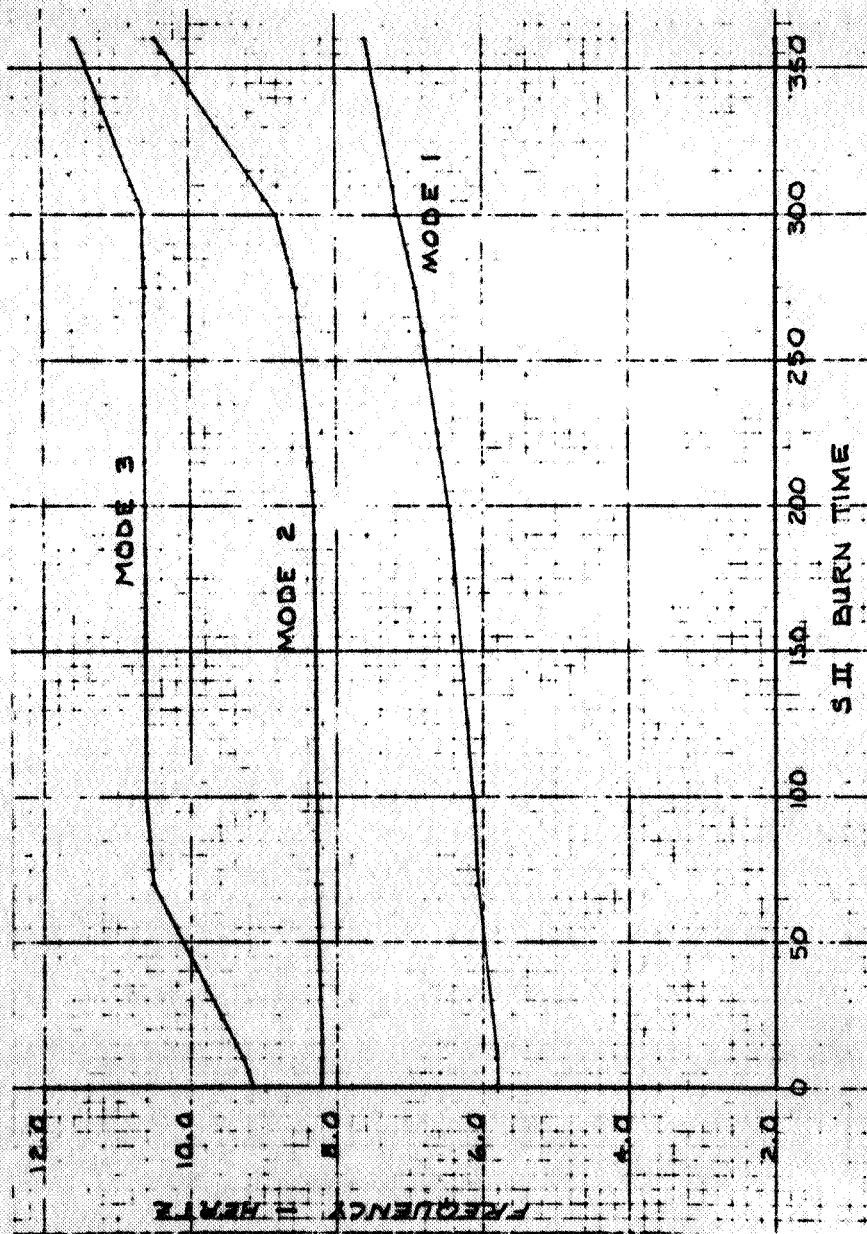
Figure 47. Structural Resonant Frequencies Predicted for AS-504

On AS-503, the accelerometers at LOX tank bulkhead, engine 1 and 5 thrust pads, and body modal longitudinal at forward and aft skirts show a pre-dominant frequency of 11.5 Hz early in the S-II burn time (370 seconds RT). Beginning at 450 seconds through 490 seconds, the 17.5-Hz oscillation and its subharmonic were apparent in the accelerometer data. These accel-erometers had the roll-off characteristic which strongly attenuated the 17.5-Hz amplitude so that it did not appear to predominate as much as it did on the engine pressure data. This is illustrated in Fig. 48 which shows the frequencies of LOX pump discharge pressure on engine No. 5 and the acceleration at the LOX tank bottom for various times. Then, as time increases, the 10.5- to 11.0-Hz frequencies again become predominant.

On AS-504, the 9- to 10-Hz oscillations were apparent on some accelerom-eters prior to the buildup of the 17-Hz oscillations; these earlier oscil-lations are shown in Fig. 49. After the 17-Hz oscillations became so large, the subharmonic was predominant in the skirt accelerometers and the 17-Hz data in the engine and tank bottom accelerometers as shown in Fig. 50. Figure 51 shows the engine No. 5 chamber pressure measurement filtered from 5 to 12 Hz. The 17-Hz data are still very apparent although atten-uated because they are beyond the range of the filter. However, the pri-mary interest in Fig. 51 is the data at approximately 516 seconds RT which have every other cycle at a low amplitude, probably indicating the presence of the subharmonic.

Because the subharmonic frequency is related to the 17-Hz frequency, elim-ination of the latter will also eliminate the former. However, the 10.0- to 11.5-Hz data have no apparent relationship to the 17-Hz data.

ENGINE STRESS AND RELIABILITY PERFORMANCE

All of the components in the J-2 LOX high-pressure system from the turbo-pump to the thrust chamber were reviewed to determine the allowable pres-sure amplitude at 18 Hz for safe operation for 365 seconds. The results

AS-503 shows strong 10- to 11-Hz oscillations (400 to 520 seconds range time) in:

LOX tank bulkhead
Engine No. 1 thrust pad
Engine No. 5 thrust pad

Body modal longitudinal forward skirt
Body modal longitudinal aft skirt
Command module

AS-503 shows one-half 18-Hz oscillations (488 to 494 seconds range time) in:

LOX tank bulkhead
Command module
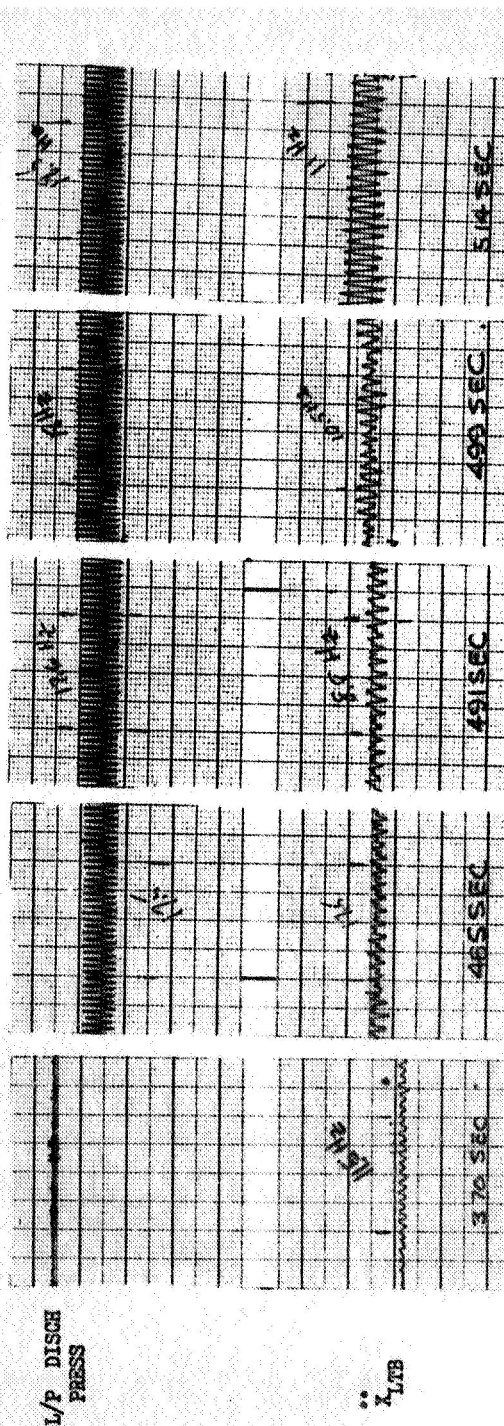
Figure 48. AS-503 S-II 18-Hz Oscillations
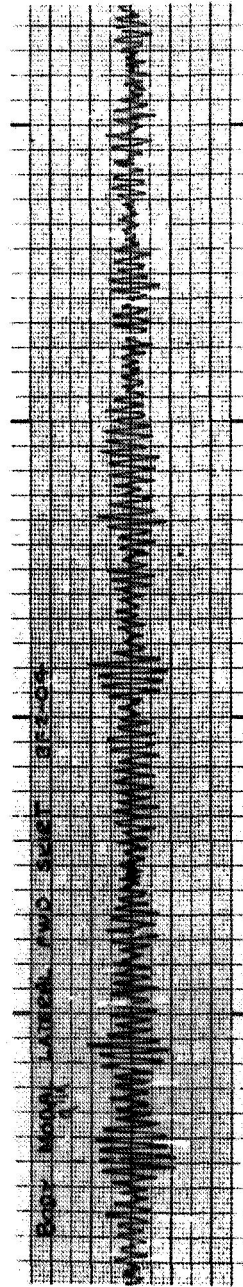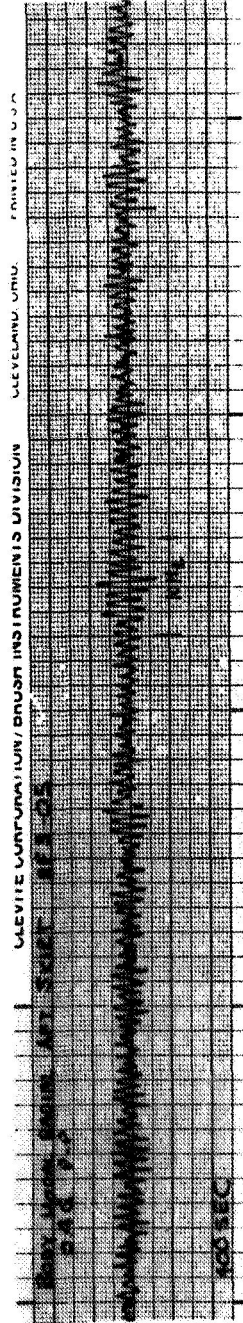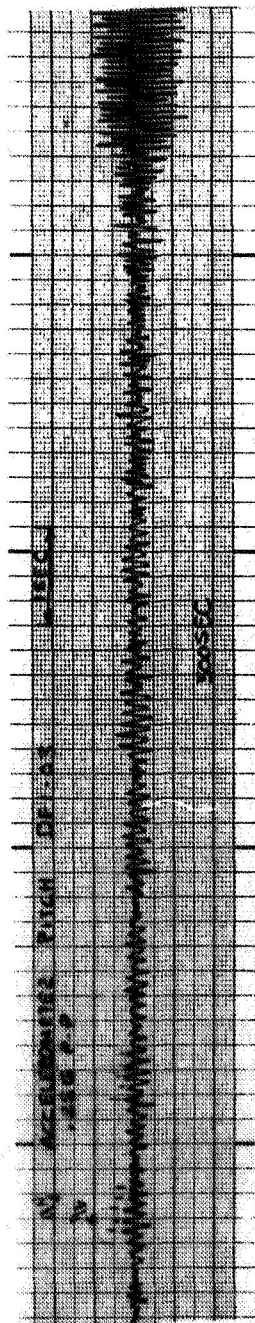
Figure 49. AS-504 S-II 17-Hz Oscillations (Low-Frequency Oscillations 9 to 10 Hz Prior to 17-Hz Instability)

Unfiltered oscillogram BF2-02, body modal radial aft skirt, shows

8.8 to 9.5 Hz from 517 to 528 seconds range time,

exactly 1/2 the 17-Hz oscillation $\dot{x}_5$ same time period.

Amplitude = 0.075 G p-p (no correction for roll-off)
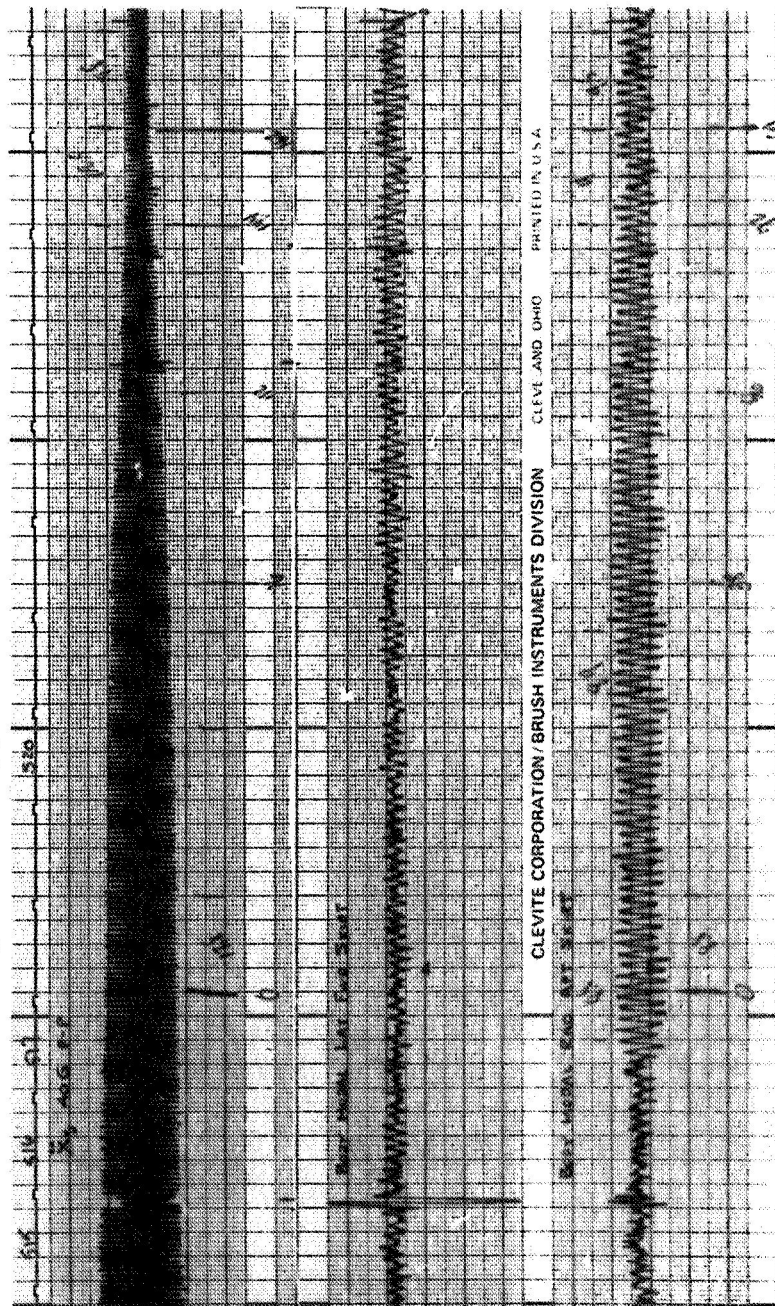
Figure 50. AS-504 S-II 17-Hz Oscillations

P_{c5} filtered 5 to 12 Hertz, bandpass 515 to 518 seconds every other cycle is low amplitude; may indicate 1/2 frequency in P_{c5}

Figure 51. AS-504, S-II 17-Hz Oscillations

R 7970
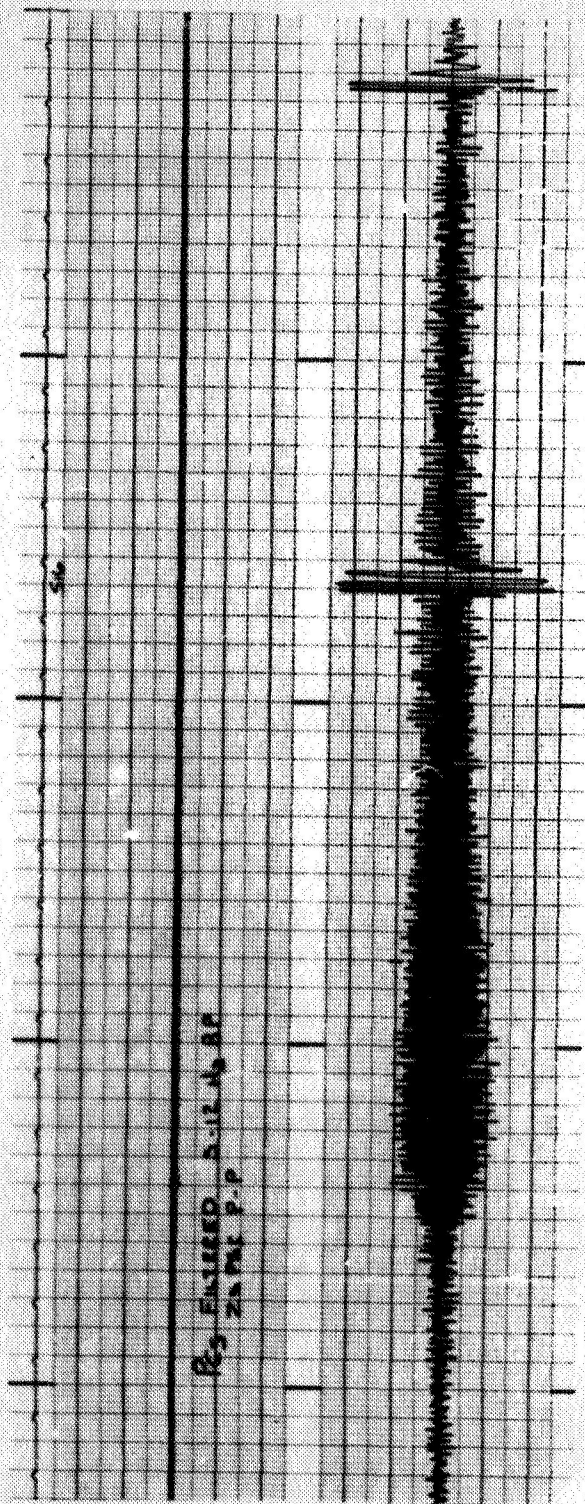
of this analysis are given in Table 5 . All components are safe u der
the loading of flights AS-503 or -504, the thrust chamber assembly having
the lowest margin of safety.

A shift in engine No. 5 performance during the 18-Hz oscillations has
already been discussed. The performance shift appears to be a result of
cavitation at the LOX pump inlet with no other detrimental effects from
the large oscillation amplitudes. If the chamber pressure oscillations
exceeded 100 psi, p-p, adverse combustion phenomena could occur; e.g.,
main chamber injector degradation or gas generator flameout.

The one other area investigated relative to engine reliability was the
ability of the engine to withstand the longitudinal g levels experienced
in flight and the margin of safety. The only actual data available are
the flight data which indicate that the engine can successfully withstand
g levels as large as 24 g, p-p, for a short duration. A Rocketdyne
study indicates that the J-2 engine is capable of withstanding 40 g,
p-p, in the longitudinal direction at 17 Hz. This study included the
major components with the limiting component being the electrical control
package mount strut. A factor of safety of 1.5 was maintained on all of
the components. Secondary lines such as control lines and electrical lines
were not specifically evaluated.

TABLE 5

STRESS LIMITS FOR 18-HERTZ OSCILLATIONS

Component	Allowable Peak-to-Peak Pressure, psi	Peak-to-Peak Pressure Seen on AS-503
Mark 15-0 Turbopump	Over 500 psi	150
LOX Discharge Duct	Over 500 psi	150
Main LOX Valve	Over 500 psi	65
Propellant Utilization Valve	Over 500 psi	150
LOX Injector Purge Check Valve	Over 500 psi	65
Heat Exchanger Antiflood Check Valve	Over 500 psi	150
Gas Generator Control Valve	Over 500 psi	65
Oxidizer Bleed Valve	Over 500 psi	65
ASI Oxidizer Valve	Over 500 psi	65
Injector Assembly	Over 500 psi	65
Thrust Chamber Assembly	Over 100 psi	55
Gas Generator Assembly	Over 100 psi	45

PROPOSED SOLUTIONS

Two objectives must be kept in mind in determining a solution to the
oscillation problem. First, obviously, the solution by definition reduces
the instability at 17 Hz. Second, however, the structure involved is
characterized by a set of structural resonant frequencies, and elimina-
tion of a 17-Hz oscillation by shifting a feedline resonance must not re-
sult in an instability at another frequency involving a different mode.
Thus, the proposed solution cannot be assumed to be useful until both
of these design objectives are met.

The first recommendation for eliminating the 17-Hz problem was to cut off
the center engine early (early CECO). The closed-loop instability has
occurred on every flight near the end of burn, seemingly being a function
of the LOX level in the tank. Phase relationships between the chamber
pressure and accelerometer measurements have shown conclusively that the
center engine is supplying the energy for the instability. Thus, cutting
off this engine early is the most definite elimination of this instability
during the latter part of burn. As a result of this recommendation, the
center engine was cut off approximately 30 seconds early on stage static
test S-II-8. There was a marked reduction in oscillation amplitudes at
17 Hz after the early CECO, and no apparent increase in amplitude in the
lower frequency ranges. Thus, this solution was implemented on flight
AS-505, and again was successful in eliminating the instability.

A second proposed solution which has received some investigation is
use of a gas-filled accumulator on the center engine LOX feedline. Be-
cause the accumulator is not a Rocketdyne design, no attempt will be made
here to present design specifications but, rather, only a general discus-
sion of design requirements will be presented. The accumulator has an
associated inertance and compliance which, combined, define the accumulator
resonant frequency. Because the accumulator acts as a branch on the main

line, its resonant frequency is effectively an antiresonance relative to oscillation transmission in the main line. Thus, the design objective for attenuating oscillations at a given frequency in the main line is to design the accumulator resonance for this same frequency.

Of course, the addition of an accumulator on the line affects the response at all frequencies. The accumulator gives an antiresonance on the main line at its design frequency, but the main line will still have resonances at frequencies below and above this design frequency. Thus, a second design objective for the accumulator is to make the compliance sufficiently large to get a broad-band response from the accumulator. In other words, the resonant frequencies of the main line are shifted much below and much above their values that were obtained before adding the accumulator. For the S-II problem, the first structural mode of the stage has an analytically predicted resonant frequency between 5.8 and 7.6 Hz during flight. The addition of the accumulator to the feedline should yield a feedline resonance below 5 Hz, and the next resonance above 30 Hz.

In the section of this report on the "Analog Model of the Instability," the inertance, compliance, and resulting resonance for an initial accumulator concept were given. These values were

$$L_a = 2.17 \ 10^{-4} \ (sec/in.)^2$$

$$C_a = 1.0/8.2 \ in.^2$$

$$f_a = 31.0 \ Hz$$

Using these values, the first resonance for the feedline transfer function $(P_{os}/\ddot{x}_5)$ was at 7.5 Hz with the antiresonance at 31 Hz and no other resonance until above 50 Hz (see Table 4). This is acceptable as far as the response at 17 Hz is concerned but could result in a problem with lower structural modes.

The latest accumulator design being considered for the flight vehicle consists of a helium gas volume of 850 in.[3] connected to the main line by forty-four, 5/8-inch-diameter holes of approximately 0.65 inch length. Approximate calculations for the inertance, compliance, and resonant frequency for this accumulator yield

$$L_a = \frac{8 \ (5/16)/3\pi \ +0.65}{(\pi/4) \ (5/8)^2 (386)(44)} = 0.176 \ .10^{-3} \ (sec/in.)^2$$

$$C_a = \frac{70 \ (850)}{1.66 \ (1728)(40)} \cong 0.519 \ in.^2$$

$$f_a = (1/2\pi) \ \sqrt{1.0/L_a C_a} = 16.7 \ Hz$$

A frequency response of the feedline transfer function using the above value of C_a and L_a was performed and the results are shown in Fig. 52. The first resonance is now as low as 4 Hz and, at 6 Hz, the phase shift is already approximately 180 degrees. The accumulator has a broad-band response which should eliminate any closed-loop instability on the S-II stage.

There is one problem with the accumulator which needs to be mentioned here and which would have to be answered before actual use of an accumulator. That is the related problem of when to fill the accumulator with helium and how much helium will be bubbling through the engine. For example, the J-2 engine could not be successfully started if there was any performance loss of the LOX engine during the start transient because of helium flow through the engine. However, if the accumulator is filled with helium after the engine has started, then the feedline resonant frequency will be dropping through all the lower structural modes during the filling process. Thus, there will be a brief period during which the potential for a closed-loop instability exists involving several modes. It is generally true that early in the burn time, the structural gains are low so that no instability may actually be realized. But the purpose here is only to point out the potential problem which would require further study.
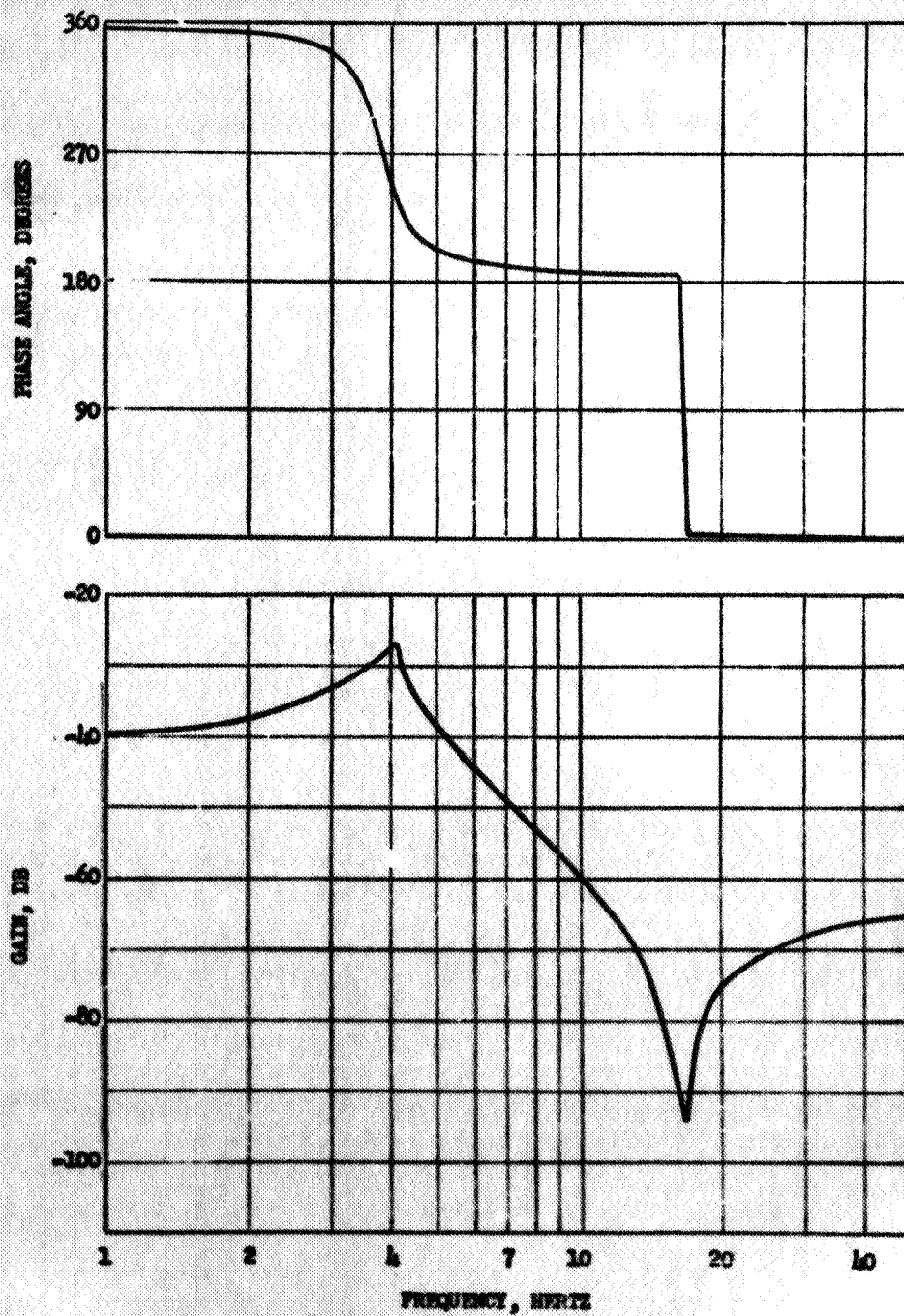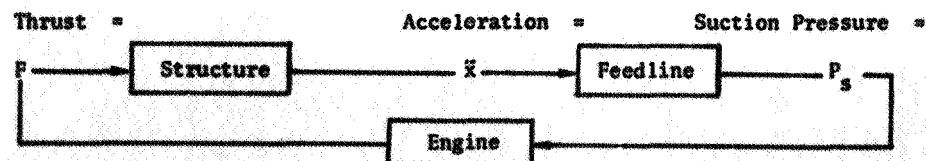
Figure 52. Analytical Transfer Function, P_{os}/V_s, With Accumulator

ENGINE AND FEEDLINE DYNAMIC CHARACTERISTICS

INTRODUCTION

The 17-Hz oscillation problem has been shown to be a closed-loop instability involving the structure, the engine, and the feedlines. The coupling between these major components is shown by the sketch below. In a case like the S-II stage which has several engines and both oxidizer and fuel feedlines, there are multiple blocks in parallel of the same type as shown in the sketch. Because the instability is a loop characteristic, each of the elements represented below must be defined sufficiently to determine this loop characteristic. Rocketdyne has no direct participation in the development of the structural portion of the loop but is responsible for the engine, and because the feedline dynamics depends on the feedline itself and the turbopump dynamics, Rocketdyne shares responsibility for this portion of the loop. The present section of this report describes Rocketdyne's efforts and their results to establish the engine and feedline dynamic characteristics.

Thrust =   Acceleration =   Suction Pressure =

```
 F ──────▶ │ Structure │ ──── x̄ ────▶ │ Feedline │ ──── Pₛ ──┐
 │                                                             │
 └──────────────────────────│ Engine │────────────────────────┘
```

A detailed description of the engine block diagram with the included turbo-pump dynamic termination of the feedline is shown in Fig. 53. This particular representation was used in Rocketdyne's initial efforts to define the engine dynamics as reported in Ref. 3. The engine itself consists of six transfer functions represented by partial derivatives. Using this particular representation, all six transfer functions and the pump dynamics must be defined for the complete description. For the J-2 engine, the LOX side has a much stronger effect on the engine dynamics (e.g., as would be measured by thrust response) than the fuel side. This was confirmed recently by comparing test data from Rocketdyne and MSFC. Rocketdyne pulsed only the LOX side of a J-2 engine, and MSFC gimbaled the engine to
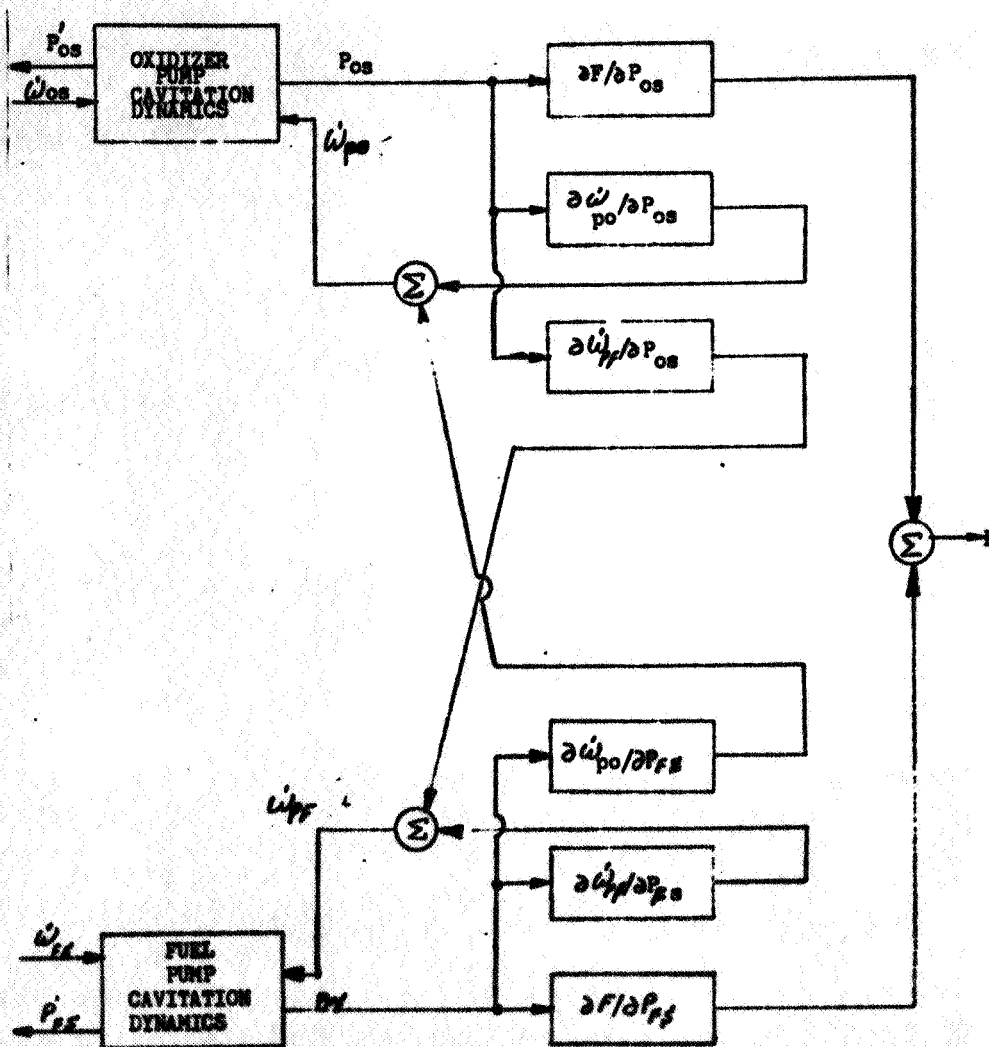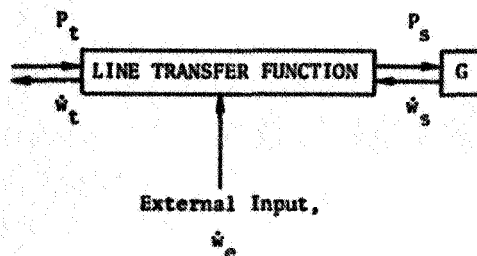
Figure 53.   J-2 Engine Block Diagram

get simultaneous inputs to the fuel and oxidizer systems. The resulting ratio of the dynamic component of thrust to LOX suction pressure was nearly identical for the two types of testing, indicating little or no effect resulting from fuel side oscillations. Analytical efforts have also indicated this same result.

The resulting simplifications, if the fuel side effects are considered negligible, are obvious. For example, in Fig. 53, only the LOX pump dynamics and two of the six transfer functions are then significant, these two being $\partial F/\partial P_{os}$ and $\partial \dot{w}_{po}/\partial P_{os}$. However, an even simpler block diagram can be derived under these conditions. In Fig. 54a is shown an engine block diagram of equal validity with that of Fig. 53. With the simplifications this reduces to the diagram of Fig. 54b. These two transfer functions were determined experimentally using an inlet positive displacement pulser. Based on these inlet pulsing tests, the transfer functions were corrected from the older values determined from discharge pulsing (Ref. 3). The other four transfer functions which were not determined experimentally in the present test program were corrected to reflect similar changes as for the two that were measured. This test program and the results obtained are described below.

A simplified block diagram of the feedline dynamics is sketched below. P is pressure; $\dot{w}$, weight flowrate, with subscripts t and s referring to conditions at the tank and at the pump inlet.
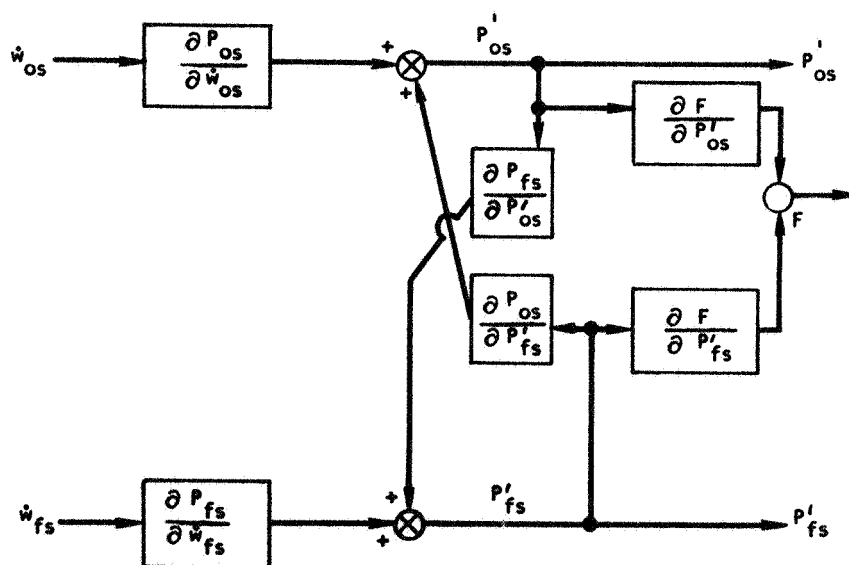
a. COMPLETE ENGINE ALTERNATE BLOCK DIAGRAM

b. SIMPLIFIED ALTERNATE BLOCK DIAGRAM

Figure 54. J-2 Engine Alternate Block Diagrams

The line transfer function at low frequencies could be as simple as a single inertance and resistance, and in fact this seems adequate for the LOX center engine line on the S-II stage. In this case

$$P_t - P_s = R\dot{w}_s + LS\dot{w}_t$$

$$\dot{w}_s = \dot{w}_t + \dot{w}_e$$

where R is the resistance, L the inertance, and S the Laplace operator (= d/dt). The termination transfer function, G, incoporates the pump dynamics and, to some extent, the influence of the pump discharge system. Thus, G can become very complex and for the most part must be determined experimentally. Both Rocketdyne and MSFC have tested to determine the feedline dynamics which can be expressed as a transfer function G. The Rocketdyne test program and results and a comparison with MSFC results are presented below.

ENGINE PULSING PROGRAM

An engine pulsing program was initiated at Rocketdyne shortly after the appearance of the S-II center engine oscillation problem on vehicle 503. The tests were set up to permit introduction of a LOX pump inlet flow oscillation as an external input and to measure the resulting response of the engine system. The purpose of the test program was fourfold:

1. To attempt to reproduce the large pressure oscillations observed in flight 503.

2. To compare a simulated flight LOX pump discharge pressure measurement with a close-coupled measurement of the same parameter.

3. To define the operating region of pump self-excited low-frequency oscillations.

4. To determine the pump and engine transfer functions, $\Delta P_{od}/\Delta P_{os}$, $\Delta\dot{w}_{od}/\Delta P_{os}$, and $\Delta P_c/\Delta P_{os}$ over a wide range of operating conditions.

The first three objectives were met by a few initial tests, more extensive testing being required to map the transfer functions.

A comment is in order here concerning the need to determine the transfer functions. In 1965, Rocketdyne was given a contract to determine J-2 engine transfer functions. At this time, Rocketdyne recommended a program for pulsing the inlet to the pump, but this required design and fabrication of inlet pulsers. Rocketdyne was given the go-ahead to fabricate the inlet pulsers, but in the meantime to use a pump discharge pulsing system, which was already available, to get estimated transfer functions. Thus, a pulse is introduced in the discharge system which is transmitted both upstream and downstream, and the resulting system response is measured. However, to adapt these results for use in a stability model where the input is an inlet pulse, a dynamic model of the engine must be assumed and the model parameters selected to fit the discharge pulsing data.

The discharge pulsing was performed, and a dynamic model was assumed which fit the data. The data clearly required more than a single pump compliance, and an in-line compliance-inertance-compliance model was used (Ref. 3). The model provided a good fit of the test data and was, therefore, an adequate model to define the system response, given a discharge pulse. However, there are other dynamic models which would give the same response to a discharge pulse but not the same response to an inlet pulse, and without actual inlet pulse data there is no way to determine which dynamic model is correct.

The inlet pulsers were developed by December of 1965, but the decision was made at that time to proceed to use the transfer functions based on discharge pulsing rather than verifying these with an inlet pulsing program. This decision was based largely on the fact that the POGO stability model was so stable that large variations in the engine transfer function produced no instability. Just before flight AS-503, some tests at MSFC gave some indication that the existing engine transfer functions were not adequate for defining engine response with an inlet pulse. Thus, the necessity of

testing again using the previously developed inlet pulser was established. The results of these tests did indeed show the old functions to be in error when used with an inlet pulse.

Test Set Up and Conditions

J-2 engine J-025-3 was made available for testing early in January 1969 on the VTS-3B test stand at the Santa Susana Field Laboratory. A hydraulically actuated piston-type pulser (Ref. 4) was used for inlet pulsing. This pulser had been specifically designed and built for J-2 LOX feed system flow pulsing as part of the POGO effort of 1965. Special instrumentation was installed and all dynamic measurements were recorded on high-frequency magnetic tape.

Figure 55 presents a sketch of the J-2 engine LOX feed system showing the locations of primary dynamic measurements. All Photocon-type transducers were flush mounted while the data sensors were close-coupled (approximately 1/2 inch recess from the duct inside diameter to the transducer diaphragm) except as noted. Table 6 presents a list of measurements recorded on magnetic tape. Some of these parameters as well as many other low-frequency signals were also sampled as a part of the normal Beckman Digital Data Acquisition System operating at Santa Susana. This instrumentation coverage permitted engine operating parameters to be defined and yet preserved the dynamic measurements in a manner permitting flexibility in later processing.

Tests were of four types: (1) attempts to duplicate the operating conditions of the center engine of the S-II stage of AS-503, (2) mapping tests, (3) LOX pump discharge pulsing utilizing the heat exchanger tap-off flow, and (4) PU transition effects tests. All tests used LOX inlet pulsing except where the heat exchanger flow in the discharge was used.

Operating conditions were simulated in an attempt to uncover any engine resonance or unusual response in the operating region. When these tests failed to uncover any unusual engine behavior, a mapping effort was

Figure 55. Sketch of Instrumentation for J-2 Pulse Tests

TABLE 6

MEASUREMENTS RECORDED ON HIGH-FREQUENCY MAGNETIC TAPE

Channel No.	Tape Recorder No. 1	Tape Recorder No. 2	Tape Recorder No. 2
1	Vibration Safety Cutoff No. 1 (Dupe)	LOX Pump Speed	
2	Vibration Safety Cutoff No. 2	Engine LOX Flow (Raw Signal)	
3	Vibration Safety Cutoff No. 3	Engine Fuel Flow (Raw Signal)	
4	LOX Pump Inlet Radial Accelerometer	Main LOX Injection Pressure No. 1 (Ph)	Fuel Pump Discharge Pressure
5	Fuel Pump Inlet Radial Accelerometer	LOX Pump Axial Accelerometer	Fuel Pump Inlet Pressure (Ph)
6	LOX Dome Radial Accelerometer No. 1	Fuel Pump Axial Accelerometer	Engine LOX Inlet Pressure (DS) (Dupe)
7	LOX Dome Radial Accelerometer No. 2	VSC No. 1 (Dupe)	LOX Pump Inlet Pressure (Tb)(*)
8	Hydraulic Pulser Position (Dupe)	Hydraulic Pulser Position (Dupe)	LOX Pump Inlet Pressure (DS)
9	Engine LOX Inlet Pressure (DS) (DUPE)	Engine LOX Inlet Pressure (DS)(Dupe)	LOX Pump Discharge Pressure (Flight Instrument)
10	ASI Fuel Injection Pressure	LOX Pump Discharge Pressure (DS)	
11	LOX Injection Pressure No. 2 (Ph)	Main P_c (DS)(*)	Spec. LOX Pump Discharge Pressure AC
12	T/C Fuel Injection Pressure (Ph)	Fuel Pump Speed	Spec. LOX Pump Discharge Pressure DC
13	T/C Fuel Inlet Manifold Pressure (Ph)	ASI LOX Injection Pressures	
14	Time Code (IRIGB)	Time Code (Dupe)	Time Code (Dupe)

NOTE: DS = Data Sensor   * = Not close-coupled
      Ph = Photocon   Dupe = Duplicate recording
      Tb = Tabor

undertaken to determine the J-2 engine response to LOX pump inlet flow disturbances in the 10- to 25-Hz frequency range. The operating parameters varied during the mapping effort were LOX pump available NPSH and PU (propellant utilization) valve position. Data were taken at every 5 feet of LOX pump NPSH between 15 feet and 60 feet and at PU valve positions of full open, 10 degrees from full open, null or center tap, and full closed.

Discharge pulse tests were undertaken to uncover any possible sensitivity of the LOX feed system to heat exchanger flow oscillations or other discharge flow disturbances. The discharge pulse was obtained using an oscillating bleed valve. Several tests were run at various bleed flow oscillation amplitudes. However, in all the tests the pulse amplitudes were not amplified by the engine and were small enough to be insignificant, and it was concluded that flight oscillations were in no way connected with an instability resulting from the heat exchanger flow. No further discussion of these particular results will be presented.

Finally, several PU effects tests were run where rapid PU excursions were undertaken with the inlet pulser operating at various frequencies. These tests provided test data over a continuous PU valve excursion. A complete summary of these 21 dynamic tests outlining conditions and duration is presented in Table 7. Table 8 presents the targeted test matrix for mapping tests illustrating the test number where information was gained for each condition. Operating conditions for vehicle 503 are noted on the matrix.

Figures A-1 through A-7 (Appendix A) present actual PU valve position and LOX pump NPSH for the mapping tests as obtained from digital data and plotted as functions of the time during a test. An envelope about the nominal NPSH value is given to show the extent of any low-frequency oscillations (less than 30 cps) in this parameter. These data, when correlated with high-frequency tape data provided an accurate estimate of engine operating condition at all times during a test.

TABLE 7

SUMMARY OF J-2 ENGINE TESTS WITH PULSING ON LOX SIDE

Test No.	Description
316-011	Attempt to duplicate AS-503 oscillations, and establish one point on mapping matrix
-012	Attempt to duplicate AS-503 oscillations
-013	Mapping test* with inlet pulsing from 10 to 25 Hz
-014	
-015	
-016	
-017	
-018	No pulsing data because of pulser problems
-019	Mapping test with inlet pulsing from 10 to 25 Hz
-020	Repeat of Test No. 316-013
-021	No pulsing data because of pulser problems
-022	Discharge pulsing test using servovalve downstream of heat exchanger
-023	No pulsing data because of electrical problems
-024	PU valve effects test. Rapid excursions of PU valve while inlet pulsing
-025	Discharge pulsing with heat exchanger bypass system
-026	
-027	Mapping test with inlet pulsing from 10 to 25 Hz
-028	
-029	
-030	
-031	Mapping test with inlet pulsing from 1 to 30 Hz and PU valve effects test.

*Mapping test--targeted values of NPSH and PU valve position are shown in Table 8. Actual values obtained are shown in Fig.A-1 through A-7 in Appendix A.

TABLE 8

OXIDIZER INLET PULSE TEST MATRIX

LOX NPSH, feet	PU Valve Position			
	Full Open	10-Degrees Open	Null	Full Closed
60 ±2.5	016	030	014 (65 feet) 030	030
55 ±2.5	016*	017	014	030
50 ±2.5	011*	017	014	030
45 ±2.5	016*	017	029	029
40 ±2.5	016*	017	029	029
35 ±2.5	013 020	013 020	013 020	029
30 ±2.5	015	027	028	029
25 ±2.5	019	027	028	**
20 ±2.5	019	028	028	**
15 $^{+0}_{-3}$	019	028	**	**

*Region of AS 503 center engine oscillation
**Region does not meet NPSH requirements for mainstage operation

NOTE: 1. Frequency sweep all tests:

   011 to 027   10 to 25 Hz in 1-Hz increments, 2-second dwell
    028 to 030   10 to 24 Hz in 2-Hz increments, 2-second dwell

  2. All tests between 1-17-69 and 2-3-69 at VTS-3B

During testing, several special problems were encountered which should be noted. First, a maximum engine inlet pressure disturbance of approximately 15 psi peak-to-peak at the input frequency was all that could be achieved. More typical values were less than 10 psi p-to-p. This limitation was the result of pulser size and also the very large area, low inertia, LOX inlet line at VTS-3B. Figure 56 illustrates the LOX facility feed system at VTS-3B with the pulser as installed. A further detraction to inlet pulse amplitude was the requirement of an angled adapter between the piston unit and the flow distribution manifold. This adapter was required to avoid an interference between the pulser and the J-2 LOX pump. This more remote location of the piston and the added potential for heat transfer to the LOX and GOX formation in the piston cavity doubtless reduced its amplitude potential. Because of this limitation, the effects of large amplitude oscillations upon engine response could not be explored, and the large oscillations experienced in flight could not be reproduced.

An additional limitation was the uncertainty in the dynamic LOX pump inlet flow. The oscillatory flow could not be measured with accuracy. The large diameter, low inertia facility feed system with its many bellows, a large flowmeter, and a large area change made dynamic flow estimation uncertain. Pressure measurements above the engine LOX inlet pressure along the facility LOX inlet line could have provided additiona. data, but the scope and time-table of the program did not permit the installation of these measurements. Further, inlet line vibration where elbows are present has since been shown to have a very significant influence (CTL-I testing). Considerable accel-erometer instrumentation and possible structural modifications would be required to ensure that mechanical vibration modes were at low levels or out of the test frequency range. Because of these problems, dynamic LOX pump inlet flow could not be determined and engine test data analysis was limited to inlet pressure transfer functions relating to downstream parameters.

Another engine test problem requiring special attention was that of J-2 LOX pump self-excited oscillations. These oscillations appear mainly in J-2 LOX pump inlet pressure in the frequency range of 10 to 21 Hz and at amplitudes
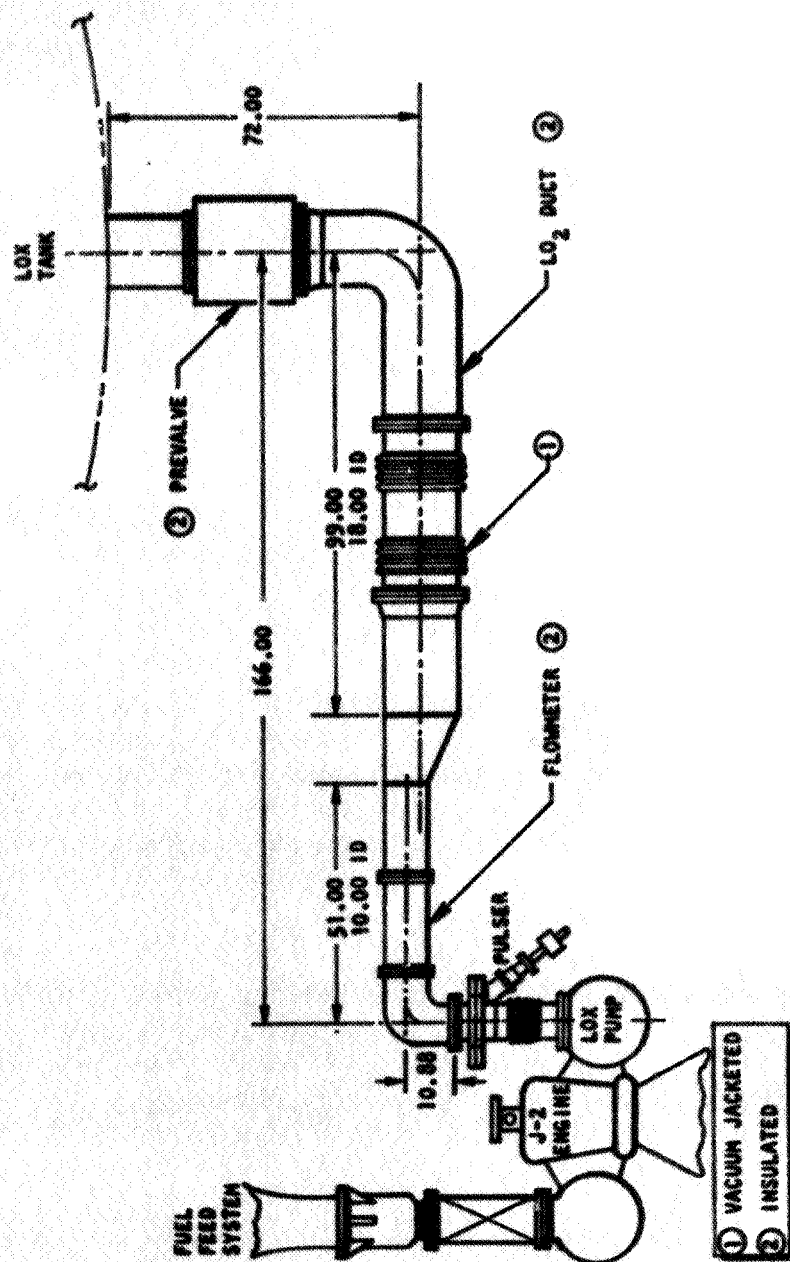
Figure 56. VTS-3B LOX Feed System

R-7970

of approximately 5 psi p-to-p. They appear to have no detrimental effect
upon engine operation. The operating region in which self-excited oscil-
lations were encountered was found to be a function of available NPSH and
pump operating point (PU valve position). Figure 28 presents the J-2
LOX pump self-excited inlet pressure oscillation region as a function of
NPSH and PU valve position. Although this area lies below the flight
vehicle operating region, a number of the mapping tests were run in the
self-excited region. As a result, some inlet pulse data are contaminated
with self-excited oscillations in the same frequency range and of a similar
amplitude. The transfer functions were determined in this region to pro-
vide a complete map, but the extent of the effect of the self-excited
oscillations on the transfer functions is uncertain.

Data Processing

The magnetic tape data were initially transcribed on Brush records, both
direct with a-c coupling and 35-Hz low-pass filtered. This processing
technique is relatively fast and was used to get a quick look at the data
to establish those regions where the data appeared to be good and to
estimate trends in the data. The Brush record data were also used to in-
dicate regions of self-excited pump oscillations and to compare the results
of different types of instrumentation measuring the same parameter.

The transfer functions were obtained from data processed by the Rocketdyne
"A-Bar" Spectrum Analyzer. The A-Bar technique computes the Fourier co-
efficient amplitudes calibrated for average peak values, hence the name
$\bar{A}$ or A-Bar, and parameter relative phase angles. The technique will
analyze a segment of data from 0.001 to 10 seconds in duration over any
frequency range from 0 to 20K Hz. It can give a maximum of four spectral
amplitudes, three relative phase angles, and three amplitude ratios,
simultaneously. The most significant advantages of the technique in the
present application are its ability to separate closely spaced *frequency*
components and to produce relative phase angles of parameters on a common
tape and its low sensitivity to transients (in comparison with standard
cross power spectral density methods).

The gain (relative amplitude) and relative phase information obtained
from the A-Bar analysis were plotted as a function of frequency. The
reduced data were inspected for points that looked inconsistent; data
points verified as being bad were rejected. Causes of bad data included:

1. Insufficient length of time at a stabilized operating condition
    and frequency (typically 2.0 seconds of engine operation were
    spent at each frequency for a valid data point)

2. Insufficient signal level

3. Periodic noise contamination (such as oscillations generated
    by something other than the pulser input)

4. Poor choice of time segment to perform A-Bar analysis

5. Instrumentation failures

After removing obviously bad data points, the remaining data points for
a given engine operating condition were submitted to a digital computer
frequency response curve-fit program. The curve-fit program used a con-
ventional least-squares-error criteria on both gain and phase to provide
a "best fit" of the data to suggested transfer function formats. Thus,
the data are presented in the form of both Bode plots and curve-fit
transfer functions. However, it must be kept in mind that in represent-
ing the transfer functions as curve fits, the terms that make up the curve
fits do not necessarily represent physical elements in the engine system,
and they do not necessarily have orderly trends with engine operating
point variations. Also, the curve fits are only applicable in the fre-
quency range of the test data and are not to be extrapolated. In almost
all tests, the frequency range of the test data was from 10 to 25 Hz.
Thus, even the steady-state value should not be projected from the curve-
fit function.

Engine Transfer Functions

$\Delta P_c / \Delta P_{os}$. The most important transfer function obtained from the engine pulsing test program was $\Delta P_c / \Delta P_{in}$. Two close-coupled LOX pump inlet pressure measurements were made, one approximately 4-inches and the other approximately 3.5-feet upstream of the pump inlet. Rocketdyne experience has shown that a measurement near the pump inlet can give erratic results because of the inducer backflow and tip-vortex cavitation. Thus, the measurement 4-inches upstream of the pump inlet is not considered sufficiently reliable for use in determining the engine transfer function, and the measurement 3.5-feet upstream was used.

Initially, it was assumed that it made little difference which inlet pressure measurement was used. This assumption is valid if the external input flowrate is right at the pump inlet and the total facility inertance is large compared to the inertance of the line between the two measurements. This can be shown by writing the simplified acoustic equations for the system sketched below.
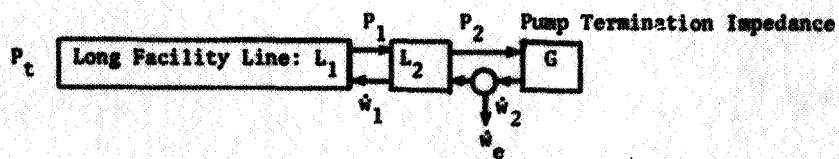
$$P_t - P_1 = S L_1 \dot{w}_1 \tag{20}$$

$$P_1 - P_2 = S L_2 \dot{w}_1 \tag{21}$$

$$P_2 / \dot{w}_2 = G \tag{22}$$

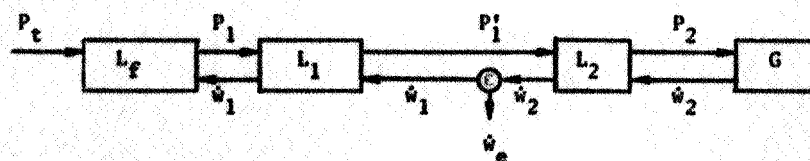$$\dot{w}_2 = \dot{w}_1 + \dot{w}_e \tag{23}$$

From Eq. 20 and 21

$$P_t - P_2 = S (L_1 + L_2) \dot{w}_1$$

If now the tank pressure, P_t, is assumed to be zero,

$$\frac{P_2}{P_1} = \frac{L_1 + L_2}{L_1} \qquad (24)$$

which is a constant nearly equal to one if $L_2 \ll L_1$.

However, if the external flowrate is input upstream of P_2, but downstream of P_1, as in the engine pulsing tests, then

$$P_t - P_1 = SL_f \dot{w}_1 \qquad (25)$$

$$P_1 - P_1' = SL_1 \dot{w}_1 \qquad (26)$$

$$P_1' - P_2 = SL_2 \dot{w}_2 \qquad (27)$$

$$\dot{w}_2 = \dot{w}_1 + \dot{w}_e \qquad (28)$$

$$P_2/\dot{w}_2 = G \qquad (29)$$

Now with $P_t = 0$ and combining equations,

$$\frac{P_2}{P_1} = \frac{1 + L_1/L_f}{1 + \frac{SL_2}{G}} \qquad (30)$$

Assuming $L_1/L_f \ll 1.0$, where L_f is the facility line inertance, then

$$\frac{P_2}{P_1} \sim \frac{1.0}{1 + SL_2/G} \tag{31}$$

and the pressure ratio depends on the complex pump termination impedance and the inertance between the flow input and the pump inlet. Assuming, by way of example, a very simple function G

$$G = \frac{R}{1 + RCS} \tag{32}$$

where R denotes a resistance and C a compliance, then

$$\frac{P_2}{P_1} = \frac{1}{1 + \dfrac{SL_2}{R} + S^2 L_2 C} \tag{33}$$

Equation 33 represents a simple resonance so would have a response curve as sketched below,
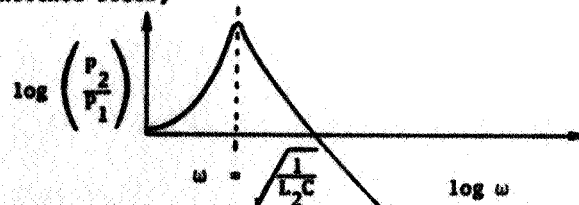
and the difference resulting from using P_1 rather than a true value of P_2 could be very significant.

The function, G, is as difficult to determine as the transfer function $\Delta P_c/\Delta P_{in}$. In fact, G is itself a transfer function being equal to $\Delta P_{in}/\Delta \dot{w}_{in}$. If $\Delta P_c/\Delta P_1$ is known and $\Delta P_c/\Delta P_2$ is required, then

$$\frac{\Delta P_c}{\Delta P_2} = \frac{\Delta P_c}{\Delta P_1} \cdot \frac{\Delta P_1}{\Delta P_2} \tag{34}$$

Using Eq. 31

$$\frac{\Delta P_c}{\Delta P_2} = \frac{\Delta P_c}{\Delta P_1} \left[1 + \frac{SL_2}{G} \right] \qquad (35)$$

From the engine pulsing test program, $\Delta P_c/\Delta P_1$ was determined and these
results are presented in this section. From the LOX pump pulsing test
program, the pump termination impedance, G, was determined combining both
experimental and analytical techniques. These results are presented in
the section on the pump test program. The combined results making use
of Eq. 35 are presented in the last section.

In Fig. A-8 through A-37 (Appendix A), Bode plots of the transfer function
$\Delta P_c/\Delta P_{in}$ are shown as determined from the pulsing tests. P_{in} is the pres-
sure 3.5-feet upstream of the pump inlet as discussed above. All but two
of the tests were run over the frequency range 10 to 25 Hz and so the data
cover only that range. The approximate average NPSH was estimated from
the actual data of Fig. A-1 through A-7(Appendix A). The data are seen
to be relatively well-behaved and consistent from test-to-test.

For convenience in using these data in stability analyses on computers,
some of the transfer functions were curve fit using a suggested transfer
function format of the form,

$$\frac{\Delta P_c}{\Delta P_{in}} = \frac{K(1 + S/2\pi f_1)(1 + 2\zeta_2 S/2\pi f_2 + S^2/4\,\pi^2\,f_2^{\,2})}{(1 + S/2\pi f_3)(1 + S/2\pi f_4)(1 + 2\zeta_5 S/2\pi f_5 + S^2/4\pi^2 f_5^{\,2})} \qquad (36)$$

The parameters $f_1, \ldots, f_5$ are frequencies in units of Hz, ζ_2 and ζ_5 are
damping ratios, and S is the Laplace operator or in this case S = iω where
i = $\sqrt{-1}$ and ω is circular frequency. Again, it should be emphasized that
the terms making up the curve fits of the transfer functions do not neces-
sarily represent physical elements in the engine system nor do they neces-
sarily have orderly trends with engine operating point variations. The
curve fits should also not be used outside the frequency range of the data.

Even the gain term K should not be interpreted as the real steady-state gain because the data did not extend to low frequencies.

The values of K, f_1, f_2,..., f_5, ζ_2, and ζ_5 are given in Table 9 along with the approximate engine operating point. (An infinite value of frequency simply indicates that that particular term from Eq. 36 was not required to obtain a good curve fit.) The curve fits of Table 9 are also plotted as dashed lines in the appropriate Bode plots of Fig. A-8 through A-37 (Appendix A). In every case, the curve fit is seen to fit the data well. Table 10 presents the root-mean-square error between data and the curve fit in gain and in phase for each of the 12 curve fits of Table 9. The maximum rms gain error is 1.63 db's and the maximum phase error is 19.7 degrees, and both of these occur at a NPSH of 35 feet which is near the region of engine self-driven oscillations.

The effect of pump operating point, i.e., NPSH and PU valve position, on the engine transfer function is shown in Fig. 57 and 58. In Fig. 57, the gain of the transfer function increases as NPSH decreases, and there is a general tendency for it to increase as the PU valve moves from the closed to the open position. The phase angles do not correlate as well with NPSH at the open PU valve position, but for the PU valve closed and 10 degrees open, the phase angle is slightly larger for the smaller NPSH. There also tends to be a slightly larger phase angle as PU valve position moves from the closed to open position.

In addition to the Rocketdyne engine tests, tests were conducted at MSFC using a LOX suction bleed pulser and gimbal pulsing, and the resulting transfer function $\Delta P_c/\Delta P_{in}$ was determined. The MSFC data were generally in agreement with the Rocketdyne data and in some cases extended the range of data, but there were some discrepancies as well. The inlet pressure measurement used in the MSFC transfer function was 2-feet upstream of the pump inlet (measurement No. D504A) and approximately 1-foot downstream of the suction bleed pulser. Therefore, Eq. 35 would have to be used to get the transfer function using an inlet pressure right at the pump inlet,

TABLE 9

COEFFICIENTS FOR $\Delta P_c / \Delta P_{in}$ TRANSFER FUNCTION AS A
FUNCTION OF LOX PUMP OPERATING POINT

Data Set No.	NPSH, feet	PU	K	f_1	f_2	ζ_2	f_3	f_4	f_5	ζ_5
1	60	Closed	0.426	19.9	∞	-	25.3	53.3	34.9	0.43
2	55	Closed	0.412	17.4	∞	-	25.9	70.1	35.1	0.47
3	50	Closed	0.413	7.2	∞	-	13.8	32.7	62.4	0.4
4	60	Null	0.58	11.6	45.5	0.12	18.0	18.8	35.1	0.37
5	60	10 Degrees From Open	0.63	14.3	29.9	0.001	18.1	21.5	27.0	0.111
6	52	↓	0.61	18.8	∞	-	21.5	27.6	29.5	0.135
7	50	↓	0.81	∞	∞	-	∞	∞	27.8	0.34
8	60	Open	0.98	23.9	∞	-	8.7	72.7	37.8	0.03
9	50	Open	0.733	7.7	∞	-	15.4	15.6	43.3	0.4
10	45	Open	0.89	18.4	∞	-	23.4	29.6	32.8	0.29
11	40	Open	0.73	13.1	∞	-	19.8	20.4	29.6	0.1
12	35	Open	0.91	31.7	∞	-	15.0	∞	23.6	0.06

TABLE 10

SUMMARY OF RMS ERRORS BETWEEN CURVE FITS AND DATA

Data Set No.	Run No.	NPSH, feet	PU	εG	εφ
1	30(1)	60	Closed	0.98	6.65
2	30(2)	55	Closed	1.14	6.7
3	30(5)	50	Closed	0.86	8.0
4	30(3)	60	Null	0.74	5.28
5	30(4)	60	10 Degrees From Open	0.93	5.46
6	17(4)	52	10 Degrees From Open	1.12	3.62
7	17(3)	50	10 Degrees From Open	0.57	11.62
8	16(4)	60	Open	0.64	6.59
9	11	50	Open	1.2	12.8
10	16(2)	45	Open	1.12	6.01
11	16(1)	40	Open	1.14	5.88
12	13(1)	35	Open	1.63	19.7

$$\epsilon G = \left[\frac{\Sigma (\text{gain error})_i}{I} \right]^{1/2} \qquad \text{in db's}$$

$$\epsilon \phi = \left[\frac{\Sigma (\text{phase error})_i}{I} \right]^{1/2} \qquad \text{in degrees}$$

$$I = \text{number of data points}$$
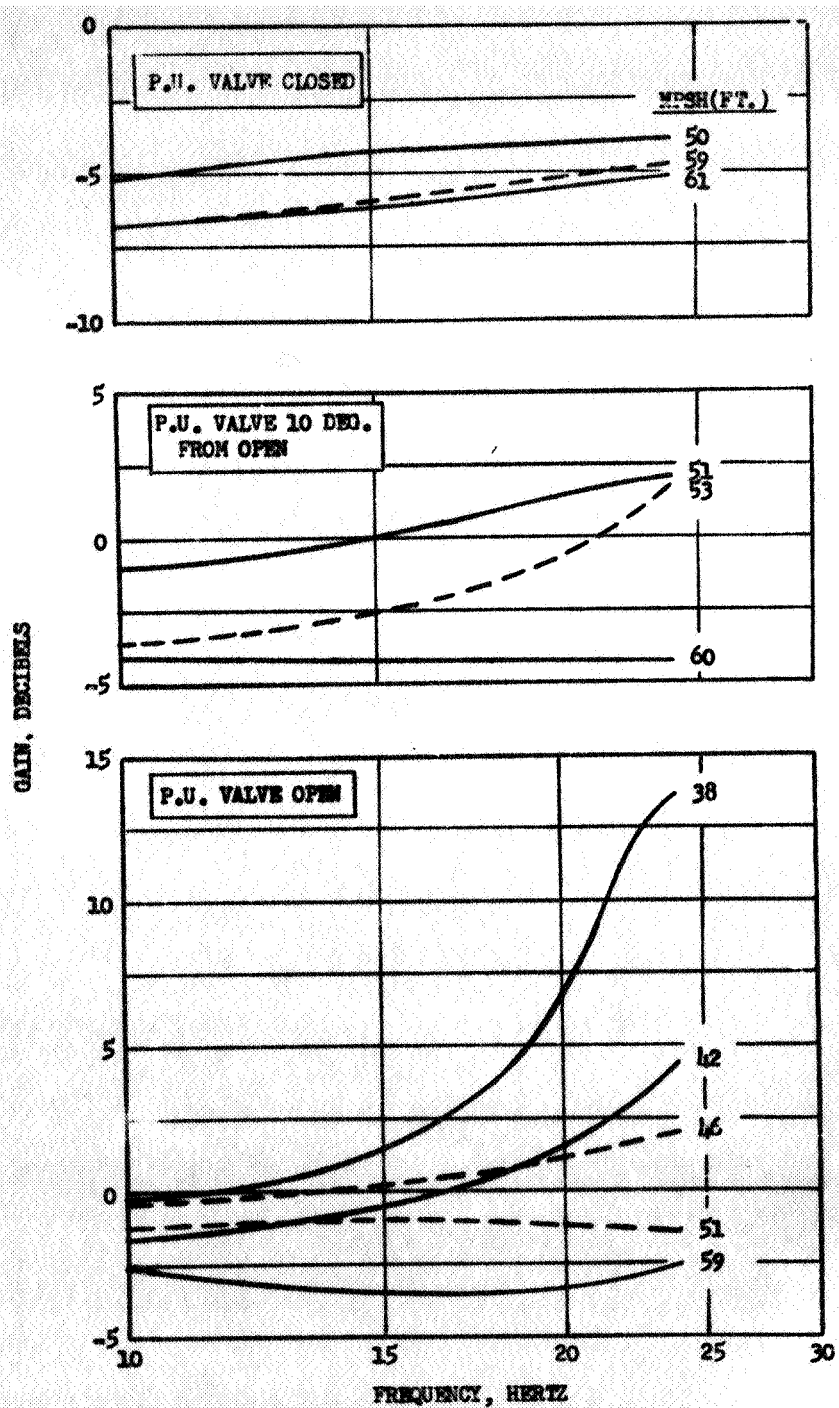
Figure 57. Curve Fit Transfer Function, $\Delta P_c/\Delta P_{in}$
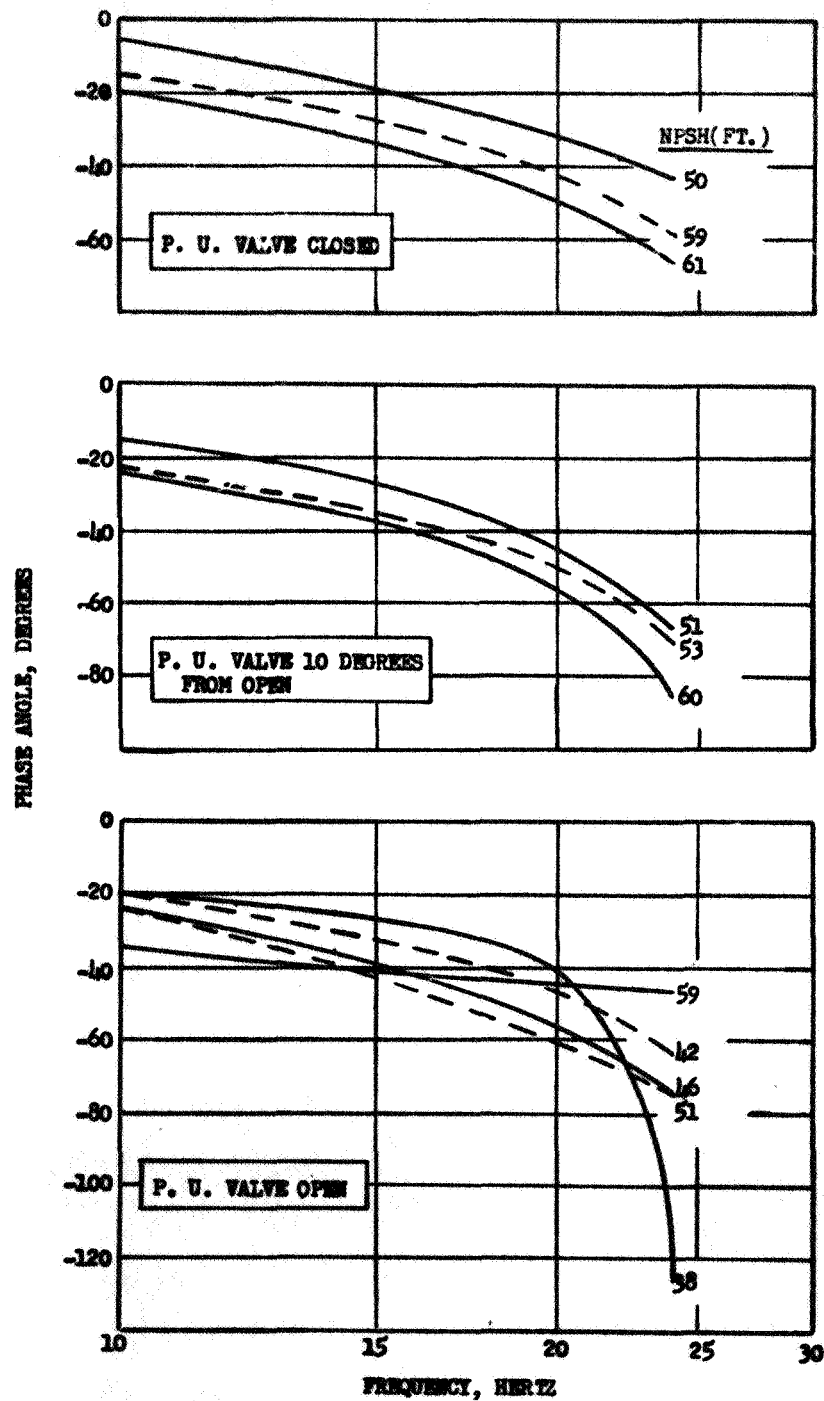
Figure 58. Curve Fit Transfer Function, $\Delta P_c / \Delta P_{in}$

where L_2 for the MSFC data is the inertance between the pressure tap and the pump inlet and is approximately equal to the L_2 for the Rocketdyne tests. The MSFC data are not presented here, but a brief discussion of their results follows.

At the high mixture ratio, closed PU valve, the MSFC data were in fair agreement with Rocketdyne data. In some cases the amplitudes were a little lower (less than 6 db's) than the Rocketdyne data, but MSFC recommended (Ref. 5) using the Rocketdyne curve-fit transfer functions in this region and to extend the application of these curve fits to 35 Hz. MSFC did recommend use of the transfer function

$$\frac{\Delta P_c}{\Delta P_{in}} = \frac{0.355}{1 + \frac{2(0.375)S}{2\pi(38.4)} + \frac{S^2}{4\pi^2(38.4)^2}} \tag{37}$$

for NPSH = 74 feet and PU valve closed. Rocketdyne did not have good data at this operating point but the trends of Rocketdyne data would indicate somewhat higher gain than would be obtained from Eq. 37.

At the null position for the PU valve, MSFC had data at 54 and 44 feet. The data at 54 feet agreed well with Rocketdyne data as did the phase data at 44 feet. However, the gain for 44 feet NPSH was low particularly in the frequency range of 10 to 20 Hz. MSFC did recommend using the Rocketdyne curve fit which was specified for 60 feet NPSH for both 50 and 60 feet NPSH.

The largest discrepancies in the Rocketdyne and MSFC transfer function data were at the operating point of full-open PU valve, or 4.5 mixture ratio. The phase data were generally in agreement even when the Rocketdyne curve fits were extended to 35 Hz. However, the gains for the MSFC data were generally lower by about a factor of two from the Rocketdyne curve fits. MSFC recommended using the transfer functions of Table 11 using the same format as in Eq. 36. These transfer functions are applicable from approximately 10 to 35 Hz. Until the discrepancies between the Rocketdyne and

MSFC data can be explained, it is recommended that the Rocketdyne transfer functions be used because they represent the more conservative value.

TABLE 11

MSFC RECOMMENDED COEFFICIENTS FOR $\Delta P_c / \Delta P_{in}$ TRANSFER FUNCTION,
PU VALVE POSITION: OPEN

NPSH	K	f_1	f_2	ζ_2	f_3	f_4	f_5	ζ_5
70*	0.316	∞	∞	--	∞	∞	31.6	0.825
60	0.224	∞	∞	--	∞	∞	33.5	0.415
50**	0.733	7.7	∞	--	15.4	15.6	43.3	0.4
44	0.75	∞	∞	--	20.0	∞	34.1	0.38
40	0.75	∞	∞	--	∞	15.3	32.2	0.3
35	1.0	∞	37	0.625	∞	∞	68	1.0

*No Rocketdyne data at this high NPSH
**Same as Rocketdyne

Other Engine Transfer Functions. Referring again to Fig. 53, there were six transfer functions required for definition of the engine dynamics. Because all six were previously reported (Ref. 3), the same six are discussed here although all are not used in the present problem. The one more significant transfer function, apart from $\partial P_c / \partial P_{os}$ which has been presented already, is $\partial \dot{w}_{op} / \partial P_{os}$ where $\dot{w}_{op}$ is the flowrate out of the cavitation bubble at the pump inlet. This flowrate was not determined in engine testing but the pump discharge flow $\dot{w}_{od}$ was measured. Assuming that fuel pressure P_{fs} has a very small effect on $\dot{w}_{od}$, then $\partial \dot{w}_{od} / \partial P_{os} \approx d\dot{w}_{od} / dP_{os}$. Then,

$$\frac{\partial \dot{w}_{od}}{\partial P_{os}} \approx \frac{\Delta \dot{w}_{od}}{\Delta P_{od}} \frac{\Delta P_{od}}{\Delta P_{os}} = \frac{\Delta \dot{w}_{od}}{\Delta P_{od}} \frac{\Delta P_c}{\Delta P_{os}} \frac{\Delta P_{od}}{\Delta P_c} \tag{38}$$

The values of $\Delta\dot{w}_{od}/\Delta P_{od}$ and $\Delta P_c/\Delta P_{od}$ were determined analytically and verified experimentally. Thus,

$$\frac{\partial\dot{w}_{od}}{\partial P_{os}} \simeq \frac{0.694\left[1 + S/(2\pi*4.91)\right]}{\left[1 + S/(2\pi*8.45)\right]} \cdot \frac{\Delta P_c}{\Delta P_{os}} \tag{39}$$

Previously, it was assumed that the LOX pump dynamics could be represented by a single compliance and that $\dot{w}_{op} = \dot{w}_{od}$. Thus, the above transfer function was used as an approximation to $\partial\dot{w}_{op}/\partial P_{os}$. However, the model developed for deriving G ($= \Delta P_{os}/\Delta\dot{w}_{os}$) from the pump pit tests indicates that $\dot{w}_{op} \neq \dot{w}_{od}$. If the function G is assumed to consist of a pump compliance B and a function G', then
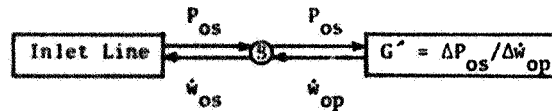
$$P_{os} = \frac{B}{S}(\dot{w}_{os} - \dot{w}_{op})$$

$$\frac{P_{os}}{\dot{w}_{os}} = G = \frac{B}{S}(1 - \frac{\dot{w}_{op}}{\dot{w}_{os}})$$

$$G = \frac{B}{S}(1 - \frac{G}{G'})$$

or

$$G' = \frac{G}{1 - SG/B}$$

Assuming no influence from the fuel side

$$\frac{\partial\dot{w}_{op}}{\partial P_{os}} = \frac{d\dot{w}_{op}}{dP_{os}} = \frac{1}{G'}$$

Thus,

$$\frac{d\dot{w}_{op}}{dP_{os}} = \frac{1 - SG/B}{G}$$

The discharge pulsing tests gave valid information for inputs from the high-pressure side of the system. Hence, the fuel pump flowrate variations with chamber pressure ($\Delta\dot{w}_{fs}/\Delta P_c$) resulting from inputs from the LOX side is known from the old data,

$$\Delta\dot{w}_{fs}/\Delta P_c = \frac{-0.00266\left[1-S/(2\pi* 17.3)\right]}{\left[1+S/(2\pi*5.14)\right]\left[1+S/(2\pi* 43.0)\right]} \qquad (40)$$

Because $\Delta P_c/\Delta P_{in}$, where P_{in} is LOX inlet pressure 4-feet upstream of pump, is known from the engine pulsing tests, then $\Delta\dot{w}_{fs}/\Delta P_{in}$ can be determined,

$$\frac{\Delta\dot{w}_{fs}}{\Delta P_{in}} = \frac{\Delta\dot{w}_{fs}}{\Delta P_c} \cdot \frac{\Delta P_c}{\Delta P_{in}} \qquad (41)$$

No new data were determined using fuel side pulsing. In the fuel side transfer functions using discharge pulsing data, a double-compliance model was assumed as on the LOX side. Because this double-compliance model did not give proper LOX transfer functions with inlet pulsing, similar difficulties are expected on the fuel side. Thus, the decision was made to represent the fuel side transfer functions based on a single-pump-inlet compliance, but using the data from discharge pulsing tests. The resulting transfer functions are

$$\frac{\partial F}{\partial P_{fs}} = \frac{16.8\left[1+S/(2\pi* 2.27)\right]}{\left[1+S/(2\pi* 3.88)\right]\left[1+S/(2\pi* 75.8)\right]} \qquad (42)$$

$$\frac{\partial\dot{w}_f}{\partial P_{fs}} = \frac{0.0416\left[1+S/(2\pi* 13.3)\right]}{\left[1+S/(2\pi* 17.1)\right]} \qquad (43)$$

$$\frac{\partial\dot{w}_{op}}{\partial P_{fs}} = \frac{-0.059}{\left[1+S/(2\pi* 41.9)\right]} \qquad (44)$$

where all flows are in lb/sec, pressures in psi, and thrust in pounds. The single compliance to be used on the fuel pump is the first compliance determined for the double-compliance model. This compliance is shown in Fig. 59.
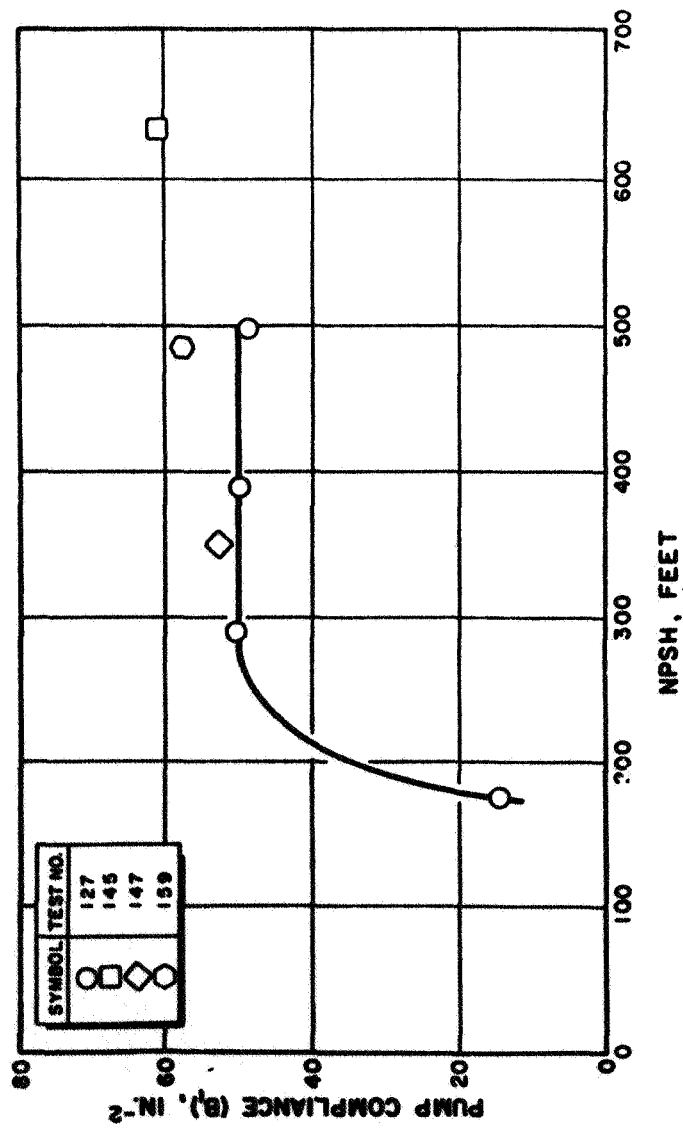
Figure 59. J-2 Fuel Pump Compliance vs NPSH From Tests Performed in 1965

Because of the lack of test data, accuracy and limitations of these transfer functions are not known. Low-frequency dynamic effects resulting from pump speed variations have been removed so that the transfer functions are invalid below about 5 Hz. Current POGO studies have indicated that the fuel system is of minor importance in the study of the 18-Hz problem and can be ignored with negligible error.

Other Results. One of the results established early in the engine pulsing test program was the region of LOX pump NPSH and PU valve position in which the LOX pump experienced self-excited oscillations in the low-frequency range. These self-excited oscillations are commonly experienced in some regions of operation and are assumed to be strongly associated with cavitation in the inducer. For the J-2 LOX pump, it was known previous to this test program that the self-excited oscillations were most frequently in the frequency range of 14 to 18 Hz, close to the frequency of the instability during flight. As a result, initial explanations of the cause of the flight oscillations listed pump self-excited oscillations as the primary candidate. The testing was to verify the region of such oscillations.

The results of testing have already been presented in Fig. 28 to which the reader is referred again. The upper bound shown on this figure was also supported by tests at MSFC. The one most important conclusion from the tests was that during flight the operating point never dropped into the region of the self-excited oscillations experienced in ground testing, as can be verified by comparing Fig. 25 and 28.

It was also pointed out previously that the amplitude of self-excited oscillations experienced on the test stands are always low for the J-2 LOX pump. Usually, the complex wave amplitude was only very slightly larger than the general noise level previous to the self-excited oscillations, but appeared as a distinct low frequency in contrast to the broad frequency spectrum of the noise. Thus, even if the pump were operated in the region of self-excited oscillations, the large amplitudes observed in flight would not

be expected. Furthermore, when pulsing the pump using an inlet piston pulser at the same frequency of the self-excited oscillations, the amplitudes generally are approximately the same as without pulsing, indicating that the mechanism which causes the pump oscillations has some amplitude limiting characteristics. Thus, even if the pump is self-driving at the structural resonance, there is an indication that coupling between the two would not cause large amplitude oscillations.

The engine pulsing tests were also used to compare the response of flight-type measurements with their long sense line and that of a close-coupled measurement. Both LOX pump inlet and discharge pressure were studied for this effect. The data from the study have already been presented in Fig. 15 , 16, and 18 in connection with the discussion of the validity of the flight measurements of these two parameters. The sense line on the discharge pressure was seen to cause a response higher than the actual value by a factor as large as 6 to 8 at some frequencies. The sense line on the inlet pressure measurement gave a response which was lower than the actual value and was amplitude-sensitive.

The long sense line contains stagnant LOX which when it warms up can form a two-phase mixture. As soon as a two-phase mixture is obtained (and the gaseous phase is intentionally at the transducer end of the line), the line has a low resonant frequency as was observed in Fig. 16 for the discharge measurement. This sense line must be kept short enough so that even if a two-phase mixture is obtained the resulting resonance is high enough to still get accurate response. For example, on the J-2 LOX pump, if it is required to get good response at 20 Hz, then the resonant frequency should not be below 40 Hz. To achieve this, the inlet sense line should be no more than about 4-inches long. The discharge line should be no longer than 24-inches long, the longer length being allowed because of the higher steady-state pressure.

J-2 LOX PUMP PULSING PROGRAM

During J-2 engine LOX inlet flow pulsing on VTS-3B, it became apparent
that LOX pump dynamic behavior could not be derived from these tests
alone. Not only was one important variable (dynamic LOX pump inlet flow)
an unknown, but potentially significant variables (such as PU valve posi-
tion, pump flow coefficient, inlet line configuration, and pump available
NPSH) could not be independently perturbed. Further, the inability to
generate inlet pressure oscillations of greater than 15 psi peak-to-peak
made it impossible to generate the magnitude of inlet oscillations which
were experienced in flight. Consequently, J-2 engine tests were com-
pleted, and an extensive J-2 LOX pump dynamic test program was initiated
in a component test pit, CTL-1, pit 2.

The purpose of the dynamic pump test program was to generate inlet flow
pulsing data in the low-frequency range for a variety of pump operating
conditions and several inlet line configurations. These data would then
be used to derive the J-2 LOX pump low-frequency characteristics. In
addition, any significant pump inlet line behavior could be determined.

Test Setup and Conditions

The CTL-1, pit 2, propellant feed system was modified to permit pulser
installation and three different inlet line test sections. These sections
were the S-II inboard LOX pump inlet duct excluding the elbow and sump,
a Rocketdyne inlet duct as used on S-II outboard engines and on the S-IV-B,
and a solid or hard line to be used as a reference.

Figure 60 depicts the general configuration of the pump test facility. A
detailed schematic of the entire test system including dimensions and
dynamic instrument locations is shown in Fig. 61.
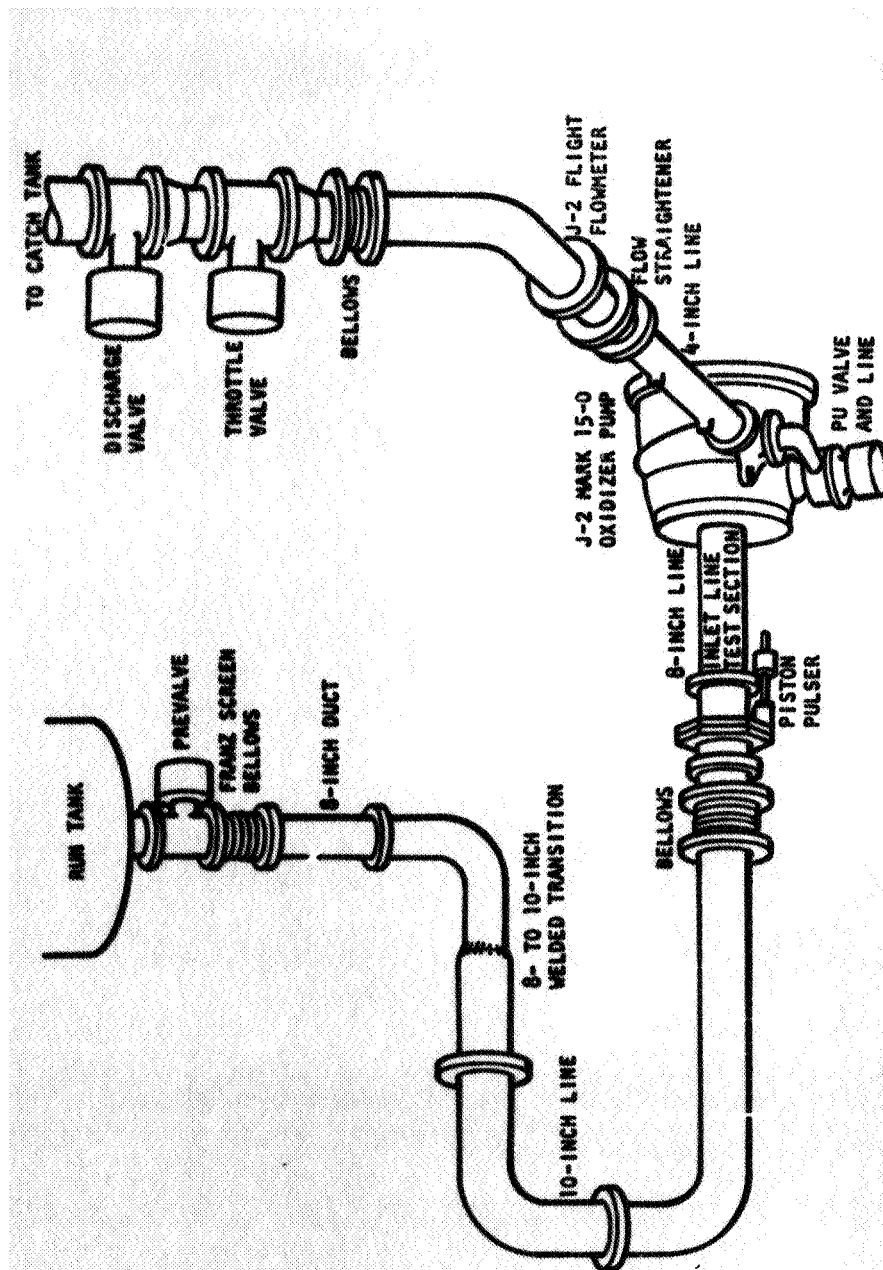
Figure 60. J-2 Oxidizer Pump Test Facility

R-7970
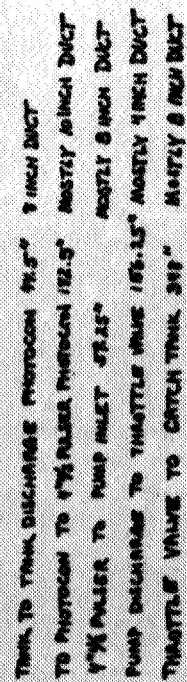
Figure 61. CTL 1, Pit 2 Dynamic LOX Pump Test Configuration

In the CTL-1 test facility, the pump was driven by an electric motor to permit accurate speed control. Pump flowrate (steady state) was controlled by the facility throttle valve in the pump discharge line. The throttle valve was servocontrolled by an active feedback system sensing the flight flowmeter output signal. This J-2 flight flowmeter is capable of responding to dynamic flow oscillations (it was, in fact, used as the sensor for discharge flow perturbations). Consequently, the discharge throttle valve control system frequency response characteristics had to be estimated, and the possible effects of a dynamically active element in the discharge line on the data and upon the modeling effort were considered.

NPSH (net positive suction head at the pump inlet) was controlled by the run-tank pressurization system utilizing a feedback control sensing LOX run-tank discharge pressure. The run tank was vented until just prior to each test to give a uniform LOX temperature. The PU (propellant utilization or LOX pump impeller bypass) valve was manually set before testing and held in place by a locking screw. Figure 62 shows the PU valve hydraulic resistance as a function of valve position. Set positions determined by a gage and locking screw holes are indicated by the numbers. A one indicates full-open position while five is full closed.

The hydraulically driven pulser was located immediately upstream of the inlet line test section, Fig. 60. Pulsing of the inlet system was accomplished by a moving piston causing a sinusoidally varying flow in and out of the pump inlet line. High-quality LOX was assured throughout the stroke by means of a constant LOX bleed through the piston and hence overboard. Peak-to-peak inlet pressure amplitudes of as high as 50 psi were achieved. However, inlet pressure amplitudes greater than 15 psi peak-to-peak proved to be undesirable because of the nonlinear pressure wave and the associated large-amplitude inlet line mechanical vibrations. These vibrations introduced additional inlet compliance of unknown amplitude which could not be determined analytically. Stiffening of the inlet line by increasing the number and rigidity of bracing struts along with low-pulsing pressure amplitudes (less than 15 psi peak-to-peak) permitted data acqusition with a minimum of vibration contamination.
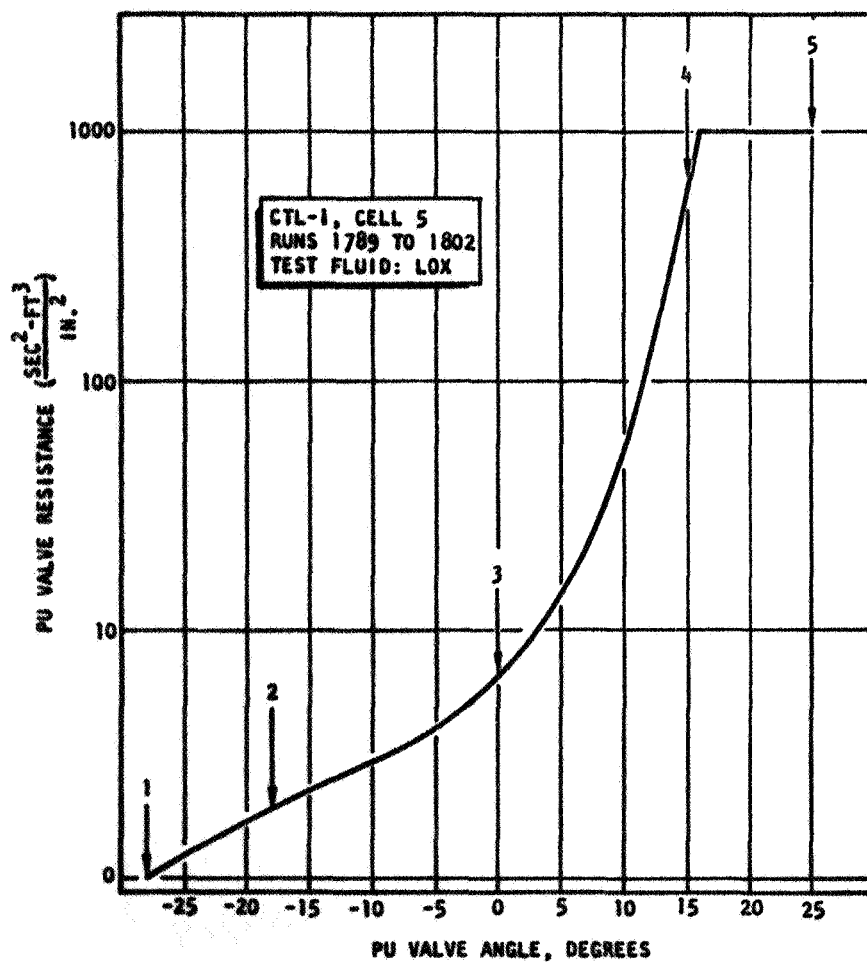
Figure 62. J-2 PU Valve Hydraulic Resistance Characteristics

High-frequency pressure sensors were located along the inlet line to permit an accurate reconstruction of inlet line behavior. This modeling of inlet line behavior was then used to estimate the inlet line dynamic flow. Both Photocon and Data Sensor dynamic pressure transducers were utilized, often redundantly (Fig. 61 presents exact locations). The former were flush mounted, while the latter, though recessed approximately 1/2 inch, were less subject to d-c drift. Static pressure measurements were located nearby to permit accurate measurement of steady-state pressure. Pump discharge and PU valve pressures were measured in a similar manner. Dynamic discharge flow was measured utilizing the J-2 flight flowmeter. This turbine-type flowmeter has been shown to respond to dynamic flow perturbations to frequencies well above the range of interest (35 Hz). In addition, six Statham low-frequency accelerometers were installed at critical points on the inlet duct and supporting structure to monitor vibration levels. Figure 61 includes the locations of key dynamic measurements. Table 12 presents a complete list of parameters recorded on magnetic tape. Table 13 lists the measurements recorded on the low-frequency Beckman system to give accurate steady-state operating point data and to monitor critical pump parameters.

Tests were of two major types: pump inlet flow pulsing tests with the pump operating, and inlet duct pulsing tests with the inlet line blanked off at the pump flange. The former were run to establish LOX pump low-frequency dynamic behavior, while the latter were run in an attempt to verify inlet line fluid behavior and to establish differences between inlet line test sections. The tests were run over a range of pump operating points and PU angles with available NPSH ranging from 70 feet to 30 feet. Pulser frequency was swept from 4 to 35 Hz with some 1- to 10-Hz sweeps also included on selected tests. Essentially, the same operating regions were covered for the pump operating with each of the three inlet line test sections.

TABLE 12

HIGH-FREQUENCY MAGNETIC TAPE RECORDED MEASUREMENTS

Tape Recorder Number   1

Channel Number

1 Inlet Pressure 4 Inches Downstream of Pulser (Ph)
2 Inlet Pressure 4 Inches Downstream of Pulser (DS)
3 Propellant Utilization Valve Discharge Pressure (DS)
4 Propellant Utilization Valve Inlet Pressure (DS)
5 Discharge Pressure 12 Inches Downstream of Pump (Ph)
6 Discharge Pressure 12 Inches Downstream of Pump (DS)
7 Pump Discharge Flowmeter (Raw Signal)
8 Inlet Pressure 4 Inches Upstream of Pump (Ph)
9 Inlet Pressure 4 Inches Upstream of Pulser (Ph)
10 Low-Frequency Accelerometer No. 1 (Tank Discharge)
11 Low-Frequency Accelerometer No. 2 (Bellows)
12 Pulser Actuator Position
13 Tank Discharge Pressure (Ph)
14 Time Code (IRIG B)

Tape Recorder Number   2

Channel Number

1 Inlet Pressure 4 Inches Downstream of Pulser (Ph)(Duplicate)
2 Inlet Pressure 4 Feet Upstream of Pulser (Ph)
3 Inlet Pressure Near Upper Flange (DS)
4 Inlet Pressure 4 Inches Upstream of Pump (DS)
5 Low-Frequency Accelerometer No. 3 (Upper Flange)
6 Low-Frequency Accelerometer No. 4 (Lower Flange)
7 Pump Speed
8 Inlet Pressure 4 Inches Upstream of Pulser (DS)
9 Inlet Pressure 4 Inches Upstream of Pulser (Ph)(Duplicate)
10 Low-Frequency Accelerometer No. 5 (4 Inches Upstream of Pump)
11 Low-Frequency Accelerometer No. 6 (Wall Support)
12 Pulser Actuator Position (Duplicate)
13 Discharge Pressure 3 Feet Downstream or Pump (DS)
14 Time Code (IRIG B)

(Ph) Photocon Transducer
(DS) Data Sensor Transducer

TABLE 13

LOW-FREQUENCY MEASUREMENTS
(Recorded on the Beckman System)

1. Inlet Static Pressure 4 Feet Upstream of Pulser (Piezometer Ring)

2. Inlet Static Pressure 4 Inches Upstream of Pulser (Piezometer Ring)

3. Inlet Static Pressure 4 Inches Downstream of Pulser (Piezometer Ring)

4. Inlet Temperature 4 Inches Downstream of Pulser

5. Discharge Pressure 12 Inches Downstream of Pump Flange (Piezometer Ring)

6. Discharge Pressure 3 Feet Downstream of Pump Flange (Piezometer Ring)

7. Discharge Temperature 3 Feet Downstream of Pump Flange

8. Discharge Flowmeter Fluid Temperature

9. Pump Speed

10. Pump Bearing Coolant Pressure

11. Pump Bearing Coolant Temperature

12. Pump Drive Torquemeter Signal

13. Pump Primary Seal Cavity Pressure

14. Pulser Actuator Cylinder Pressure

A total of 195 dynamic tests was run over a 2-month period. On the early tests, the inlet line was found to have excessive vibrations. These line vibrations represent a mechanical "softness" or compliance in the system which must be eliminated or accounted for so that the resulting fluid compliance could be determined. Because it was not considered practical to account for inlet line mechanical vibrations by theoretical techniques, an effort was made to stiffen the facility line and thus reduce the vibration amplitude to an acceptable level. Further, the pulser was operated at a reduced amplitude for the remainder of the tests in an attempt to avoid exciting mechanical vibrations. Because all tests using the Rocketdyne inlet line were run prior to the facility modification, these results were considered invalid. With a few exceptions, all tests with the flight-type (SD) duct and the solid line were valid.

Results from the pulsing tests with the blanked-off flange were also invalid. Although considerable effort was made to ensure good-quality LOX, these tests showed erratic behavior even between two frequency sweeps in a single test, thus indicating the presence of significant quantities of trapped GOX. For this reason, duct pulsing test data were not used in the analysis. The resulting tests which yielded valid data are presented in Table 14.

Data Handling

The data from pulsing tests of the LOX pump were recorded on magnetic tape. The FM tape was then analyzed by using the Rocketdyne tracking filter technique. The tracking filter technique used the pulser position signal as a reference signal to control a variable center frequency of matched band-pass filters and to act as a phase reference. Individual data channels were simultaneously processed by the band-pass filters to obtain the components of the data at the frequency of the pulser input. Up to four component amplitudes, three relative phases, and three amplitude ratios can be computed simultaneously. The frequency range must be

TABLE 14

J-2 LOX PUMP PRESSURE OSCILLATION TESTING, CTL-1, CELL 2

Test Number	NPSH, feet	N, rpm	Q, gpm	PU Valve Position	Duct	Pulser Frequency, Hz
084, 085, ..., 088*	70, 60, ..., 30	8676	2917	Closed	SD	4-35
089, 090, ..., 093	70, 60, ..., 30	8676	2622	Closed	SD	4-35
094, 095, ..., 098	70, 60, ..., 30	8120	2551	Null	SD	4-35
099, 100, ..., 103	70, 60, ..., 30	8120	2300	Null	SD	4-35
104	50	8120	2300	Null	SD	0-10
105, 106, ..., 109	70, 60, ..., 30	7248	2092	Open	SD	4-35
110, 111, 112	60, 40, 70	7248	2092	Open	SD	1-10
113, 114, ..., 117	70, 60, ..., 30	7248	1890	Open	SD	4-35
118	60	8676	2917	Closed	SD	4-35
119	60	8676	2917	Closed	SD	1-10
128, 129, ..., 132	70, 60, ..., 30	8676	2917	Closed	Solid →	4-35
133	60	8676	2917	Closed		1-10
135, 136, ..., 139	70, 60, ..., 30	8676	2917	15 Deg Closed		4-35
140, 141, ..., 144	70, 60, ..., 30	8120	2551	Null		4-35
145	60	8120	2551	Null		1-10
146, 147, ..., 150	70, 60, ..., 30	8120	2551	18 Deg Open		4-35
151	50	8120	2551	18 Deg Open		4-35
152, 153, ..., 156	70, 60, ..., 30	7248	2092	18 Deg Open		4-35
157, 158	70, 60	7248	2092	Open		4-35
160, 161, 162	50, 40, 30	7248	2092	Open		4-35
163	60	7248	2092	Open		1-10
164, 165, ..., 168	70, 60, ...,30	7248	2092	Open		4-35
169, 170	70, 80	8120	2551	Null		4-35
171, 172	80, 70	8120	2551	18 Deg Open		4-35

*Indicates successive tests with the only parameter change being NPSH which is decreased in 10-foot increments.

limited to one decade in the 0- to 20K-Hz range. The tracking filter yields a much sharper filtering of the data than does an ordinary filtered Brush record but is only about one-third as selective as a Power Spectral Density (PSD) plot. The advantage of the technique over the PSD is its ability to process a continuous span of data, whereas numerous PSD's must be obtained to analyze an expanded time segment.

Typically, the ratios of inlet line pressure, discharge line pressure, and discharge line flowrate to pulser position were obtained for each test. Inlet flowrate was analytically determined using the inlet pressure measurements. These inlet pressure measurements indicated that the facility ducting could be adequately modeled as a fluid inertance, and with pressure measurements at the two extremes of the duct, flow could be computed using the relation $\Delta P = SL\dot{w}$ where L is the inertance.

Test Results

The test data were plotted as a function of frequency for each of the parameters of interest, and an estimated best-fit curve was traced through the data for each test. Typical results are shown in the figures of Appendix B. In these curves, the gain and phase of pump inlet pressure (4 inches upstream of the pulser) divided by pulser position is plotted as a function of frequency. Each figure presents data for a common inlet line and target LOX pump NPSH. The pump operating conditions (i.e., flow, speed, and PU valve position) can be determined by comparing the test numbers with the results presented in Table 14. Similar data were obtained for pump discharge pressure divided by pump inlet pressure and pump discharge flow divided by pulser position, but these curves are not included.

The data clearly indicate multiple resonances in the frequency range of 5 to 35 Hz. On each figure, the frequencies of the resonant peaks are fairly consistent from test to test, but the gains, or indicated damping factors, vary significantly. It was found in reviewing the Brush records

of t e raw data that whenever the structural vibration levels tended to
increase during a test, the response of the inlet pressure tended to
decrease giving a rounded-off resonant peak. Thus, those curves which
indicate the sharper resonances are considered to be a better representa-
tion of the pump dynamics.

The effect of pump NPSH on the resonant frequencies and amplitudes can be
determined by comparing the various figures. The first and second resonant
and antiresonant frequencies are plotted as a function of NPSH in Fig. 63
and 64 for the S-II inboard duct and a solid duct, respectively. Both of
the resonances are seen to occur at a lower frequency as NPSH decreases.
A comparison of these two figures indicates the influence of the inlet
duct configuration on the resonant frequencies. The first resonance and
antiresonance are essentially identical for both ducts. The second reso-
nance and antiresonance are at slightly lower frequencies for the S-II
inlet duct. This is believed to be the influence of the additional mechan-
ical compliance of the S-II duct. PU valve position appears to have some
effect on amplitude. The peaks at the null PU position are generally the
highest peaks of a particular set. At the full-open or closed positions,
no consistent difference can be determined. It is not certain whether
the null position results in higher pressure response or results in less
mechanical vibrations which yields higher pressure response. The effects
of pump speed and flow are even less pronounced. It should be kept in
mind that in the pump test facility, speed, flow, and PU valve position
can be set independently.

In a later section, the results of the pump and facility analytical model
are correlated with the test data. The data are presented in that section
as bands of data representing the scatter observed in the figures of
Appendix B.
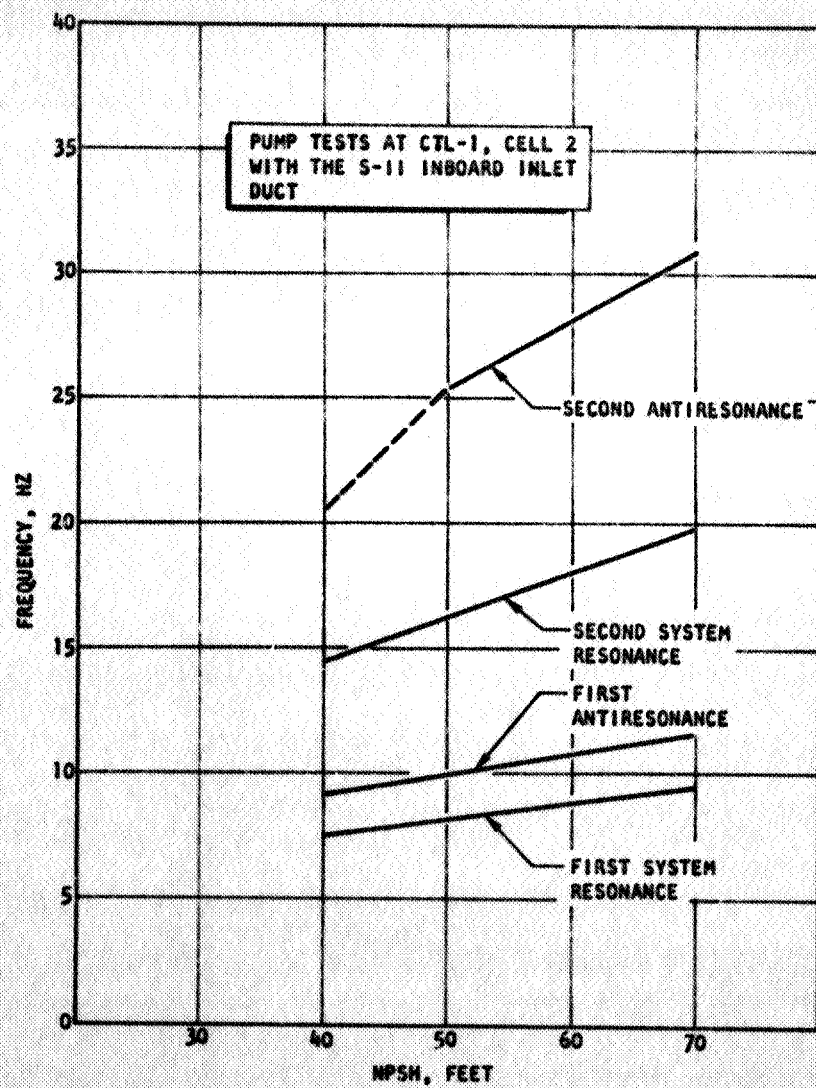
Figure 63. Observed Characteristic Frequencies for S-II Inboard Duct
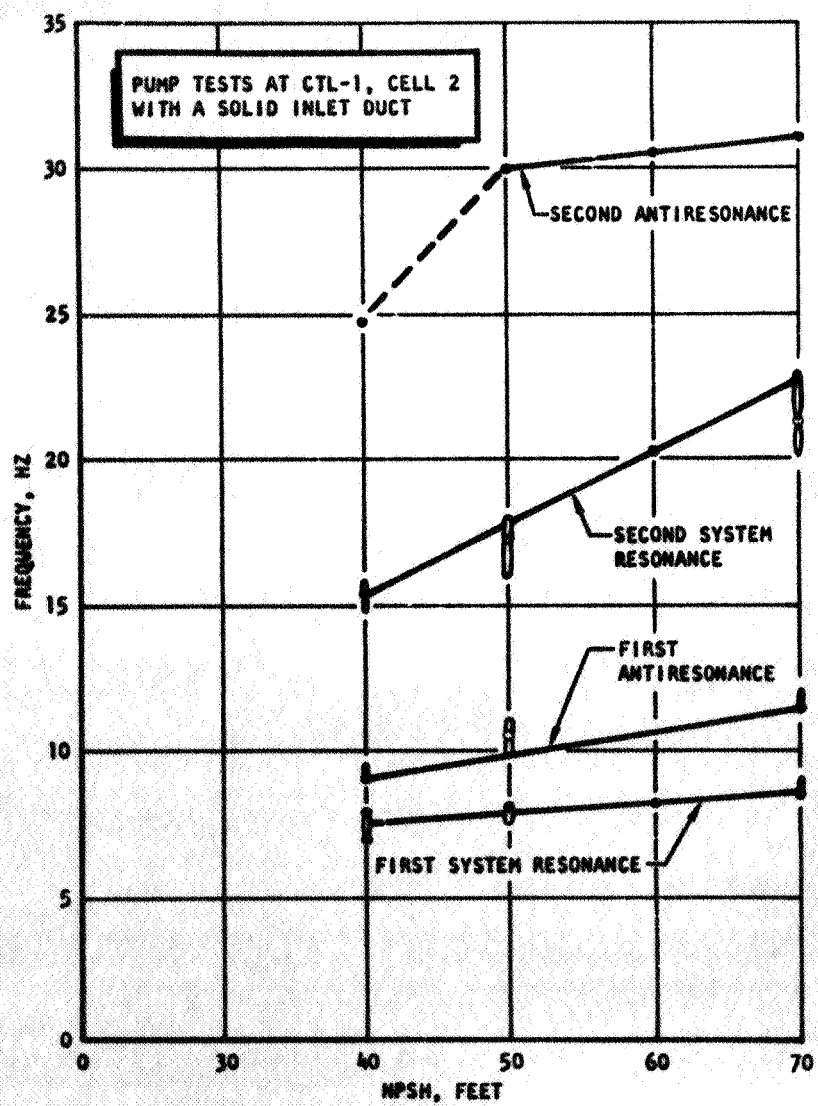
Figure 64. Observed Characteristic Frequencies for Solid Inlet Duct

Pump Analytical Model

An analytical model of the low-frequency dynamics of the CTL-1 test facility with the pulser and the LOX pump was developed. The model parameters were then determined by matching the test results of pump inlet pressure divided by pulser position. The model was then checked further by comparing the analytical and experimental response of other parameters. The purpose of the model is to understand the data from the tests, to determine the pump suction impedance for use in any other dynamic environment, and to attempt to gain better understanding of the relationship between pump design and the resulting dynamics.

The one parameter required but not directly measurable is pump inlet flow. The tests with the inlet line blanked off at the pump inlet flange were designed to determine an empirical relationship between inlet flow and inlet pressure. Extensive attempts were made to ensure that there was no trapped gas in the inlet lines during these tests, but the results indicated that gas must be present. As a result, these tests were not usable for determining the relation between suction pressure and inlet flow, and the analytical model of the inlet system was used. The facility line from the tank to the pulser was modeled using the familiar time-delay equations for acoustics in a straight duct. This model indicated no acoustic resonances for the duct in the 1- to 35-Hz range such that the duct could be treated as a simple inertance. As a simple inertance, the pressures along the duct should be in phase. The pressure amplitude at the tank is zero, and the amplitude should increase along the duct in proportion to the inertance between a station and the tank and the total line inertance. These phase and amplitude relationships were both veri- fied by the data from the pump tests and yielded confidence in the facility inlet line analytical model.

The dynamic flow input due to the pulser was computed from pulser posi- tion and the piston area. This calculation is exact if no cavitation was experienced on the withdrawal stroke of the piston. An overboard

bleed through the piston was used to assure good quality LOX, and the
pulser stroke was reduced at the higher frequencies. The data transcrip-
tion techniques filtered the input data to determine the amplitude at
the fundamental frequency so that an assumed pure sinusoidal input in
the dynamic model is a good approximation.

The duct between the pulser and the pump was treated as an inertance.
The S-II inboard duct was seen from Fig. 63 and 64 to have an associated
mechanical compliance, but this compliance was lumped together with the
pump inlet compliance. Previous experience with pump low-frequency fluid
dynamic behavior had indicated that a "cavitation compliance" or "bubble"
existed at the pump inlet, but this was not sufficient to explain pump
dynamic behavior over the frequency range of testing. A detailed phys-
ical model of the J-2 oxidizer pump was formulated which included all
potentially significant fluid passages which might contribute to the pump
dynamic behavior. Figure 65 is a cross section of the MK 15-O pump show-
ing the pertinent cavities. Aside from the main flow path, there are
three other fluid passages in the pump. First is the stress relief vol-
ume just to the side of the impeller. This cavity must contain high-
pressure LOX during pump operation. Second is the propellant utilization
passage. Flow is tapped off the discharge volute and routed to a return
point between the inducer and impeller. Depending on the PU valve posi-
tion, this flow may vary from 10 to 130 lb/sec of LOX. This passage is
presumably filled with LOX although this is by no means certain at the
low flowrates.

The third cavity is behind the impeller and extending into the area
around the bearings. This cavity is also connected to the inducer dis-
charge through passages in the impeller. Flow leaks past the seal to the
back side of the impeller and is also bled from the volute through the
bearings to the back side of the impeller. It is likely that two-phase
fluid exists around the bearings as a result of high local velocities

PU
BYPASS
FLOW
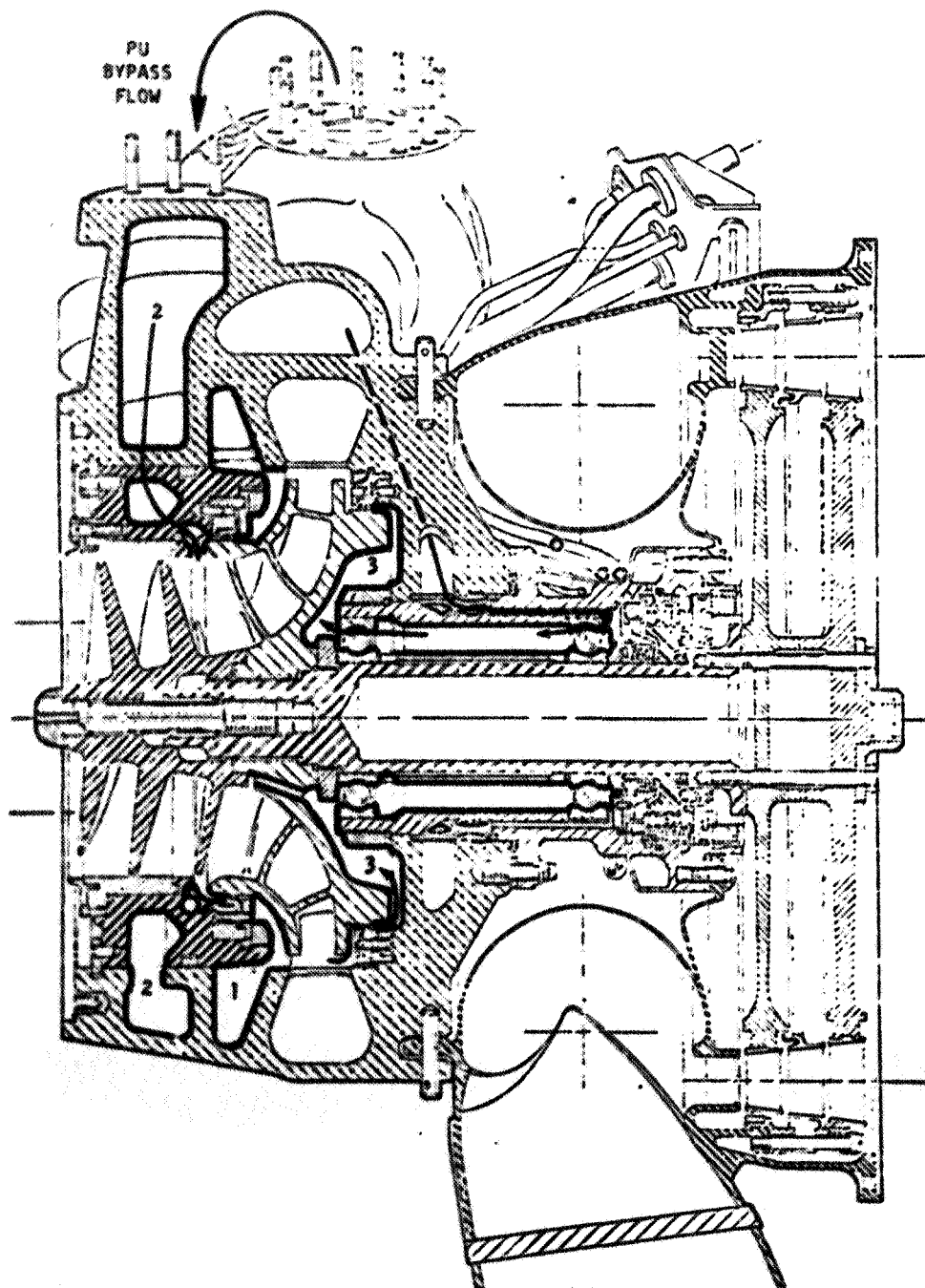
　　　　　Figure 65.　J-2 Oxidizer Pump

and bearing friction heat input. In addition, the antivortex vanes installed behind the impeller to prevent vortexing in the direction of impeller rotation almost certainly induce vortexes at 90 degrees to this plane. In other words, this is an area for potential two phase oxygen.

Recognizing the fluid dynamic potential of these cavities, it was determined that the initial model should include them all. Figure 66 illustrates the postulated lumped parameter pump model representing this system.

The facility discharge system of the pump was modeled analytically using the same techniques as used on the inlet system. It was found that there was a flow throttle valve control which was active below 10 Hz. The effect of this flow control was studied using the analytical model. The results indicated that the control had very little effect on the response of inlet pressure divided by pulser position as shown in Fig. 67. Probably even more significant, these results indicate that the inlet pressure is relatively insensitive to the discharge system behavior and that any reasonable dynamic approximation of the discharge system is adequate in the analytical model. Of course, the influence of the discharge system dynamic representation would be greater on the discharge parameters of pressure and flow. Figure 68 indicates the effect on discharge pressure of this flow control.

The complete pump-facility model is shown schematically in Fig. 69. The model equations are given below with explanations. Only certain coefficients are unspecified in the equations, and these were studied to determine their influence and then to match the test data. These unspecified coefficients are the pump inlet compliance, B_1 of Eq. 52, the impeller back-side cavity compliance, B_2 of Eq. 56, the inertia and resistance associated with the back-side cavity, L_2 and R_2 of Eq. 55, and the factor K used to relate inducer head rise to NPSH, Eq. 53. If K is zero, inducer head rise is independent of NPSH, but as cavitation is encountered in the inducer the value of K assumes some small value.
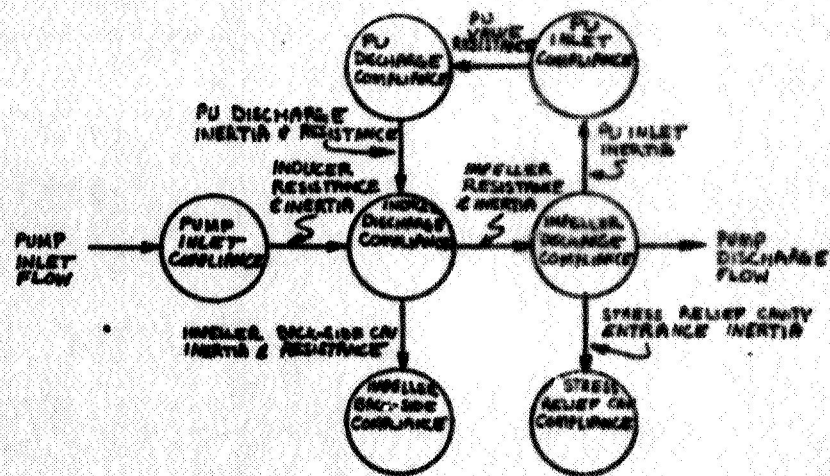
Figure 66. J-2 LOX Pump Lumped Parameter Fluid Dynamic Model
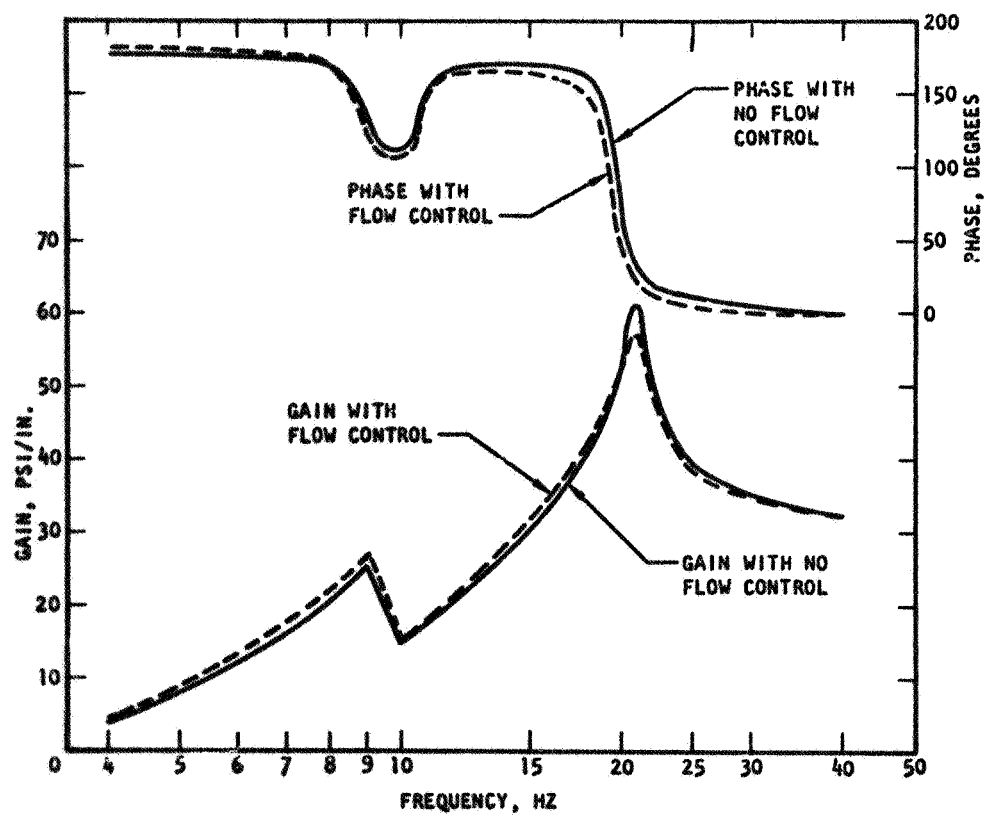
Figure 67. Inlet Pressure to Pulser Position Transfer Function for Two Different Discharge Systems
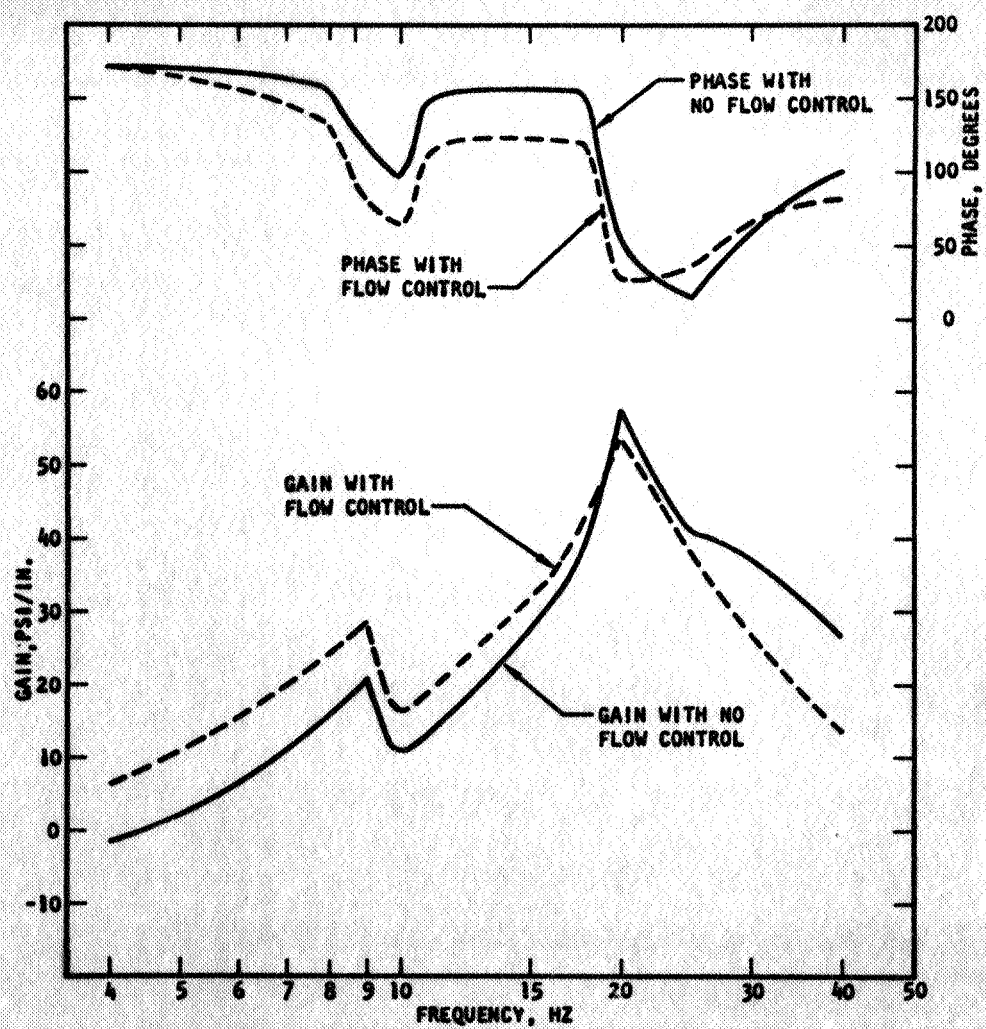
Figure 68. Discharge Pressure to Pulser Position Transfer Function for Two Different Discharge Systems
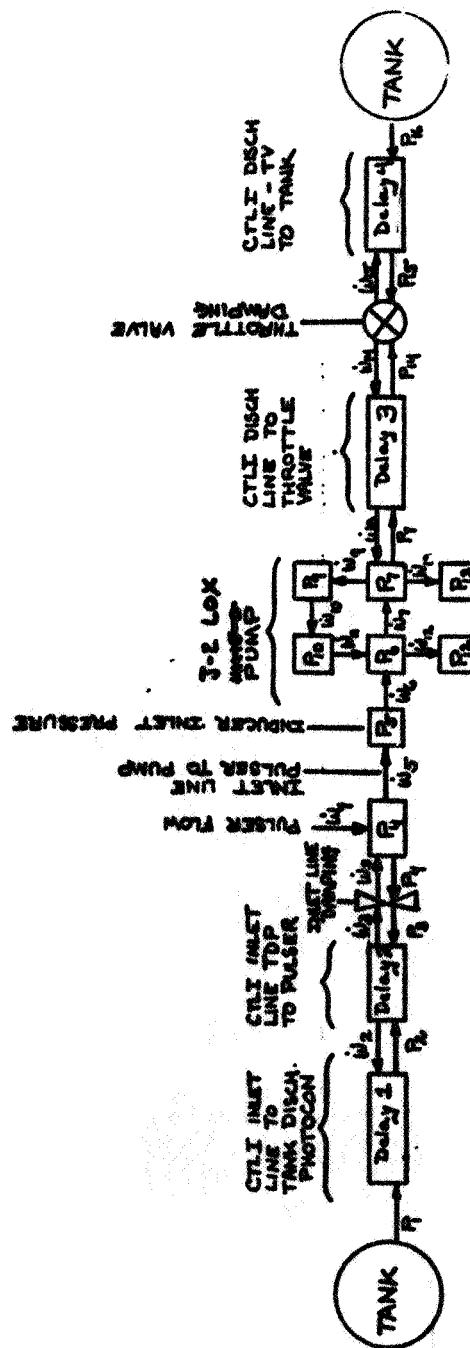
Figure 69. Block Diagram of Dynamic Model of CTL-1 Facility With J-2 LOX Pump

166

PUMP FACILITY DYNAMIC MODEL EQUATIONS

(45) $0 = -P_2 - P_2 e^{-0.002576S} - 1.788 \dot{w}_2 + 1.788 \dot{w}_2 e^{-0.002576S}$ Time Delay 1

(46) $0 = -\dot{w}_2 + \dot{w}_2 e^{-0.010562S} - 1.7634 P_3 e^{-0.005281S}$
$\qquad +0.8817 P_2 (1.0 + e^{-0.01056S})$

(47) $0 = -\dot{w}_3 + \dot{w}_3 e^{-0.010562S} + 1.7634 P_2 e^{-0.005281S}$
$\qquad -0.8817 P_3 - 0.8817 P_3 e^{-0.010562S}$

Time Delay 2
Equations
Tank Discharge
Photocon
to Pulser

(48) $P_3 = P_4 + 0.01 \dot{w}_3$ Inlet Line Damping

(49) $\dot{P}_4 = 10,000 (\dot{w}_3 + \dot{w}_4 + \dot{w}_5)$ Flow Effects at Pulser

(50) $\dot{w}_4 = 0.2035 \dot{x}$ Pulser Input

(51) $\ddot{w}_5 = 326.3 (P_4 - P_5)$ Pulser-to-Pump Inlet Line

(52) $\dot{P}_5 = B_1 (\dot{w}_5 - \dot{w}_6)$ Pump Inlet Compliance

(53) $\ddot{w}_6 = 400 \left[(1 + K)P_5 - P_6 - 0.363 \dot{w}_6 \right]$ Inducer Flow

(54) $\dot{P}_6 = 1000 (\dot{w}_6 + \dot{w}_{11} - \dot{w}_{12} - \dot{w}_7)$ Interstage Pressure

(55) $\ddot{w}_{12} = L_2 (P_6 - P_{12} - R_2 \dot{w}_{12})$ Impeller Cavity Flow

(56) $\dot{P}_{12} = B_2 \dot{w}_{12}$ Impeller Cavity Pressure

(57) $\ddot{w}_7 = 1000 (P_6 - P_7 - 1.0 \dot{w}_7)$ Impeller Flow

(58) $\dot{P}_7 = 10,000 (\dot{w}_7 - \dot{w}_{13} - \dot{w}_9 - \dot{w}_8)$ Impeller Discharge Pressure

(59) $\ddot{w}_{13} = 10,000 (P_7 - P_{13})$ Stress Relief Cavity Flow

(60) $\dot{P}_{13} = 56,370 \dot{w}_{13}$ Stress Relief Cavity Pressure

(61) $\ddot{w}_9 = 92.85 (P_7 - P_9)$ PU Inlet Flow

(62) $\dot{P}_9 = 135,800 \ (\dot{w}_9 - \dot{w}_{10})$ PU Inlet Pressure

(63) $\ddot{w}_{10} = 295.9 \ (P_9 - P_{10} - 4 \ \dot{w}_{10})$ PU Valve Flow

(64) $\dot{P}_{10} = 34,390 \ (\dot{w}_{10} - \dot{w}_{11})$ PU Discharge Pressure

(65) $\ddot{w}_{11} = 719.4 \ (P_{10} - P_6 - 2 \ \dot{w}_{11})$ PU Discharge Flow

(66) $0 = -P_{14} - P_{14} \ e^{- \ 0.008918S} + 2 \ P_7 \ e^{- \ 0.004459S}$

$\qquad - 7.124 \ \dot{w}_{14} + 7.124 \ \dot{w}_{14} \ e^{- \ 0.008918S}$

(67) $0 = - \ \dot{w}_8 - \dot{w}_8 \ e^{- \ 0.008918S} + 2 \ \dot{w}_{14} \ e^{- \ 0.004459S}$

$\qquad - 0.1404 \ P_7 \ e^{- \ 0.008918S} + 0.1404 P_7$

$\left. \begin{array}{l} \\ \\ \\ \\ \\ \\ \end{array} \right\}$ Time Delay 3
Equations
Pump Discharge
to
Throttle Valve

(68) $\dot{w}_{14} = (P_{14} - P_{15})/4$ Throttle Valve Damping

(69) $0 = -P_{15} - P_{15} \ e^{- \ 0.01472S} - 1.8126 \ \dot{w}_{14} \ e^{- \ 0.01472S}$

$\qquad + 1.8126 \ \dot{w}_{14}$

$\left. \begin{array}{l} \\ \\ \\ \\ \end{array} \right\}$ Time Delay 4
Equation,
Throttle Valve
to Tank

DERIVATION OF DYNAMIC MODEL COEFFICIENT VALUES

Equation Number	Coefficient Value	Derivation
(48)	0.01 psi/(lb/sec)	Inlet line damping based on an estimated 4-psi friction loss at 400 lb/sec flow
(49)	10,000 $1/in.^2$	Estimated pulser compliance (all liquid oxygen)
(50)	0.2035 $(lb/sec)/(lb/in.^2)$	Pulser piston velocity-flow relation for 5-sq in. pulser
(51)	326.3 $(lb/sec^2)/psi$	Pulser-to-pump inlet inverse fluid inertia, $50.03\text{-}in.^2$ line 59.25 inches long
(52)	B_1 $1/in.^2$	Pump inlet compliance (including the inlet bellows effect) 150 $1/in.^2$ to 50 $1/in.^2$ range based on model matching
(53)	400 $(lb/sec^2)/psi$	Inverse pump inducer inertia
(53)	K psi/psi	Effect of inlet pressure (NPSH) on inducer head rise experimentally determined to be 0.5 by model matching
(53)	0.363 psi/(lb/sec)	Linearized damping resulting from inducer head-flow characteristic
(54)	1000 $1/in.^2$	Estimated inducer discharge compliance (perturbation studies show this to be a reasonable value)
(55)	L_2 $(lb/sec^2)/psi$	Inverse inertia of impeller back-side cavity passage calculated = $\frac{1}{0.02}$ = 50 $lb/sec^2/psi$ based on pump data
(55)	R_2 psi/lb/sec	Linearized damping of impeller back-side cavity passage experimentally determined equal to 0.5 psi/lb/sec by model matching

Equation Number	Coefficient Value	Derivation
(56)	B_2 1/in.^{2}	Impeller back-side cavity compliance 150-1/in.^{2} to 90-1/in.^{2} range based on model matching
(57)	1000 lb/sec^2/psi	Estimated LOX pump impeller inverse inertia
(57)	1.0 psi/lb/sec	Linearized damping resulting from impeller head-flow characteristic
(58)	10,000 1/in.^{2}	Estimated impeller discharge compliance (high-pressure liquid)
(59)	10,000 lb/sec^2/psi	Estimated stress relief cavity passage inverse inertia
(60)	56,370 1/in.^{2}q	Stress relief cavity calculated compliance (high-pressure liquid)
(61)	92.85 lb/sec^2/psi	Calculated PU valve inlet inverse inertia
(62)	135,800 1/in.^{2}	Calculated PU valve inlet cavity compliance
(63)	295.9 lb/sec^2/psi	Estimated PU valve and discharge inverse inertia
(63)	4 psi/lb/sec	Estimated linearized damping resulting from PU valve
(64)	34,390 1/in.^{2}	Estimated PU discharge compliance
(65)	719.4 lb/sec^2/psi	Estimated PU return passage inverse inertia
(65)	2 psi/lb/sec	Estimated linearized damping resulting from PU return passage

$a = 34,560$ in./sec   acoustic velocity of LOX in inlet lines

$a = 35,040$ in./sec   acoustic velocity of LOX in discharge lines

Initially, each of these parameters were to be perturbed to determine its influence on the inlet pressure response. Some of the early analytical results indicated that the side-branch inertia, L_2, was not varying with NPSH and its value could be determined analytically. The form of the data and the model results indicate that the response curve of inlet pressure at the pulser divided by pulser position has the asymptotes as indicated in the sketch below.
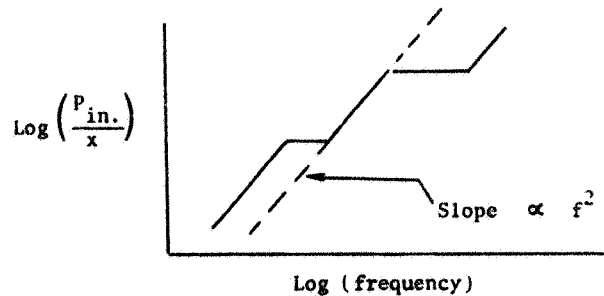
The location of the break points on the frequency scale is determined by the resonances and antiresonances of Fig. 63 or 64. The intercepts of the asymptotes with the ordinate scale are primarily a function of the inertances of the system.

Assuming that the inertance of the facility lines, inlet line, and the inducer and impeller are independent of NPSH, the only significant inertance which could vary would be L_2, the side-branch inertance. However, the asymptote along the dashed line in the sketch above is independent of NPSH, thus indicating that L_2 is independent of NPSH. The required value of L_2 to get this asymptote is in the range of 0.0183 to 0.026 $(sec/in.)^2$, the lower values appearing to be more realistic. Thus, a value $L_2 = 0.02$ was used, and it was not necessary to vary this parameter in the studies correlating the analytical model with the experimental data.

Thus, there are four parameters which were varied to arrive at model-data correlation. The effect of all four on the pump parameters are shown in Fig. 70 through 81. The first three of these figures indicate the effect of the pump inlet compliance (B_1). This compliance is seen to have a strong effect on the second resonant and antiresonant frequencies and amplitudes. Because these frequencies vary with NPSH, B_1 will have to vary with NPSH, but this was expected because B_1 is an indication of the pump cavitation. The side-branch compliance (B_2) has a similar effect on the first resonance and antiresonance. The factor $(1 + K)$ tends to shift the second resonant frequency and to flatten the first resonance-antiresonance pair of pump inlet pressure (Fig. 76). The side-branch resistance, R_2, tends to lower the amplitude of both resonant peaks without shifting the frequencies.

Correlation of Model With Data

It now remains to select those values of the four unknown parameters which will result in correlation with the data. As there was a rather large amount of data scatter, the data had to be weighted to establish what were considered the most representative results apart from contamination by noise, vibrations, etc. Part of this weighting is reflected in the figures to follow where bands of data are presented for each NPSH, but some of the actual data falls outside these bands. In general, the analytical resonant peaks were selected to match the higher values in the data band. This yields results which are more conservative but are also expected to be more accurate. In each case, the pump inlet pressure (at the pulser) divided by pulser position was selected as the parameter to be matched by the model. The data for this parameter is more consistent and reliable, and the suction side impedance is the desired output of the model. The comparison of model results with data of other parameters added confidence to the validity of the model.

The bands of data are shown in Fig. 82 through 89 , and the model results are indicated by dashed lines on the figures. The correlation is generally seen to be good. If it were desired to match the data to the lower gains,

this could be accomplished by increasing the resistance, or damping, terms, e.g., R_2. Considering specific curves, the fit of P_1/X is good in each case for both gain and phase with the one possible exception of the second resonant frequency at a NPSH of 50 feet. This particular resonance was less consistent from test-to-test so that the data scatter itself prevents the correlation from appearing as good. This resonance could be lowered by decreasing B_1, but this would lower its amplitude as well (Fig. 70). There is enough scatter in the flow data to render any attempt at correlation uncertain. However, each time the model results indicate resonant and antiresonant peaks, there are some data which also indicate a corresponding response of gain. The correlation of flow phase angle is as good as could be expected from the flow data. Certain aspects of the pump gain (=pump discharge/inlet pressure) are matched well by the model, e.g., the gain trends at the higher frequencies. However, the correlation is not as good for gain at lower frequencies, but the discharge parameters at the lower frequencies are contaminated by the active flow control valve in the discharge line.

To arrive at these data correlations, the side-branch resistance, R_2, and the NPSH factor, $1 + K$, were constant with respect to NPSH. The values used were

$$R_2 = 0.5 \text{ sec/in.}^2$$

$$1 + K = 1.5$$

The two cavitation compliances used are shown as a function of NPSH in Fig. 90.

The comparison of model results and test data demonstrates that the model is capable of matching the features of the test results. In fact, considering the nature of the data and the difficulties encountered in obtaining good data, the overall agreement of model and data is believed to be quite good. This means that the model is sufficient to obtain pump suction impedance, but it cannot be shown that this model formulation is

unique, i.e., the only possible form. Furthermore, it cannot be proven that the elements of the model correspond to the physical cavities which suggested their use. It does seem to be more than coincidence, however, that a model derived from the physical pump drawings matches the test data so well. Further effort would be required to demonstrate model uniqueness and to definitely associate physical cavities with model elements.
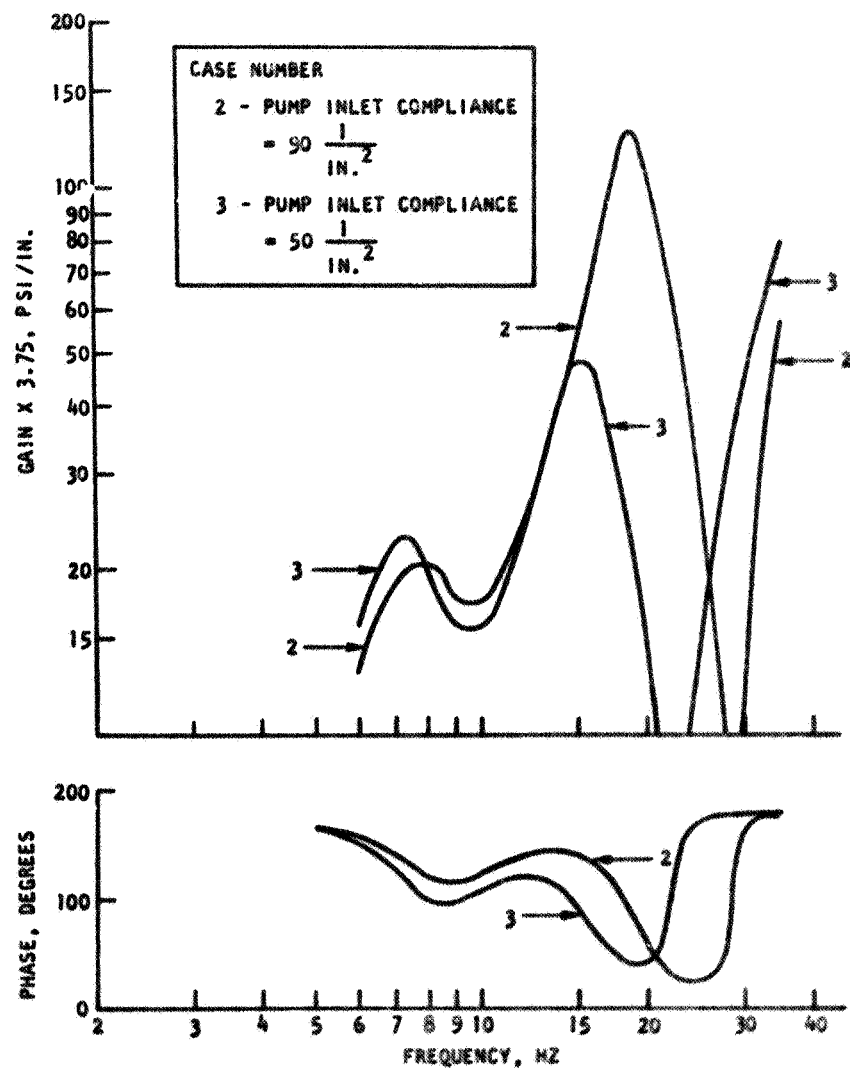
Figure 70. Predicted Effect of Pump Inlet Compliance (B_1) on Pump Inlet Pressure Gain (P_4/X)
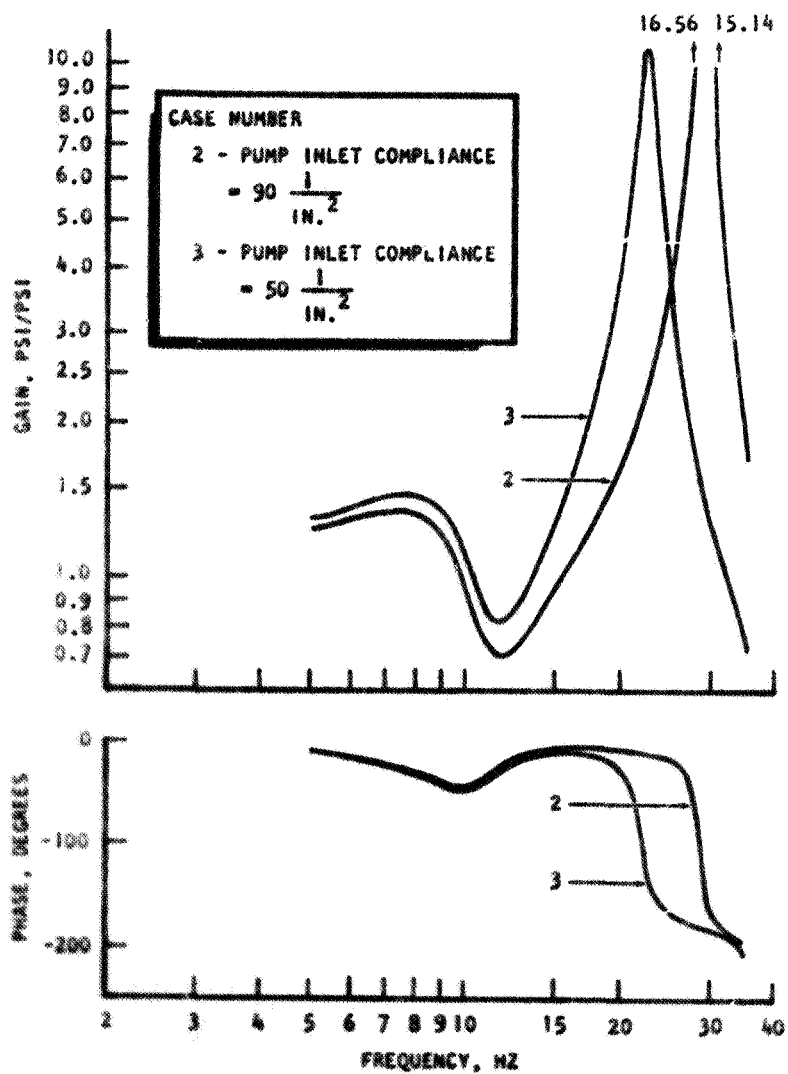
Figure 71. Predicted Effect of Pump Inlet Compliance on Pump Gain (P_7/P_4)
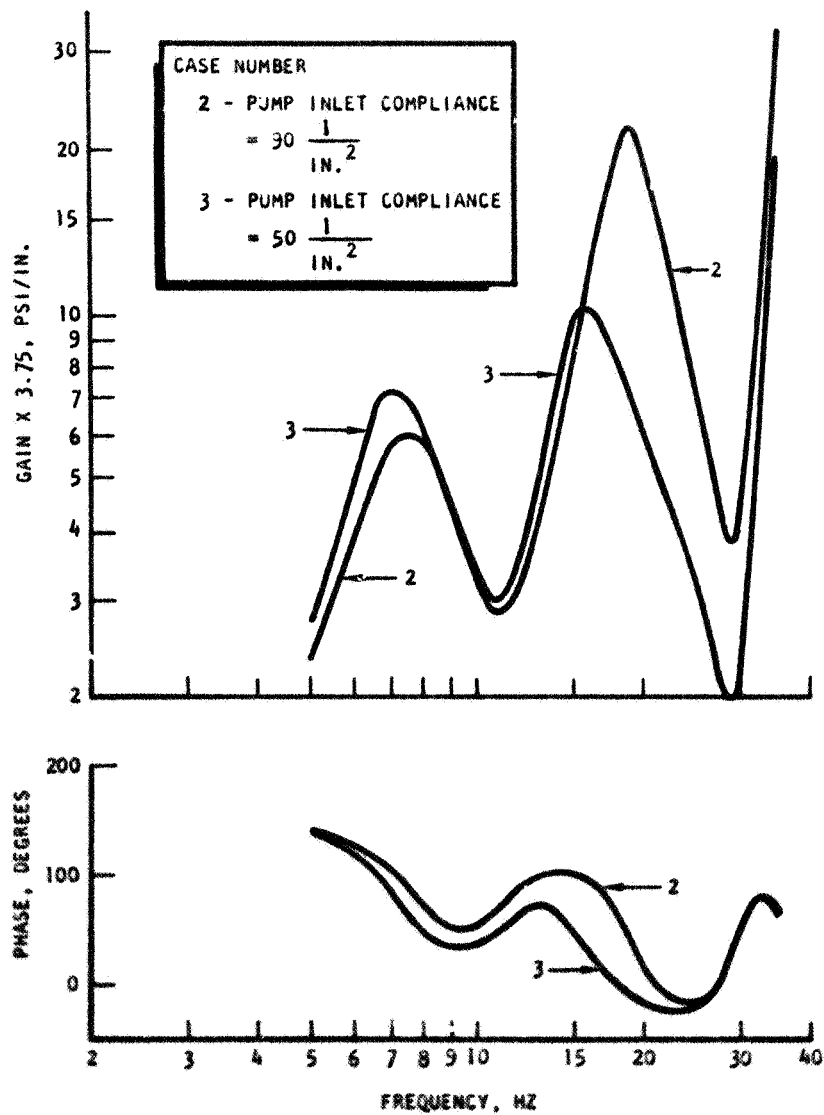
Figure 72. Predicted Effect of Pump Inlet Compliance on Pump Discharge Flow ($\dot{w}_g/x$)
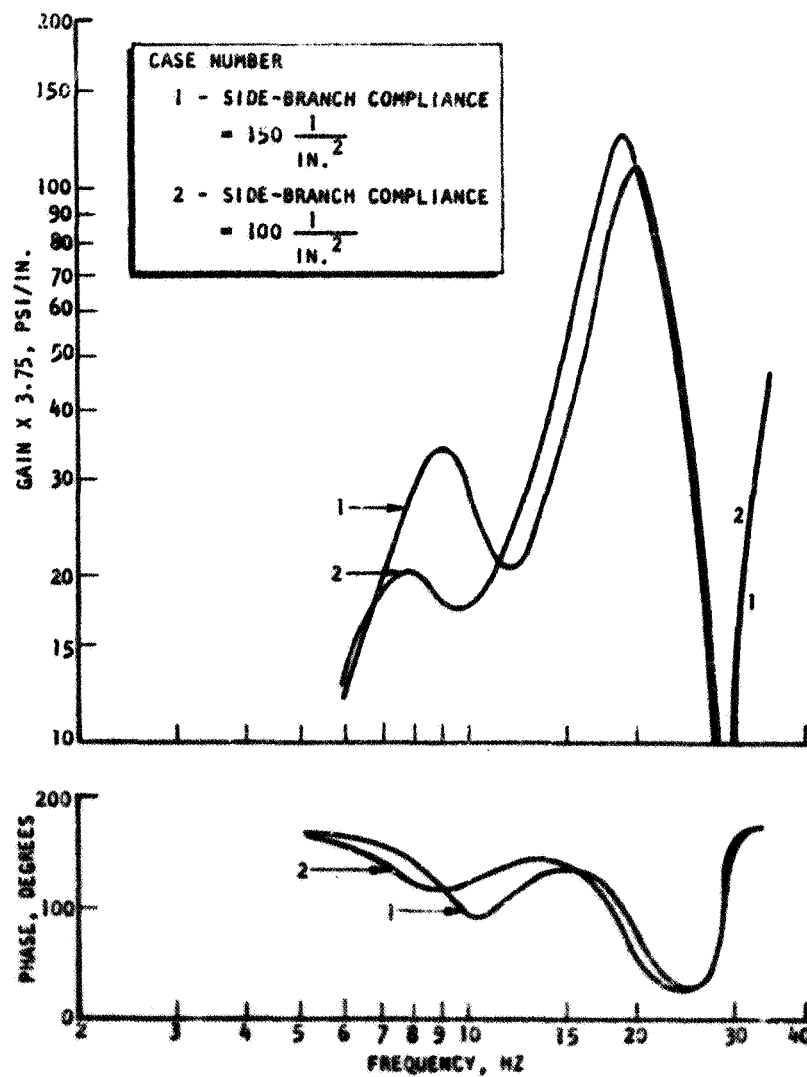
Figure 73. Predicted Effect of Pump Side-Branch Compliance (n_2) on Pump Inlet Pressure Gain (P_4/X)
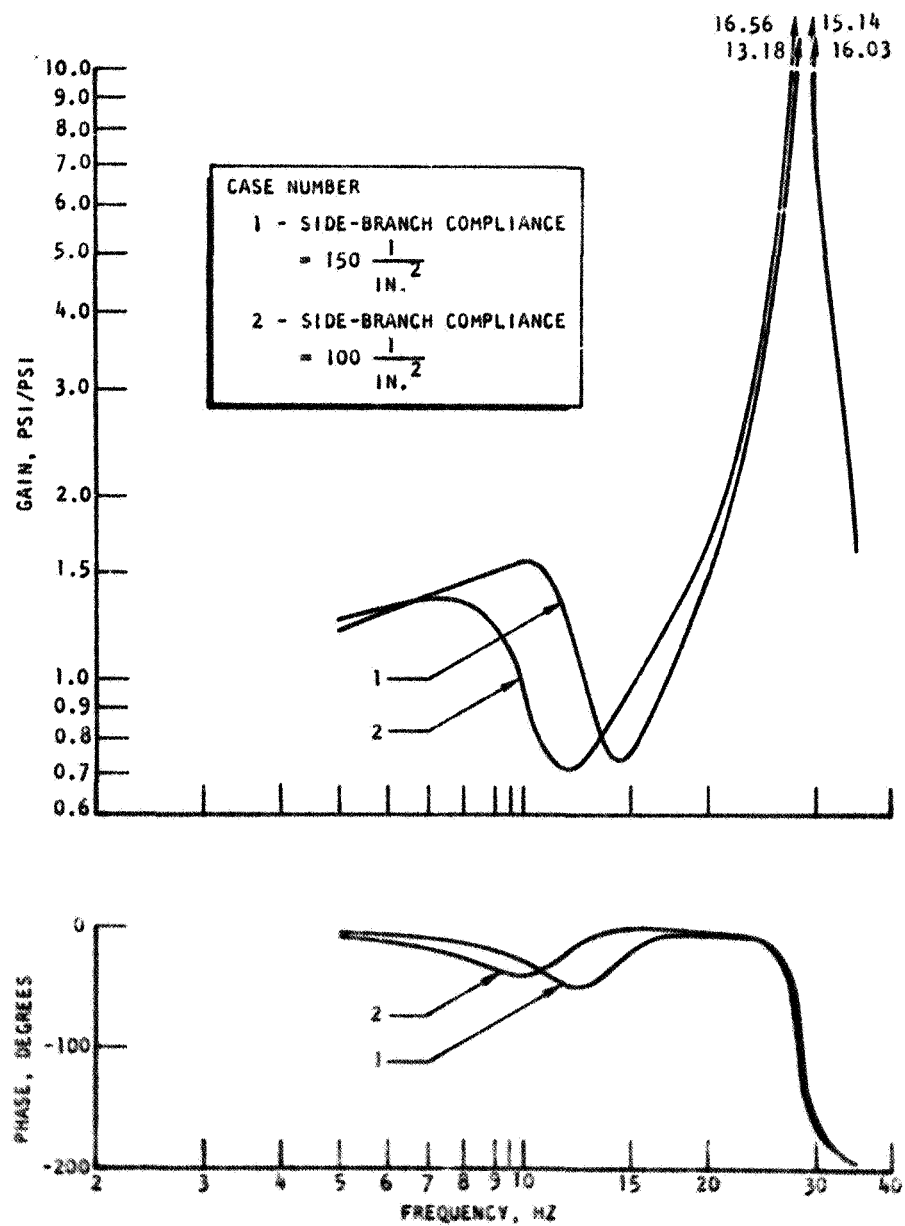
Figure 74. Predicted Effect of Pump Side-Branch Compliance (B_2) on Pump Gain (P_7/P_4)
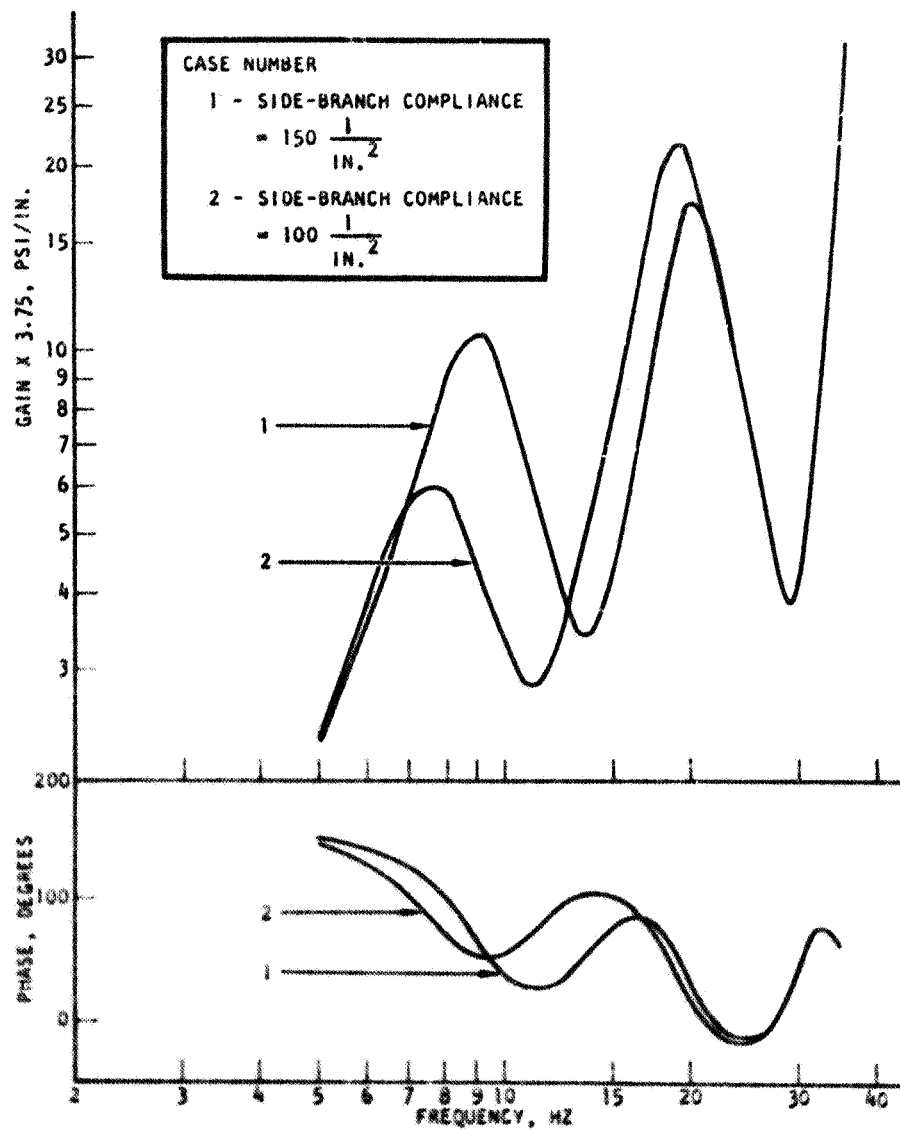
Figure 75. Predicted Effect of Pump Side-Branch Compliance (S_2) on Pump Discharge Flow Gain ($\dot{q}_8/X$)
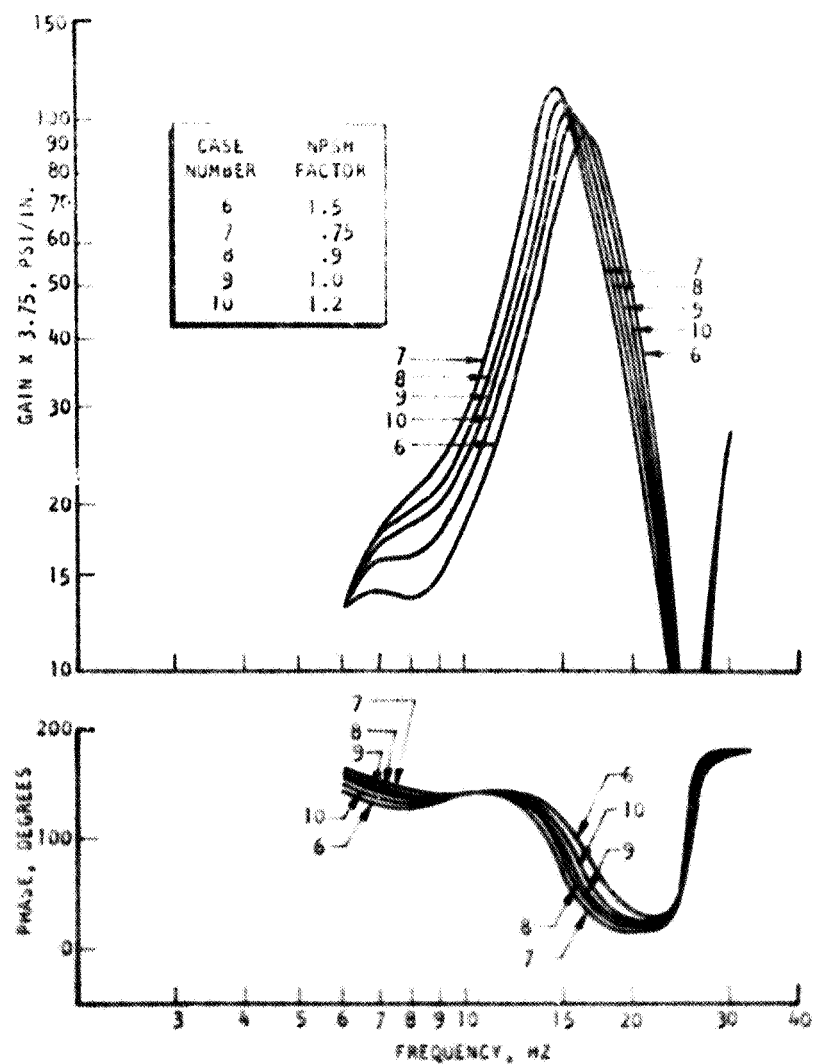
Figure 76.   Predicted Effect of NPSH Factor (1+K) on
Pump Inlet Pressure Gain (P$_s$/X)
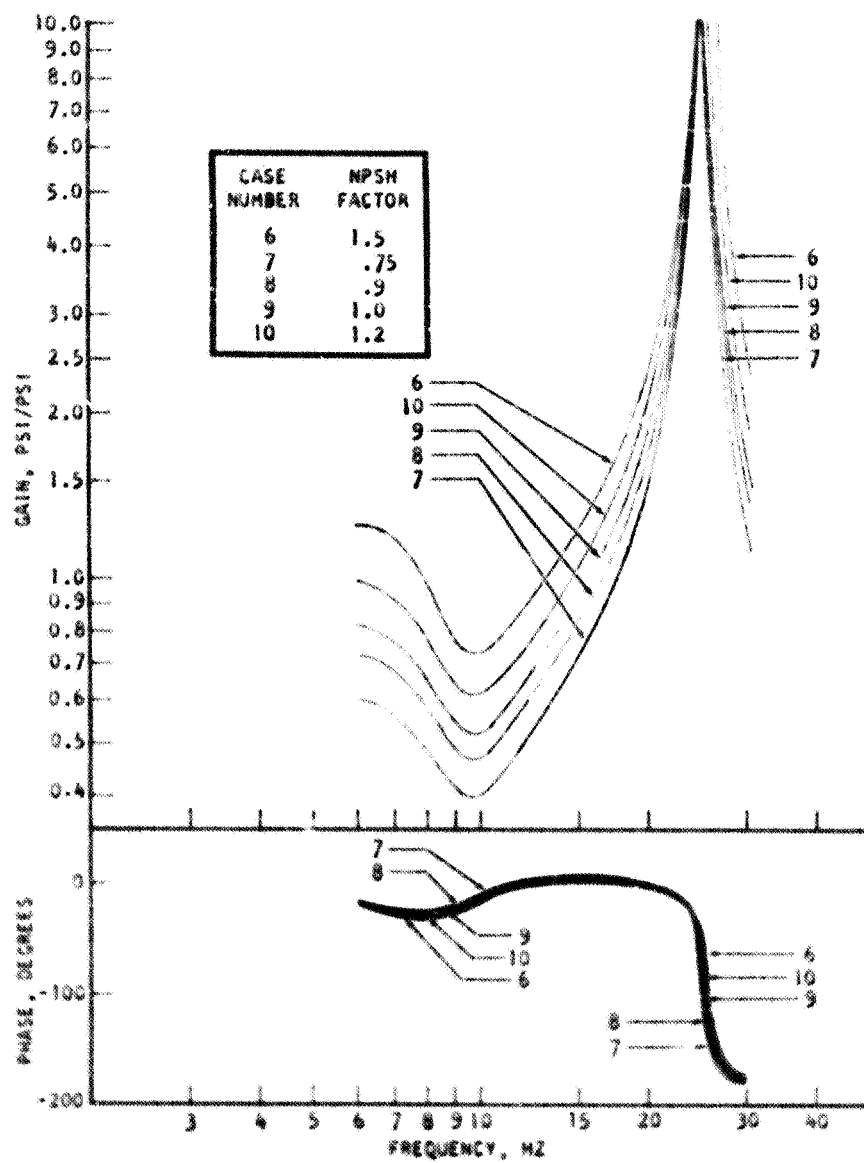
Figure 77. Predicted Effect of NPSH Factor on Pump Gain (P_o/P_i)

CASE NUMBER	NPSH FACTOR
6	1.5
7	.75
8	.9
9	1.0
10	1.2
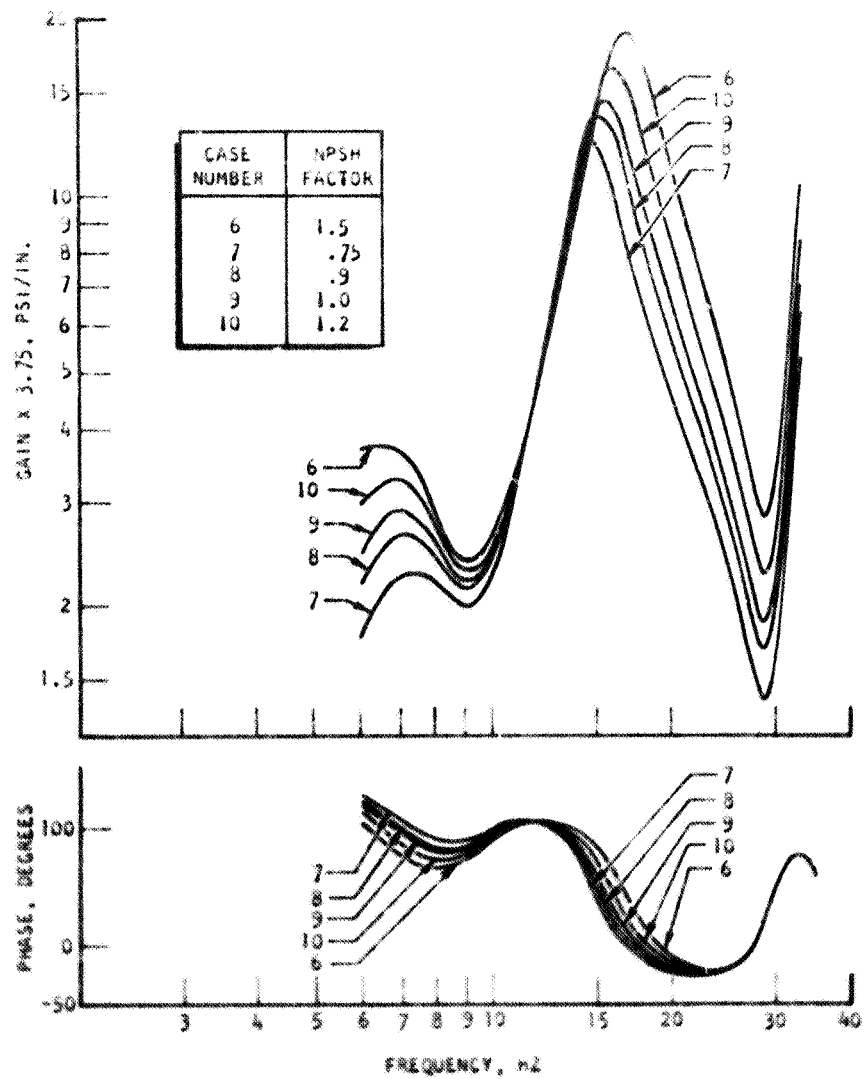
Figure 78. Predicted Effect of NPSH Factor on Pump
Discharge Flow ($\dot{w}_D/X$)

CASE NUMBER	NPSH FACTOR
6	1.5
7	.75
8	.9
9	1.0
10	1.2
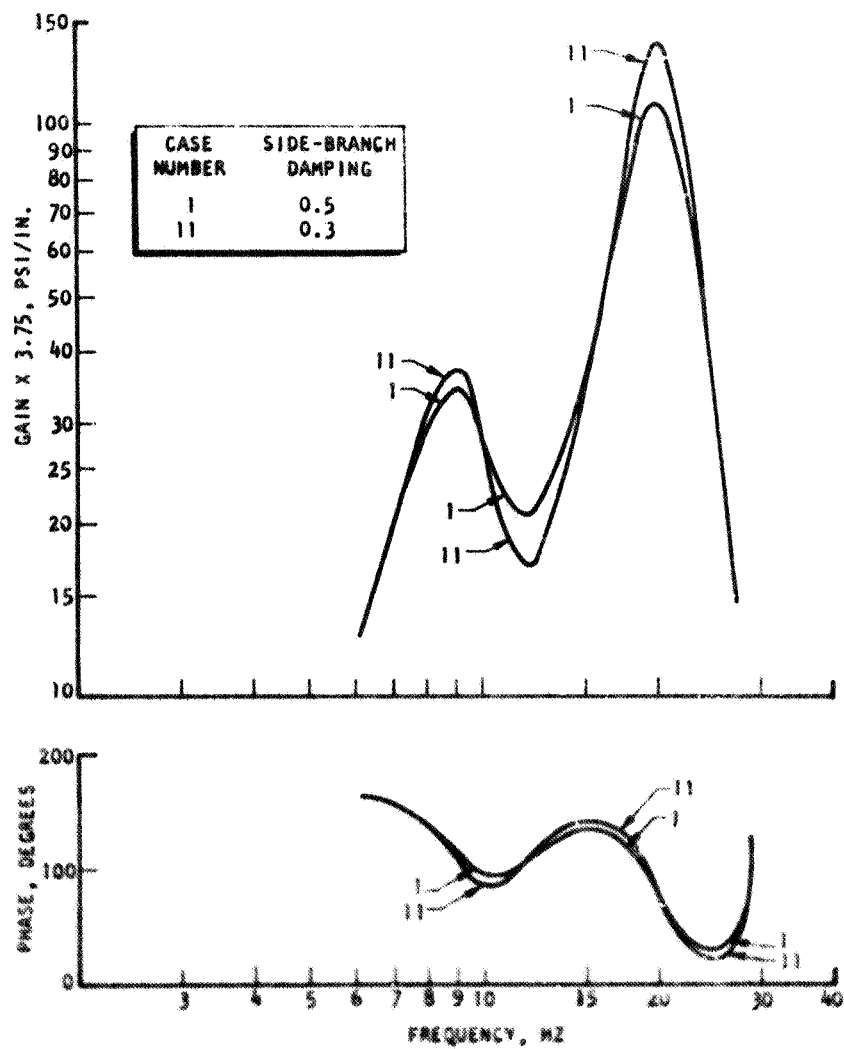
Figure 79. Predicted Effect of Side-Branch Damping (R_2) on Pump Inlet Pressure Gain (P_4/X)
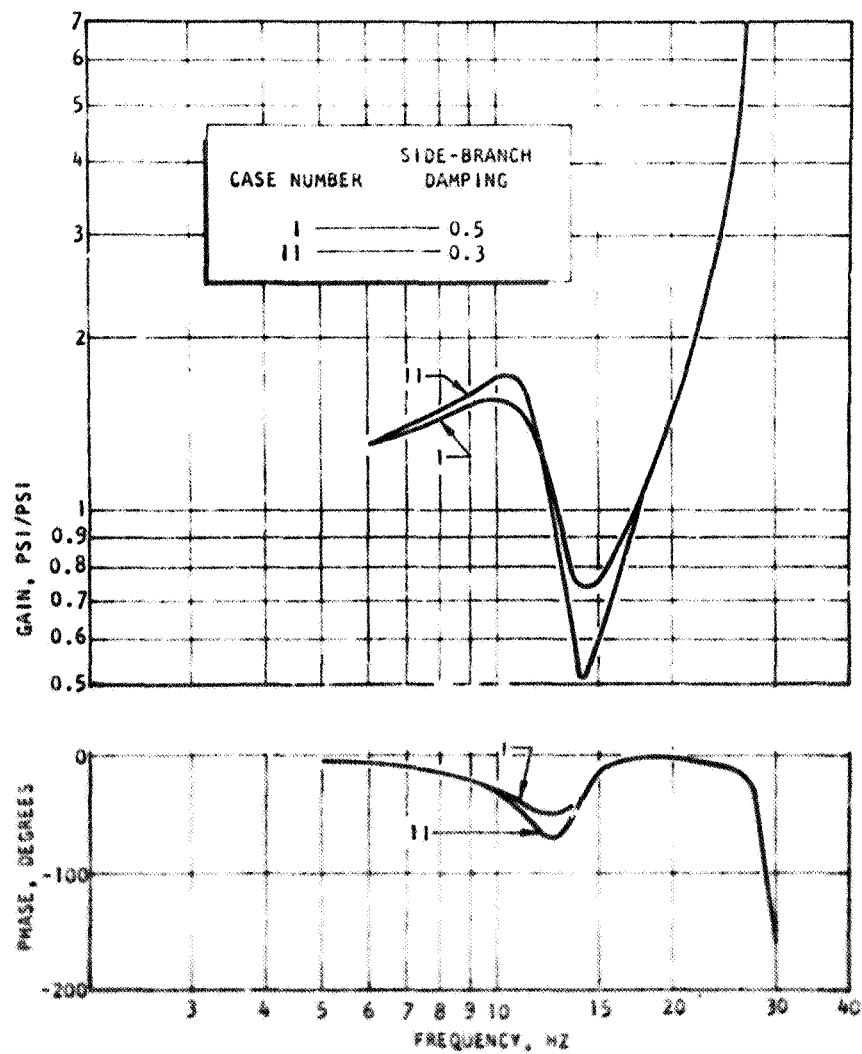
Figure 80. Predicted Effect of Side-Branch Damping (P_2) on Pump Gain (P_7/P_8)
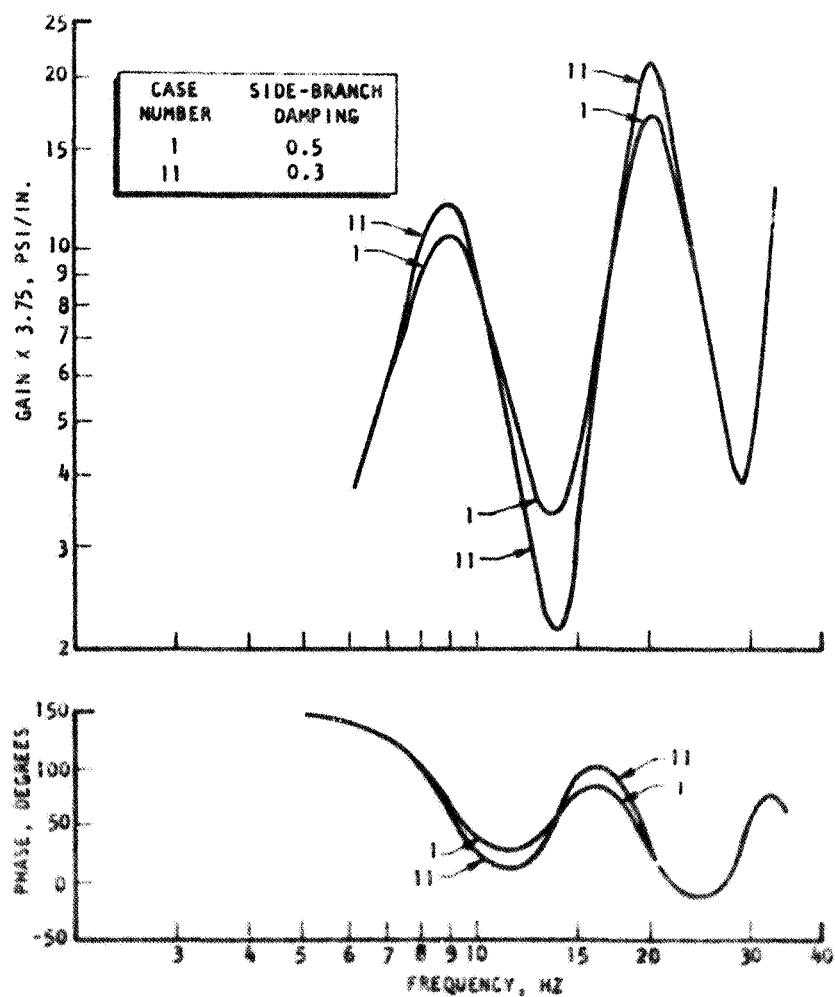
Figure 81. Predicted Effect of Side-Branch Damping (R_2) on Pump Discharge Flow ($\dot{m}_8/\lambda$)
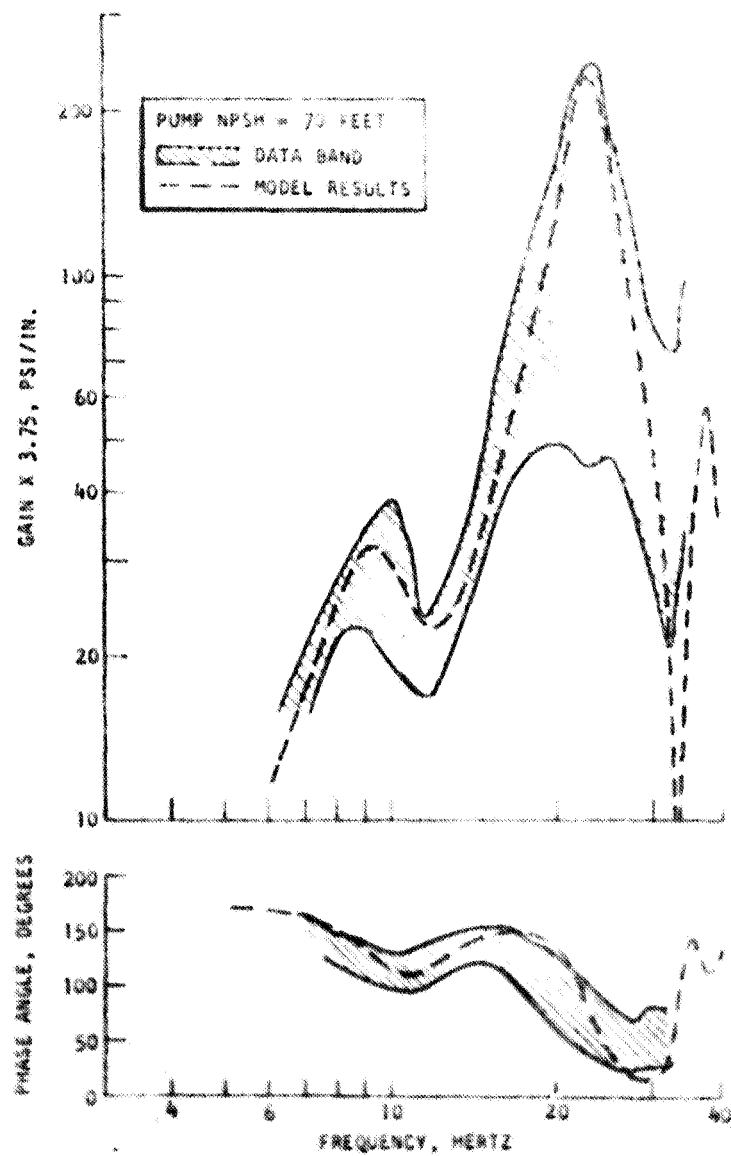
Figure 82. Comparison of Analytical and Experimental Results for Pump Inlet Pressure Divided by Pulser Position
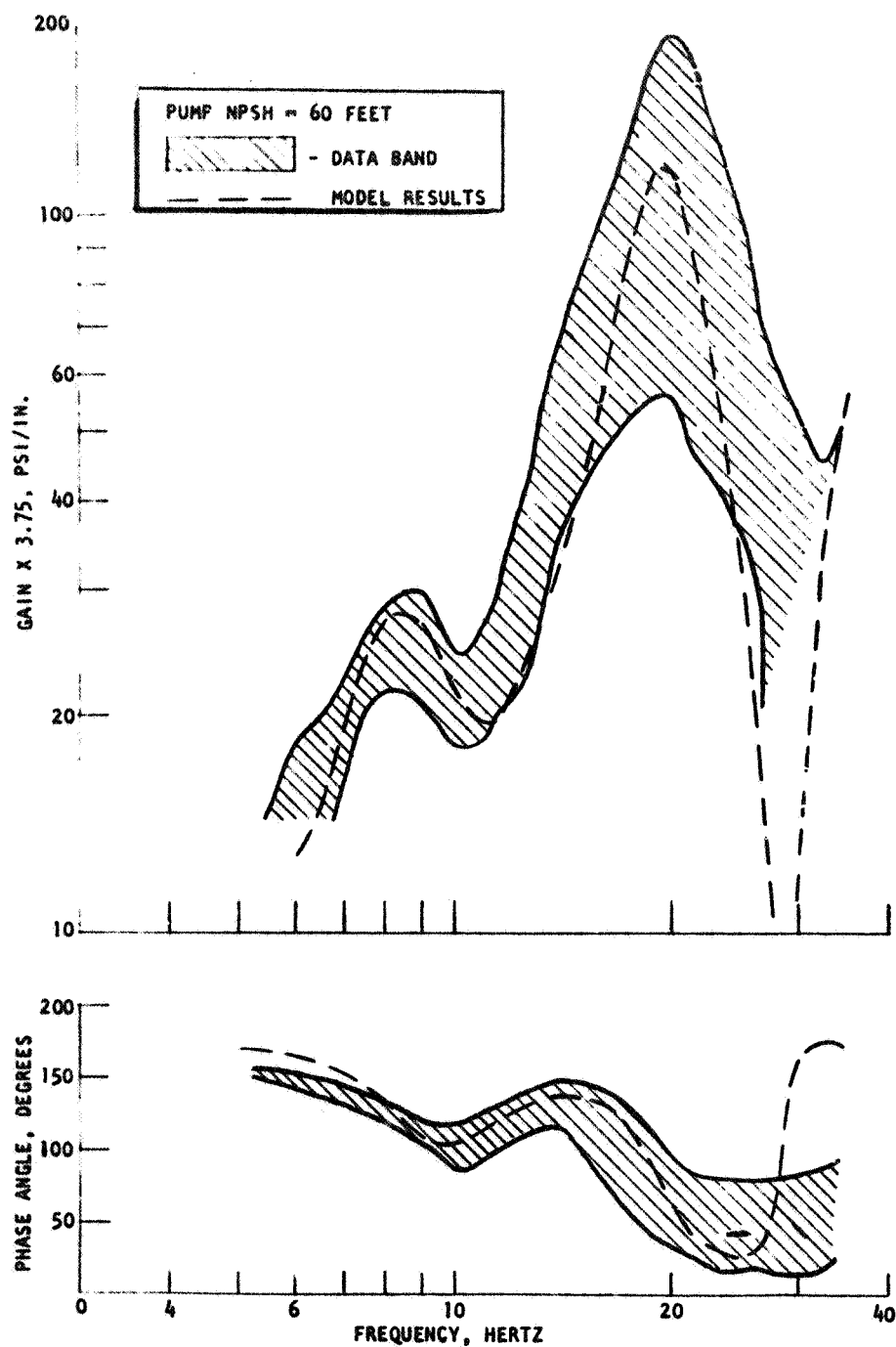
Figure 83. Comparison of Analytical and Experimental Results for Pump Inlet Pressure Divided by Pulser Position

R-7970
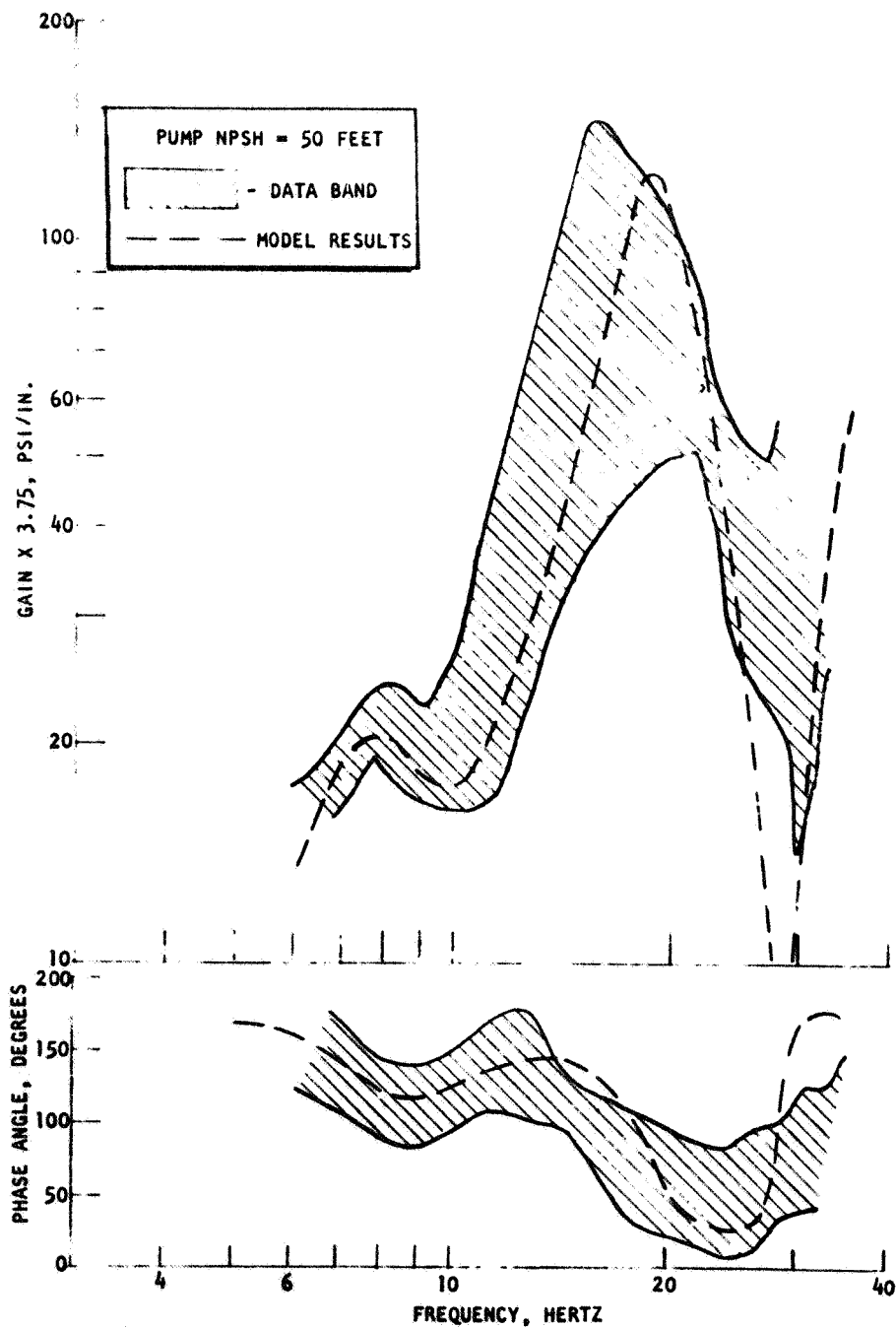
Figure 84. Comparison of Analytical and Experimental Results for
Pump Inlet Pressure Divided by Pulser Position
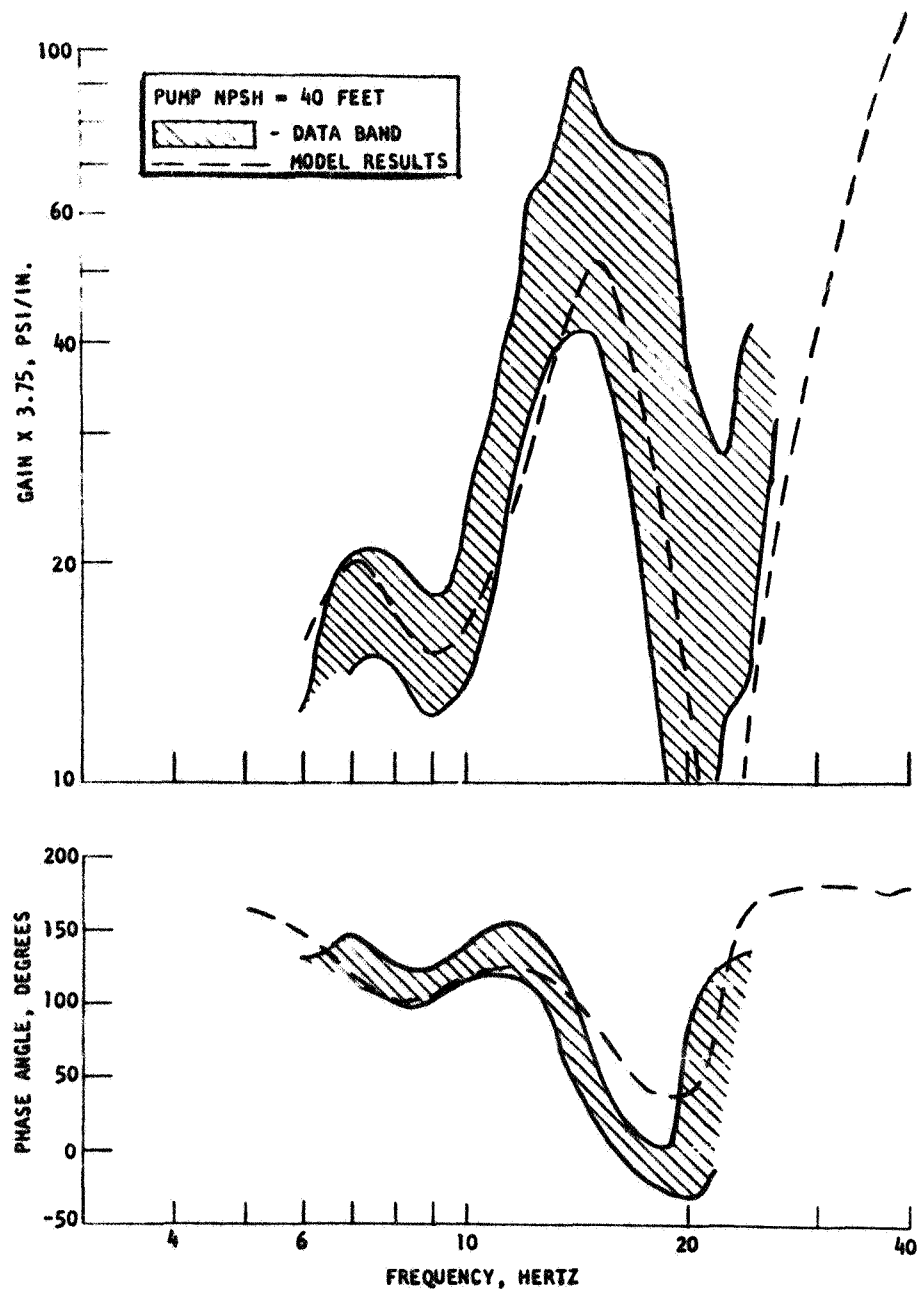
Figure 85. Comparison of Analytical and Experimental Results for Pump Inlet Pressure Divided by Pulser Position

R-7970
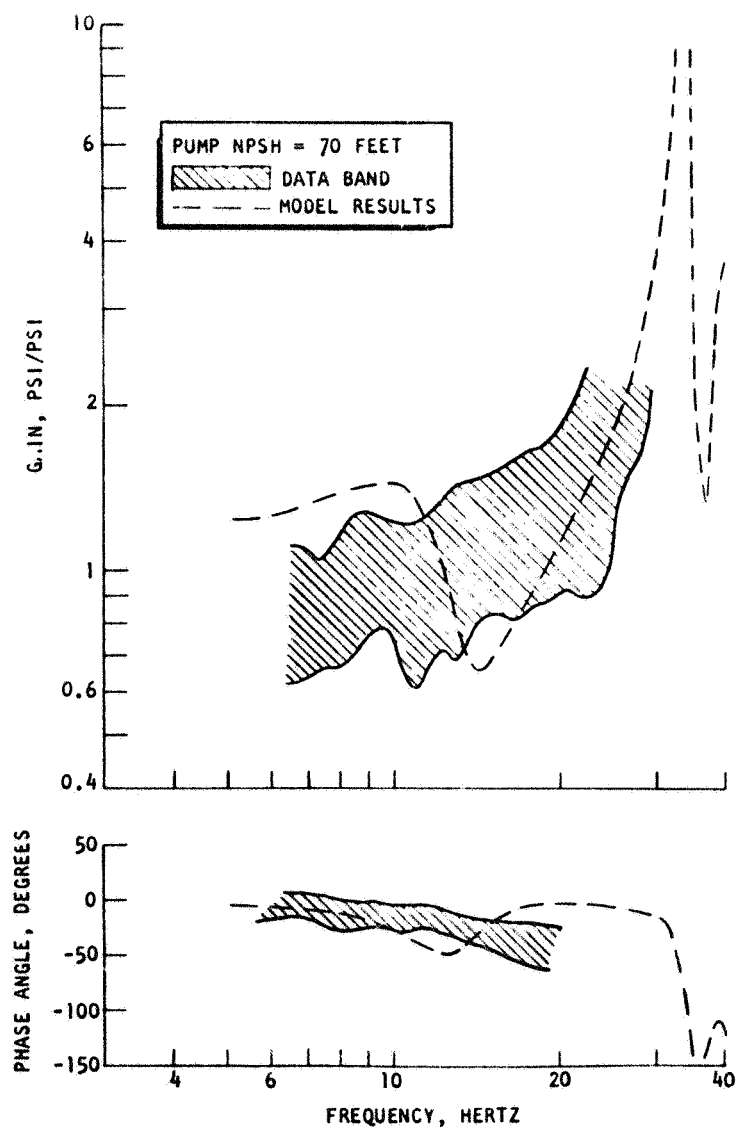
Figure 86.   Comparison of Analytical and Experimental Results for
Pump Gain (= Discharge/Inlet Pressure)
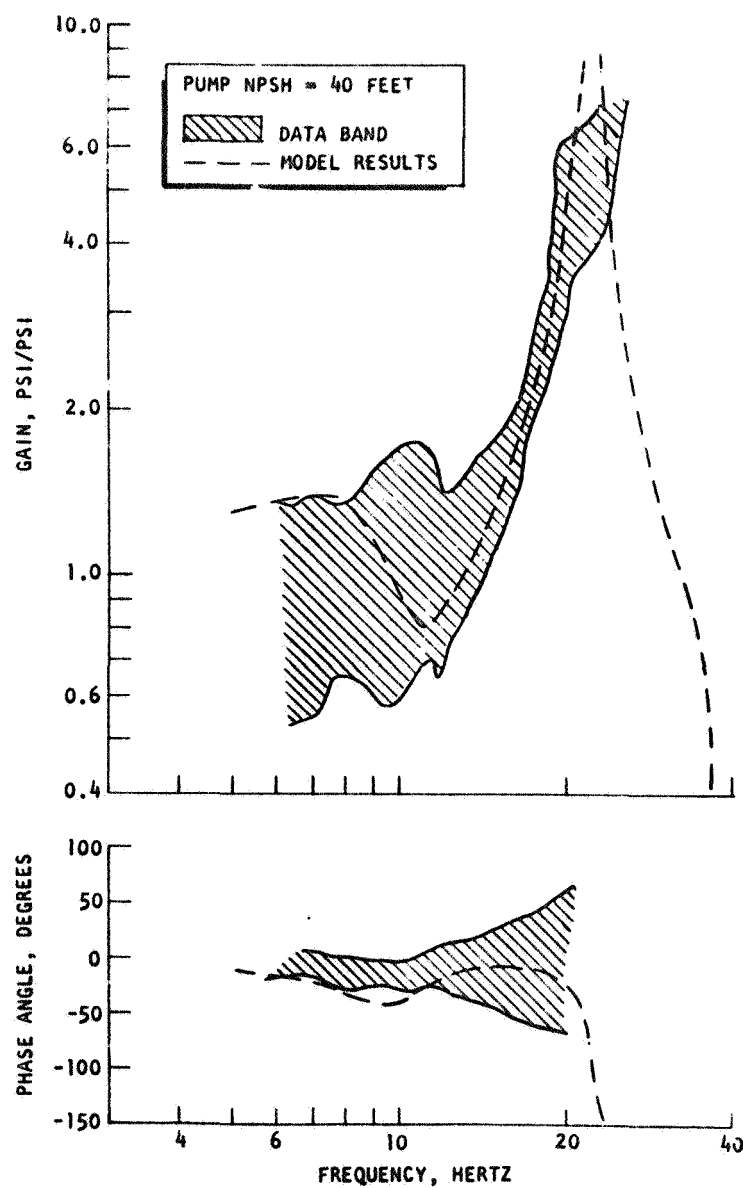
Figure 87. Comparison of Analytical and Experimental Results for
Pump Gain (= Discharge/Inlet Pressure)
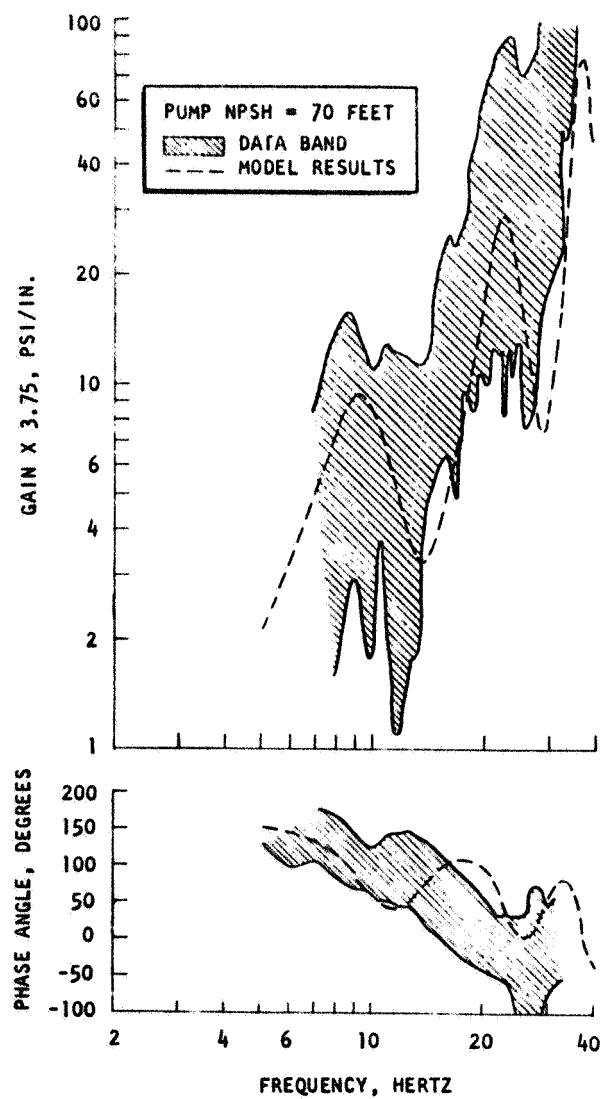
Figure 88. Comparison of Analytical and Experimental Results for Pump Discharge Flow Divided by Pulser Position
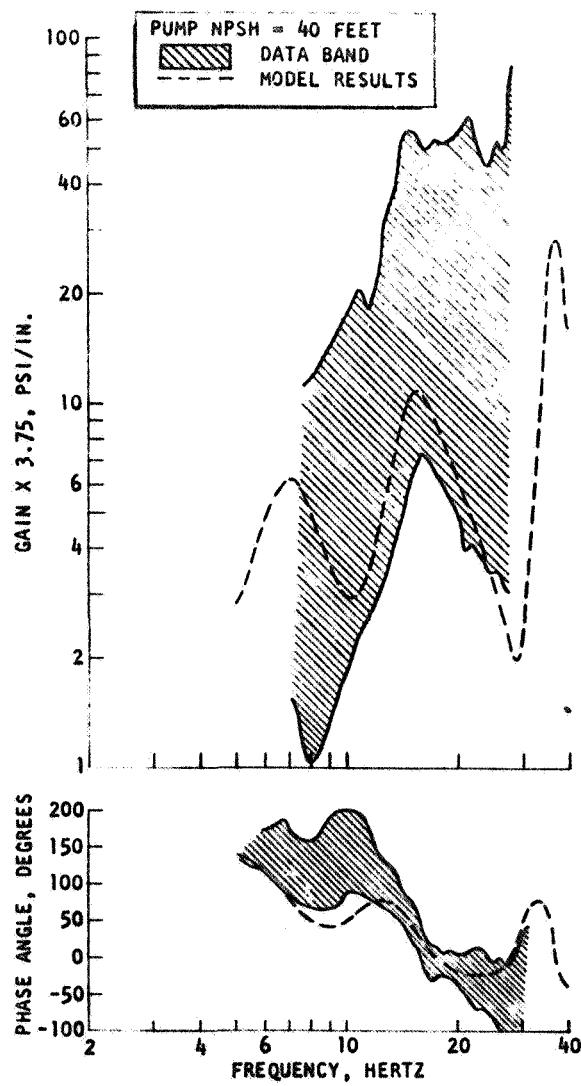
Figure 89. Comparison of Analytical and Experimental Results for
Pump Discharge Flow Divided by Pulser Position
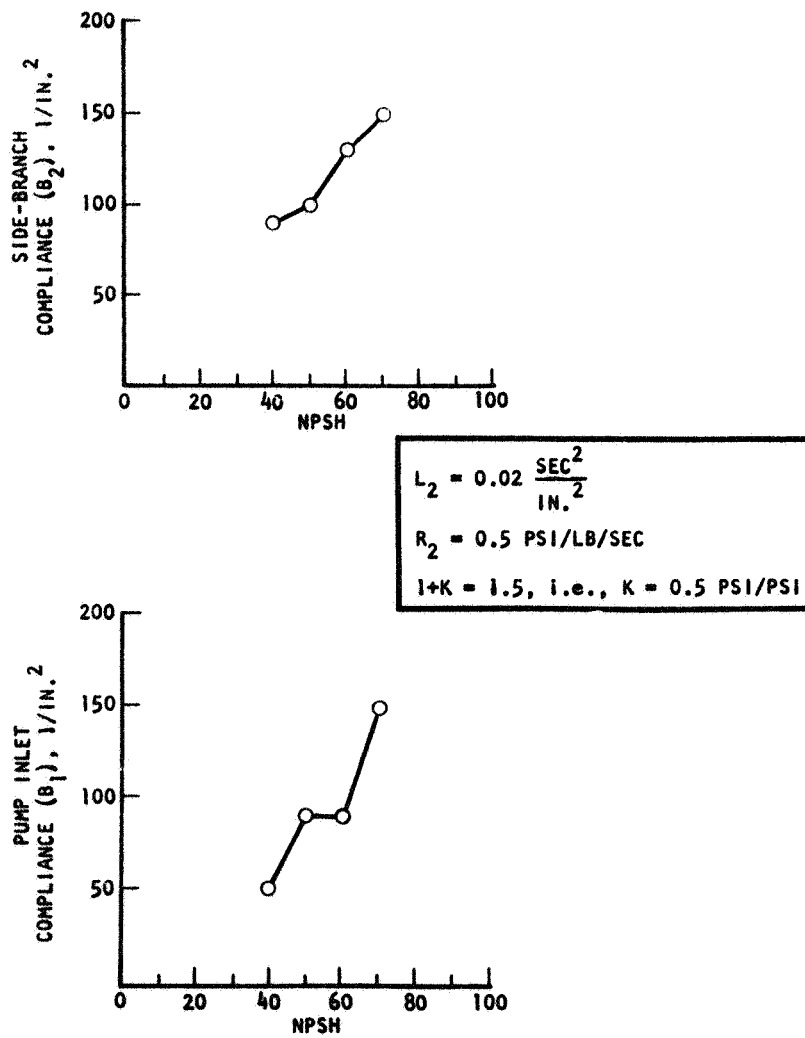
Figure 90. Variation of Pump Model Compliances With NPSH

COMBINED DYNAMIC CHARACTERISTICS
OF ENGINE AND FEEDLINE

Having established an analytical model which is in agreement with the
pump pulsing test data, the model can be used to determine the pump
termination impedance function, G. This function was defined in Eq. 22
to be

$$G = P_2/\dot{w}_2$$

where P_2 and $\dot{w}_2$ are pressure and flow at the pump inlet flange. The
function G was determined for an NPSH of 40, 50, 60, and 70 feet with
no dependence upon PU valve position or inlet duct configuration. The
function for these four conditions is shown in Fig. 91 and 92. The trends
are seen to be consistent with NPSH as would be expected from the data
trends. The shape of the curve is also reasonable being representable
of a resistance at very low frequency followed by alternate dominance
by the compliance and then the inertial terms. These curves were curve
fit using an equation of the form

$$G = \frac{K \left[1 + \dfrac{2\zeta_2 S}{2\pi f_2} + \dfrac{S^2}{4\pi^2 f_2^2} \right]}{\left[1 + \dfrac{S}{2\pi f_1} \right] \left[1 + \dfrac{2\zeta_3 S}{2\pi f_3} + \dfrac{S^2}{4\pi^2 f_3^2} \right]} \tag{70}$$

The curve fits are applicable up to a frequency of 33 Hz, and in each
case the curve fit function was in excellent agreement with the original
curve. The values of the parameters appearing in Eq. 70 are given below:

Parameter	Equivalent NPSH, feet 40	50	60	70
K, db	10.77	11.32	10.8	11.03
f_1, Hz	1.29	1.66	2.06	2.64
f_2, Hz	10.47	11.1	12.62	13.64
f_3, Hz	13.58	16.0	16.95	19.71
ζ_2	0.29	0.291	0.243	0.233
ζ_3	0.209	0.184	0.166	0.145
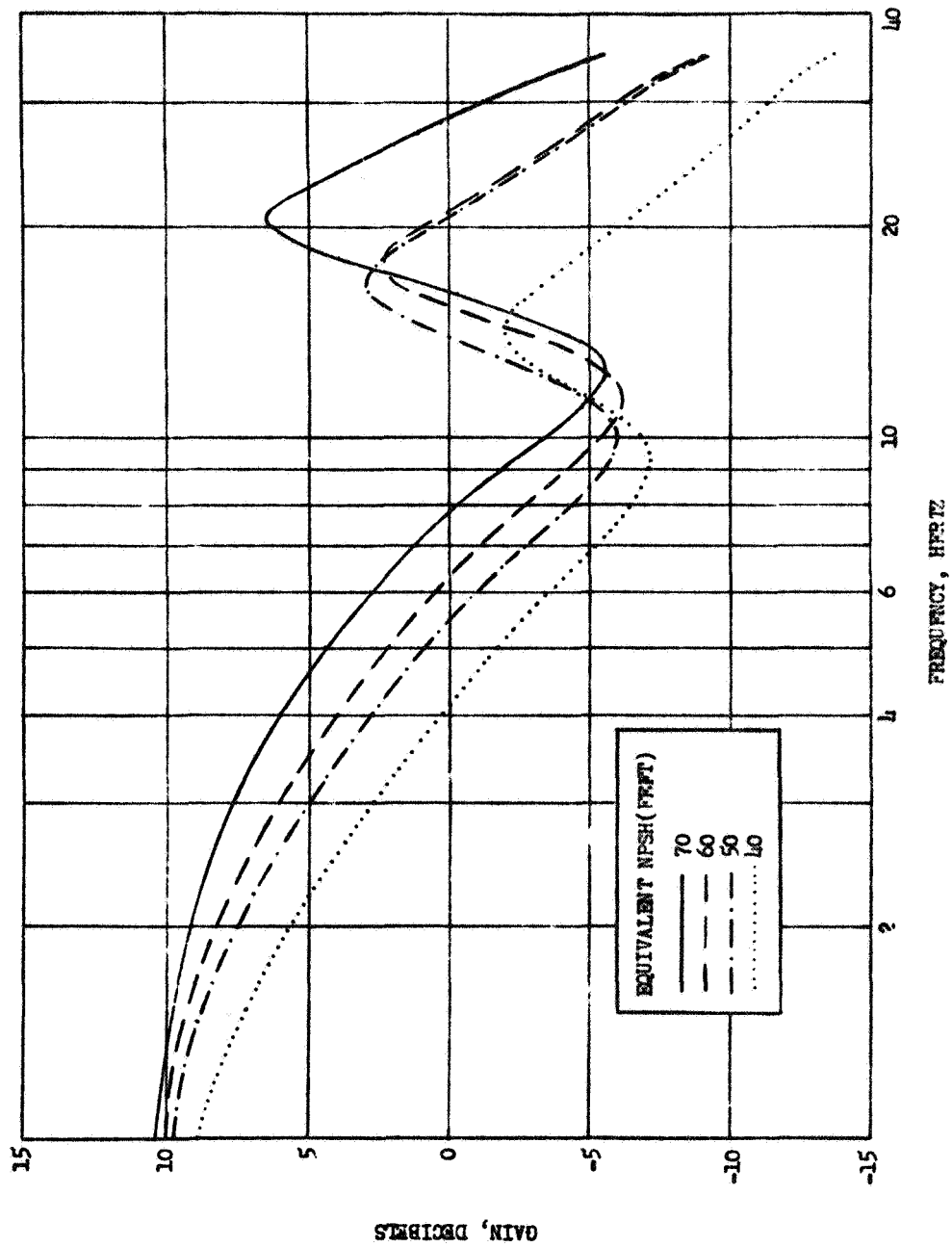
Figure 91. Pump Termination Impedance, G ($=P_2/\dot{w}_2$), From Pump Dynamic Model

R-7970
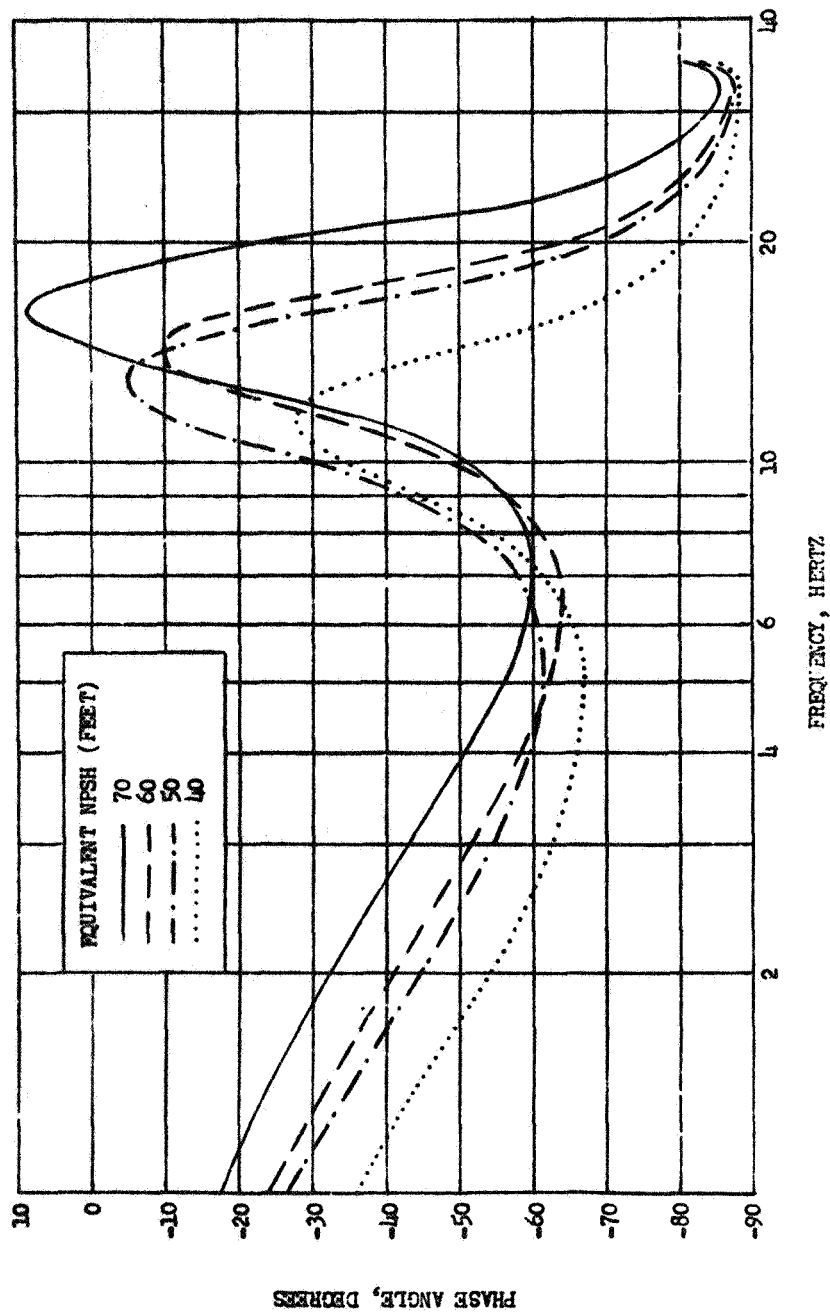
Figure 92. Pump Termination Impedance, G (=$P_2/\dot{w}_2$), From Pump Dynamic Model

It was shown that this pump termination impedance is required to arrive at engine transfer functions $\Delta P_c/\Delta P_2$ based on an inlet pressure at the pump inlet flange. The equation for determining this function was Eq. 35 which is repeated below:

$$\frac{\Delta P_c}{\Delta P_2} = \frac{\Delta P_c}{\Delta P_1} \left\{ 1 + \frac{SL_2}{G} \right\} \tag{71}$$

where P_1 is pump inlet pressure upstream and L_2 is the inertance of the line between the pulser and P_2. Because the Bode plots of engine transfer functions are for $\Delta P_c/\Delta P_1$, it is now required to determine the function $Z = \left[1 + SL_2/G\right]$. The pulser in the engine pulsing test program was located 21 inches above the pump inlet flange on a duct of 8 inches diameter. Thus,

$$L_2 = 21/\left[\pi/4 \; (8)^2 * 386\right] = 0.001081 \left(\frac{sec}{in.}\right)^2$$

Using this value in Eq. 71, the function Z was calculated. The results are listed in Table 15 as a function of frequency, and the results for a NPSH of 50 feet are plotted in Fig. 93. The function has very little effect until frequency gets as large as 20 Hz. The phase angle is less than 10 degrees up to 30 Hz, and the gain is within 0 ±3 db up to 25 Hz except at a NPSH of 40 feet. Using the transfer function, Z, the Bode plots of the engine transfer function, $\Delta P_c/\Delta P_{in}$, could now be corrected to get $\Delta P_c/\Delta P_2$. However, because the function Z has such a small effect on the engine transfer function, no plots of $\Delta P_c/\Delta P_2$ are presented here.

One final relationship of interest is P_c as a function of structural acceleration which would be applicable to the flight vehicle. To derive this functional relationship, the following assumptions are made:

1. The feedline can be represented by a single resistance and inertance, R+SL.

2. The pump dynamics are defined by the pump termination impedance, G

TABLE 15

TRANSFER FUNCTION $Z = 1 + SL_2/G$

Frequency, Hz	Equivalent NPSH							
	40 Feet		50 Feet		60 Feet		70 Feet	
	Gain, db	Phase, degrees	Gain, db	Phase, degrees	Gain, db	Phase, degrees	Gain, db	Phase, degrees
1	-0.01	0.1	-0.01	0.1	-0.01	0.1	-0.01	0.1
2	-0.05	0.2	-0.04	0.2	-0.03	0.2	-0.02	0.2
4	-0.21	0.6	-0.15	0.6	-0.13	0.5	-0.09	0.5
6	-0.50	1.6	-0.36	1.3	-0.31	1.0	-0.22	0.9
8	-0.83	4.2	-0.62	3.4	-0.59	2.2	-0.43	1.7
10	-0.69	7.6	-0.52	7.2	-0.85	5.3	-0.70	3.9
12	-0.50	6.8	-0.08	7.2	-0.51	9.0	-0.61	8.2
14	-0.77	5.1	-0.08	5.3	-0.12	7.5	0.04	8.9
16	-1.28	4.2	-0.33	4.1	-0.25	5.3	0.20	6.3
18	-1.94	3.6	-0.67	3.3	-0.58	4.1	0.03	4.5
20	-2.75	3.4	-1.08	2.9	-1.0	3.4	-0.24	3.5
22	-3.74	3.3	-1.56	2.6	-1.49	2.9	-0.54	2.9
24	-4.99	3.3	-2.12	2.4	-2.06	2.6	-0.89	2.5
26	-6.60	3.4	-2.79	2.3	-2.73	2.5	-1.29	2.2
28	-8.81	3.9	-3.60	2.2	-3.53	2.3	-1.75	2.0
30	-12.19	4.9	-4.61	2.2	-4.54	2.3	-2.31	1.8
33	-27.24	35.5	-6.93	3.2	-6.86	3.1	-3.57	2.2
35	-15.07	149.1	-9.73	15.9	-9.63	15.6	-5.03	9.1
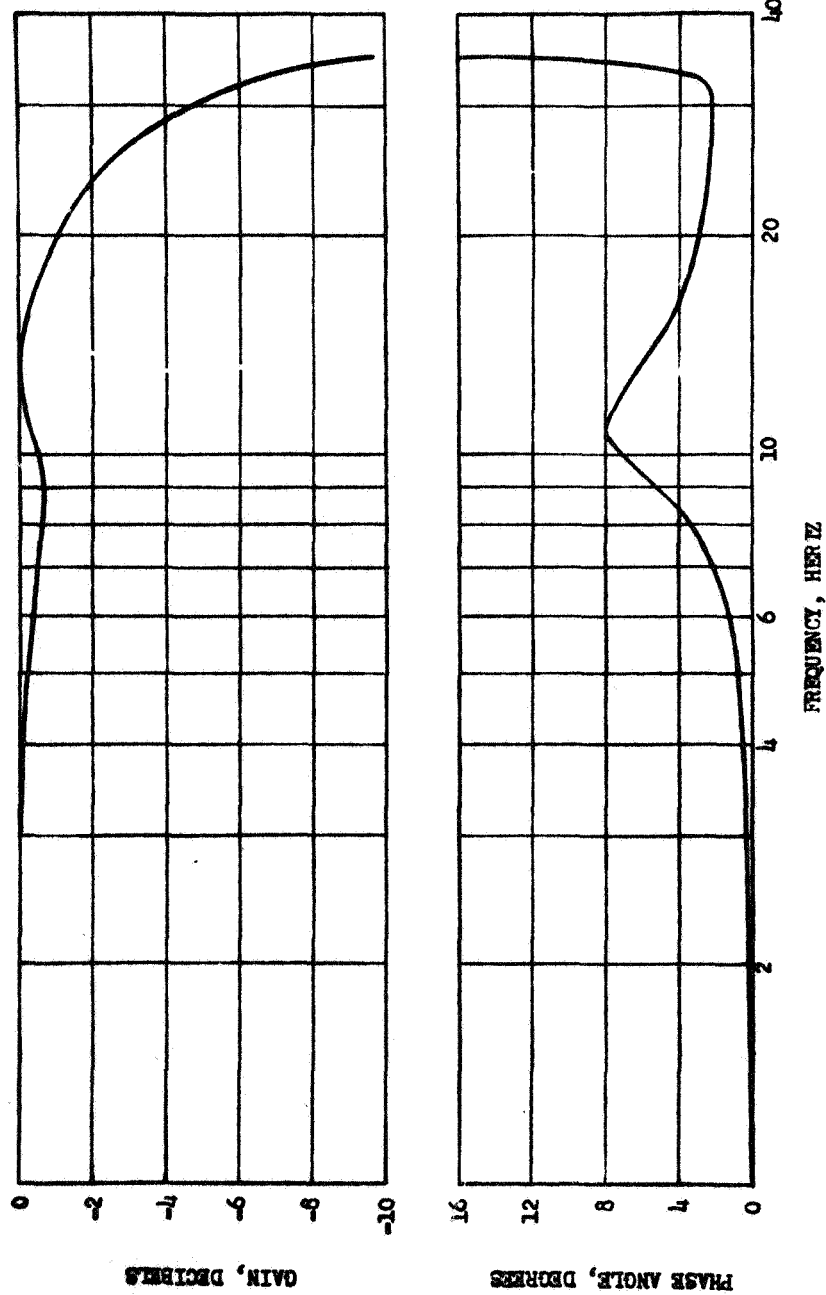
Figure 93.   Transfer Function $Z = 1 + SL_2/G$ at NPSH ~ 50 feet

3. Tank pressure is proportional to tank-bottom acceleration which is directly proportional to engine acceleration, so that $P_t = K\ddot{x}$.

Therefore,

$$P_t - P_2 = (R + SL)\,\dot{w}_1$$

$$P_2/\dot{w}_2 = G$$

$$\dot{w}_2 = \dot{w}_1 + \rho A \ddot{x}/S$$

$$P_c = \frac{\Delta P_c}{\Delta P_1}\left\{1 + \frac{SL_2}{G}\right\}P_2$$

where $\ddot{x}$ is the oscillatory acceleration at the engine mounts and other parameters are as used previously. These equations can now be combined to yield

$$P_2 = \left\{\frac{G}{G+R+SL}\right\}\left\{P_t + \rho A\,\frac{\ddot{x}}{S}\,(R+SL)\right\} \tag{72}$$

$$P_c = \frac{\Delta P_c}{\Delta P_1}\left\{\frac{G+SL_2}{G+R+SL}\right\}\left\{P_t + \rho\,\frac{A\ddot{x}}{S}\,(R+SL)\right\} \tag{73}$$

Assuming that the resistance of the flight duct is small, these equations can be reduced to the form

$$P_2 = \left\{\frac{1}{1+SL/G}\right\}\left\{P_t + \rho AL\ddot{x}\right\} \tag{74}$$

$$P_c = \frac{\Delta P_c}{\Delta P_1}\left\{\frac{1 + SL_2/G}{1 + SL/G}\right\}\left\{P_t + \rho AL\ddot{x}\right\} \tag{75}$$

The expression $\left[\,P_t + \rho AL\ddot{x}\,\right]$ represents a forcing function and the other terms, the dynamics of the system.

Assuming an inlet line of 4 feet length corresponding to the inboard duct on the S-II stage, the dynamic function $[\ 1/(1 + SL/G)\ ]$ was calculated. The results are tabulated in Table 16 and are plotted in Fig. 94 and 95 for a NPSH of 40, 60, and 70 feet. (The results for a NPSH of 50 feet are approximately equal to those at 60 feet). The dynamics of the feed-line and pump is seen to increase the gain of P_2 over acceleration for all but a few points, and in no case is there a significant reduction. At 17 Hz, the gain has not yet increased significantly, but it was previously shown that the static gain with no increase resulting from the dynamics of the line was sufficient to get an instability. In Fig. 95, the phase angle at 17 Hz is close to the -20 degrees which was required for zero phase shift around the closed loop representing the flight system dynamics.

The function $\left[(1 + SL_2/G)/(1 + SL/G)\right]$ which appears in Eq. 75 is plotted in Fig. 96 and 97. Again, the case of NPSH equal to 50 feet was not plotted because it is so close to the results at 60 feet. The shape of these curves are similar to those of Fig. 94 and 95, respectively. Although the function G appears in a similar term in both numerator and denominator, it is still seen to exert a significant influence on the dynamic response above 20 Hz. Using the Bode plots for $\Delta P_c/\Delta P_1$ presented as Fig.A-8 through A-37, the functions of Fig. 96 and 97 , and Eq. 75, a transfer function relating P_c to engine acceleration could be constructed.

TABLE 16

FEEDLINE-PUMP DYNAMIC FUNCTION, $\left\{\dfrac{1.0}{1 + SL/G}\right\}$

Frequency, Hz	Equivalent NPSH							
	40 Feet		50 Feet		60 Feet		70 Feet	
	Gain, db	Phase, degrees	Gain, db	Phase, degrees	Gain, db	Phase, degrees	Gain, db	Phase, degrees
1	0.03	-0.3	0.02	-0.3	0.02	-0.3	0.01	-0.3
2	0.12	-0.6	0.08	-0.5	0.07	-0.5	0.05	-0.5
4	0.49	-1.5	0.34	-1.4	0.29	-1.2	0.21	-1.2
6	1.18	-3.9	0.83	-3.2	0.71	-2.4	0.51	-2.1
8	1.93	-11.0	1.43	-8.7	1.38	-5.5	1.01	-4.2
10	1.37	-19.2	1.00	-17.7	1.91	-13.8	1.61	-10.0
12	0.96	-16.5	-0.03	-16.5	0.85	-21.7	1.13	-20.3
14	1.74	-13.2	0.08	-12.2	0.05	-17.3	-0.39	-19.9
16	3.15	-11.8	0.70	-9.7	0.46	-12.6	-0.59	-13.8
18	5.17	-12.1	1.56	-8.5	1.31	-10.2	-0.14	-10.1
20	8.20	-14.5	2.65	-8.0	2.41	-9.1	0.50	-8.2
22	13.36	-23.1	4.04	-8.0	3.80	-8.8	1.25	-7.2
24	22.68	-89.9	5.88	-8.5	5.64	-9.1	2.15	-6.6
26	12.86	-163.7	8.49	-10.1	8.19	-10.6	3.25	-6.3
28	6.72	-173.0	12.72	-14.3	12.29	-14.7	4.65	-6.3
30	2.77	-176.2	22.21	-41.1	21.22	-38.2	6.59	-6.8
33	-1.62	-177.3	11.58	-167.5	11.87	-167.2	12.54	-14.2
35	-4.32	-172.8	4.39	-160.3	4.52	-160.1	13.84	-96.0

*L = 0.00247, based on an assumed flight duct 48 inches long and 8 inches in diameter.
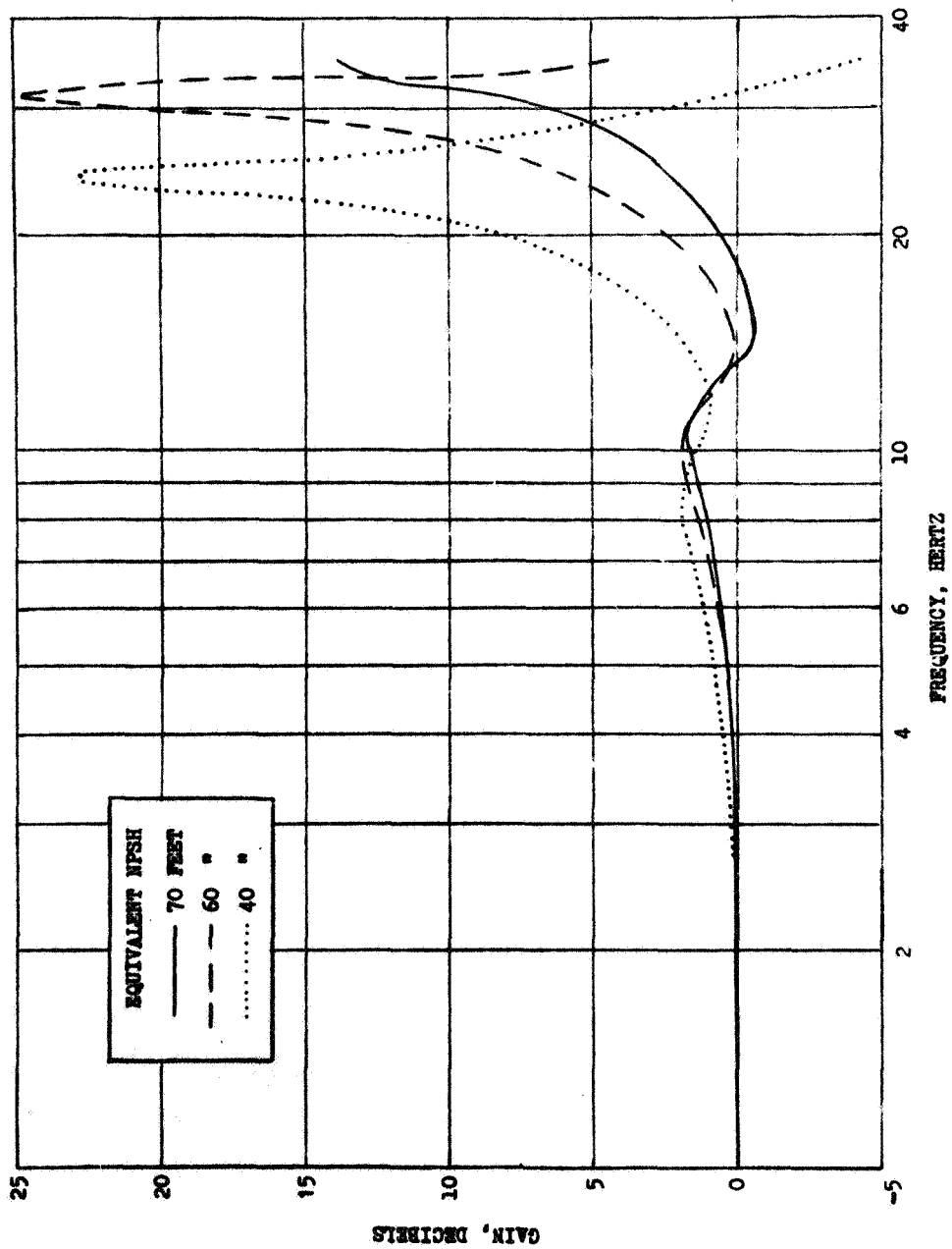
Figure 94. Transfer Function $1/(1+SL/G)$
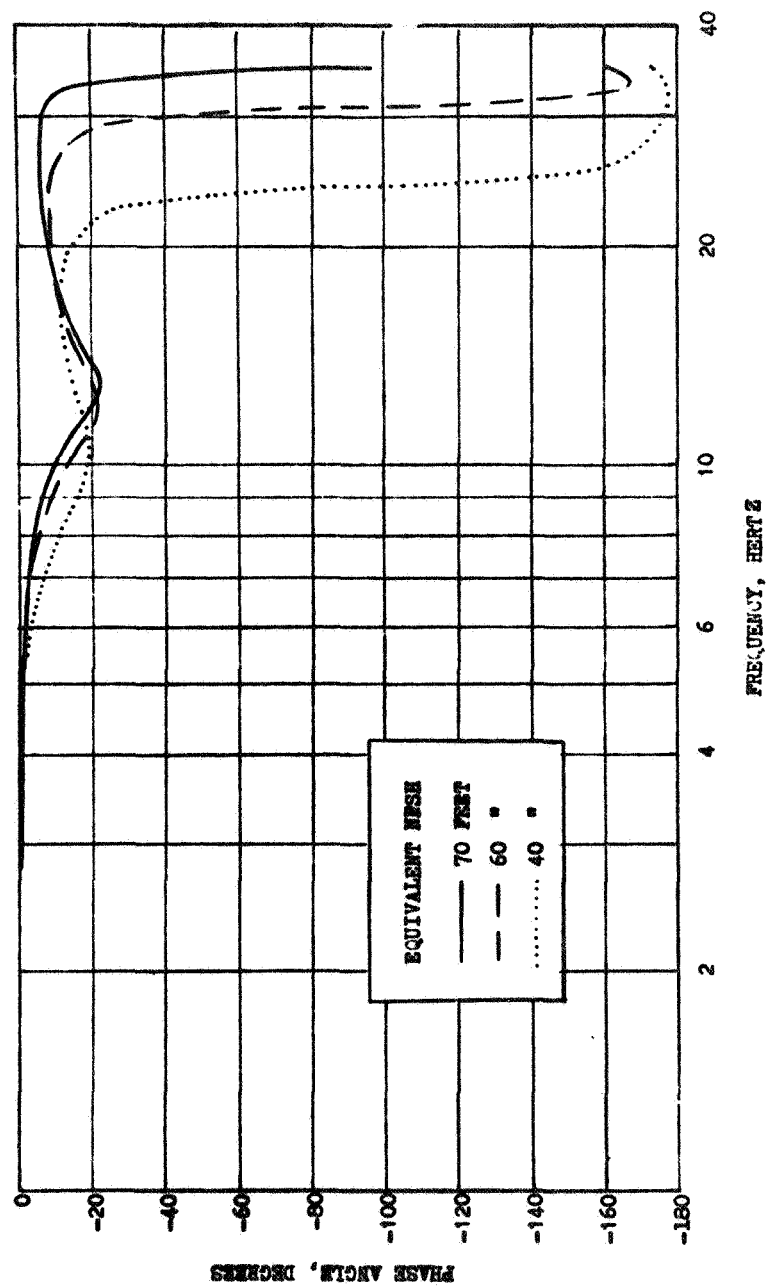
Figure 95.   Transfer Function 1/(1+SL/G)
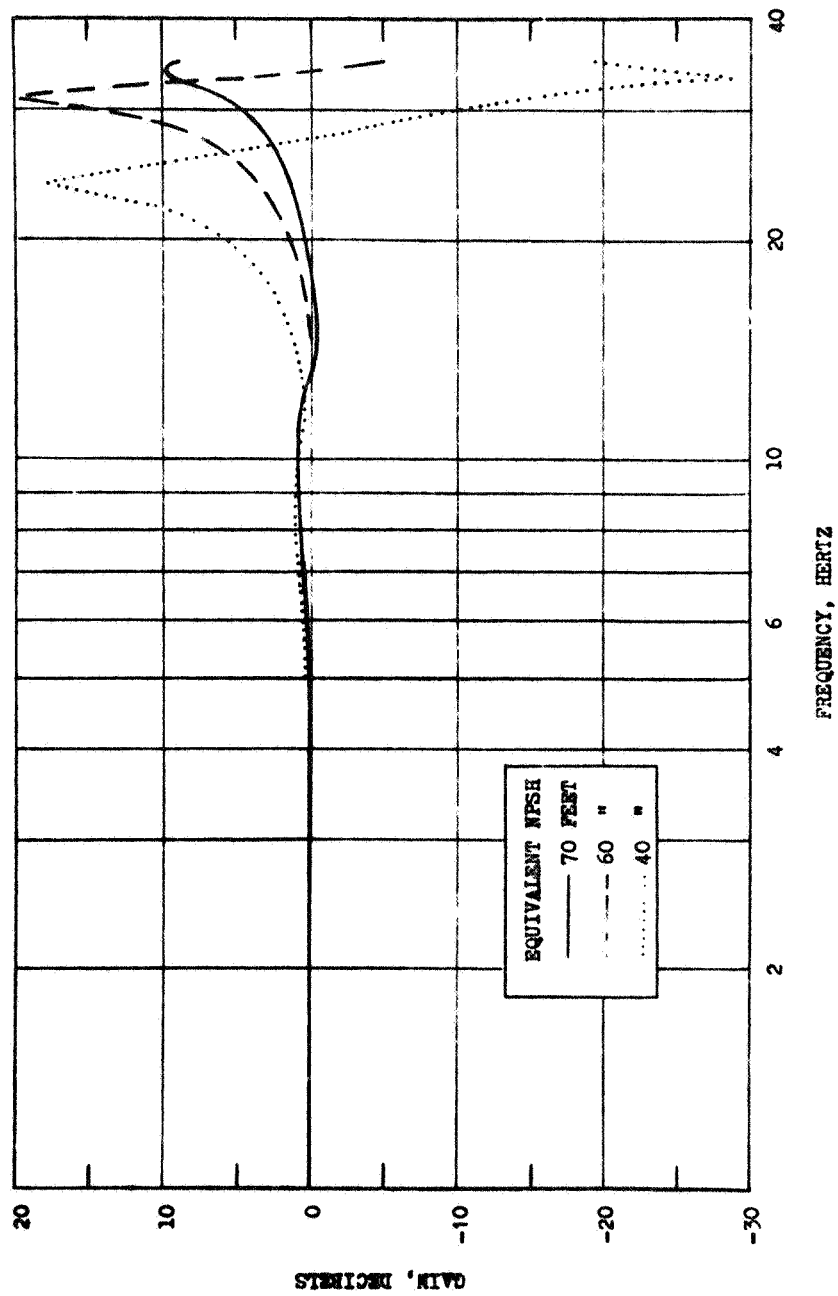
Figure 96. Transfer Function $(1+SL_2/G)/(1+SL/G)$
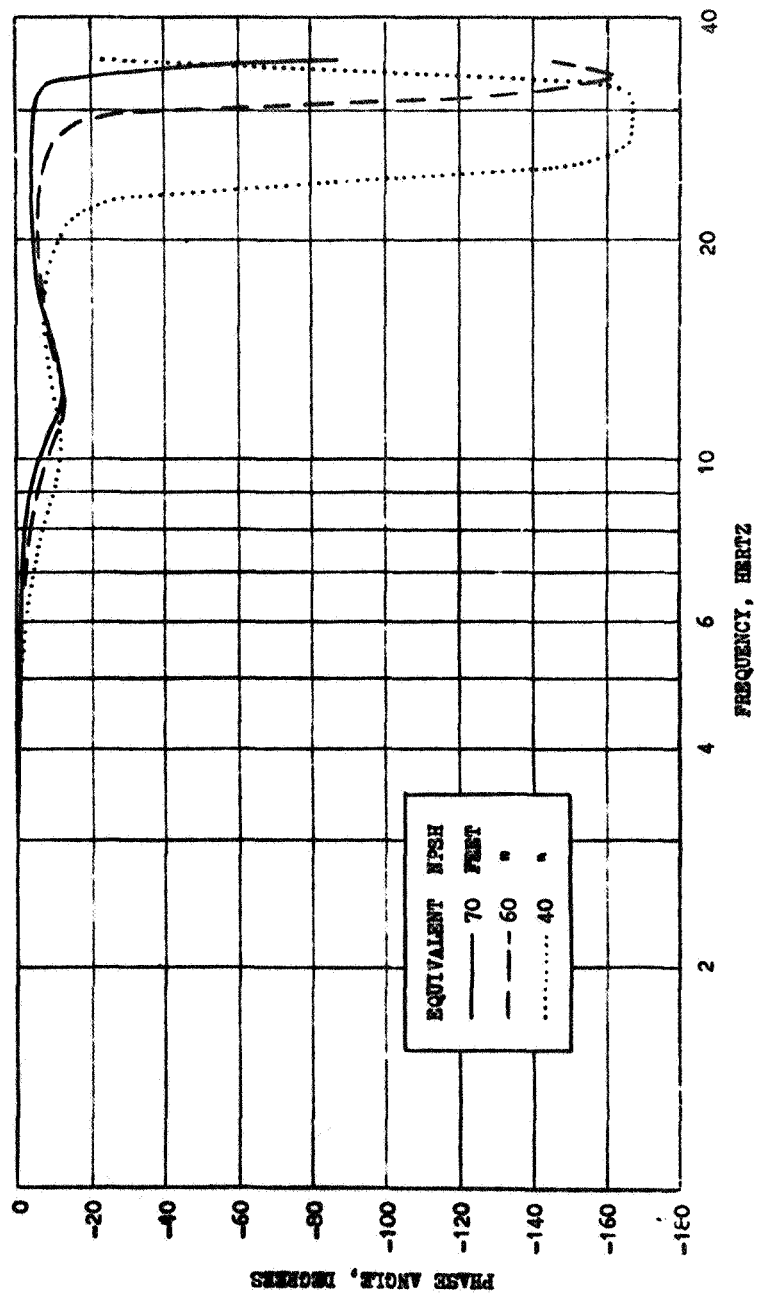
Figure 97. Transfer Function $(1+SL_2/G)/(1+SL/G)$

R-7970

CONCLUSIONS

Extensive analysis has been performed on the data from the Apollo flights to determine the source and characteristics of the 17-Hz oscillations which reach large amplitudes near the end of S-II burn. The primary measurements used to study the oscillations were chamber pressure and acceleration of engines No. 1 and No. 5 and of the LOX tank bottom. (Long instrumentation sense lines rendered the LOX pump inlet and discharge pressure measurements unreliable.) These primary measurements were analyzed to determine gain ratios, relative phase angles, and in some cases, rate of change of gain.

The most significant conclusion resulting from the data analysis was that the oscillations were caused by a closed loop instability. The loop consists of the structure, the inboard LOX feedline, and the center engine, and the instability is of the same nature as POGO oscillations except that this instability occurs at the frequency of a higher structural mode (frequently referred to as the fifth mode) which has significant displacements, or accelerations, in the LOX tank bottom, the thrust structure, and the cross beam on which the center engine is mounted. There were four reasons given for the conclusion that the oscillations were the result of an instability:

1. The gains and phases of the three main elements of the closed loop are such that the total loop gain is greater than one, and the loop phase is close to zero, two conditions which define an unstable loop.

2. The oscillations occur at a resonant frequency of the structure.

3. The shape of the oscillation amplitude curve is indicative of an instability.

4. The operating region of the engine during flight is above the region in which engine self-driven oscillations occur.

Using the rate of change of the acceleration with time, minimum closed loop damping of -1.0 percent was calculated for the instability on flight AS-504. Assuming the structure had 1.5-percent damping, then the maximum instability was 4.5 db unstable. If the structure had only 1.0-percent damping, the system was 6.0 db unstable. The occurrence of the instability was shown to correlate with LOX level in the tank on the four flights AS-501 through -504. The frequency and amplitude of this structural mode varies with LOX level, and the conditions necessary for the instability occurred near the end of burn.

An analog model of the closed loop was developed to study the instability. The transfer functions required to describe the engine were obtained from Rocketdyne tests The structural modes were derived from the flight data because the predicted modes did not agree with the data. The LOX feedline-pump dynamic model was varied from a simple model through more complex models which were derived from pump testing data. The analog model gave an instability agreeing in character and time (approximately) with the instability in flight. The model demonstrated that a nonlinear response of pump inlet pressure caused by cavitation resulted in many of the characteristics of the flight data. The model also demonstrated the significance of the pump inlet compliance on the occurrence and degree of instability. Finally, the model was used to indicate the degree of stability earlier in flight. This analysis is not conclusive because the confidence is low in the gains for the structural modes as determined from flight data. The analysis indicated that the system closed-loop gain does not vary by more than a factor of 2 at any time during the S-II burn. If this is representable of the flight hardware, the system does not meet the 6-db stability criterion at any time during burn.

The amplitudes of oscillations observed to date are not considered large enough to result in degradation of engine performance or overstress of engine components. However, an engine with fluid has not been tested at vibration levels of this magnitude, and the amplitudes are large enough that it is desirable to eliminate them, or at least significantly reduce

them. Because the instability occurred near the end of burn, the surest
method of eliminating the oscillations was to cut off the center engine
early because data proved that the center engine was the only source for
these oscillations. This solution was adopted and was effective on stage
static tests and succeeding flights. A second potential solution to the
problem is use of a gas accumulator on the inboard LOX feedline. The
analog model demonstrated that the accumulator can eliminate an instability
in the 17-Hz region. An accumulator is currently being tested at MSFC.

There are some other characteristics of flight data which were not con-
clusively understood. There were differences between the four flights
in the maximum amplitudes and amplitude envelopes which have not yet been
explained. Some of these differences may be related to the NPSH level.
There are bursts of amplitude early in flight but of low amplitude whose
origin has not been established. The amplitudes are low enough that they
are not of concern, but if these early bursts are indicative of a marginal
stability then they would be of concern for future flights. Also, there
are low amplitude oscillations at approximately 10 Hz and some at the
subharmonic of the frequency of the 17-Hz instability. Currently, the
10-Hz oscillations are believed to be independent of the 17-Hz oscilla-
tions and are probably related to another structural mode. The subharmonic
oscillations are believed to be induced by the 17-Hz oscillations through
symmetrical sloshing in the LOX tank.

In support of the oscillation analysis program, Rocketdyne conducted two
test programs, one involving the engine and the other involving only the
LOX pump. In both cases, an inlet piston pulser was used to introduce
flow perturbations in the LOX inlet line. Dynamic instrumentation was
used to evaluate the feedline-pump and engine dynamic behavior.

The data from the engine pulsing tests demonstrated (1) that the flight-
type instrumentation using long sense lines on pump discharge and inlet
pressures were unreliable, (2) that the region of engine self-driven
oscillations was rather well defined and at NPSH values below those
experienced in flight, and (3) that new transfer functions based on

inlet pulsing tests were required to describe engine dynamics. The only new transfer function directly obtainable from the engine tests was $\Delta P_c/\Delta P_{in}$ where P_c is chamber pressure and P_{in} is LOX pump inlet pressure upstream of the pump. This is the most significant of the transfer functions for the S-II oscillation problem. A second significant transfer function was determined from pump tests and is mentioned below. Based on the new transfer function for $\Delta P_c/\Delta P_{in}$, fuel-side transfer functions and cross-feed transfer functions were adjusted to what appeared to be a more correct representation, although these transfer functions have a negligible effect on the 17-Hz problem.

The transfer function $\Delta P_c/\Delta P_{in}$ was determined over an extended operating range of NPSH and PU valve position. The results indicated a consistently lower gain as NPSH increased, and a lower gain as the PU valve was moved from the full-open to the full-closed position. MSFC tests verified certain of the Rocketdyne results, but at the full-open PU valve po ition, the MSFC data indicated gains lower than Rocketdyne's by a factor of approximately two. This discrepancy is still being studied.

The primary objective of the pump tests was to determine the pump termination impedance, $G = \Delta P_{os}/\Delta \dot{w}_{os}$ where P_{os} is LOX pump suction pressure and $\dot{w}_{os}$ is LOX suction flow. The suction flowrate was not measurable, and reliable pressure measurements cannot be made at the pump inlet flange. Thus, pressure measurements upstream of the pump and pressure and flow measurements downstream of the pump were used to determine coefficient values in a pump-facility analytical model, and the model was used to generate the termination impedance function, G.

The analytical model of the facility lines appeared from test data to be adequate in the frequency range of interest. Thus, matching the model to test data depended only on successful modeling of the pump itself. The dynamic model used for the pump was generated from the physical characteristics of the pump and included all potential dynamic effects which were recognizable. The primary dynamic elements of the pump are the inlet compliance, inducer inertance, a side-branch inertance, resistance, and

compliance, and an impeller inertance. Values for these parameters were determined by matching model results with test data.

Difficulties were experienced in obtaining good test data because of vibrations of the system. The facility inlet lines had to be stiffened and the pulser stroke maintained at a low level to minimize vibrations. Many early tests did not yield any usable data, and the data from most of the tests appeared to have scatter because of some vibration contamination, noise, etc. The form of the data definitely indicated two resonant frequencies in the inlet pressure response. These resonances and the associated antiresonances were dependent on the NPSH of the LOX pump. To match the model results to the data, the data were inspected and weighted to determine those data bands, and values within the data bands, which appeared to be less contaminated from other influences; thus, most representable of the pump dynamic response.

The analytical model parameters were determined by matching the model results to the data for pump inlet pressure divided by pulser position. The model was able to match this data well. Further confidence in the validity of the model was then obtained by matching the data trends of pump discharge pressure and flow. The only operating point parameter which could be shown to have a definite effect on dynamic response was LOX pump NPSH. The data were matched by the model for NPSH of 40 to 70 feet. The two model parameters which varied with NPSH were the pump inlet compliance and the side-branch compliance associated with the pump.

After establishing the model which successfully matched the test data, the pump termination impedance, G, was determined for a NPSH of 40, 50, 60, and 70 feet. This function together with the engine transfer function $\Delta P_c/\Delta P_{in}$ are sufficient to analyze the closed-loop instability of the S-II stage. It was shown that, assuming that the flight inboard LOX feedline

can be represented by a single resistance and inertance (R+SL), then the
pump inlet pressure and chamber pressure are given by

$$P_{os} = \left\{ \frac{G}{G+R+SL} \right\} \left\{ P_t + \rho A \; \frac{\ddot{x}}{S} \; (R+SL) \right\}$$

$$P_c = \frac{\Delta P_c}{\Delta P_1} \left\{ \frac{G+SL_2}{G+R+SL} \right\} \left\{ P_t + \rho A \; \frac{\ddot{x}}{S} \; (R+SL) \right\}$$

All the terms are defined in the text, but it is noted here that G is
the pump impedance, $\Delta P_c / \Delta P_1$ is the engine transfer function measured by
Rocketdyne and shown as Bode plots in the text, and $\left| P_t + \rho A \ddot{x} \; (R+SL)/S \right|$
is the general forcing function relating structural accelerations to
the oscillations. It was particularly interesting to note that the
function G had little influence on P_c for frequencies below 20 Hz, except
that at a NPSH of 40 feet the gain was increased by a maximum of approximately
5 db at 20 Hz. Above 20 Hz, the function G had a pronounced effect on
the transmission of acceleration effects to P_c.

NOMENCLATURE

a = acoustic velocity

A = generally, the cross-sectional area of a duct

B = fluid spring rate, or hydraulic compliance in units of $in.^{-2}$

C = hydraulic compliance in units of $in.^{2}$

CECO = center engine cutoff

db = decibels

E-1,E-5 = engine No. 1 or 5 on Apollo second stage

f = frequency (Hz)

F = engine thrust

g = acceleration of gravity

G = pump termination impedance $(=\Delta P_{os}/\Delta \dot{w}_{os})$

GG = gas generator

h_{ℓ}, h_{t} = height of a liquid column in a line, or tank, respectively

i = complex variable operator $(=\sqrt{-1.0})$

K = gain term in transfer function, gain ratio of X_{LTB}/X_{5}, factor relating inducer head rise and inlet pressure

L = inertance

M = generalized mass associated with a structural vibration mode

N = pump speed

NPSH = net positive suction head

P = pressure

P_{c} = chamber pressure

$P_{c_{1}}, P_{c_{5}}$ = chamber pressure for engine No. 1 or 5 on Apollo second stage

PSD	=	power spectral density data analysis technique
PU	=	propellant utilization (valve)
Q	=	pump volumetric flow
R	=	resistance
RT	=	range time for Apollo flights
S	=	Laplace operator ($=i\omega$ or d/dt)
t	=	time
V	=	velocity
$\dot{w}$	=	weight flowrate
W	=	work
$x, \dot{x}, \ddot{x}$	=	displacement, velocity, and acceleration, respectively
$\ddot{x}_1, \ddot{x}_5$	=	acceleration of engine No. 1 or 5 on Apollo second stage
$\ddot{x}_{LTB}$	=	acceleration of LOX tank bottom at sump on Apollo second stage
Z	=	transfer function, or impedance
Δ	=	denotes incremental value of parameter
ζ	=	percent of critical damping
ζ_ℓ, ζ_s	=	percent of critical damping for a closed loop or a structure, respectively
ρ	=	weight density
$\emptyset$	=	phase angle, e.g., of a transfer function
ω	=	frequency in radians/second
ω_n	=	resonant frequency

Subscripts

a	=	accumulator
c	=	thrust chamber

e   =   external

fs   =   fuel suction

in   =   inlet, usually LOX pump inlet

ℓ =   line or loop

LTB   =   LOX tank bottom

os   =   LOX suction

od   =   LOX discharge

pf   =   fuel pump

po   =   LOX pump

t   =   tank

v   =   vapor

1,2,... =   sometimes denotes a particular engine on the Apollo
            second stage and, at other times, denotes a particular
            location or parameter

REFERENCES

1. Dodge, Franklin T.: "Vertical Excitation of Propellant Tanks," chap. 8 of The Dynamic Behavior of Liquids in Moving Containers, Ed. by H. Norman Abramson, NASA SP-106, 1966.

2. R-7753, Apollo POGO Problem Special Study, Contract NAS8-18734, Rocketdyne, a division of North American Rockwell, Canoga Park, California, May 1969.

3. R-6283, J-2 Vehicle Longitudinal Stability (POGO) Analysis Program, Contract NAS8-19, Rocketdyne, a division of North American Rockwell Corporation, Canoga Park, California, August 1965.

4. R-6428, Final Report, J-2 Special Studies, Vehicle Longitudinal Stability Analysis (POGO Signal Generators), Contract NAS8-19, Rocketdyne, a division of North American Rockwell Corporation, Canoga Park, California, December 1965.

5. Letter No. S&E-ASTN-PP-69-L-20, Letter from H. G. Paul, NASA MSFC, Huntsville, Alabama, To Dr. E. W. Larson, Rocketdyne, a division of North American Rockwell Corporation, Canoga Park, California, June 1969.

APPENDIX A

This appendix contains two sets of figures relating to the engine
pulsing test program. The first set, Fig. A-1 though A-7, presents
the actual PU valve position and LOX pump NPSH as a function of time
for the tests which were used to determine the engine transfer function
$\Delta P_c/\Delta P_{in}$. These data were obtained from the Beckman digital data acquisi-
tion system. The sampling rate on this system is high enough to reflect
the low-frequency oscillations in the inlet system so that an envelope
of NPSH data is obtained. The mean value of NPSH is quoted as the test
operating value.

The second set, Fig. A-8 through A-37, presents Bode plots of the transfer
function $\Delta P_c/\Delta P_{in}$. P_{in} is the pressure 3.5 feet upstream of the pump
inlet flange. All but two of the tests were run over the frequency range
of 10 to 25 Hz, and the data cover only that range. Some of the tests
were curve fit, and the resulting curves are plotted as dashed lines in
the figures. The form of the curve fit function and the parameter values
are given in the text in the section on the engine testing program.
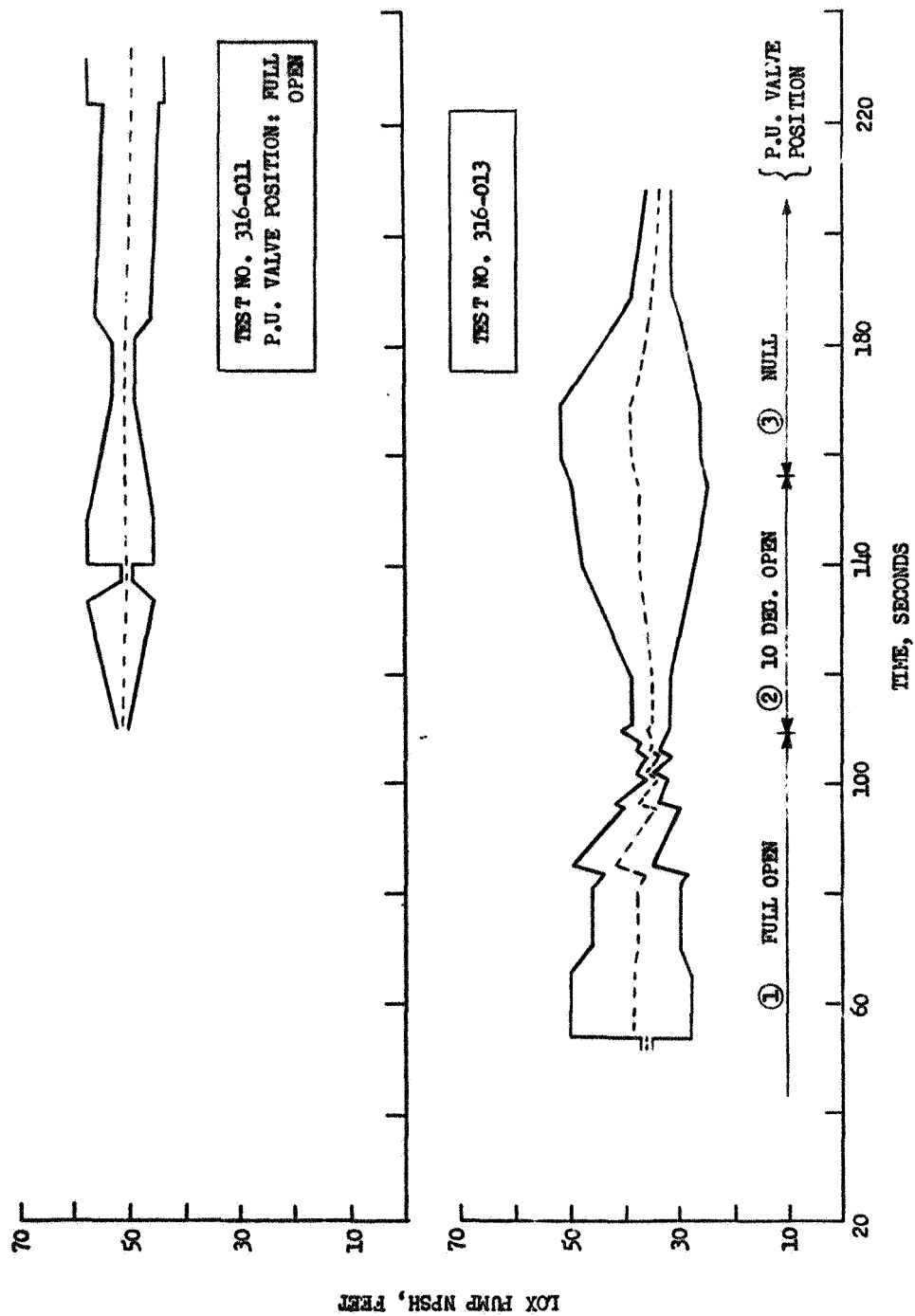
Figure A-1. Operating Conditions, J-2 Engine Pulsing Tests

TEST NO. 316-011
P.U. VALVE POSITION: FULL OPEN

TEST NO. 316-013

① FULL OPEN ② 10 DEG. OPEN ③ NULL { P.U. VALVE POSITION

TIME, SECONDS

LOX PUMP NPSH, FEET
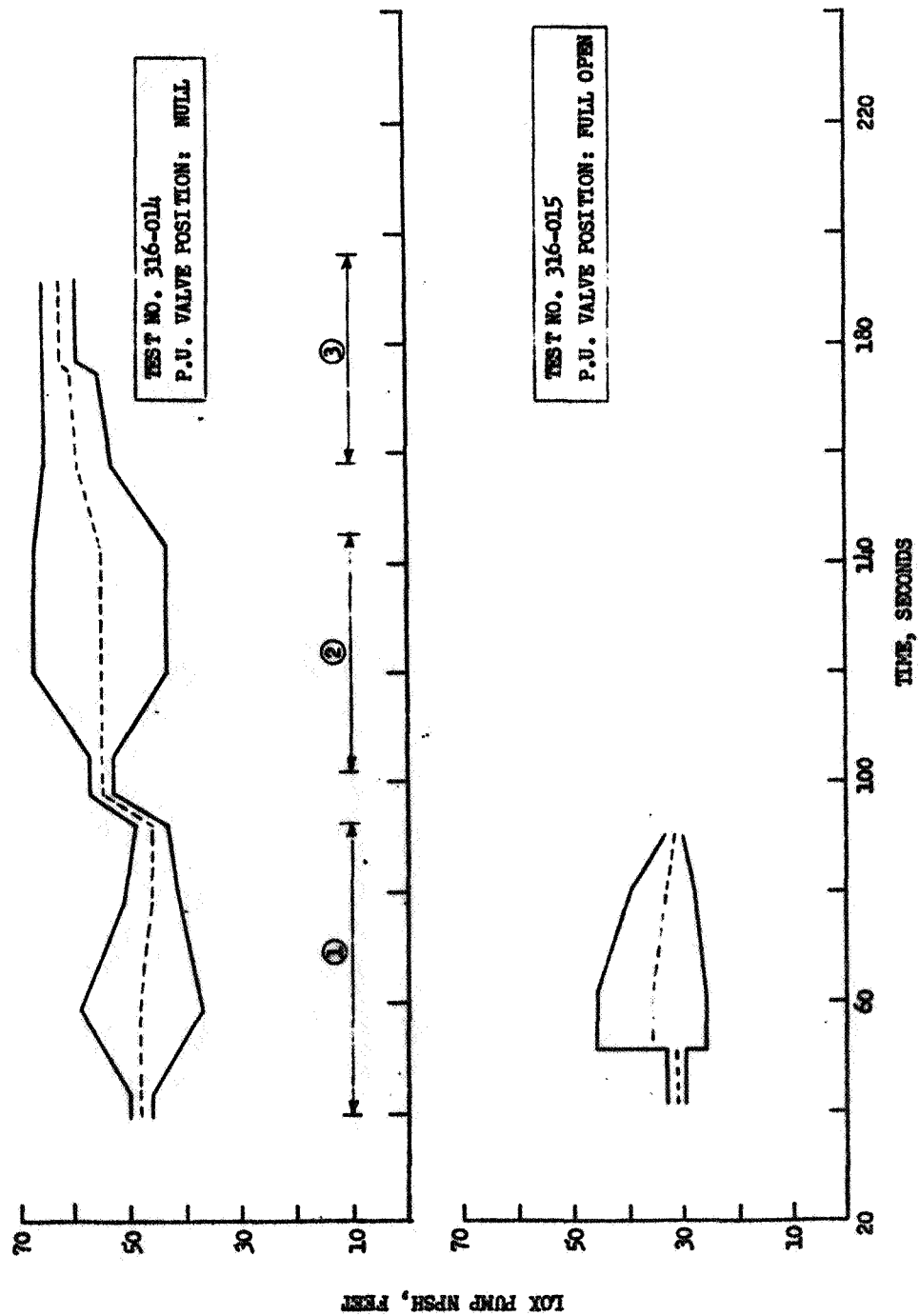
Figure A-2. Operating Conditions, J-2 Engine Pulsing Tests

TEST NO. 316-014
P.U. VALVE POSITION: NULL

TEST NO. 316-015
P.U. VALVE POSITION: FULL OPEN

LOX PUMP NPSH, FEET

TIME, SECONDS
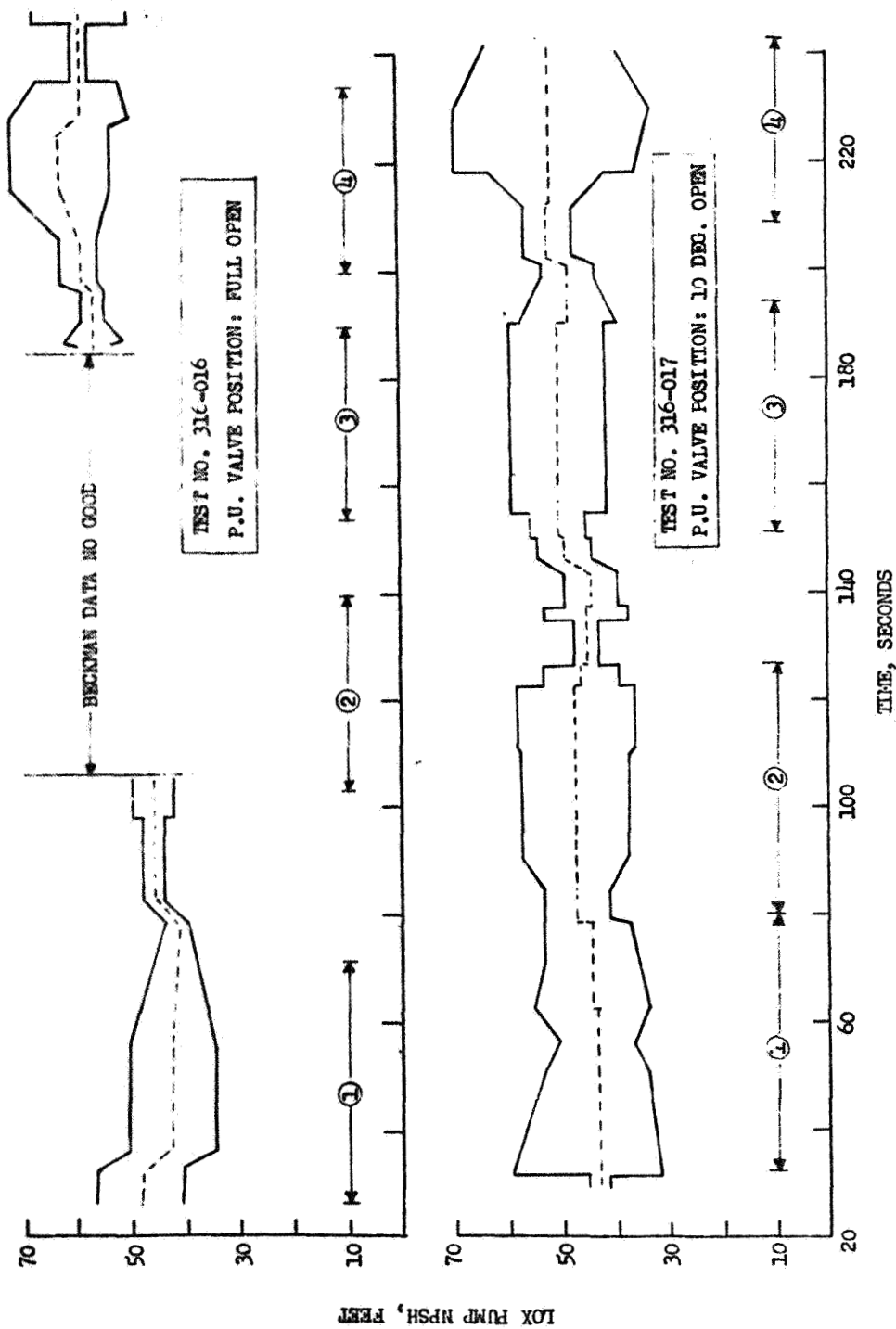
Figure A-3. Operating Cond' ions, J-2 Engine Pulsing Tests
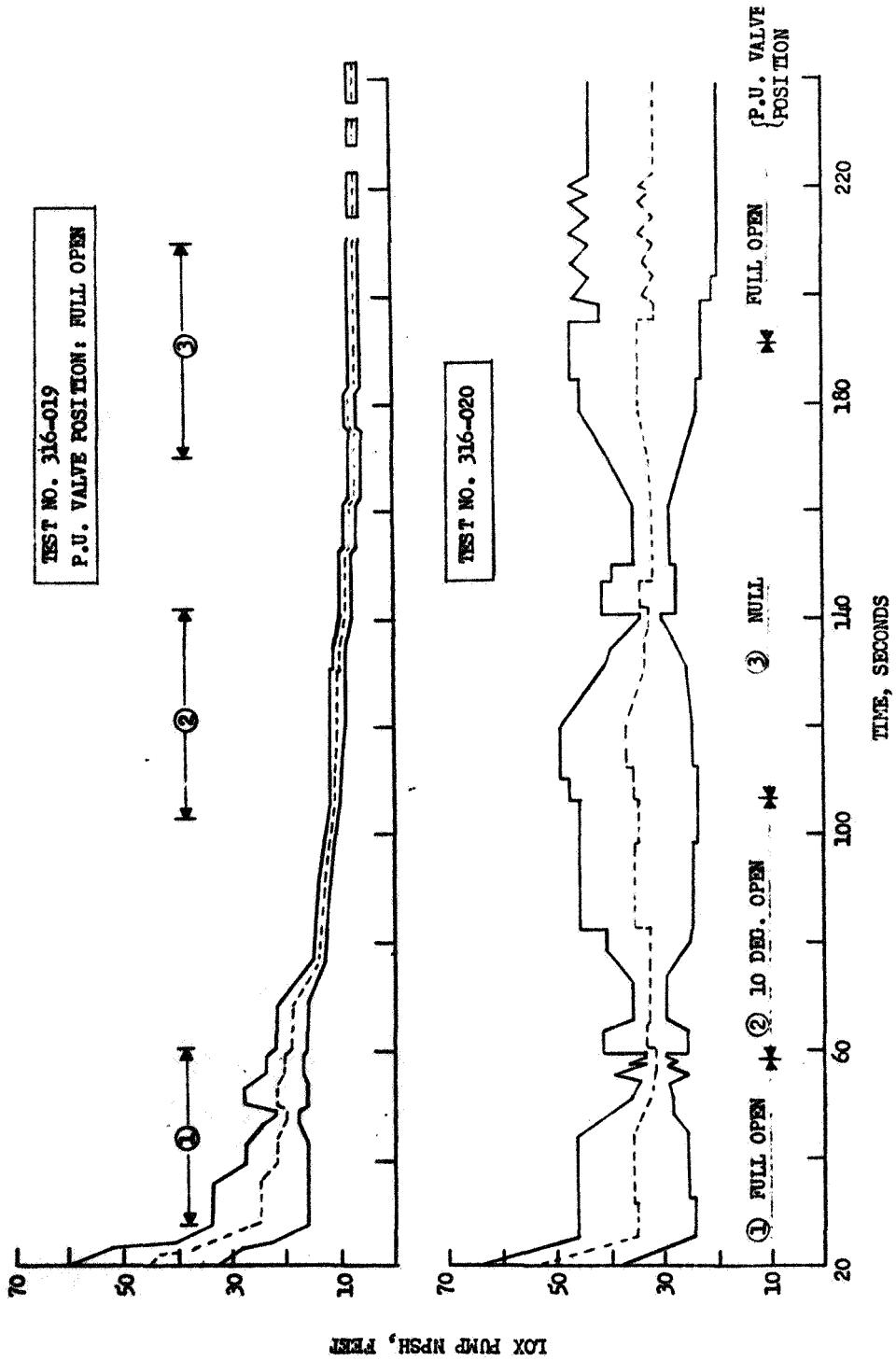
Figure A-4. Operating Conditions, J-2 Engine Pulsing Tests
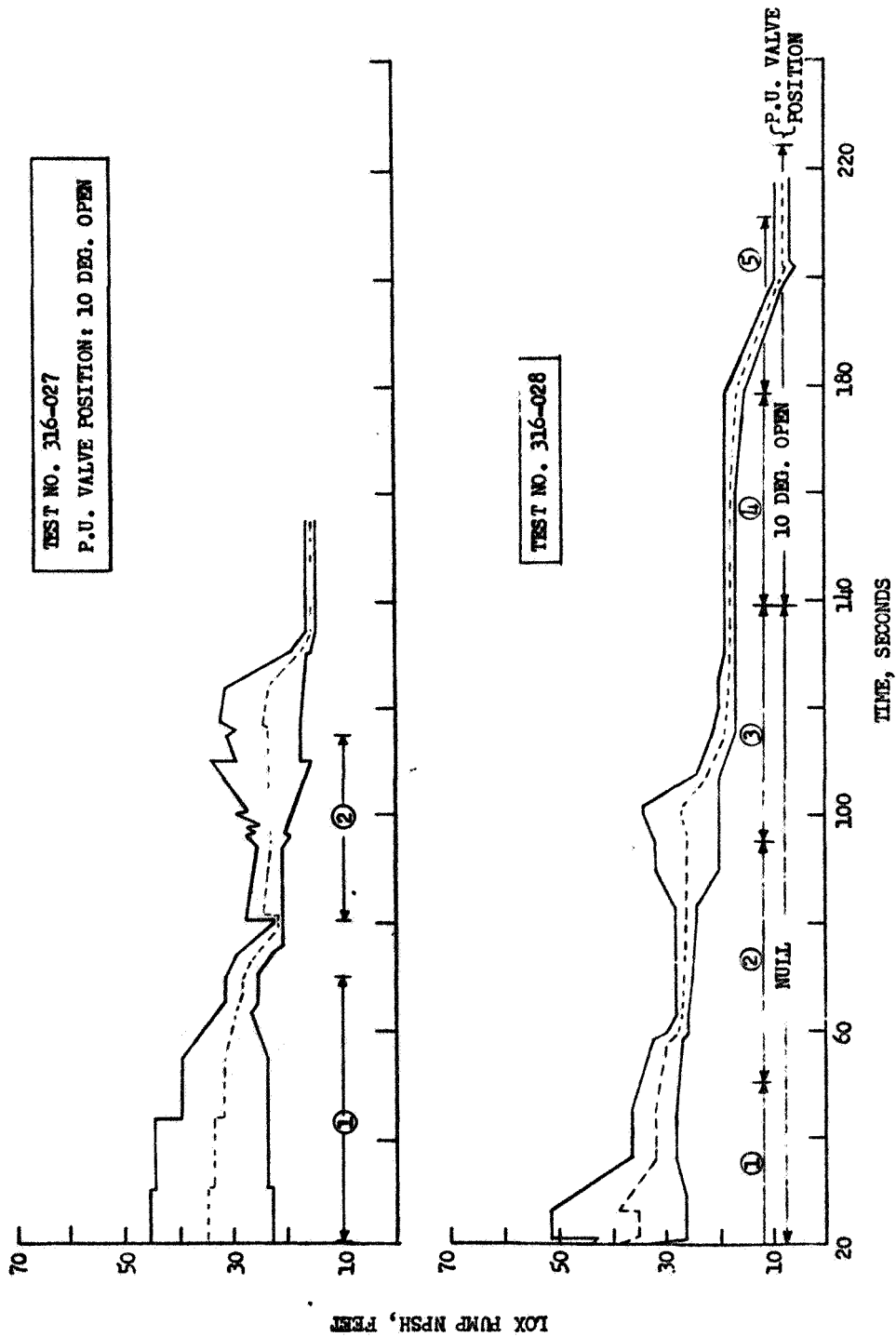
Figure A-5. Operating Conditions, J-2 Engine Pulsing Tests

A-6

R-7970
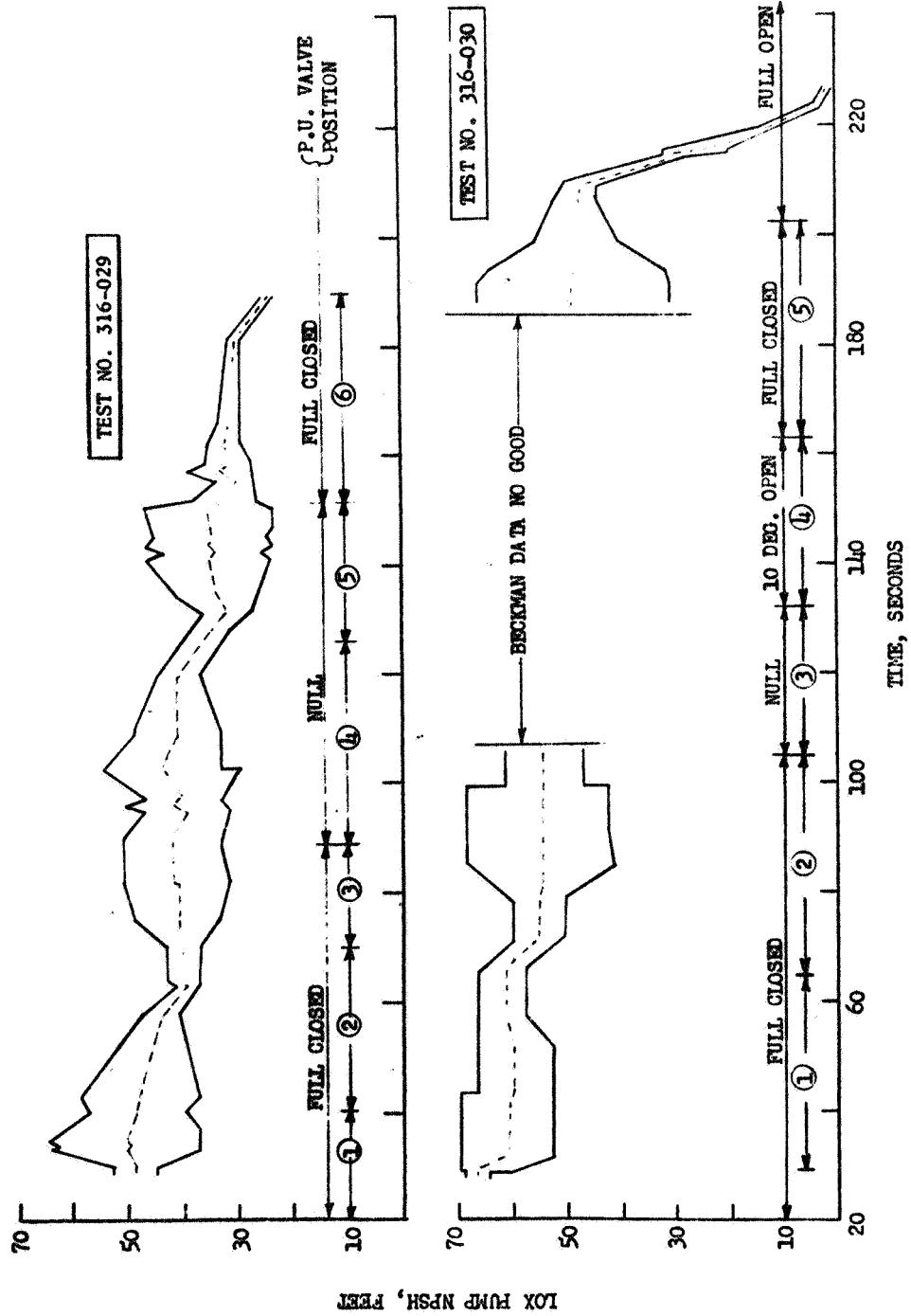
Figure A-6. Operating Conditions, J-2 Engine Pulsing Tests
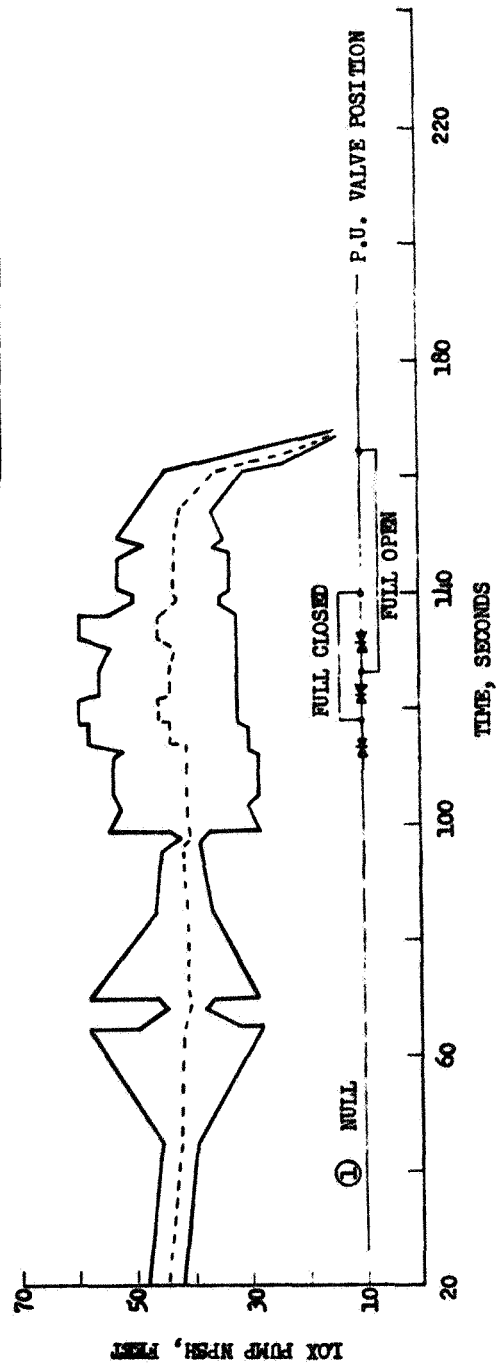
Figure A-7. Operating Conditions, J-2 Engine Pulsing Tests
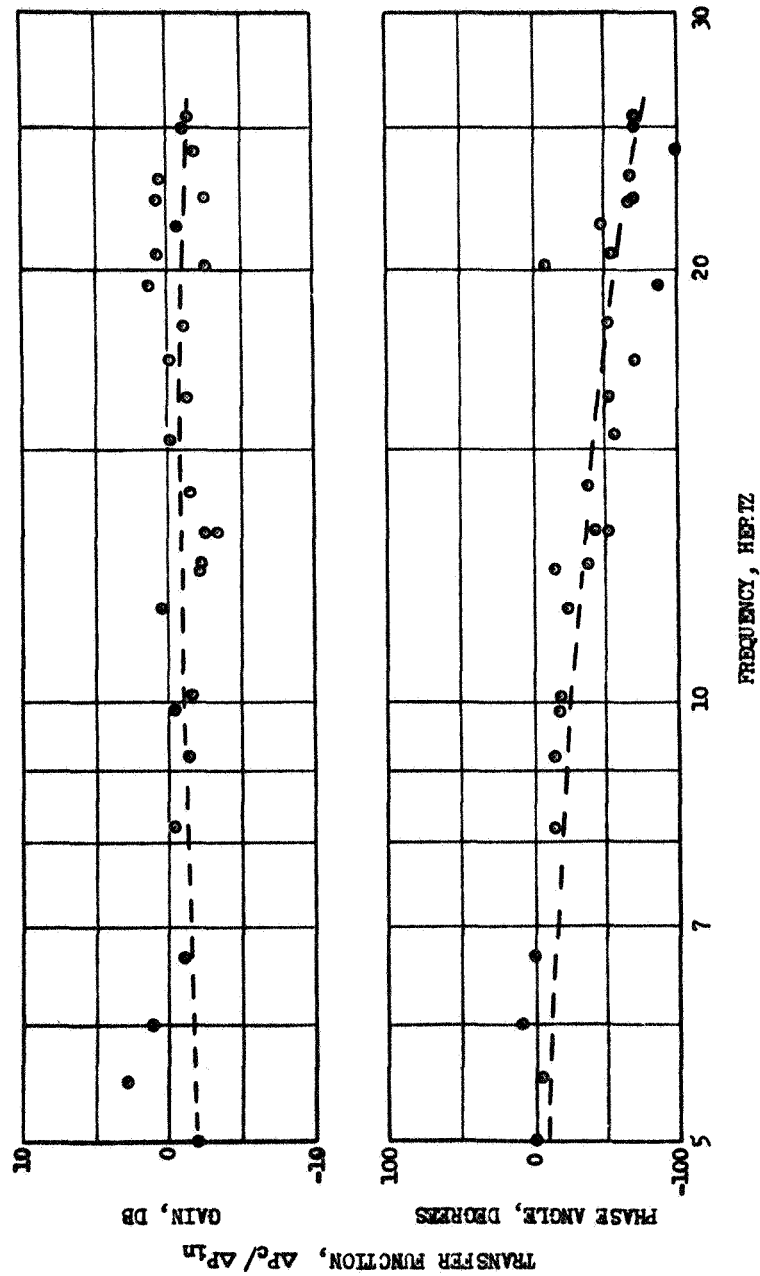
Figure A-8. J-2 Engine Test With Inlet Line Pulser, Test No. 316-011

Figure A-9. J-2 Engine Test With Inlet Line Pulser, Test No. 316-013-1

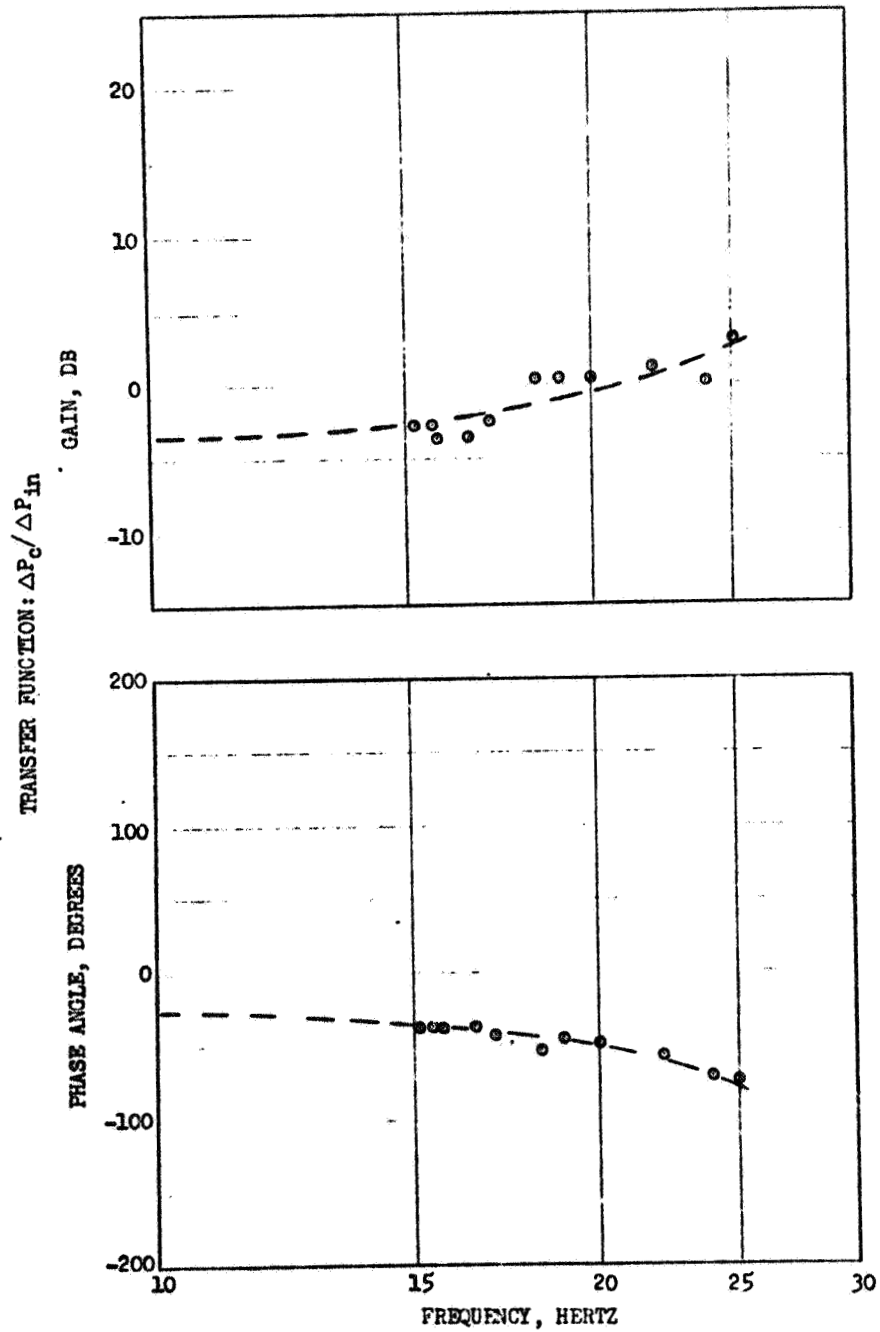P.U. VALVE POSITION: 10 DEG. OPEN
APPROXIMATE AVG. NPSH: 37 FEET
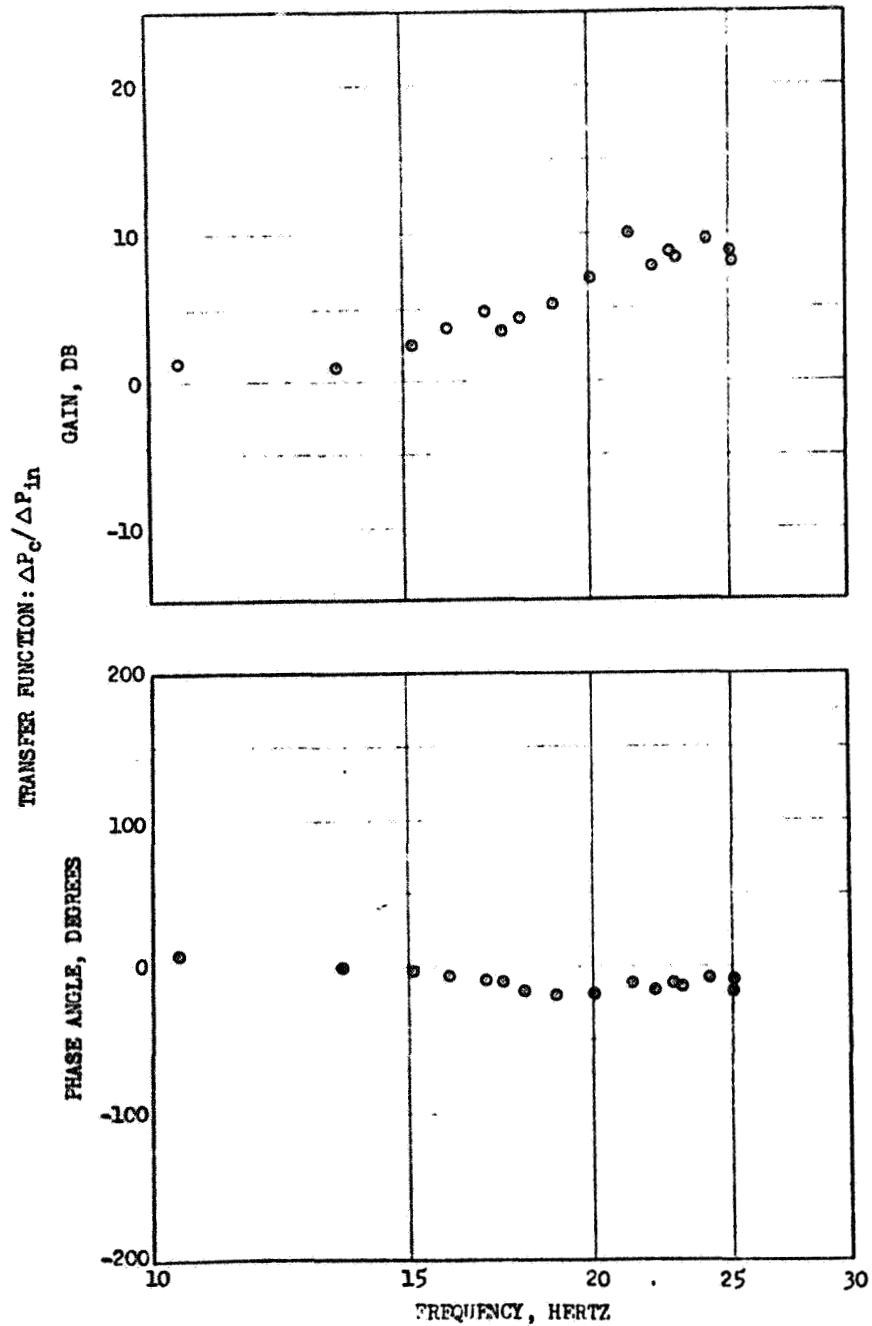
Figure A-10.   J-2 Engine Test With Inlet Line Pulser, Test No. 316-013-2
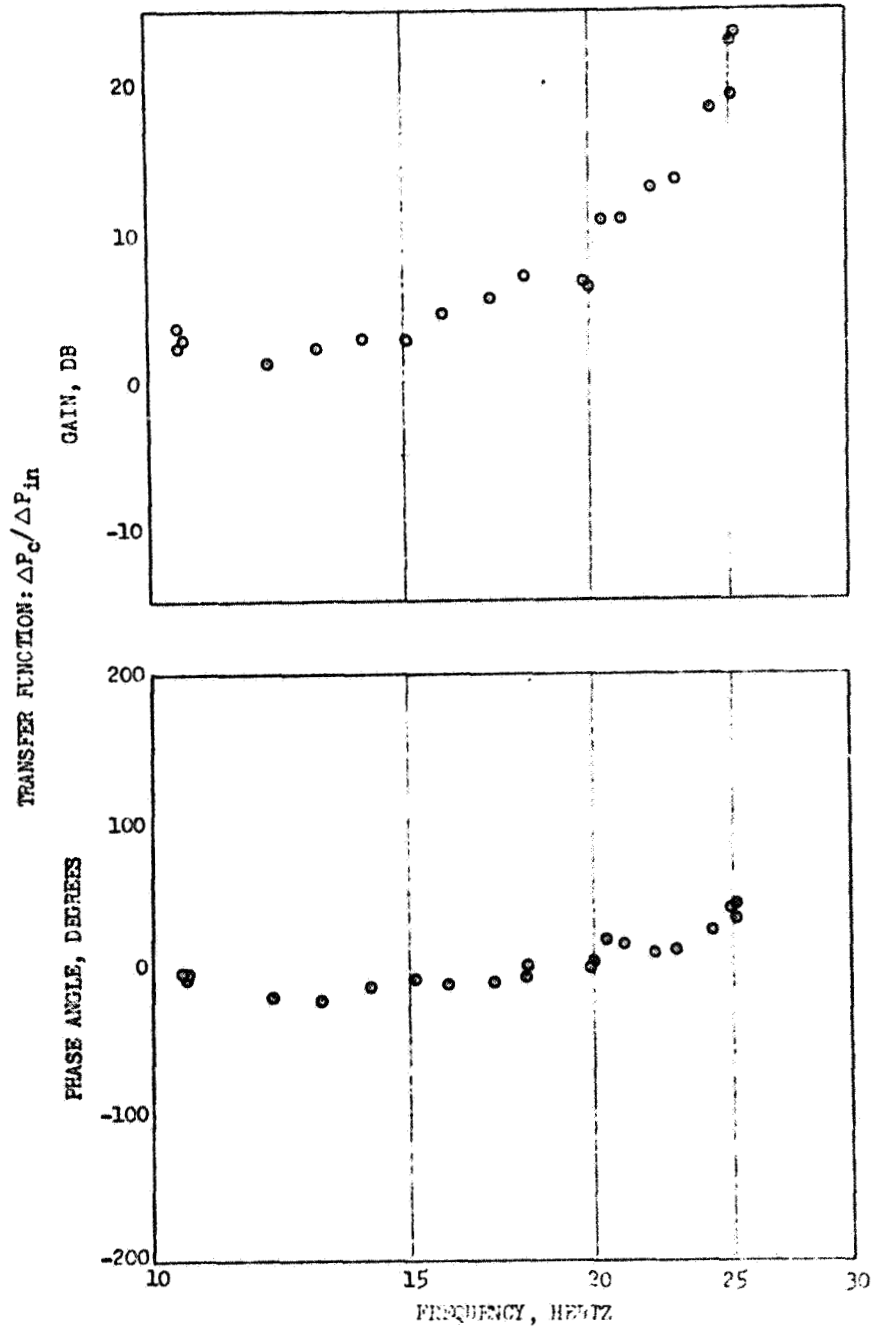
Figure A-11. J-2 Engine Test With Inlet Line Pulser, Test No. 316-013-3

P.U. VALVE POSITION: NULL
APPROXIMATE AVG. NPSH: 48 FEET
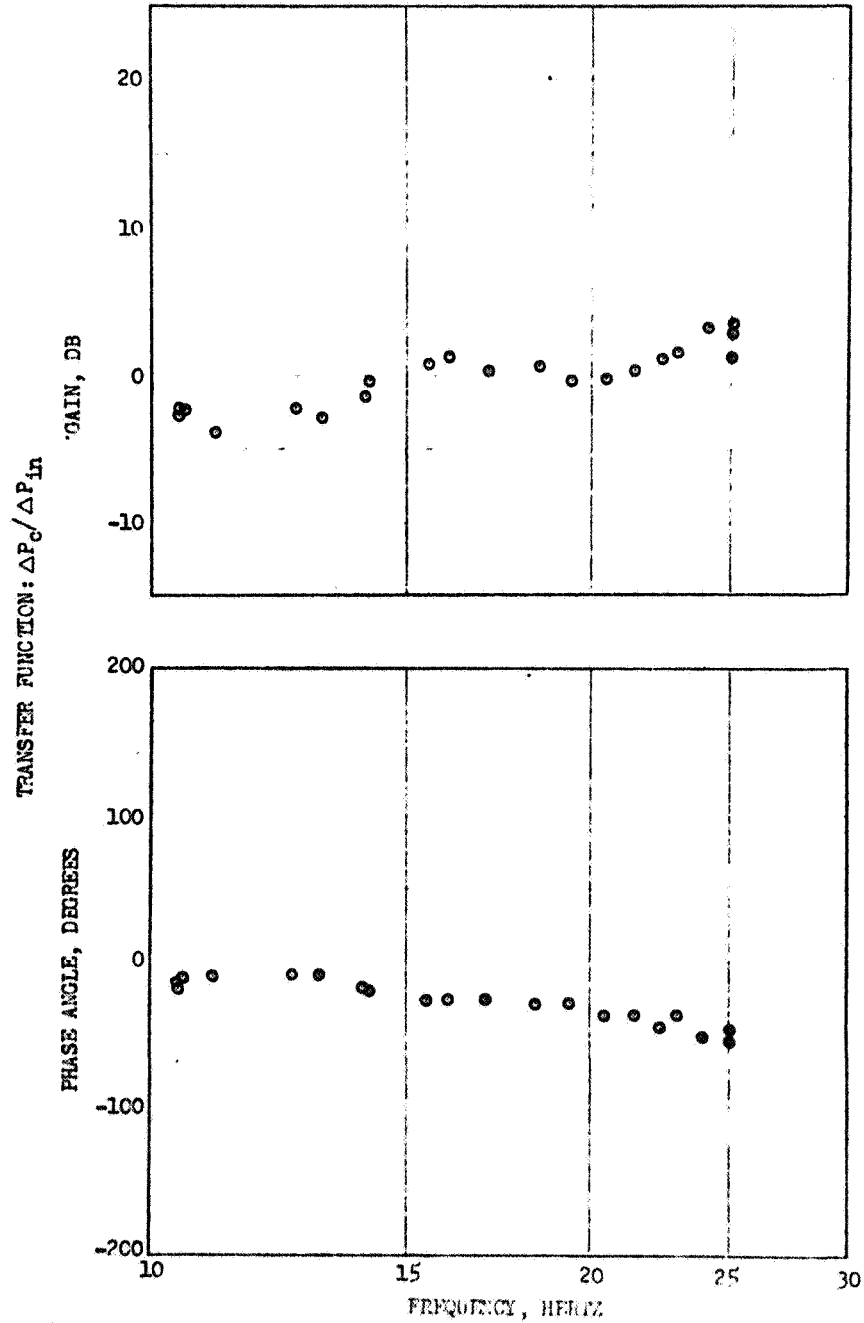
Figure A-12. J-2 Engine Test With Inlet Line Pulser, Test No. 316-014-1

P.U. VALVE POSITION: NULL
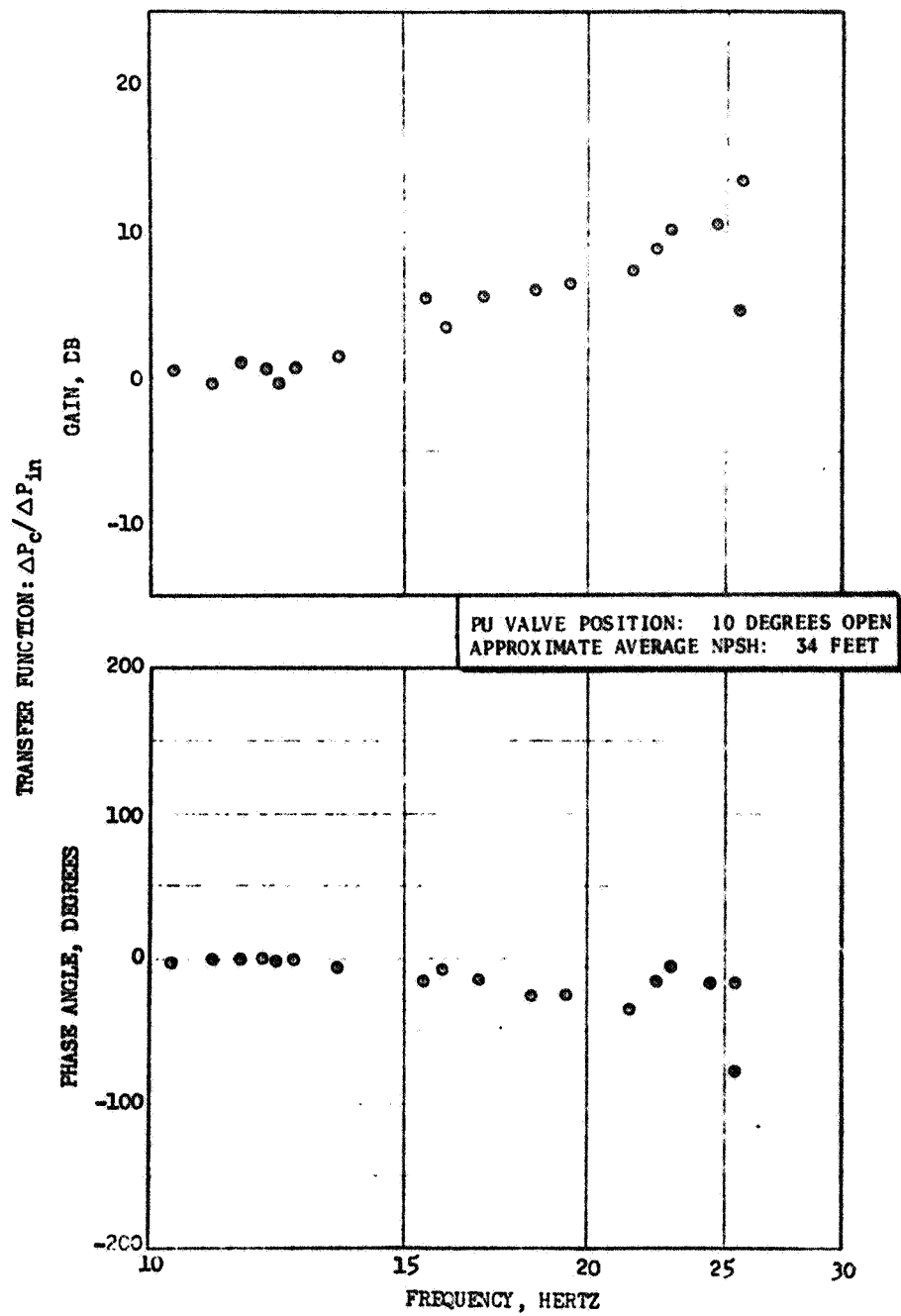APPROXIMATE AVG. NPSH: 55 FEET
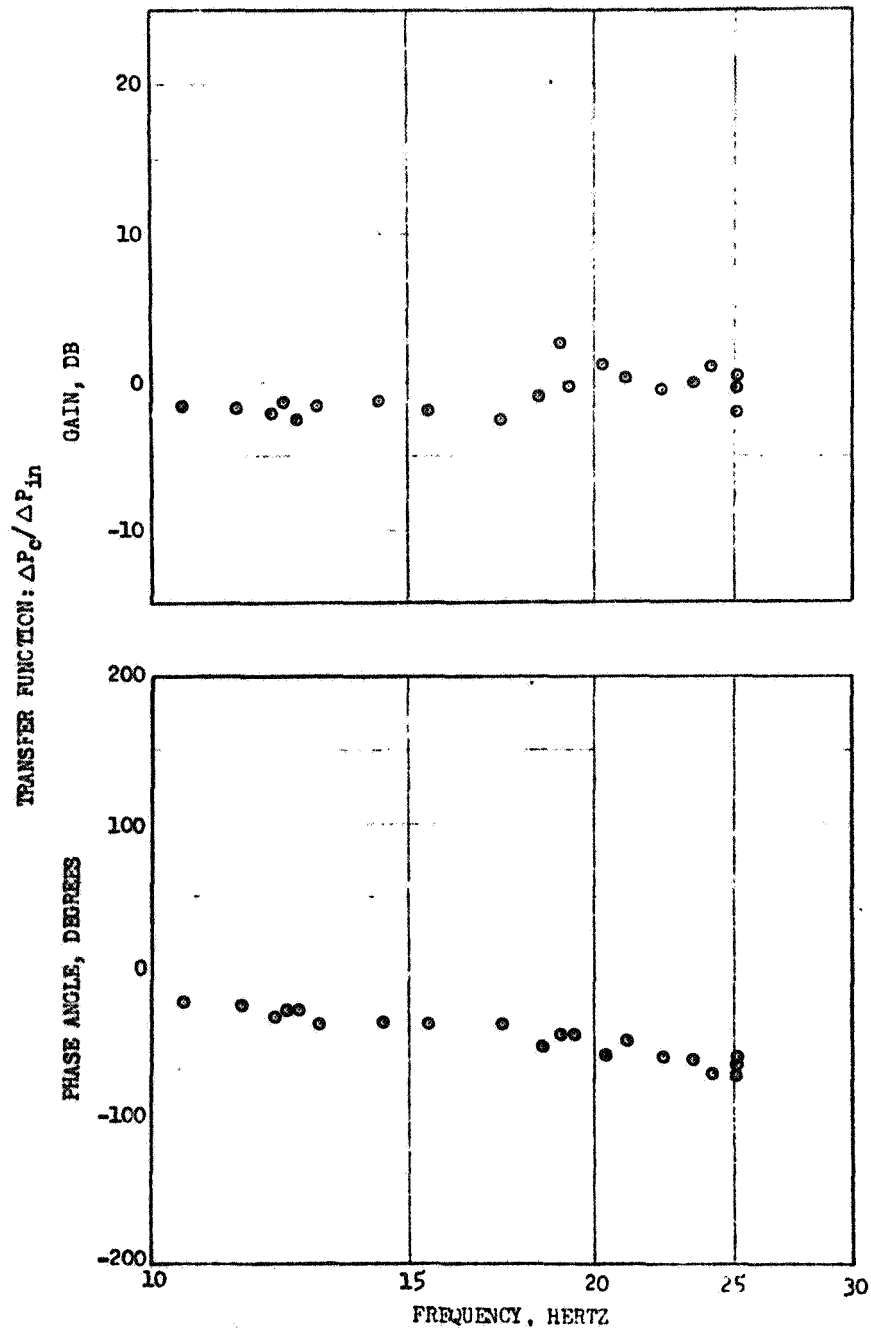
Figure A-13. J-2 Engine Test With Inlet Line Pulser, Test No. 316-014-2
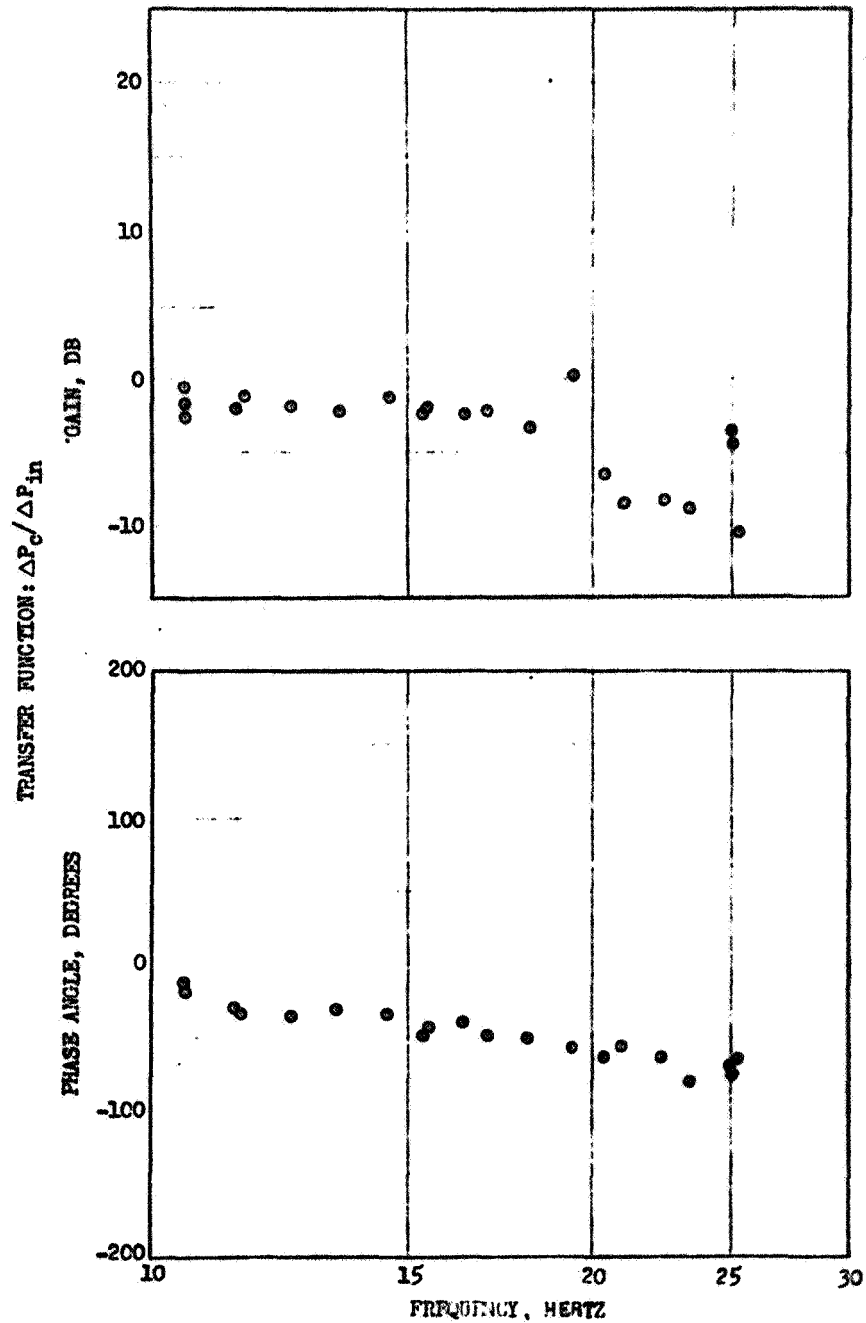
Figure A-14. J-2 Engine Test With Inlet Line Pulser, Test No. 316-014-3
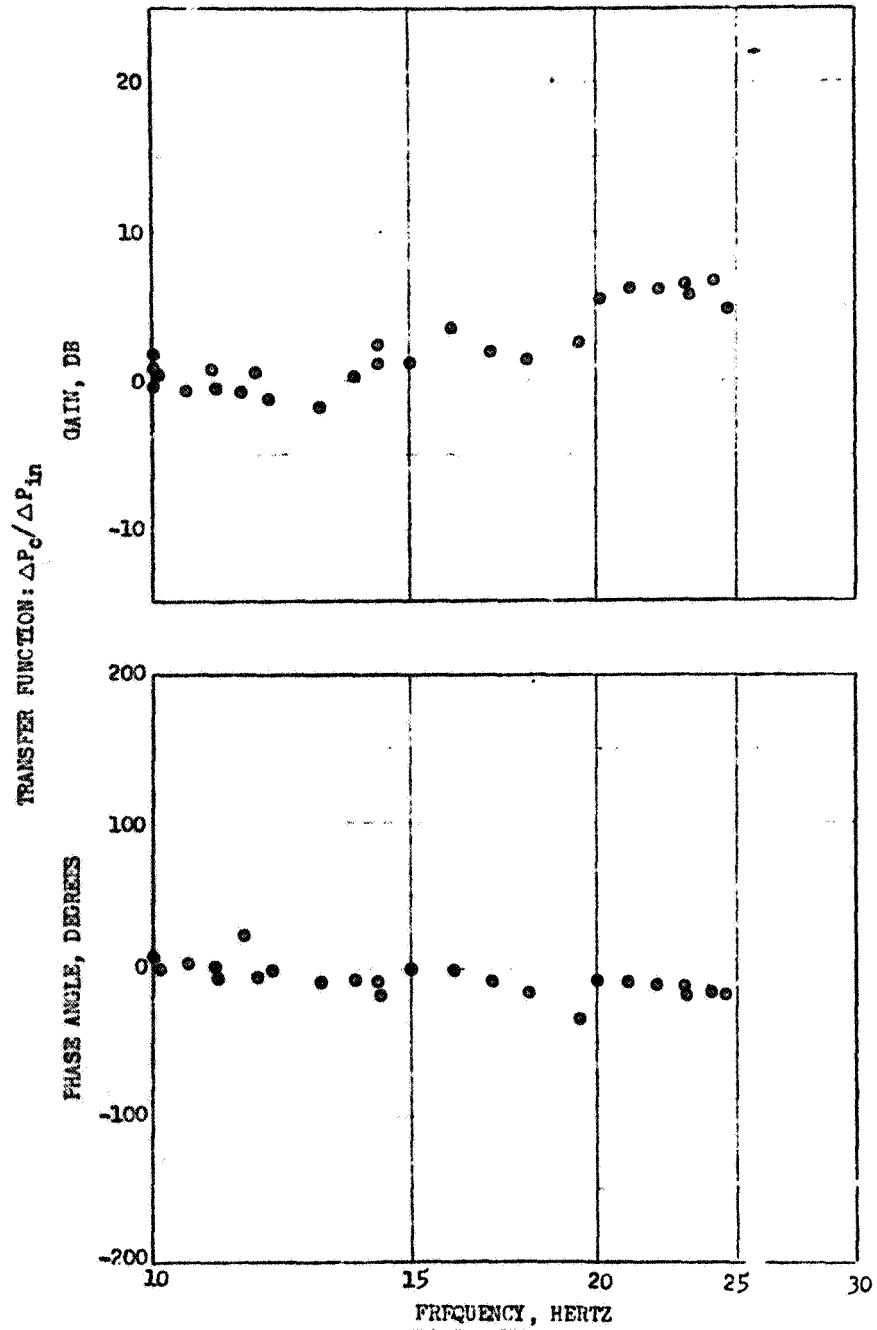
Figure A-15. J-2 Engine Test With Inlet Line Pulser, Test No. 316-015

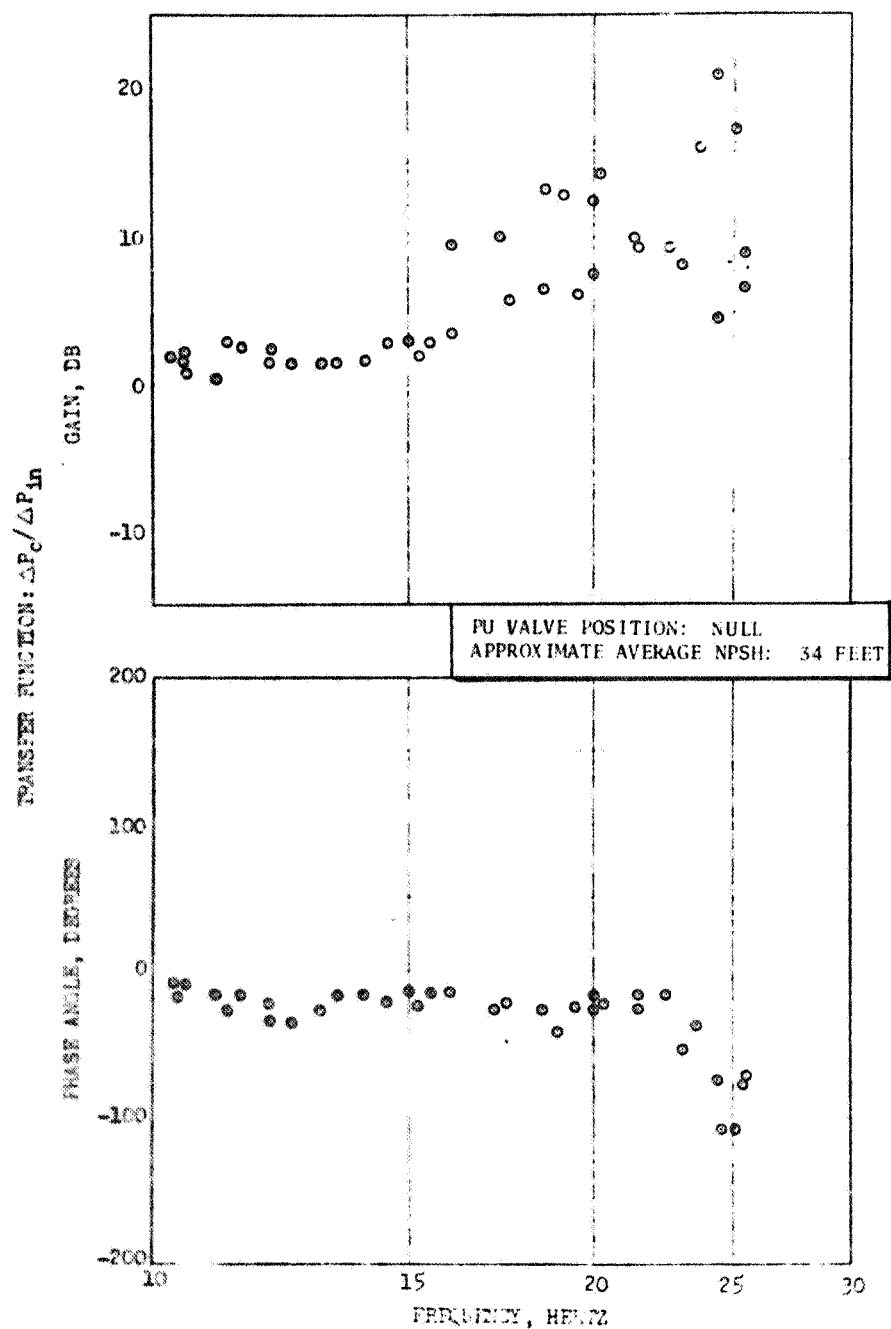Figure A-16. J-2 Engine Test With Inlet Line Pulser, Test No. 316-016-1

P.U. VALVE POSITION: FULL OPEN
APPROXIMATE AVG. NPSH: 46 FEET
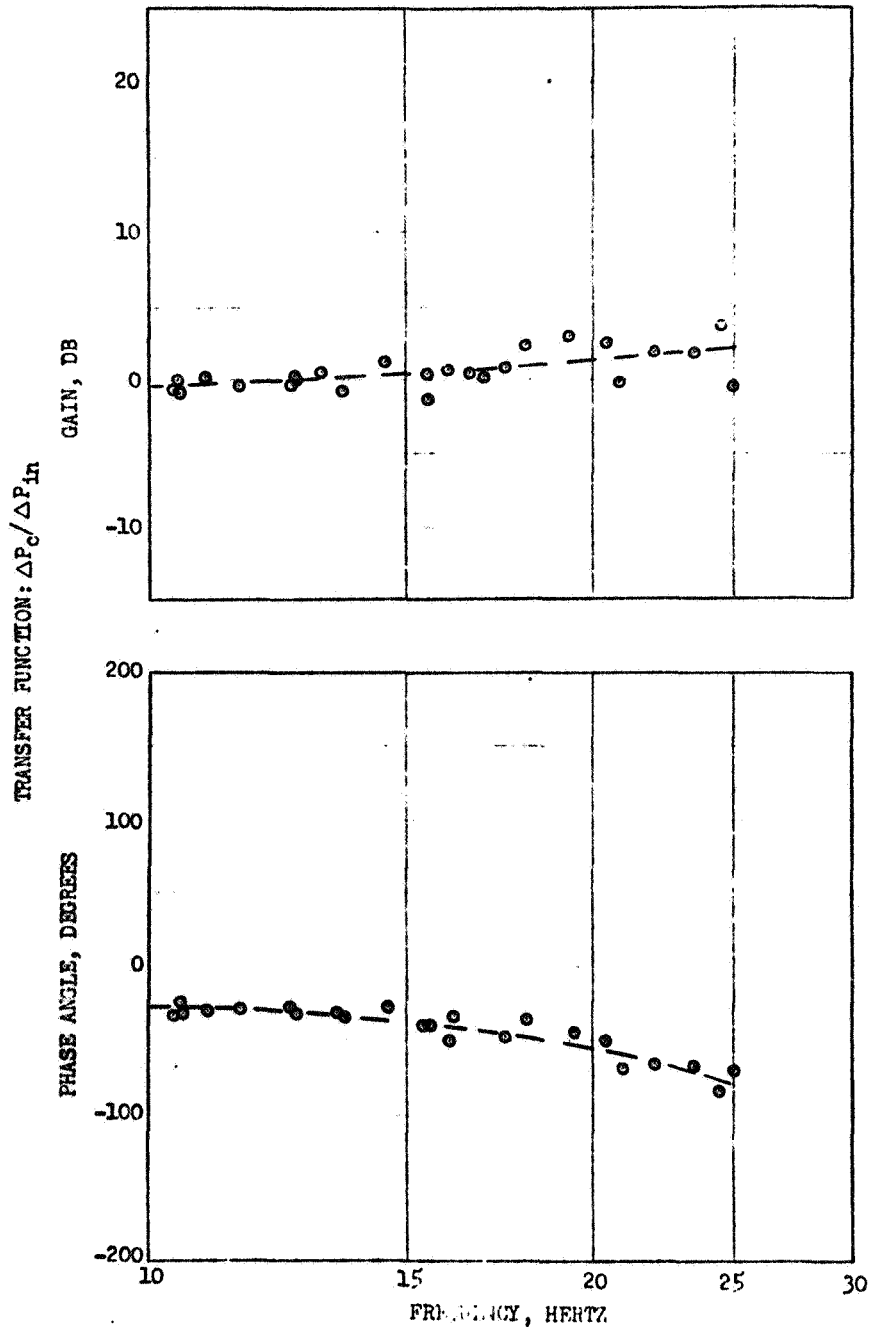
Figure A-17. J-2 Engine Test With Inlet Line Pulser, Test No. 316-016-2

F.U. VALVE POSITION: FULL OPEN
APPROXIMATE AVG. NPSH: 55 FEET
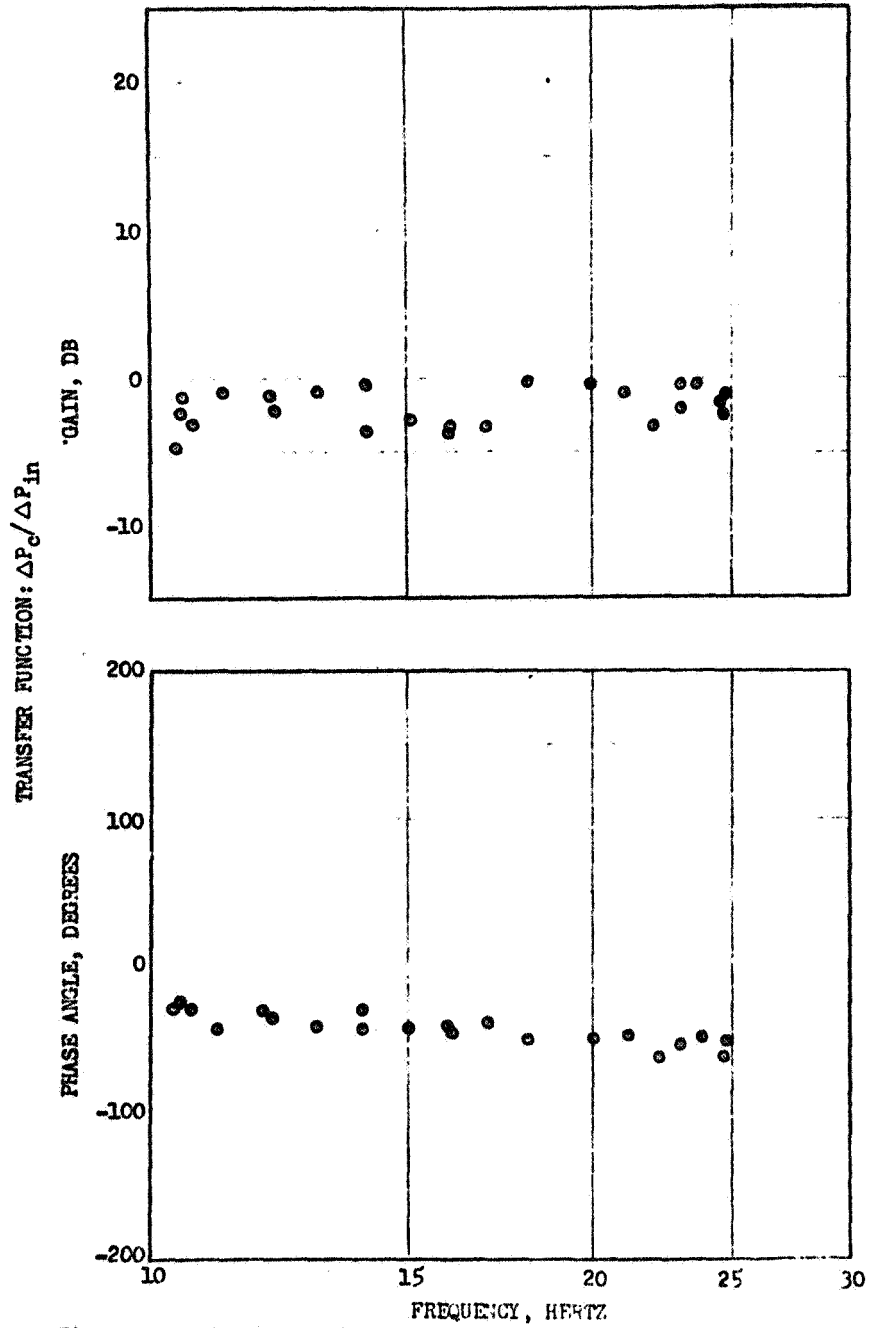
Figure A-18. J-2 Engine Test With Inlet Line Pulser, Test No. 316-016-3

P.U. VALVE POSITION: **FULL OPEN**
APPROXIMATE AVG. NPSH: 59 FEET
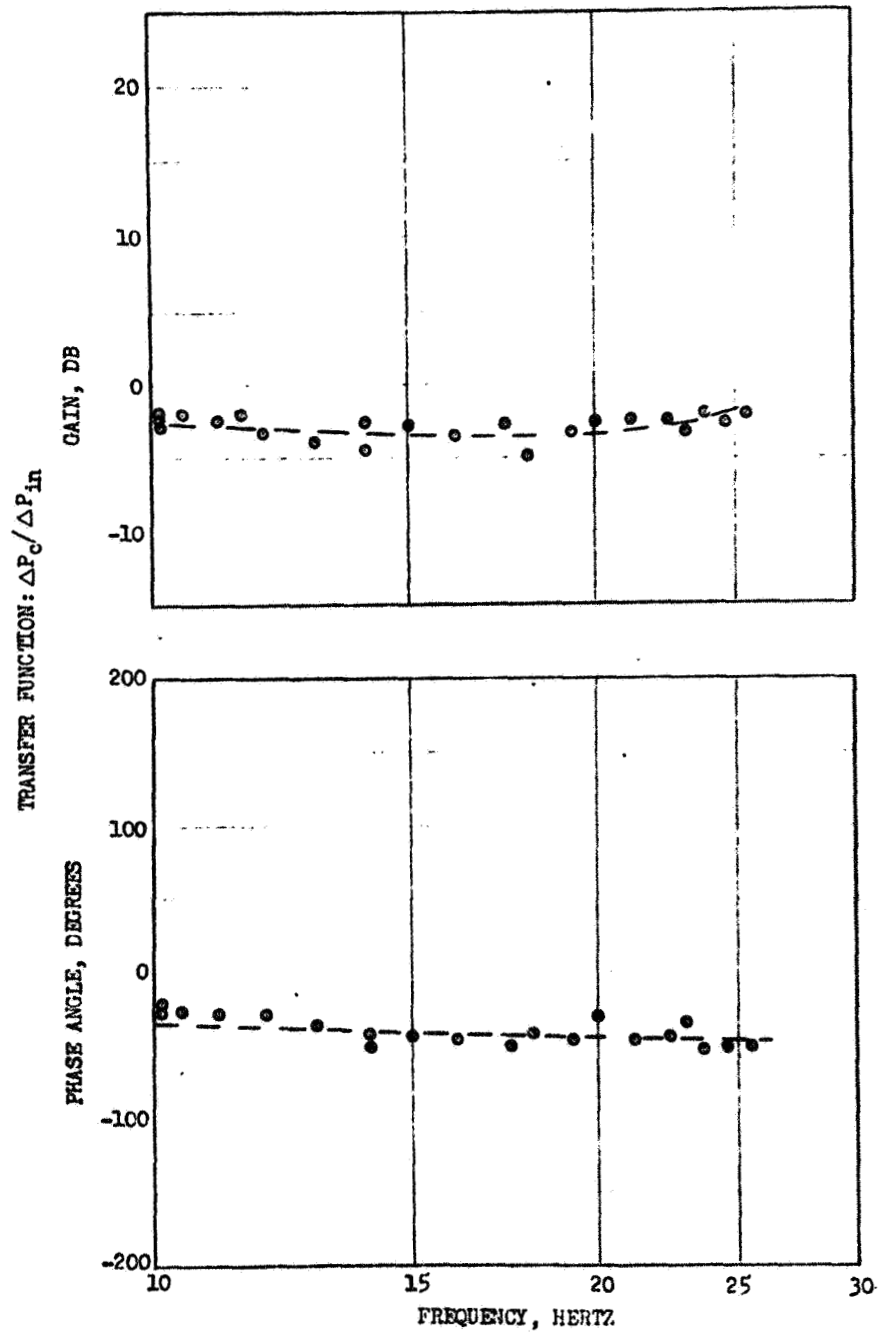
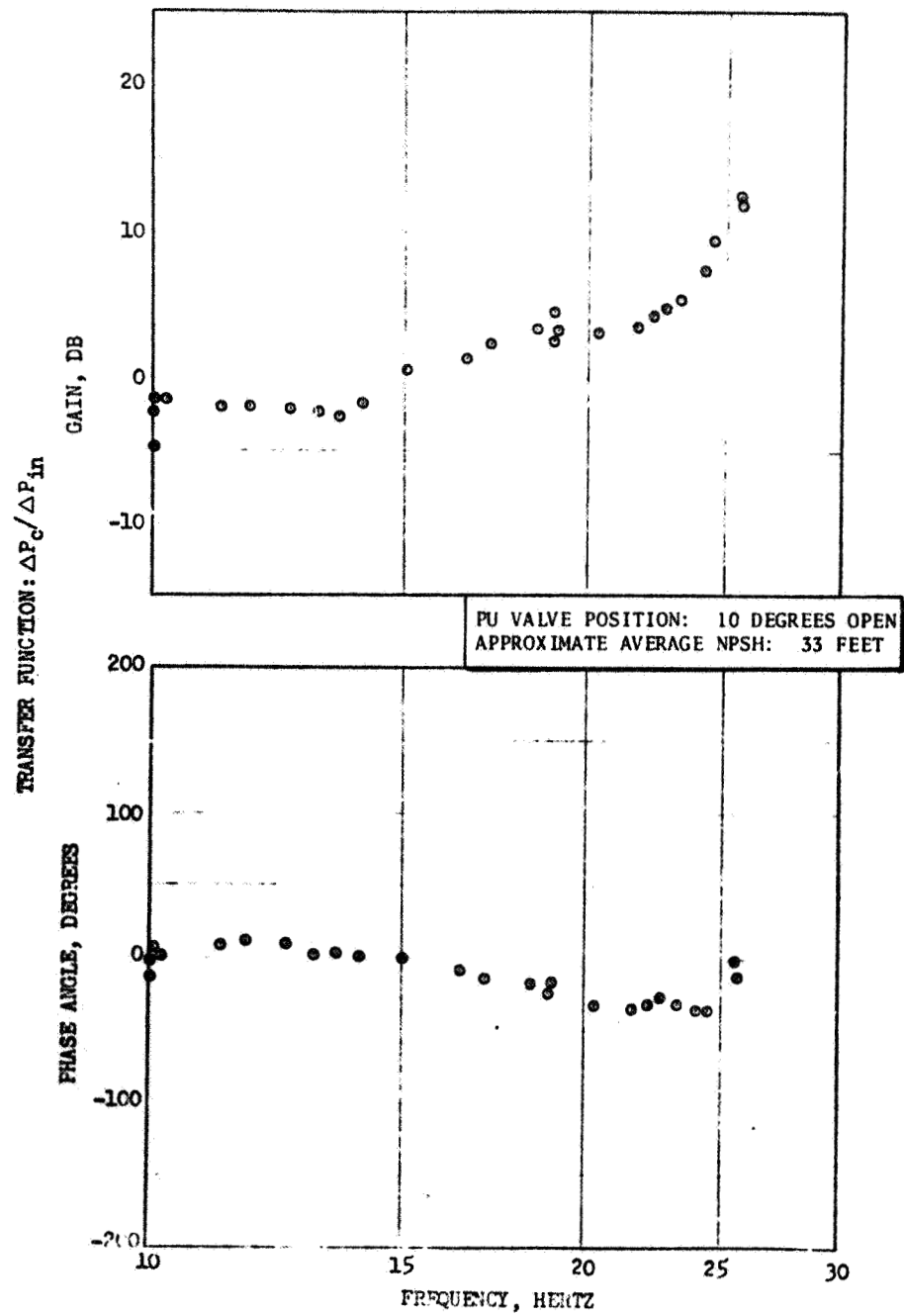Figure A-19. J-2 Engine Test With Inlet Line Pulser, Test No. 316-016-4
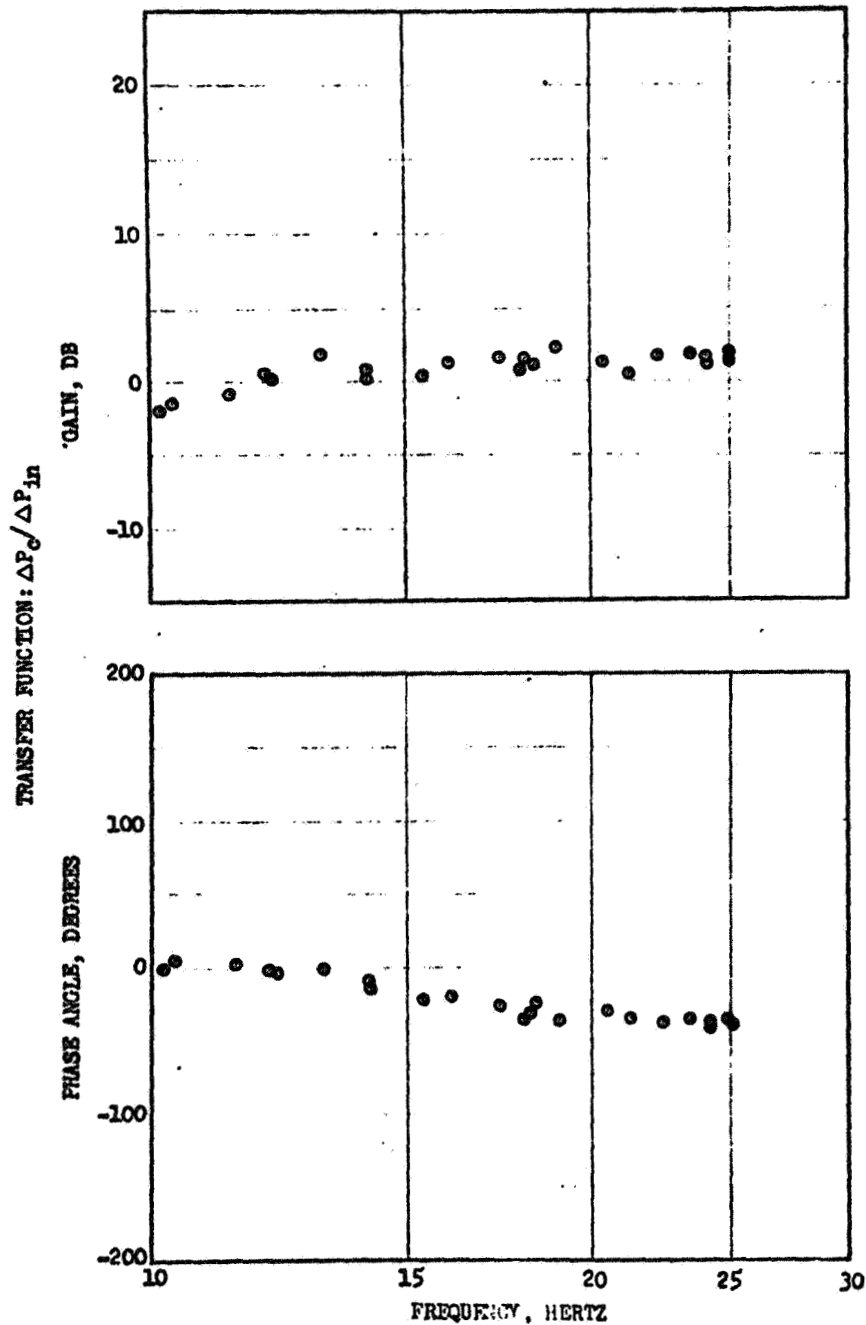
Figure A-20. J-2 Engine Test With Inlet Line Pulser, Test No. 316-017-1
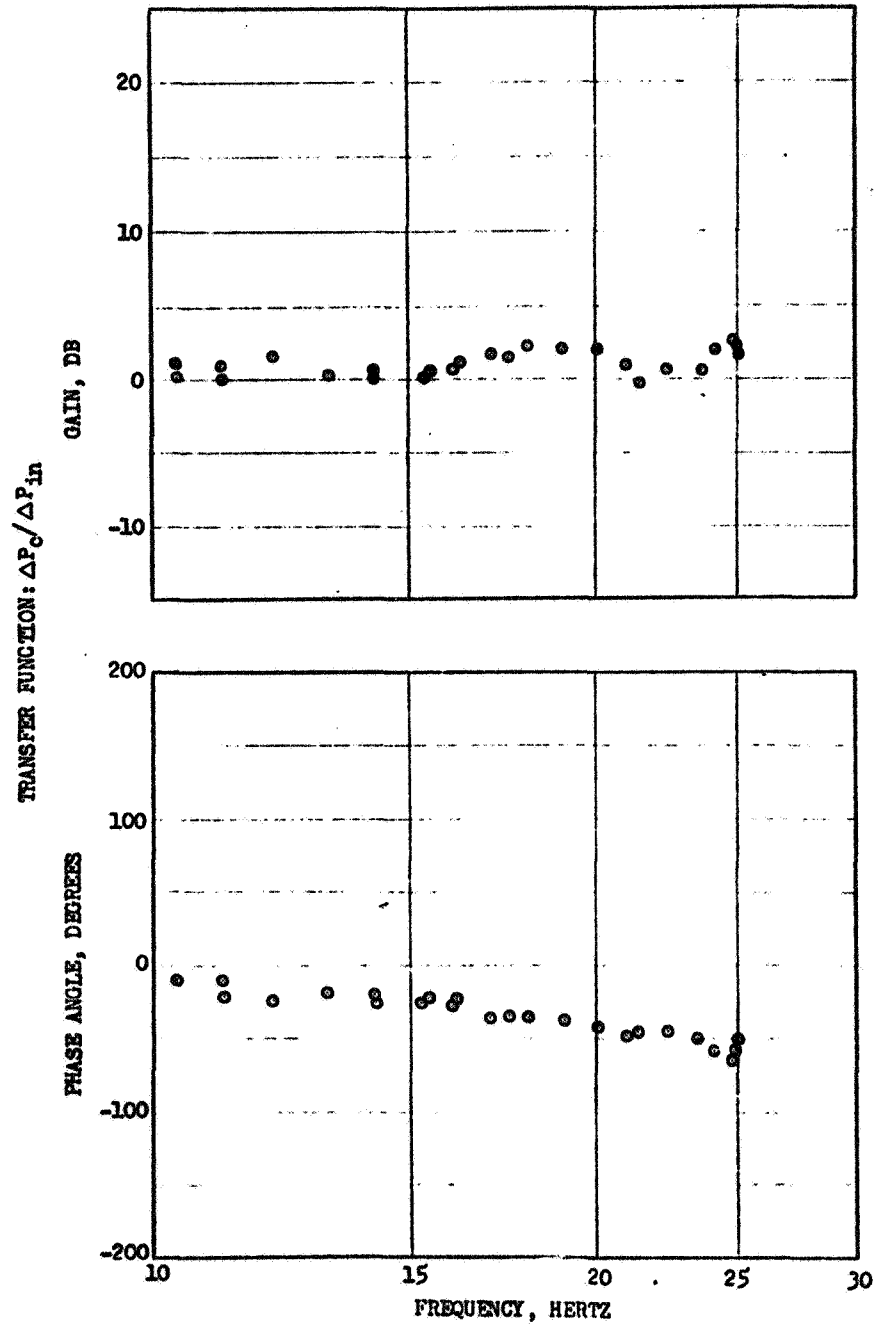
Figure A-21. J-2 Engine Test With Inlet Line Pulser, Test No. 316-017-2

P.U. VALVE POSITION: 10 DEG. OPEN
APPROXIMATE AVG. NPSH: 51 FEET
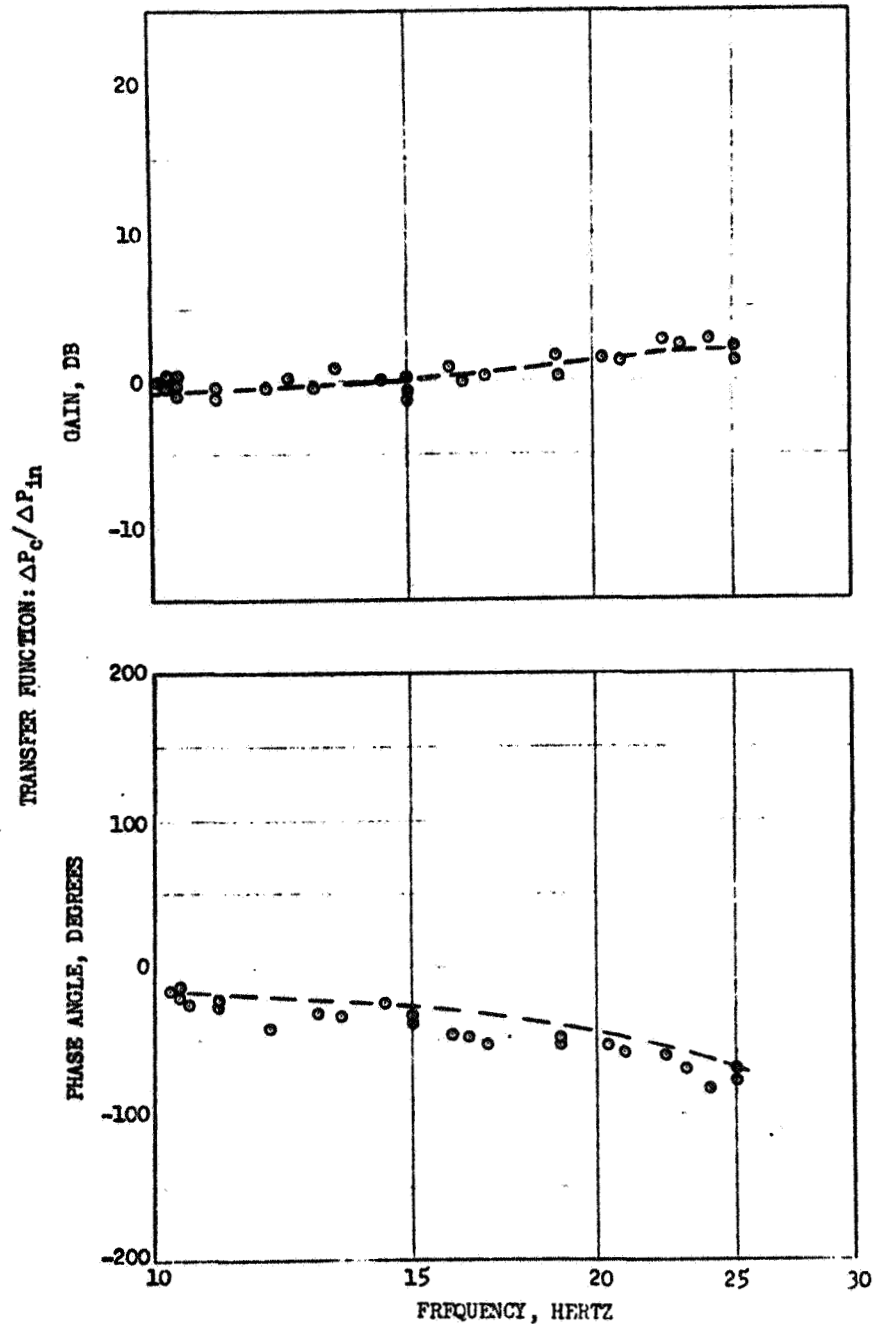
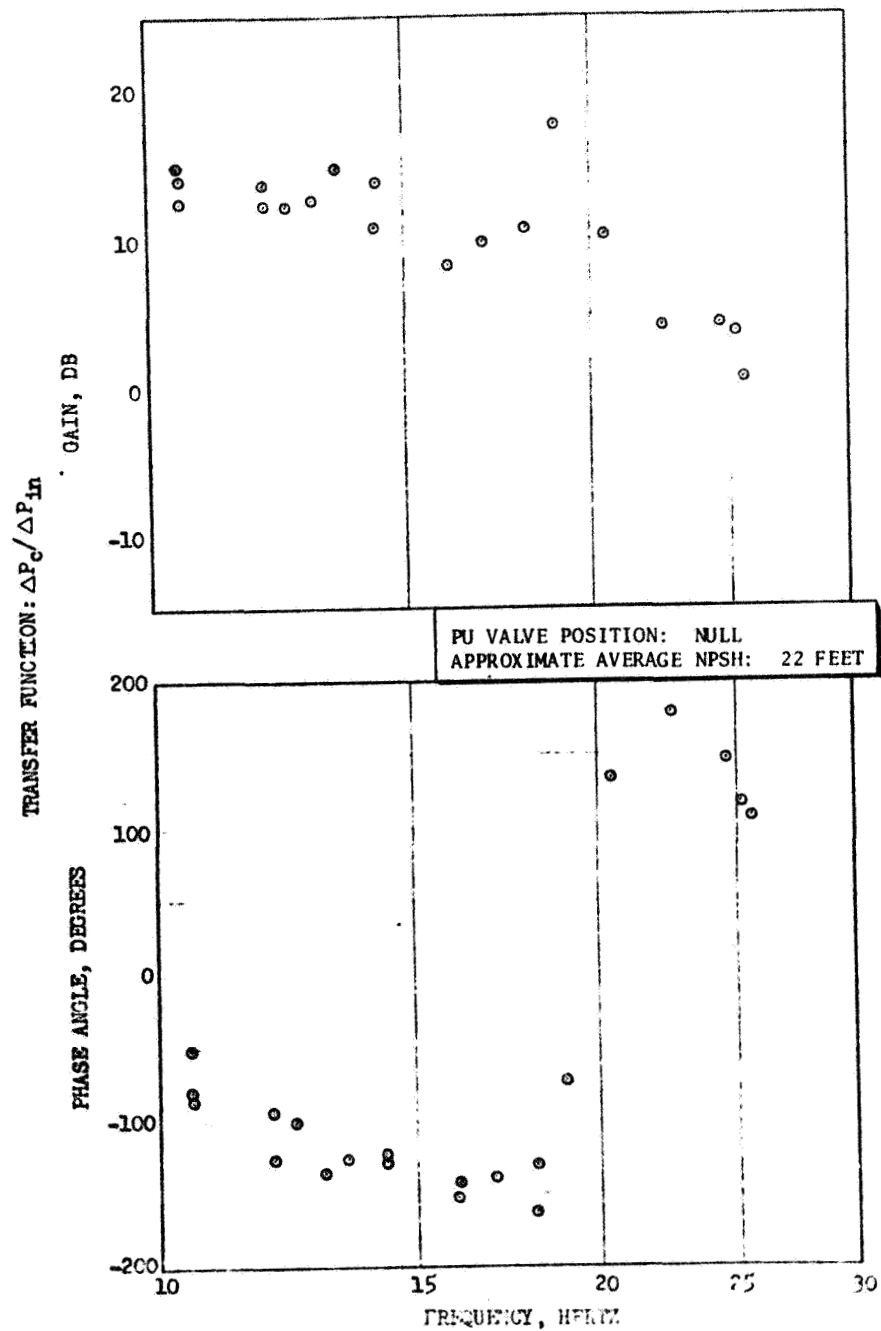Figure A-22. J-2 Engine Test With Inlet Line Pulser, Test No. 316-017-3

Figure A-23. J-2 Engine Test With Inlet Line Pulser, Test No. 316-017-4
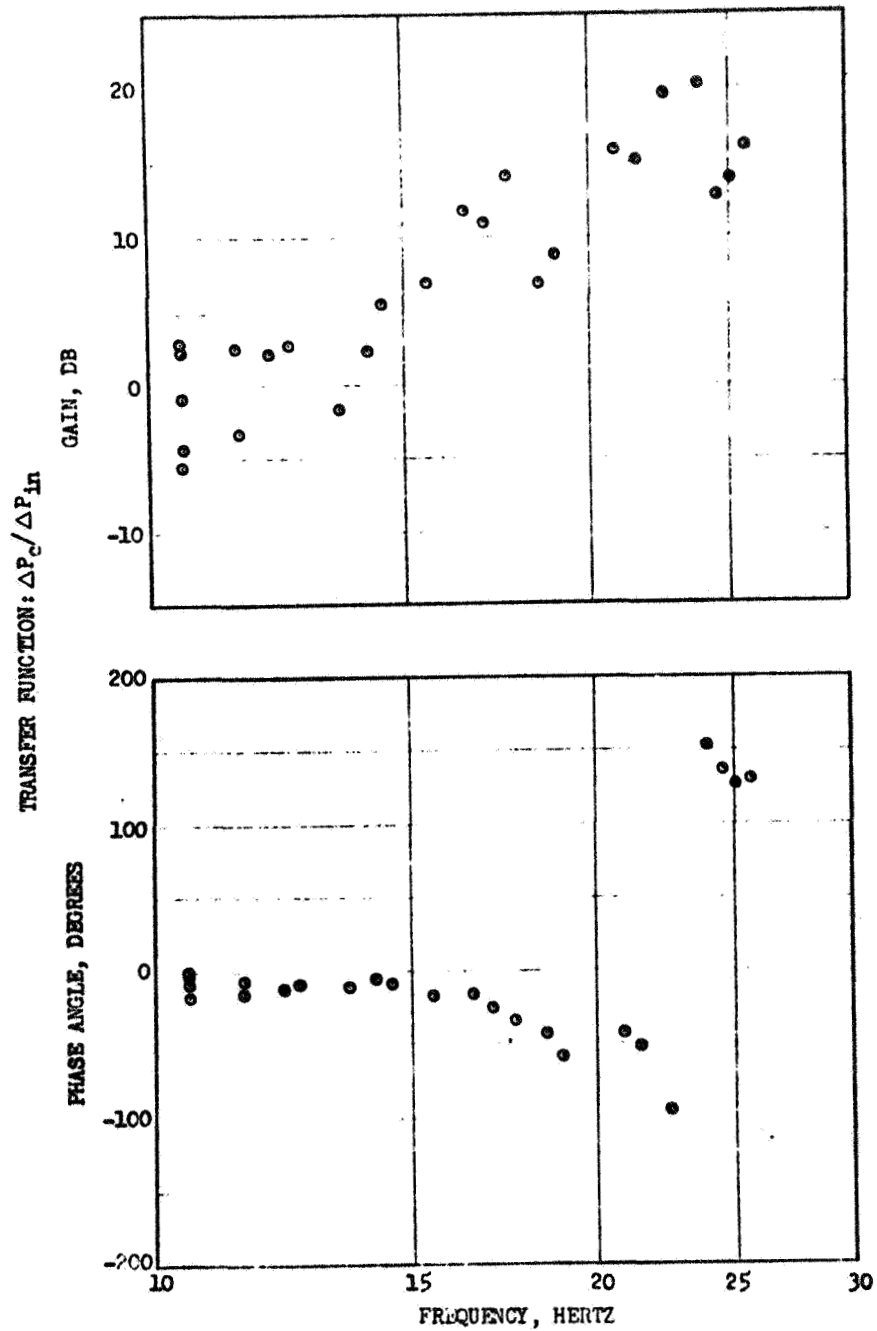
Figure A-24. J-2 Engine Test With Inlet Line Pulser, Test No. 316-019-1
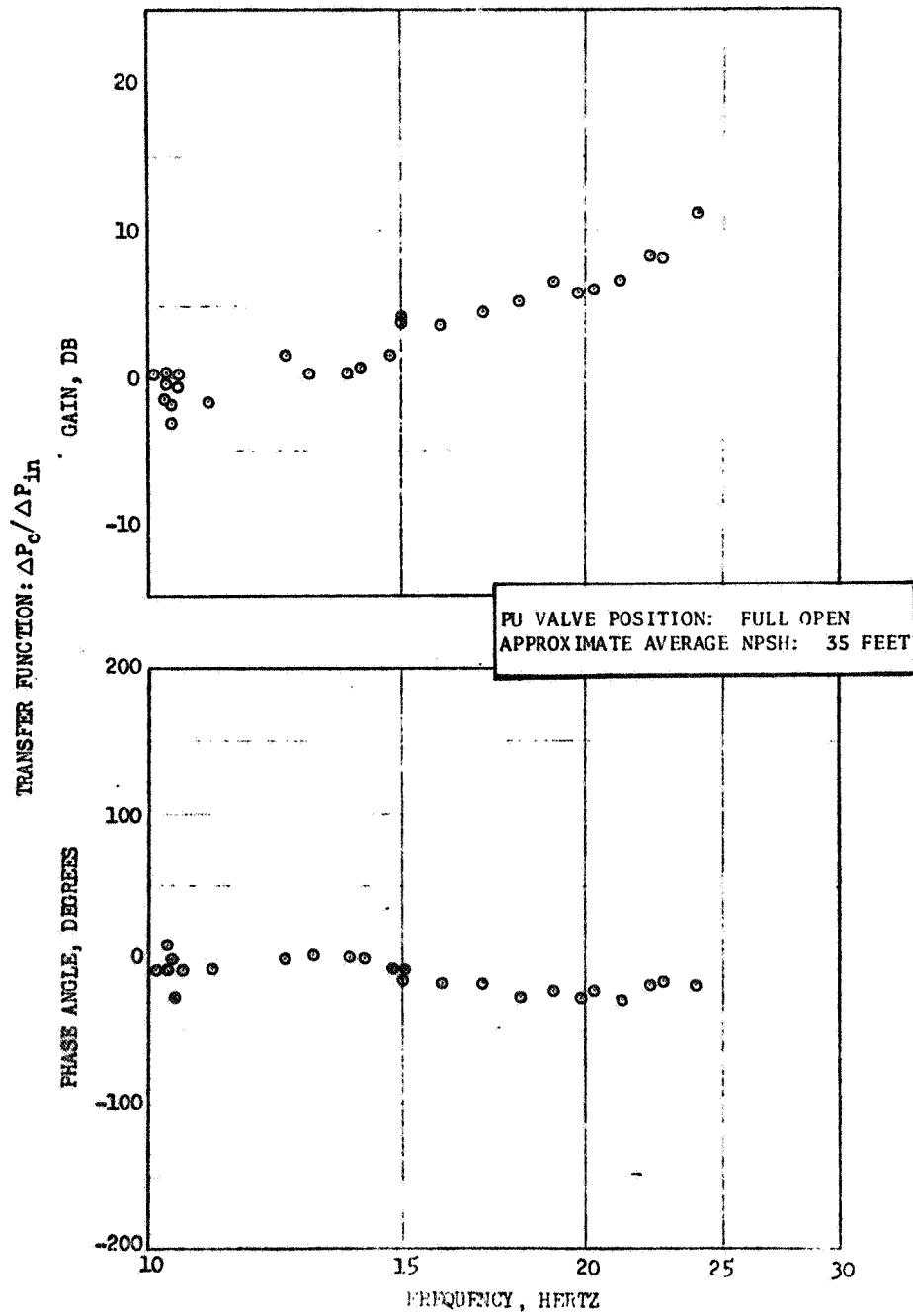
Figure A-25. J-2 Engine Test With Inlet Line Pulser, Test No. 316-020-1

Figure A-26. J-2 Engine Test With Inlet Line Pulser, Test No. 316-020-2

Figure A-27. J-2 Engine Test With Inlet Line Pulser, Test No. 316-020-3

R-7970

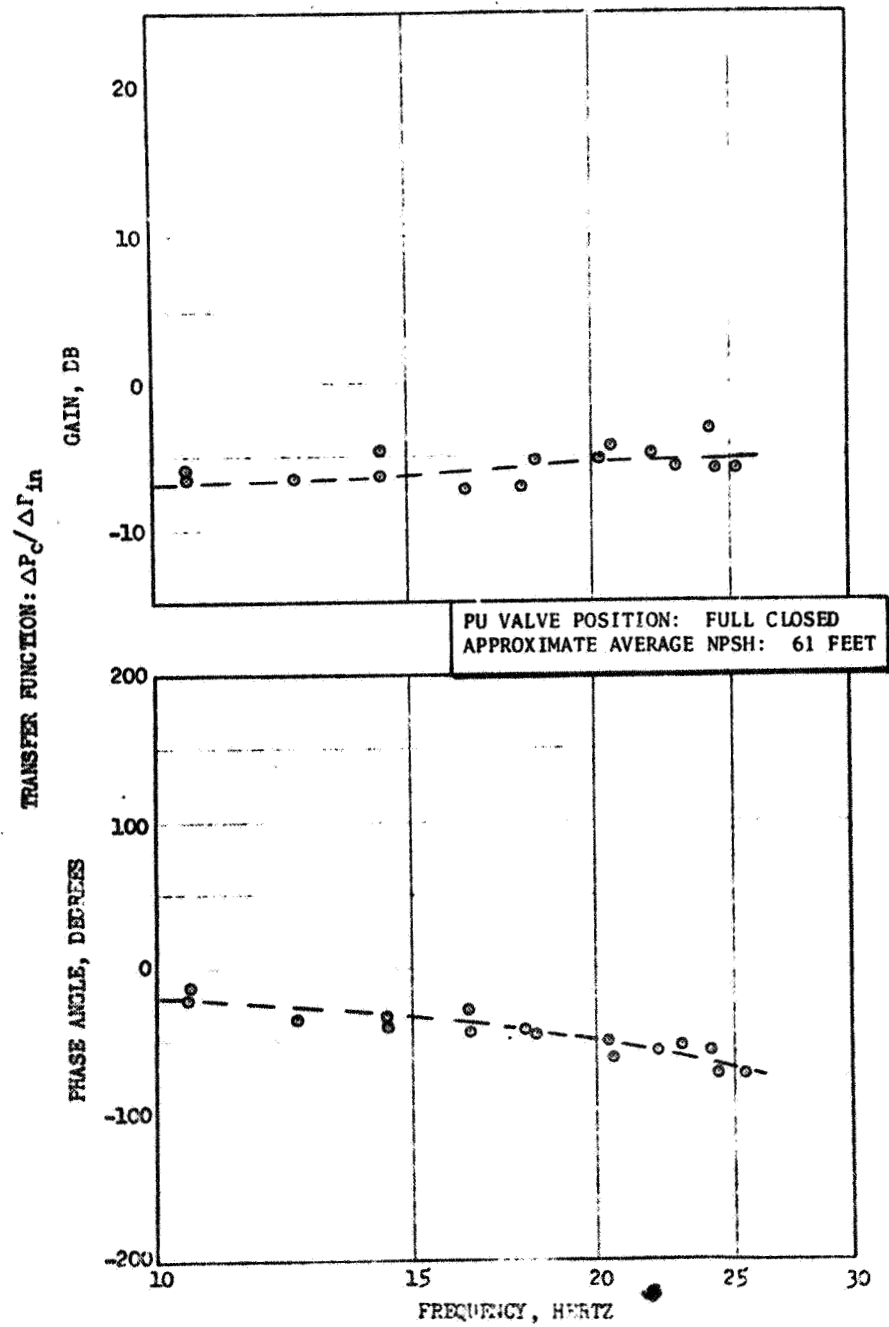Figure A-28. J-2 Engine Test With Inlet Line Pulser, Test No. 316-027-1
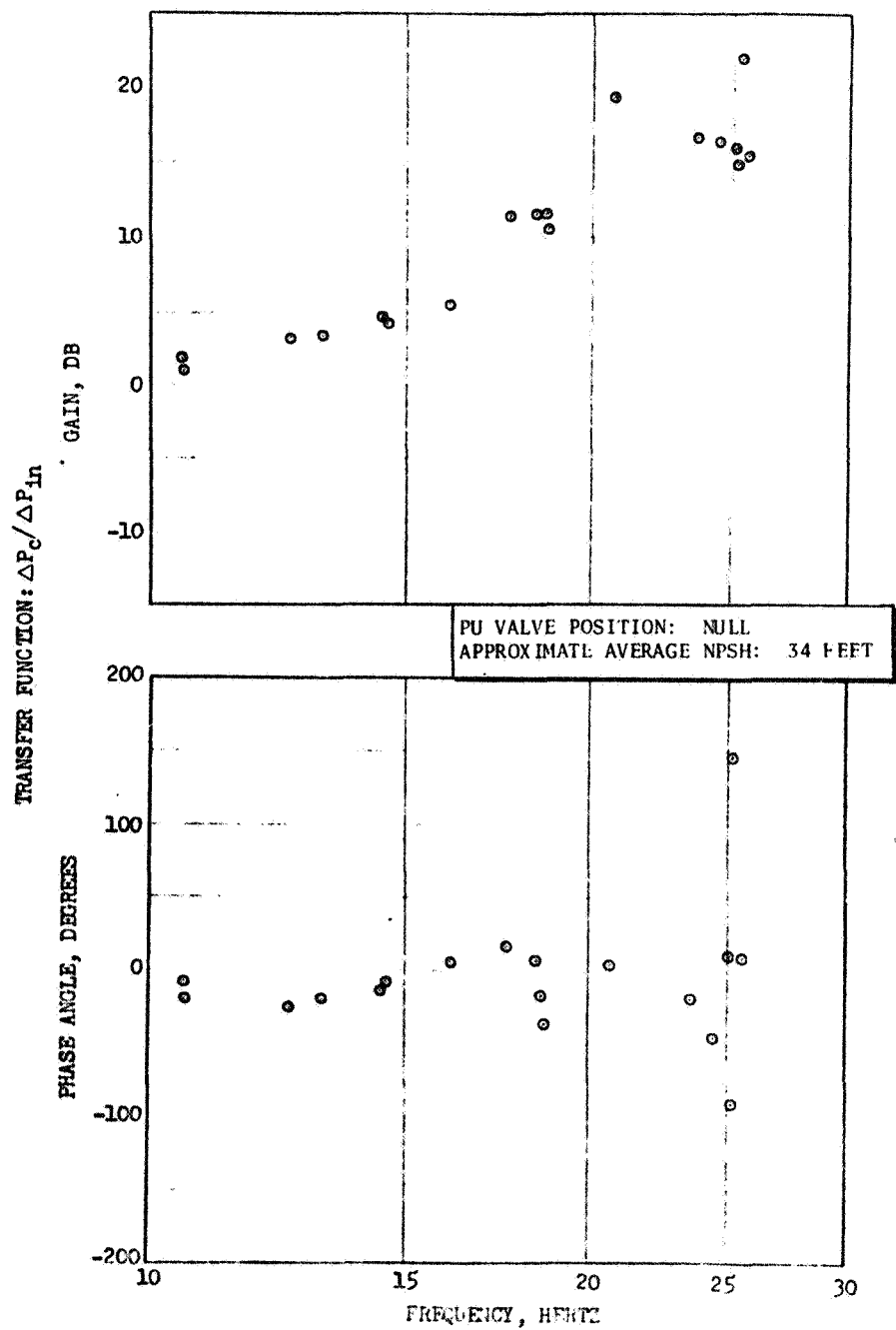
Figure A-29. J-2 Engine Test With Inlet Line Pulser, Test No. 316-028-1
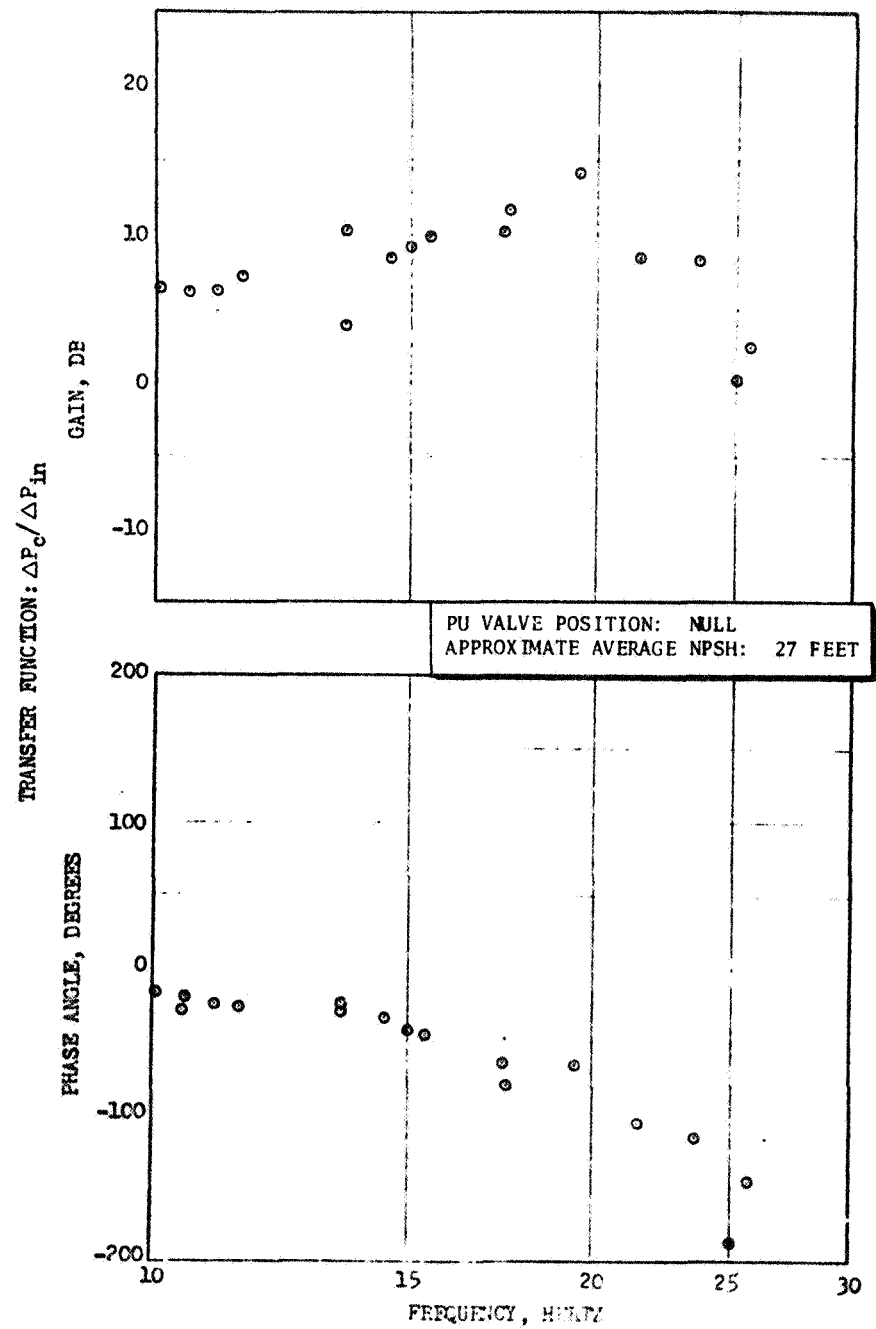
Figure A-30. J-2 Engine Test With Inlet Line Pulser, Test No. 316-028-2

Figure A-31. J-2 Engine Test With Inlet Line Pulser, Test No. 316-028-3

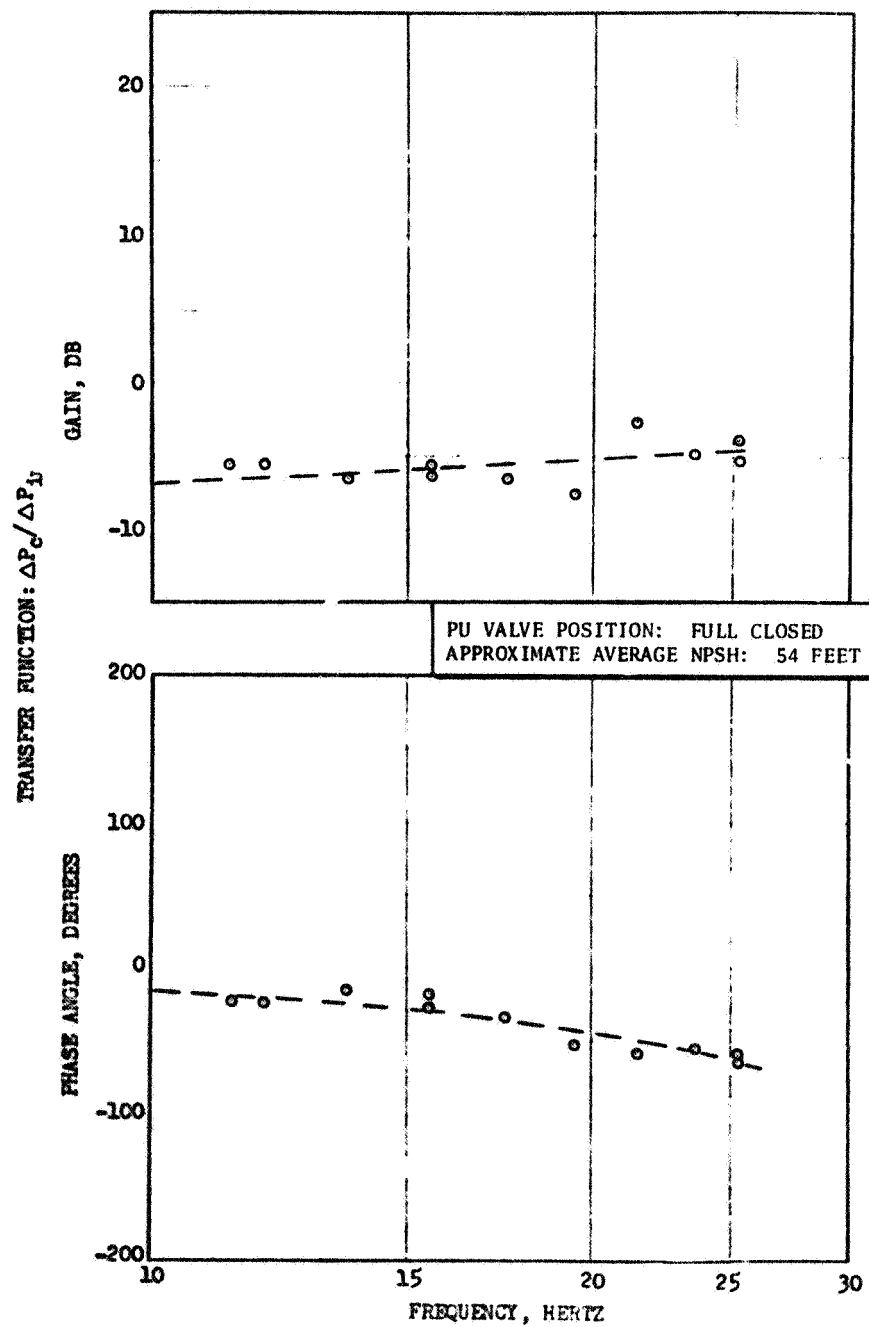Figure A-32. J-2 Engine Test With Inlet Line Pulser, Test No. 316-030-1

Figure A-33. J-2 Engine Test With Inlet Line Pulser, Test No. 316-030-2
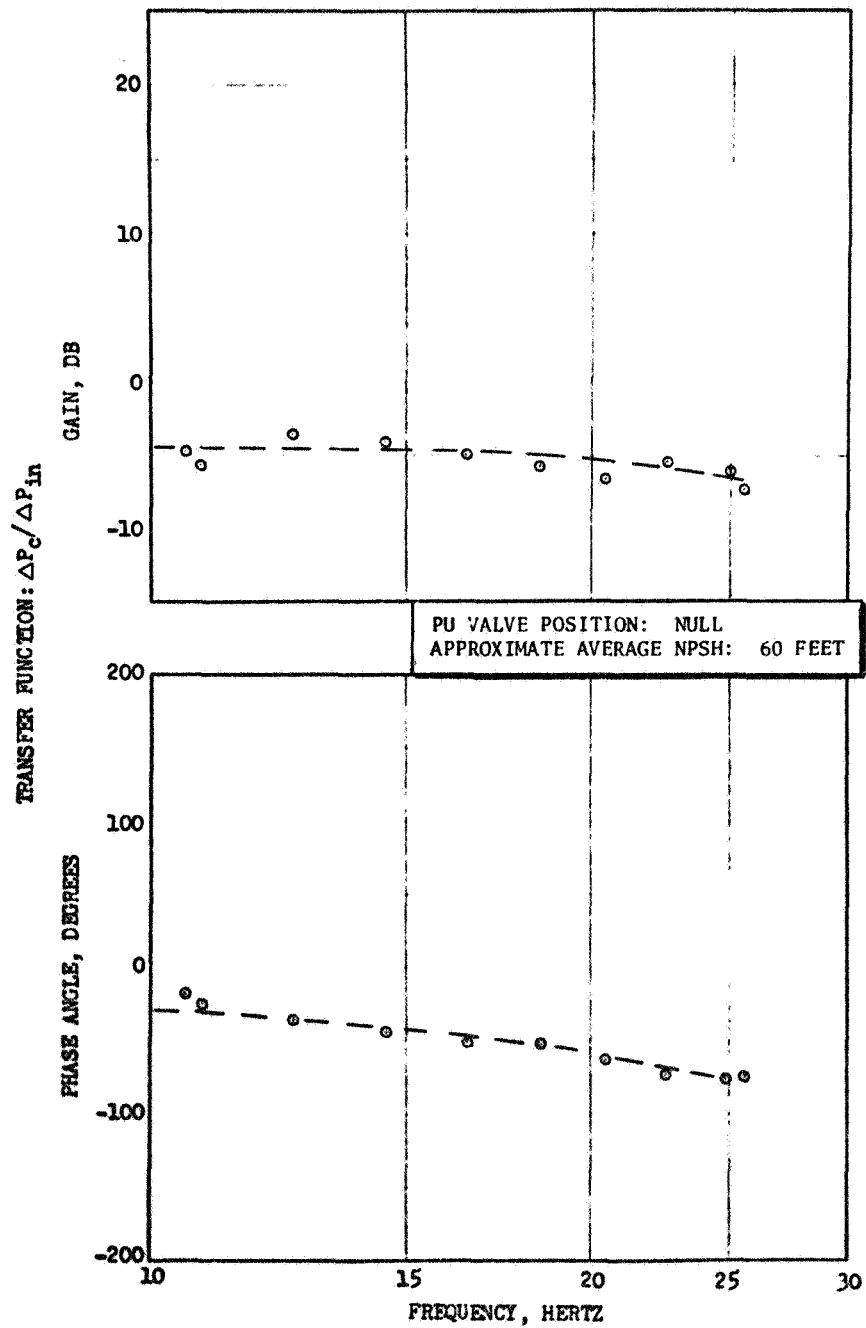
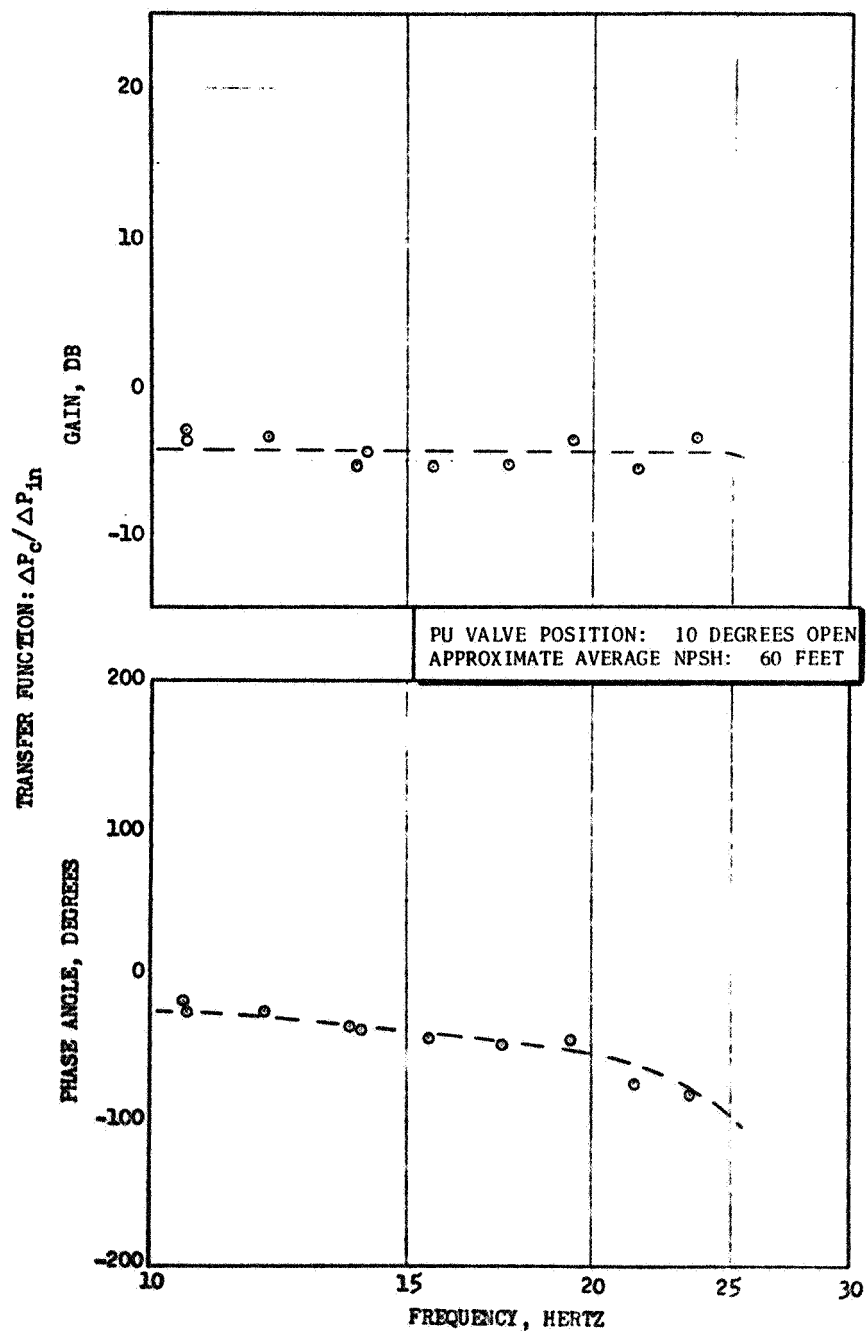Figure A-34. J-2 Engine Test With Inlet Line Pulser, Test No. 316-030-3

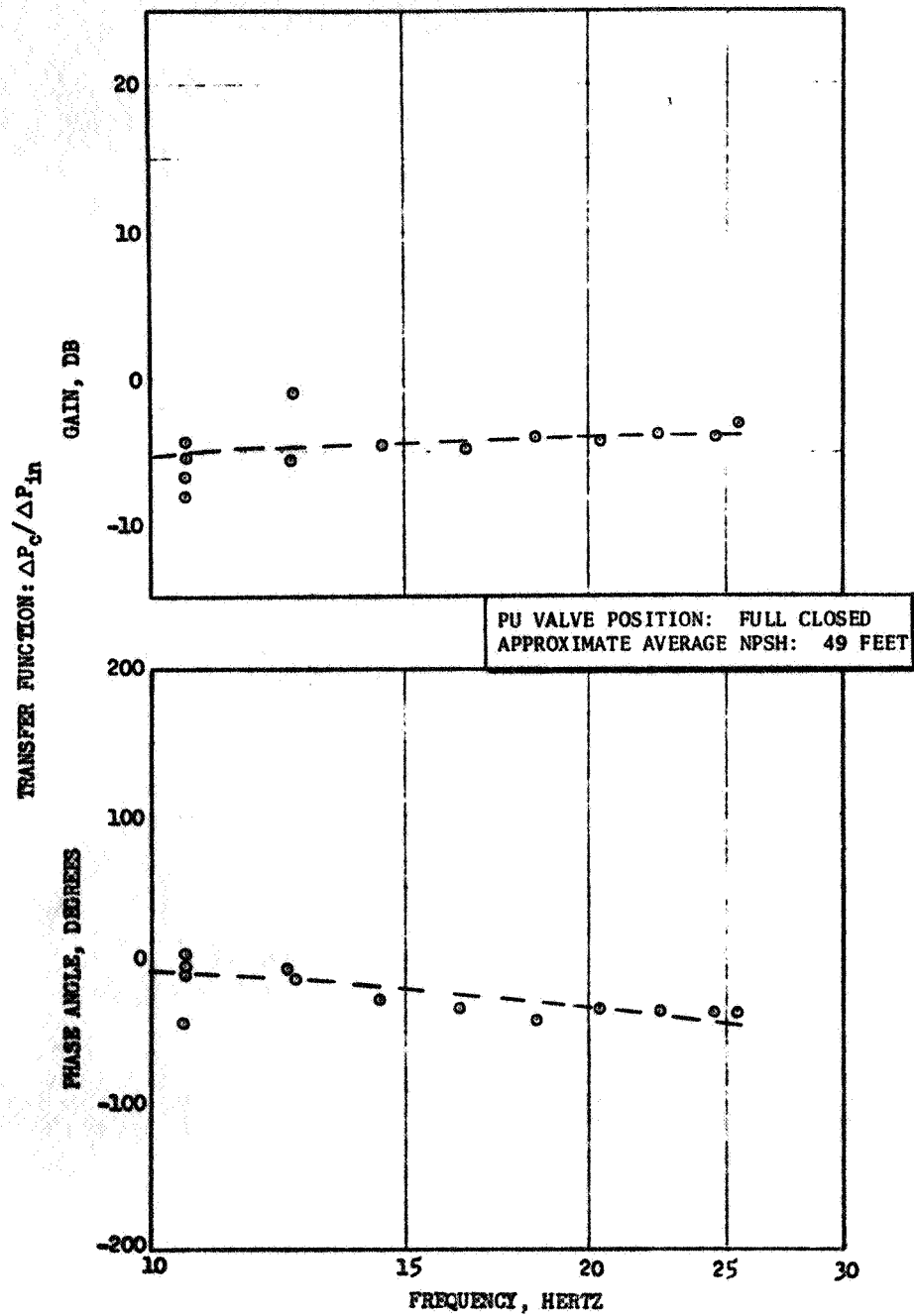Figure A-35. J-2 Engine Test With Inlet Line Pulser, Test No. 316-030-4

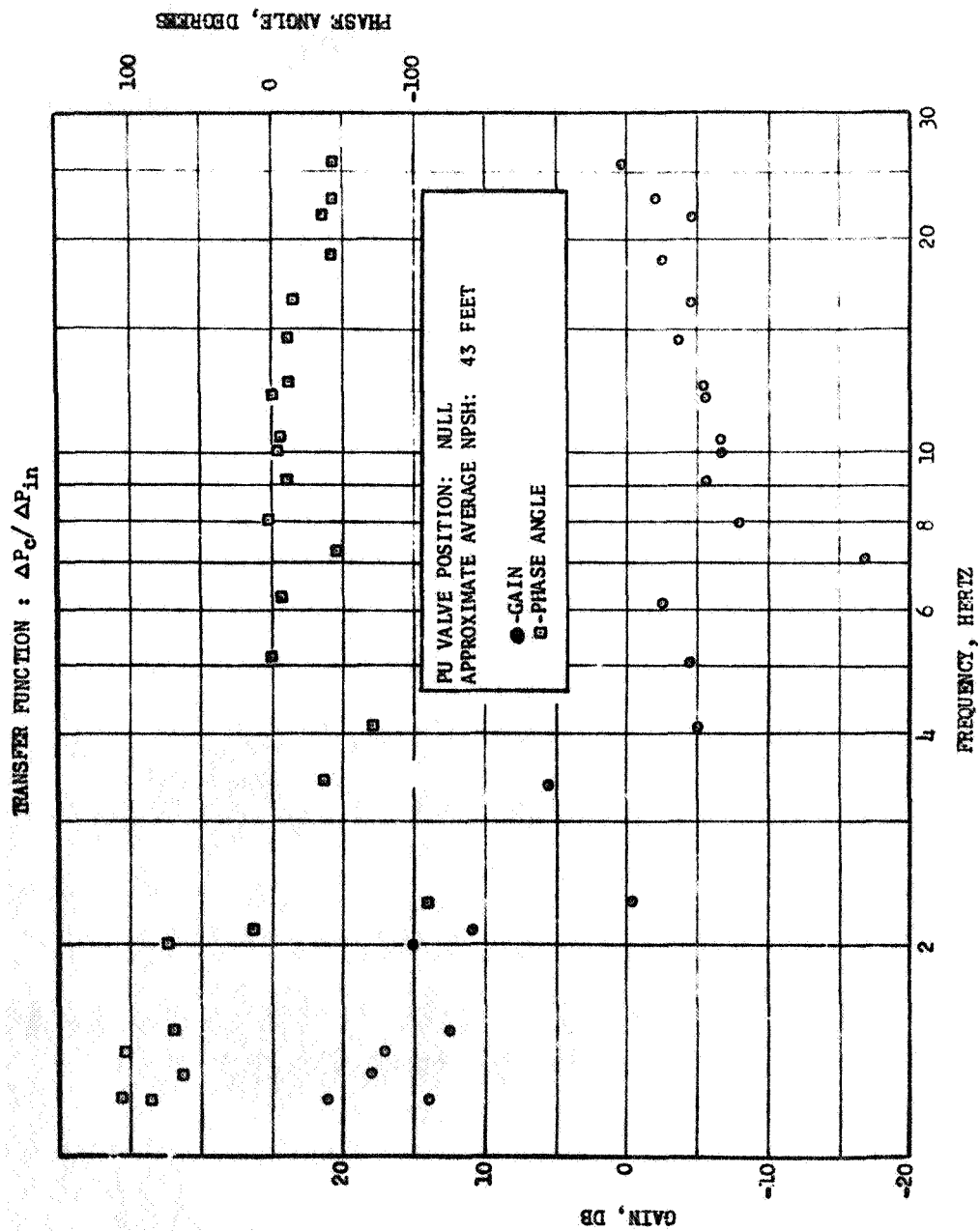Figure A-36. J-2 Engine Test With Inlet Line Pulser, Test No. 316-030-5

Figure A-37. J-2 Engine Test With Inlet Line Pulser, Test No. 316-031

R-7970

APPENDIX B

The following eight figures present some of the data from the LOX pump tests. In each case, the gain and phase of pump inlet pressure divided by pulser position (P_1/X) is plotted as a function of frequency. This pump inlet pressure is located 4 inches upstream of the pulser, which is approximately 59 inches upstream of the pump inlet flange. The eight figures present the data for both a solid inlet duct and the S-II inboard inlet duct at NPSH values of 40, 50, 60, and 70 feet. The pump operating conditions of speed, flow, and PU valve position can be determined from the test number and the corresponding data of Table 14 . Similar data, though less consistent, were obtained for pump discharge pressure and flow, but are not included here.

SOLID INLET DUCT
TARGET NPSH = 50 FEET

TEST NO.

R-7970

SOLID INLET DUCT
TARGET NPSH = 40 FEET

TEST NO.

S-II INBOARD INLET DUCT
TARGET NPSH = 70 FEET

S-II INBOARD INLET DUCT
TARGET NPSH = 60 FEET

TEST NO.

S-II INBOARD INLET DUCT
TARGET NPSH = 50 FEET

GAIN × 3.75, PSI/in.

PHASE, DEGREES

FREQUENCY, Hz

S-II INBOARD INLET DUCT
TARGET NPSH = 40 FEET